Title
Development of Heterogeneous Catalysis with Lignin Monomers and Carbohydrates Obtained from “Lignin First” Biorefinery

Author
Liu, Baoyuan

Publication Date
2021

Peer reviewed|Thesis/dissertation

University of California

Santa Barbara

Development of Heterogeneous Catalysis with Lignin Monomers and Carbohydrates Obtained from “Lignin First” Biorefinery

by

Baoyuan Liu

A dissertation submitted in partial satisfaction of the requirements for the degree Doctor of Philosophy in Chemistry

Committee members:

Professor Mahdi M. Abu-Omar, Chair

Professor Steven K. Buratto

Professor Peter C. Ford

Professor Susannah L. Scot

June 2021

The dissertation of Baoyuan Liu is approved.

Steven K. Buratto

Peter C. Ford

Susannah L. Scott

Mahdi M. Abu-Omar, Committee Chair

May 2021

ACKNOWLEDGMENT

First all of I would like to give my deepest appreciation to my family for all the care and love have been provided to my life. I want to express a special thank to my wife, Yaoyue Liu. Having you in my life is always one of the greatest pleasures, and I could not complete the doctoral study without your loving support.

I wish to formally thank my advisor, Professor Mahdi Abu-Omar, who has been providing me such great opportunities for working with him to explore chemistry in the field of catalysis and biomass. I am very indebted and thankful for his excellent guidance and tremendous encouragement throughout my academic life. This dissertation would not be possible without his fantastic support. His passions and dedications toward the excellence in science have energized me to continue pursuing my future career in academia.

A portion of my research was performed in collaboration with Professor Peter Ford, an amazing, talented, and passionate chemist. Doing research with him is an exceptional learning and working experience and I truly thank him for teaching me the reaction mechanisms and the strategies of writing research articles. It is my great honor to have Professor Ford as my committee member for my doctoral degree.

I would also like to thank Professor Susannah Scott and Professor Steven Buratto for being the members of my committee since candidacy exam in the December of 2017. I am always extremely grateful for your constructive advice and comments which have improved me a lot to become a better chemist. I am very pleased to have Professor Scott and Professor Buratto again as my committee members for the final dissertation and defense.

Last but not the least, thank you to all former and current lab members of the Abu-Omar group. Working with you in the lab has always been joyful. Beyond the lab mates, I am truly lucky to have made friends with you. I want to deliver special thanks to Ian Klein, Shou Zhao, Hao Luo, Thilina Gunasekara, Chan Young Park, Jun Hee Jang, Tayyabeh Bakhshi, Manxi Xiong, Kalin Hanson, Manhao Zeng (Danny), Julianne Truong, Joshua Speer, Yu-Hsuan Lee (Ariel), Melissa Sanchez, Jack Hopper, Justin Marlowe, and Zachary Westman for your great support and company.

Abstract

Development of Heterogeneous Catalysis with Lignin Monomers and Carbohydrates Obtained from "Lignin First" Biorefinery

by

Baoyuan Liu

Lignocellulosic biomass is composed of lignin, cellulose, and hemicellulose. Lignin is naturally formed renewable aromatic biopolymer; the cellulose and hemicellulose are polysaccharides. By far, the "second generation" biorefineries mainly use the value of cellulose pulp in paper industries or in making low-value chemicals such as ethanol while more than 98% of lignin is discarded into direct combustion. The valorizations of lignin and polysaccharides are still under development. Herein, we have studied the heterogeneous catalytic conversion of lignin monomers and polysaccharides with Ru/C catalyst with different metal oxides for making a variety of value-added chemicals. For instance, we developed a Ru/C and Nb_2O_5 co-catalyst system to funnel different lignin monomers into C9 hydrocarbons which could potentially be used as drop-in fuels. We also investigated the Ru/C and WO_x co-catalysts to convert the polysaccharides into diols and polyols. By performing the isotopic reactions and time programmed sampling, our study disclosed the mechanisms and kinetics of the catalytic reactions. To achieve the goal of biomass valorization, we also developed a purification method to avoid catalyst poisoning by the contaminations from raw biomass and thus facilitated the sustainable utilization of native lignin into valuable chemicals.

Table of Contents

List of Figures

List of Reaction Schemes

List of Tables

Chapter 1. Introduction: Lignin Extraction and Valorization using Heterogeneous Transition Metal Catalysts

1.1 Abstract

Lignocellulosic biomass is the most abundant renewable carbon source on our planet. It offers an alternative as well as a complementary source to petrochemical refining for energy and chemical production. The market of renewable energy and chemicals has been rapidly growing over the past two decades. However, utilization of biomass is still underdeveloped. Energy production from biomass has seen only moderate increases.

Today’s second generation biorefinery only uses the carbohydrate components (cellulose and hemicellulose) from the biomass and lignin is generated as a waste byproduct to be used for its low value heat. In contrast, the concept of lignin valorization can improve the economics of biorefining by producing value-added products from lignin. This can be accomplished by changing the pretreatment of biomass to provide fractionation and upgrading of lignin first into valuable products, the “lignin-first” biorefinery concept. Alternatively, pretreatment can provide a protected technical lignin byproduct which can be valorized to chemicals and/or hydrocarbon biofuels. Monomeric phenols are the major products of lignin valorization through heterogeneous catalysis. The complex structure of lignin, impurities from its preparation, and catalyst selection are among the key factors restricting yield of products. This chapter presents and contrasts preparation techniques of technical lignin, reviews the use of inorganic transition metal heterogeneous catalysts for lignin valorization into chemicals and fuels, and lastly demonstrates examples of subsequent applications of lignin derived monomers.

Keywords: Biomass; Lignin-first; Technical lignin; Heterogeneous catalysis; Biofuels

1.2 Biomass Basis

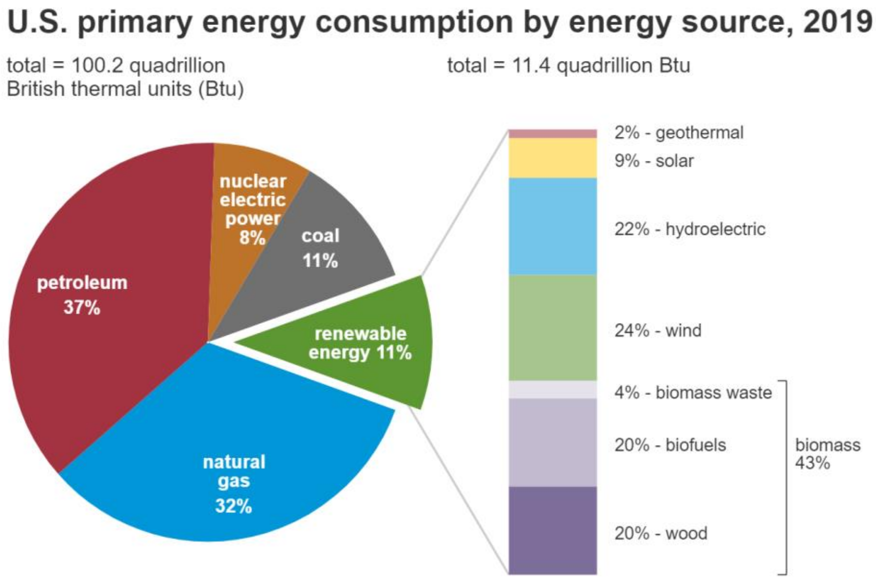

Figure 1.1 Chart of the U.S. energy consumption by energy source, 2019. Adapted from U.S. Energy Information Administration (EIA). Source: U.S. Energy Information Administration, *Monthly Energy Review*, Table 1.3 and 10.1, April 2020. (Accessed on Oct 2020 at: https://www.eia.gov/energyexplained/us-energy-facts/)

Lignocellulose is sustainably produced by photosynthesis which converts solar energy into stored chemical energy on Earth. Lignocellulosic biomass is the most abundant renewable organic feedstock for energy consumption, yielding 50-85 EJ of energy per year.[1] An annual production of ca. 1.5 billion tons of lignocellulosic biomass can be achievable by 2030.[2] Meanwhile the value of global biomass power market will be doubled from the current value of 52 billon U.S. dollars (USD) to more than 100 billion USD by 2027. However, only 11% of the total energy consumption in the U.S. is renewable energy in 2019, 43% of which comes from biomass energy (Figure 1.1).[3] During the past decade (2009-2019), energy consumption in the U.S. from biomass increased at a moderate rate of less than 3% per year.[3, 4] The major energy sources remain non-renewable fossil fuels: petroleum, natural gas, and coal. The continued reliance on fossil fuels has many negative ramifications including greenhouse emission, toxic gas release, and water pollution. Thus, a more rapid implementation of renewable resources including lignocellulosic biomass is necessary to meet a sustainable future.

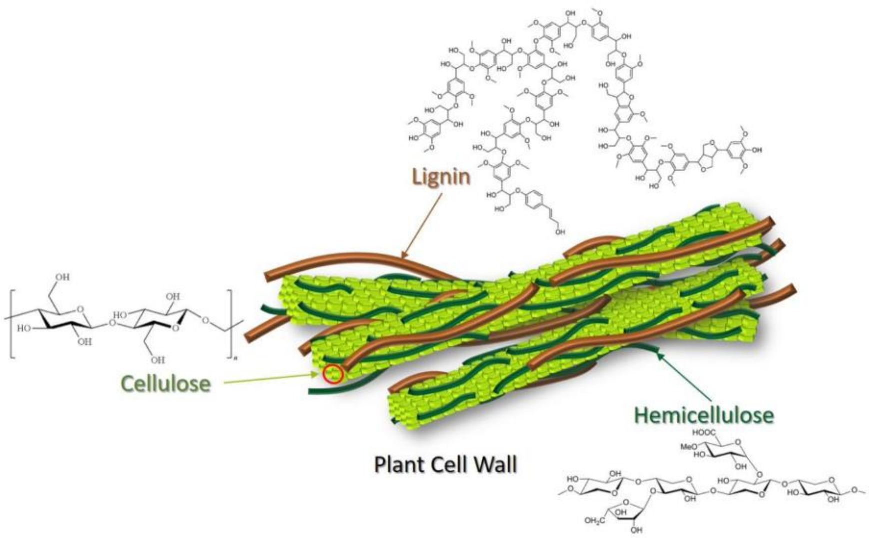

Figure 1.2 Structure of lignocellulosic biomass. Adapted from Jensen, C. U.; Guerrero, J. K. R.; Karatzos, S.; Olofsson, G.; Iversen, S. B. *Biomass Convers Bior* **2017,** *7* (4), 495-509.

Lignocellulosic biomass is composed of three major biological polymers: cellulose (50%), hemicellulose (25%), and lignin (25%).[5] They are the major building blocks of the secondary cell walls (Figure 1.2).[6] The crystalline cellulose forms the fibrous trestle of plant cell wall and is bundled with hemicellulose and lignin, which provides rigidity, ability of plants to grow against gravity, and a mechanism for water transport.[7] While cellulose and hemicellulose are polysaccharides, lignin is the only natural polymer made of aromatic monomers.[8] Interestingly, the most common industrial method of biomass utilization is direct combustion, which does not make use of the chemical differences between polysaccharides and lignin. Recent advances in fermentation of lignocellulose (second generation biorefining) to bio-ethanol has attracted commercial attention for the utilization of carbohydrates from cellulose and hemicellulose on a large scale. However, in the second generation biorefineries lignin is a waste by-product and used only for its heat value.[9-12] Similarly in the paper and pulp industries, 50-70 million tons of lignin is produced every year, of which 98% is discarded into direct combustion.[5, 13] Burning lignin for heat energy is an inefficient way of biomass utilization. It impedes lignin's potential valorization towards high energy density fuels and chemicals. Lignin because of its composition has high carbon content and the potential to provide platform aromatic chemicals and fuels.[14-18] Hence, development of efficient lignin valorization to chemicals can be a game changer for the future of biorefining.

The idea of efficient lignin valorization is to depolymerize the complex three-dimensional lignin polymer into smaller molecules that can be selectively upgraded to chemicals, fuels, and materials for further applications.[19] This approach is distinctly different from the conventional biorefinery methods where lignin is treated as the "left over" waste that can be used for heat value only. Focusing on successful lignin utilization/valorization has been referred to as "lignin first," a concept which targets chemistry that affords selective depolymerization of lignin into low molecular weight phenolic compounds.[20-22] Since native lignin is composed mostly of C-O ether bonds and chemistry for cleaving C-O ether bonds is well known, "lignin first" targets lignin valorization directly from lignocellulosic biomass.[23] In contrast, lignin liquor obtained from harsh pre-treatment in conventional biorefining (acid, base, steam explosion, and ammonia treatment) is composed of re-condensed lignin products with non-native C-C bonds, which are recalcitrant and cannot be upgraded selectively to valuable chemicals/molecules. However, "lignin first" must contend with impurities in the biomass, limitations on process intensification because of the use of solids and low density of biomass, tolerate carbohydrates (cellulose and hemicellulose), and challenges in separations.

A third approach is extraction and separation of lignin in its native form, a pretreatment that protects C-O bonds and prevents re-condensation of lignin into recalcitrant C-C bonds. In this case, lignocellulosic biomass is pre-treated under conditions and/or in the presence of specific reagents to allow for lignin isolation in which the "native" chemical connectivity is maintained as much as possible. This isolated lignin is referred to as "technical lignin." Depending on the pre-treatment, technical lignin is divided into several categories. Kraft and soda lignin refer to aqueous alkali (NaOH and Na_2SO_4) process.[24] Klason lignin is obtained after the cellulose and hemicellulose are dissolved in 72% sulfuric acid.[25] Organosolv lignin results from using various organic solvents such as formic acid, acetic acid, methanol, and acetone.[5, 26, 27] Lignin is first dissolved and extracted in an organic solvent, and recovered by precipitation. Compared to alkali (kraft and soda) and acid (Klason) pre-treatment, organosolv lignin retains chemical connectivity (C-O bonds) present in "native lignin".[5] As a result, organosolv lignin can be valorized to chemicals with reasonable yields. This contrasting approaches for handling lignin are summarized in Figure 1.3.

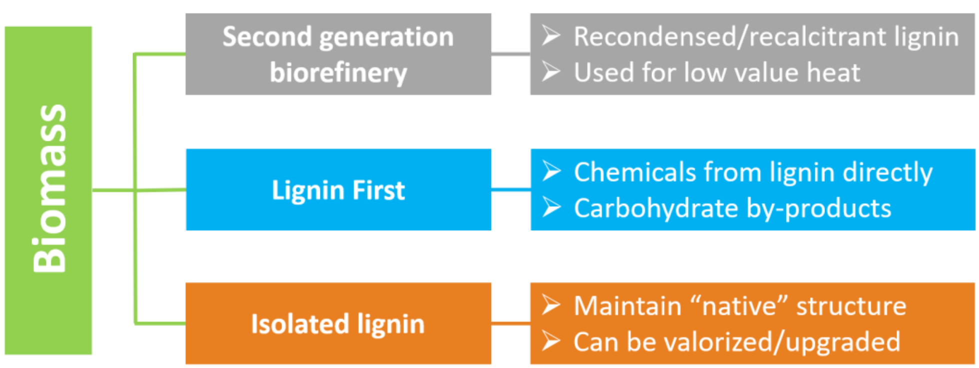

Figure 1.3 Comparison of biomass treatment with the respect to lignin separation and use.

Recent studies have investigated many lignin valorization methods including pyrolysis[28-30], gasification[31, 32], enzymatic catalysis[33, 34], and inorganic catalysis[35-38], into a broad range of high-value aromatic chemicals, such as guaiacol[5, 35, 36, 39-41], vanillin[42-45], dihydroeugenol (DHE)[5, [35-37, 46, 47], 2,6-dimethoxy-4-propylphenol (DMPP)[5, 35, 37, 48, 49], ferulic acid[39, 50, 51], and sinapyl alcohol[39, 52, 53] (Figure 1.4). Among those lignin valorization methods, the use of heterogeneous metal catalysts is a promising technology for making value-added chemicals from lignin.[35, 54, 55]

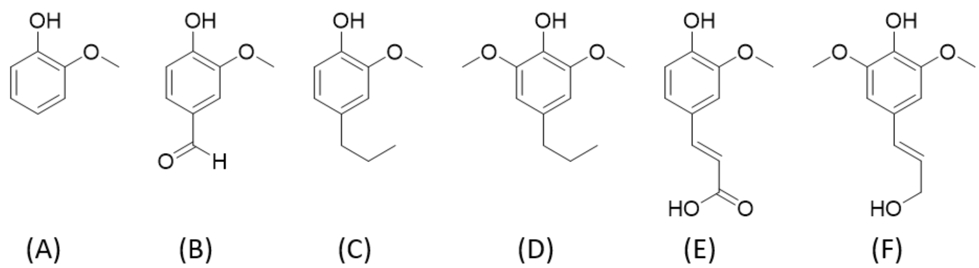

Figure 1.4 Example of lignin monomers. (A) Guaiacol. (B) Vanillin. (C) Dihydroeugenol (DHE). (D) 2,6-dimethoxy-4-propylphenol (DMPP). (E) Ferulic acid. (F) Sinapyl alcohol.

Among its attractive features are, high lignin conversion, relatively mild reaction conditions, ease of product separation, production of cellulose and hemicellulose as unscathed byproducts that can be used further in making biofuels and chemicals, and catalyst stability. The application of various metals has been demonstrated. Pd, Pt, Rh, and Ru are the most common used noble metals that have been studied to selectively cleave C-O bonds (in some instances C-C bonds) of the lignin polymer.[37, 47, 56-58] On one hand, these noble metals are usually supported on activated carbon to increase the surface area for improved catalyst activity. On the other hand, the integration of noble metals with an acidic zeolite or metal oxide support, creates a bifunctional catalyst system which can improve selectivity to deoxygenated aromatic hydrocarbons.[59] To satisfy scientific curiosity, sustainability and economics, inexpensive earth-abundant metals have been favored in recent investigations. Cu[60, 61], Ni[35, 36, 62, 63], and Co[64, 65] catalysts have been shown to give comparable results to noble metals. More interestingly, lignin depolymerization can occur under supercritical conditions in ethanol/isopropanol medium without the need for a transition-metal catalyst.[66]

In this chapter, we review “lignin first” valorization and compare it to isolation and upgrading of technical lignin with a focus on organosolv lignin. An atomic level characterization of lignin will be discussed to understand and contrast the properties of technical lignin compared to recalcitrant and not upgradable lignin. A discussion of mechanistic aspects of lignin conversion will be provided. We will end the chapter by showing how platform molecules obtained from lignin can serve as versatile monomers to make renewable plastics and as feedstock for making specialty hydrocarbon fuels, mapping a complete supply chain from lignocellulosic biomass to value-added bioproducts.

1.3 Technical Lignin

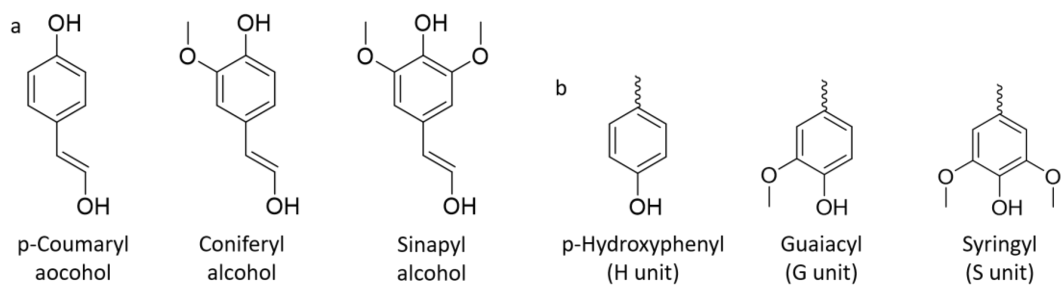

Figure 1.5 a: The three monolignols that make up lignin units; b: The key units in lignin polymer.

Lignin is an aromatic polymer made of three major monolignols: p-coumaryl alcohol, coniferyl alcohol, and sinapyl alcohol (Figure 1.5a). Through biological polymerization, the monolignols are linked by C-O and C-C bonds forming three key lignin units: p-hydroxyphenyl (H unit), guaiacyl (G unit), and syringyl (S unit) (Figure 1.5b).[5] In general, softwood lignin is composed of 90-95% G unit with a small percentage of H unit, while hardwood lignin is 50-75% S unit and 25-50% G unit.[22, 67] Even though the content of key units differ from species to species, the lignin interunit linkages are similar among all types of lignocellulose. The most common linkage is the β-O-4 ether bond, which accounts for 50-60% of the total linkages (Figure 1.6).[68, 69] Other linkages commonly found include α-O-4 and 4-O-5; connected by C-C covalent bond are 5-5, β-5, β-1, and β-β. The approximate content of each lignin linkage in softwood and hardwood is summarized in Table 1.1.[24, 69-71]

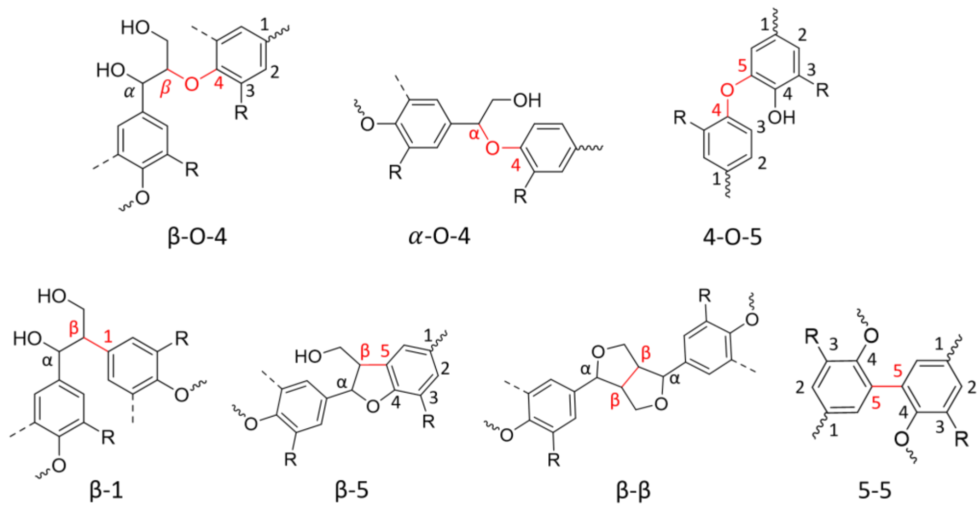

Figure 1.6 Common lignin interunit linkages (labeled in red color) in lignin polymer. Reproduced from: (1) Patil, N. D.; Tanguy, N. R,; Yan, N. In *Lignin in Polymer Composites*, Faruk, O.; Sain, M., Eds. William Andrew Publishing: 2016; pp 27-47. (2) Luo, H.; Abu-Omar, M. M. In *Encyclopedia of Sustainable Technologies*, Abraham, M. A., Ed. Elsevier: Oxford, 2017; pp 573-585.

Making technical lignin is driven by the distinct solubility of biomass components. One approach is dissolution of carbohydrates and leaving the lignin as a solid residue, such as Klason lignin. Another strategy is to extract and dissolve the lignin in aqueous alkali or organic solvent and leave other components of the biomass (cellulose) as a solid residue. Examples of the second method include Kraft, soda, and organosolv lignin. Regardless of what method is used, production of technical lignin generally requires elevated temperature and the use of acid/base to cleave the intermolecular linkages between lignin and carbohydrates, and separation of the different components. Because acid/base also catalyze lignin inter-unit cleavage, technical lignin is always a modified structure from the native form and the extent of modification varies from method to method. The differentiating characteristics between different technical lignins are type of linkages preserved and introduced, molecular weight, and elemental composition. For instance, the β-O-4 ether linkage is selectively cleaved during Kraft pulping by sulfonation and result in increased content of non-native C-C bonds. Compared to organosolv, Kraft lignin exhibits higher molecular weight and higher sulfur content.[24, 72, 73] Different pulping methods and the resulting lignins will be discussed and compared in this section.

Table 1. Proportions of Linkages in Softwood and Hardwood Lignin

Linkage type	Softwood (%)	Hardwood (%)
β-O-4	45-50	50-65
α-O-4	6-8	4-8
4-O-5	4-8	6-7
β-1	7-10	5-7
β-5	9-12	4-6
β-β	3	3-7
5-5	18-25	4-10

Table 1.1 Values were obtained from: (1) Chakar, F. S.; Ragauskas, A. J. *Ind Crop Prod* **2004,** *20* (2), 131-141. (2) Zakzeski, J.; Bruijnincx, P. C. A.; Jongerius, A. L.; Weckhuysen, B. M. *Chem Rev* **2010,** *110* (6), 3552-3599. (3) Mei, Q.; Shen, X.; Liu, H.; Han, B. *Chinese Chemical Letters* **2019,** *30* (1), 15-24.

1.3.1 Kraft lignin

The most abundant production of technical lignin is via Kraft processing, which produces 55 million tons of lignin every year in the U.S.[13] The Kraft pulping process was initially developed in the paper industry by the German chemist C.F. Dahl in 1879. Wood chips are cooked under alkaline condition with sodium hydroxide (NaOH) and sodium sulfide (Na_2S) at 170 ℃ for 2 hours to dissolve lignin and hemicellulose in the aqueous solution. The residual cellulose from Kraft pulping is a brown solid. After bleaching with hydrogen peroxide (H_2O_2) and chlorine dioxide (ClO_2) the cellulose is used for paper production. Lignin dissolved in the aqueous alkaline fraction is recovered by decreasing the pH.[74]

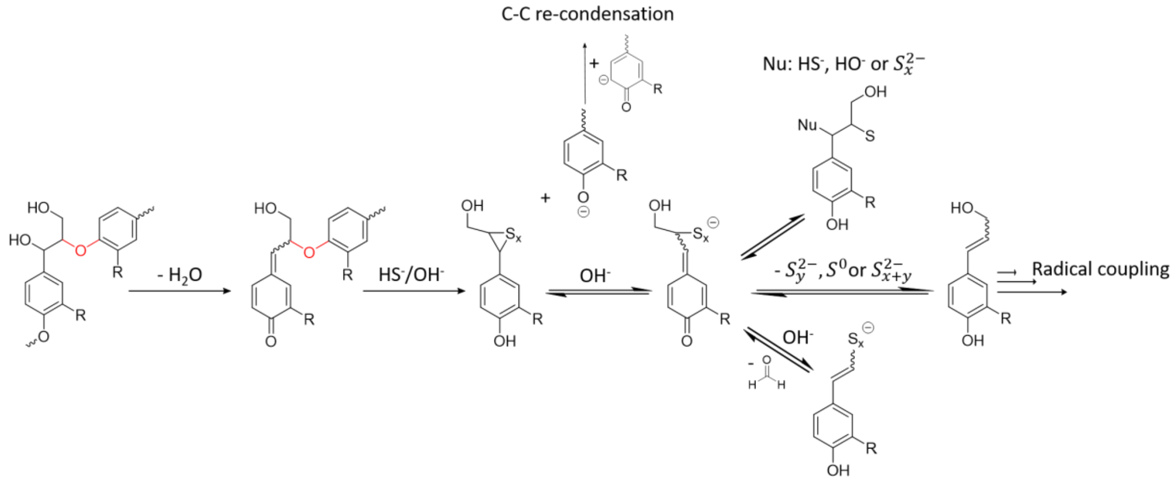

Scheme 1.1 Cleavage of phenolic β-ether bond in kraft pulping process. Reproduced from: Rinaldi, R.; Jastrzebski, R.; Clough, M. T.; Ralph, J.; Kennema, M.; Bruijnincx, P. C. A.; Weckhuysen, B. M. *Angew Chem Int Edit* **2016,** *55* (29), 8164-8215.

Studies have proved that the solubilization of lignin into the aqueous phase is accompanied with the cleavage of both α and β ether bonds (α-O-4 and β-O-4 linkages).[75] Content of α-O-4 linkage is relatively low in most lignin structures (6-8%). Therefore, one characteristic of Kraft lignin is the low content of β-O-4 linkage. Advanced 2D (^{1}H and ^{13}C) Heteronuclear Single Quantum Coherence NMR (2D HSQC NMR) spectroscopy has been widely used to analyze linkages and functional groups on the lignin framework.[76] Quantitative HSQC NMR indicates up to 86% of β-O-4 linkages are cleaved during Kraft pulping.[77] Scheme 1.1 illustrates the mechanism of cleaving β-O-4 linkage in the presence of sulfide and hydroxide ions. The cleavage of C-O ether bonds is initiated by dehydration and ring rearrangement to form quinone methides and thiirane intermediates resulting in a coniferyl alcohol type fragment.[77, 78] The sulfonation and sulfur extrusion promote an increase in sulfur content as well as recondensation in Kraft lignin. This mechanism explains the high sulfur content and increased amount of recalcitrant C-C bonds in Kraft lignin. Giummarella et al. recently reported their findings of C-C direct coupling between S and G units in Eucalyptus Kraft lignin.[79] Analysis by 1D ^{13}C NMR indicated non-native C-C bond formation is common through retro-aldol and subsequent radical condensation between aromatic carbons. Oxidized quinone-like byproduct from the condensation reaction gives Kraft lignin its amber color. Besides the direct coupling of aromatic carbons, Lancefield et al. demonstrated another possibility of repolymerization by a different type of C-C linkage between homovanillin and formaldehyde to a lactone structure.[78] This complex condensation reaction can result in over 100 new C-C linkages in Kraft lignin. Rinaldi et al. have summarized the bond dissociation energy (BDE) of both β-O-4 linkages in native lignin and C-C linkages in Kraft lignin. Accordingly, a typical BDE of β-O-4 is 54-72 kcal/mol while the BDE of C-C linkage falls into a higher value range 86-118 kcal/mol.[77] As a result, the valorization of Kraft lignin is hindered by its recalcitrant C-C bonds formed during the extraction process.

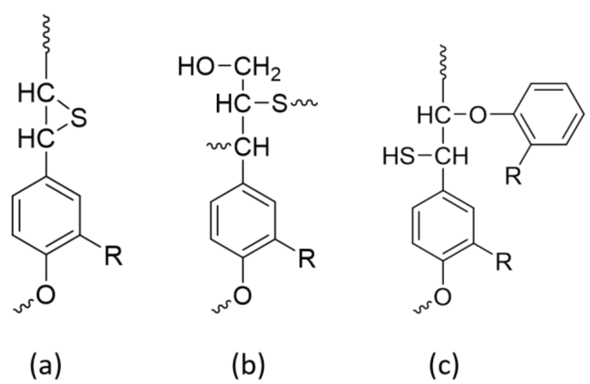

Figure 1.7 (a), (b) and (c) represents the -S-, -S-S- and -SH types sulfur structure in kraft lignin. Reproduced from: Evdokimov, A. N.; Kurzin, A. V.; Fedorova, O. V.; Lukanin, P. V.; Kazakov, V. G.; Trifonova, A. D. *Wood Sci Technol* **2018,** *52* (4), 1165-1174.

Another characteristic of Kraft lignin is its high sulfur content. Sulfur exists in both organic and inorganic structures during the growth of native biomass.[80, 81] In general, raw biomass contains less than 0.1% of sulfur.[82] However, the Kraft process increases the sulfur content up to 7% in lignin.[13, 68, 83, 84] The sulfonation within Kraft lignin is caused by the residual sulfur from sodium sulfide. It forms a variety of sulfur-containing structures in the Kraft lignin including: thiol (-SH), sulfide (-S-), and disulfide bonds (-S-S-) (Figure 1.7).[85] Although several desulfurization methods have been investigated, such as sulfur extraction by organic solvent, sulfur removal by O_2 oxidation, reduction by Raney nickel, and sodium sulfite treatment etc., the typical sulfur content remains between 1-3% in Kraft lignin. Inwood et al. studied the elemental analysis and proposed the chemical formula of Kraft lignin to be $C_9H_{10.09}O_{3.23}S_{0.53}$, $C_9H_{7.98}O_{5.67}S_{0.59}$, and $C_9H_{9.96}O_{3.76}S_{0.19}$.[84] The increased sulfur content can also prevent Kraft lignin from further valorizations. Osada et al. reported sulfur-free lignin could be completely converted to syngas (mixture of methane, carbon monoxide, and hydrogen) over Ru/TiO_2 catalyst.[86] However, the yield of syngas is significantly lowered when sulfur is present because of catalyst poisoning. As a result, only catalysts resistant to sulfur poisoning can be used with Kraft lignin.[87] Instead, fast pyrolysis at high temperature (up to 850 ℃) is a common way to utilize Kraft lignin. The thermal decomposition at high temperature overcomes sulfur poisoning; however, sulfur byproducts such as SO_2, H_2S, CH_3SH, CH_3SCH_3, and CH_3SSCH_3 must be scrubbed and managed to avoid pollution.[88]

1.3.2 Lignosulfonates

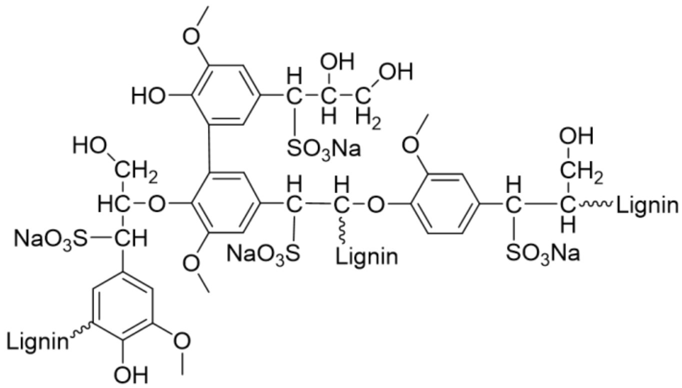

Figure 1.8 Illustration of main building blocks in sodium lignosulfonate molecule. Reproduced from: Flatt, R.; Schober, I. In *Understanding the Rheology of Concrete*, Roussel, N., Ed. Woodhead Publishing: 2012; pp 144-208

Lignin made with sulfite ions (SO_3^{2-} or HSO_3^-) is referred to as lignosulfonate. It is a byproduct from the paper industry. The process of making lignosulfonates, sulfite pulping, has been used as a delignification technique since the 1930s. It is the second lignin source in the market after Kraft lignin. 1 million tons of lignosulfonate solids is produced annually .[89] Lignosulfonate pulping also generates sulfur-containing lignin. The sulfur content in dry lignosulfonate is around 3-8%.[68, 90] While sulfur in Kraft lignin is mainly covalent sulfur, in lignosulfonates it is anionic as salt of typical ions such as sodium (Na^+) , potassium (K^+), and calcium (Ca^{2+}).[68, 91] Figure 1.8 displays an example of sodium lignosulfonate.[92] Because of its highly charged structure, lignosulfonate is water-soluble.

Sulfite pulping takes up to 14 hours.[68] After that, the lignosulfonate is extracted into an aqueous phase. In most cases, acidic (pH 1-5) and neutral (pH 5-7) conditions are applied to the sulfite pulping process. Reactions described in Scheme 1.2 represent the major mechanism of sulfonation and condensation pathways during acidic sulfite pulping.[90, 93] The α ether linkages are first cleaved through hydrolysis catalyzed by acid (H^+) at 130-160 °C followed by sulfonation on the resulting benzylic cations. Competitive condensation of the benzylic cation with the aromatic ring of another lignin unit forms C-C bonds. In contrast to acidic conditions, the β ether bond is selectively cleaved under neutral conditions.[93] Therefore, the properties of lignosulfonate are highly dependent on pH and the sulfite reagent used in pulping. The large variety makes lignosulfonate a broad range of molecular weight (10 to 50 kg/mol) with distinct properties. For example, lignosulfonate made with ammonium-based sulfite is more condensed and results in higher molecular weight product. On the other hand, sodium lignosulfonates exhibit the lowest viscosity because of the strong electro-kinetic repulsive force of sodium ions.[90]

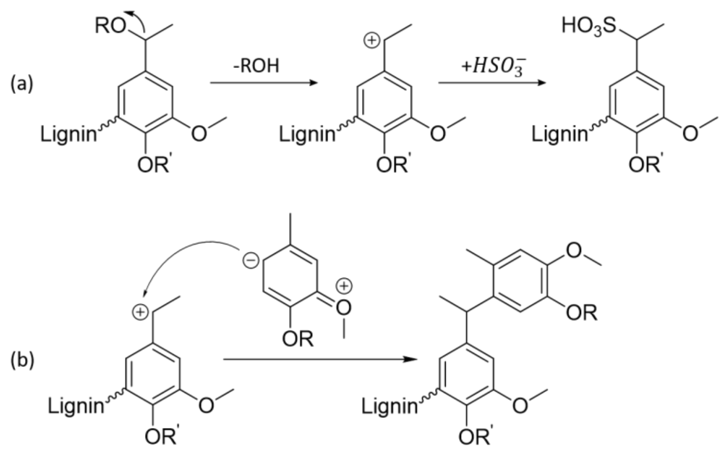

Scheme 1.2 Illustration of (a) sulfonation and (b) condensation pathways in acidic sulfite pulping. Reproduced from: Aro, T.; Fatehi, P. *Chemsuschem* **2017,** *10* (9), 1861-1877

Compared to Kraft lignin, lignosulfonates are generally of low purity. Carbohydrates, ash, and inorganic salts can take up to 30% by mass of lignosulfonate. The high sulfur content, highly condensed structure, and low lignin purity make lignosulfonate a less attractive feedstock for production of chemicals. Instead, utilizing lignosulfonate polymer directly is more prevalent. For example, the sodium lignosulfonate is a well-known dye dispersant.[94, 95] Besides, a recent study by Huang et al. also demonstrated the comprehensive electrostatic repulsion and steric hindrance on the anionic surface-active structure makes lignosulfonate potentially a good water reducer additive to improve the quality of concrete.[96]

1.3.3 Soda lignin

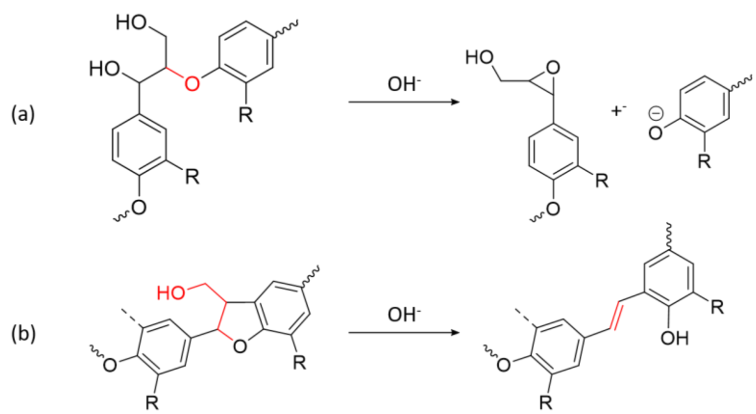

Scheme 1.3 Illustration of lignin linkages modified in soda pulping. (a) describes the reaction of β-O-4 linkage in alkaline condition. (b) represents the change of β-5 linkage in alkaline condition. Reproduced from: (1) Schutyser, W.; Renders, T.; Van den Bossche, G.; Van den Bosch, S.; Koelewijn, S.-F.; Ennaert, T.; Sels, B., Catalysis in Lignocellulosic Biorefineries. 2017; pp 537-584. (2) Rinaldi, R.; Jastrzebski, R.; Clough, M. T.; Ralph, J.; Kennema, M.; Bruijnincx, P. C. A.; Weckhuysen, B. M. *Angew Chem Int Edit* **2016,** *55* (29), 8164-8215.

Soda lignin is made from the soda pulping process. Compared to Kraft lignin and lignosulfonates, soda lignin is sulfur-free and has higher purity.[89, 97, 98] The soda pulping method is mainly used for processing annual crops such as straws, bagasse, and hardwood. In fact, the alkaline process of delignification in soda pulping is quite comparable to the Kraft method. Sodium hydroxide (NaOH) is used to generate an aqueous alkaline medium. Delignification reaction occurs within the hot alkaline solution and can modify several lignin inter-units such as β-O-4 and β-5 linkages (Scheme 1.3).[77, 99] The chemical treatment in soda lignin generates many vinyl ether and p-hydroxyl units.[68, 97] Condensation within in soda lignin often occurs on the vinyl ether units. Nevertheless, most soda lignin still has low molecular weight of 0.3-3 kg/mol.[68]

After delignification, the dissolved soda lignin can be recovered from the alkaline solution by lowering the pH. Mousavioun et al. reported an interesting two-stage acid precipitation in which the soda lignin collected at pH 5.5 gives higher purity and larger particle size than that produced at pH 3.[98] Because of its low sulfur content and high purity, soda lignin is more suited for chemical upgrading to functional biopolymers,[100] phenols and hydrocarbons[101] than Kraft lignin and lignosulfonates. Besides, soda lignin can also serve as a natural feed additive for monogastric animals.[102]

1.3.4 Organosolv lignin

The organosolv process is another important method for making sulfur-free lignin from biomass. To date, there is no commercial organosolv lignin on the market. Most efforts are still on the laboratory scale. The principle of organosolv method is to extract lignin by solubilization in organic solvent or solvent mixtures. Methanol,[5, 103] ethanol,[104] acetone,[5, 105] ethylene glycol,[106] and 1,4-dioxane have been among the most commonly used organic solvent for lignin extraction and isolation.[107] Organosolv lignin is highly soluble in organic solvents but insoluble in water.[108] Due to this hydrophobic characteristic, organosolv lignin can be easily precipitated and recovered by adding water to the solution.

Besides the simple recovery, organosolv lignin is attractive for the following reasons: (1) The organosolv methodology affords complete fractionation of biomass major components: cellulose, hemicellulose, and lignin into three separate streams. Cellulose is collected as the leftover solid, lignin is recovered from the organic solvent phase, and hemicellulose (and its derivatives) are washed out in the aqueous phase. This complete fractionation of biomass establishes the possibility of utilizing every component of the biomass efficiently. (2) Organosolv lignin has excellent chemical characteristics. It is sulfur-free, high in lignin purity, and low in ash content (1.75 wt%).[13] Thus, organosolv lignin is an ideal precursor for production of chemicals and biopolymers.[5, 109-111] (3) The preparation of organosolv lignin requires moderate conditions. (4) Compared to Kraft, sulfite, and soda lignin, organosolv lignin shows the least chemical modifications and resembles "native" lignin the most.[76, 112, 113] (5) The production of organosolv lignin is environmentally friendly.[114, 115] Organosolv lignin is generally made with low energy input, reduced use of strong acid/base and metal catalyst. The organic solvent can be recycled and reused. As a result, organosolv treatment exhibits low cost, no water pollution, and no sulfur dioxide (SO_2) emission, while providing high quality lignin.

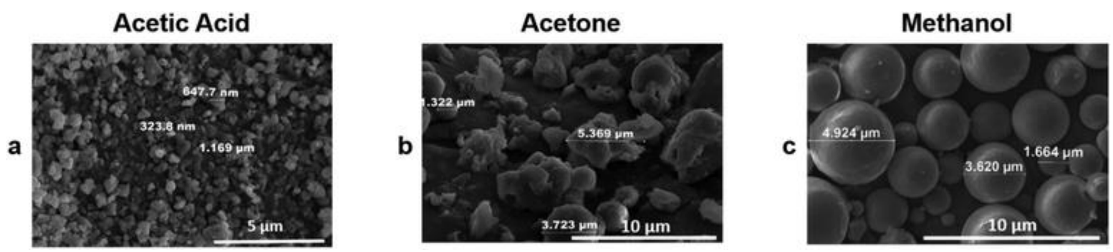

Figure 1.9 Scanning electron microscopy (SEM) images of the isolated organosolv lignin from wild-type poplar using different solvent extraction methods. (a) lignin sample from FA/AA treatment. (b) lignin sample from acetone/formaldehyde treatment. (c) lignin sample from methanol treatment. Imiage was acquired from: Luo, H.; Abu-Omar, M. M. *Green Chem* **2018,** *20* (3), 745-753.

Organosolv lignin from different solvent systems may share similar properties such as high lignin purity and low molecular weight.[68, 89] However, studies have shown the quality of organosolv lignin is highly dependent on the solvent system. A recent study from our group[5] compared formic acid/acetic acid (FA/AA), acetone/formaldehyde, and methanol with dilute sulfuric acid (0.045 N) for the preparation of poplar wood organosolv lignin. A narrow range of molecular weight was observed (1.8-2.5 kg/mol) for the isolated organosolv lignins. Despite this similarity in molecular weight average, the aggregation and shape of the resulting organosolv lignin varied significantly. Scanning electron microscopy (SEM) images showed organosolv lignin from methanol to be highly regular and spherical in structure while those from FA/AA and acetone to irregular (Figure 1.9).

Two-dimensional (^{13}C, ^{1}H) HSQC-NMR analysis revealed the presence of alcohol (methoxy group) on the α position of the β-O-4 linkages (Scheme 1.4a). Another unique signal at around δ_C/δ_H 94/5 ppm was only detected in the lignin made from acetone/formaldehyde mixture. This signal was due to the dioxane structure formed by addition of formaldehyde to the lignin linkage (Scheme 1.4b). Therefore, methanol and formaldehyde serve as protection groups to trap the active α carbon cation intermediate and prevent formation of recalcitrant C-C bond (Scheme 1.4c).

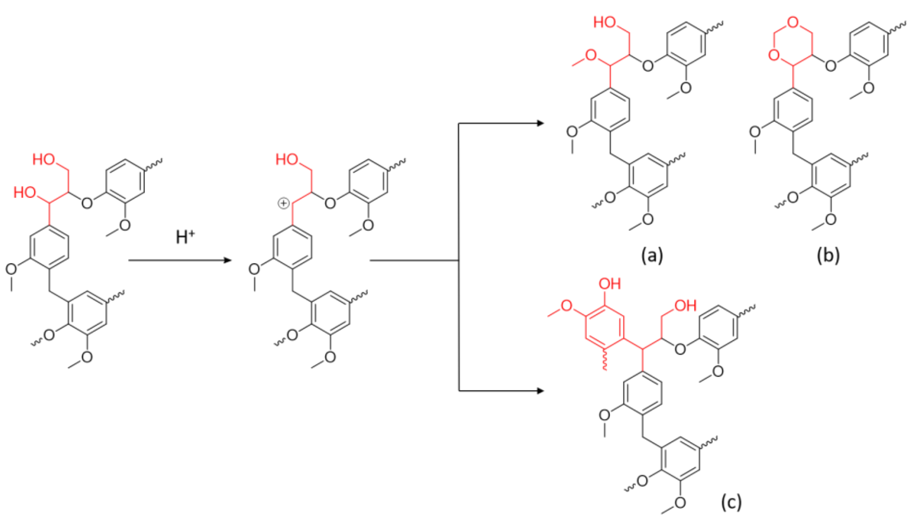

Scheme 1.4 Illustration of acid catalyzed modifcation of lignin linkages within different organic solvents. (a) nucleophil protected α-aryl ether bond in methanol sloution. (b) dioxane structure by formaldehyde addition. (c) condensation occurs on the α carbon through recalcitrant c-c bond**.** Adapted from: Luo, H.; Abu-Omar, M. M. *Green Chem* **2018,** *20* (3), 745-753.

Overall, the organosolv extraction of lignocellulosic biomass is an attractive alternative to Kraft, sulfite, and soda methods. It has potential for making high quality lignin and cellulose fractions for further upgrading. Many studies have shown promising yields of phenolic products from lignin by various heterogeneous catalysts. Compared to direct catalytic conversion of lignin from lignocellulosic biomass where lignin is only a 20-30 wt% component, catalysis of organosolv lignin has the advantage of process intensification because organosolv lignin is pure lignin and it is soluble in most common organic solvents. Studies of heterogeneous catalysis for lignin valorization to phenolic monomers will be discussed next in terms of feedstock, reaction mechanism, and catalyst selection.

1.4 Catalytic Depolymerization of Lignin

"Lignin first" refers to fractionation of lignocellulosic biomass and in the same step depolymerizing lignin and upgrading it to bioproduct-chemicals and/or fuels.[23] The lignin first approach begins with the raw biomass directly. Lignin valorization can also start from technical lignin and simplify products separation.

Catalytic depolymerization of lignin (CDL) is one of the most common strategies within the "lignin first" valorization to produce value-added lignin monomers.[5] As described in Figure 4, lignin monomers are aromatic phenols with aldehyde or alcohol attached to the end of the alkyl sidechain. Transition-metal heterogeneous catalysts have been well-studied for the conversion of lignin into monomeric phenol derivatives. The approach of reductive lignin depolymerization dates back to the 1940s when it was used to characterize the lignin structure in woody biomass.[22] In the presence of a transition-metal catalyst and under reductive conditions, lignin selectively undergoes CDL at temperatures < 250 °C and the cellulosic fibers are left intact.[35, 116, 117] The catalytic conversion requires elevated temperature to overcome the activation barriers of the abundant C-O and C-C lignin linkages.[118, 35, 119, 120] The high temperature and pressure may limit the scalability of reductive lignin valorization.[121] Therefore, the use of hydrogen transfer reagents instead of hydrogen gas promotes milder conditions. Alcohols, such as methanol, ethanol, and 2-propanol can serve as a hydrogen source in lignin valorization.[23, 47, 122] These alcohols can provide hydrogen through reforming over a metal catalyst. Thus, reforming catalysts such as Pt, Ru and Raney-Ni can be ideal for CDL.[47, 123] Due to the easy recovery, low cost, and non-toxic characteristics, methanol and ethanol make good solvents for CDL processes. They have also been found to reduce lignin re-condensation and avoid char formation.[122, 124, 125] Formic acid as an additive to ethanol has been shown as a good source of in situ hydrogen.[126, 127]

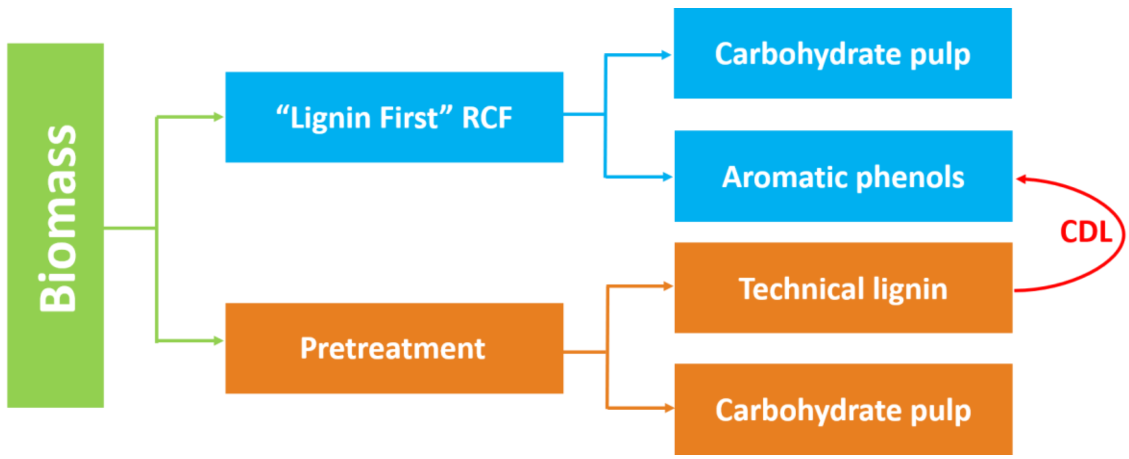

Figure 1.10 Illustration of reductive catalytic fractionation (RCF) and technical lignin valorization via catalytic depolymerization of lignin (CDL).

Regardless of what H-source is used, catalytic fractionation of carbohydrate along with lignin depolymerization is generally referred to as reductive catalytic fractionation (RCF), Figure 1.10.[23] RCF is a convenient way of biomass valorization in a one-pot reaction. However, the low-density of biomass (150-205 kg/m^3)[128] and complexity of products separation may limit the future scalability of RCF. In contrast, a concentrated lignin feedstock can be obtained from the organosolv process, and its subsequent conversion via CDL can be intensified and as a result more amenable to industrial scaling. Most catalysts that are effective for RCF were found to work well in CDL. Accordingly, upgrading lignin is protected by catalyst from re-condensation. In this section, we review metal-catalyzed lignin valorizations that apply to both RCF and CDL.

1.4.1 Palladium

Palladium is well known for its ability to catalyze hydrogenation and hydrogenolysis reactions. Previous work by Pandarus et al. showed that supported metallic palladium was active for direct C-O hydrogenolysis to cleave benzylic ether bonds.[129] They investigated several model compounds and achieved 100% C-O cleavage with palladium catalyst in methanol under hydrogen pressure. Up to 65% of lignin linkages are composed to C-O ether bonds (Table 1.1). Pd/C has been shown as an effective catalyst for lignin valorization to cleave β-O-4, 4-O-5, α-O-4, and even β- β linkages.[22, 130]

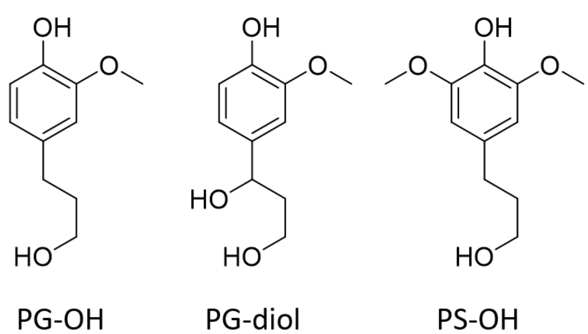

Figure 1.11 Molecular structure of PG-OH, PG-diol, and PS-OH. Reproduced from: Klein, I.; Marcum, C.; Kenttamaaa, H.; Abu-Omar, M. M. *Green Chem* **2016,** *18* (8), 2399-2405.

We employed model compounds and poplar woody biomass to understand the mechanism of β-O-4 cleavage over Pd/C catalyst.[37] The catalytic conversion was performed in methanol under hydrogen pressure at 225 ℃. The primary result indicated the phenolic products were mainly PG-OH and PS-OH when the monometallic Pd/C catalyst was used; product yields were 59%. The two products were consistent from both poplar wood and model compounds. The molecules defined as PG-OH and PS-OH are the DHE and DMPP with a hydroxyl group (OH) attached to the γ carbon on propyl sidechain (Figure 1.11).[37] This result confirmed the Pd/C catalyst is active in breaking the C-O ether bond in the lignin polymer. Our findings also indicated the OH at the α position of β-O-4 linkage is cleaved by Pd/C as well. The experimental results agreed with computational prediction from density function theory (DFT) for C-O ether model compound and Pd (111) species by Lu et al.[131]

However, Pd/C should not catalyze the hydrogenolysis of the hydroxyls at the γ carbon of β-O-4 linkage. This hypothesis was confirmed by the reaction of PG-diol and Pd/C which yielded PG-OH. A modified Pd/C catalyst was also studied to understand the effect of introducing Lewis acids to the reaction mixture. $ZnCl_2$ and $Zn(OAc)_2 \cdot 2H_2O$ were added as a co-catalysts. Hydrogenolysis of the γ carbon hydroxyl of β-O-4 linkages was observed in the presence of Zn^{2+}. DHE and DMPP were the major products. The addition of a Lewis acid facilitated the hydrogenolysis of γ C-OH. However, applying this Pd-Zn^{2+} co-catalyst system to PG-diol, the major product was still PG-OH (63% yield). DHE was only observed as minor product. Therefore, PG-OH was not an intermediate and the hydroxyl group at the γ position must be activated and cleaved by Zn^{2+} prior to hydroxyl removal from the α position by Pd/C. Also, PG-OH was unreactive with the Pd-Zn^{2+} co-catalyst.

Further investigations and spectroscopic evidence for coordination between the α/γ OH and Zn^{2+}, led to a proposed mechanism for β-O-4 cleavage by the Pd-Zn^{2+} co-catalyst system (Scheme 1.5). Hydride transfer from the Pd surface to the C-O ether bond initiates the reaction. Coordination between Zn^{2+} and the substrate made the γ OH a better leaving group. Lastly, Pd/C catalyzed hydrogenolysis cleaved the benzylic OH on the α carbon and hydrogenation of the terminal C=C bond completed the reaction. Other Lewis acids such as $FeCl_3$, $NiCl_2$, and $AlCl_3$ were also investigated and shown to be effective for producing DHE and DMPP from lignin.

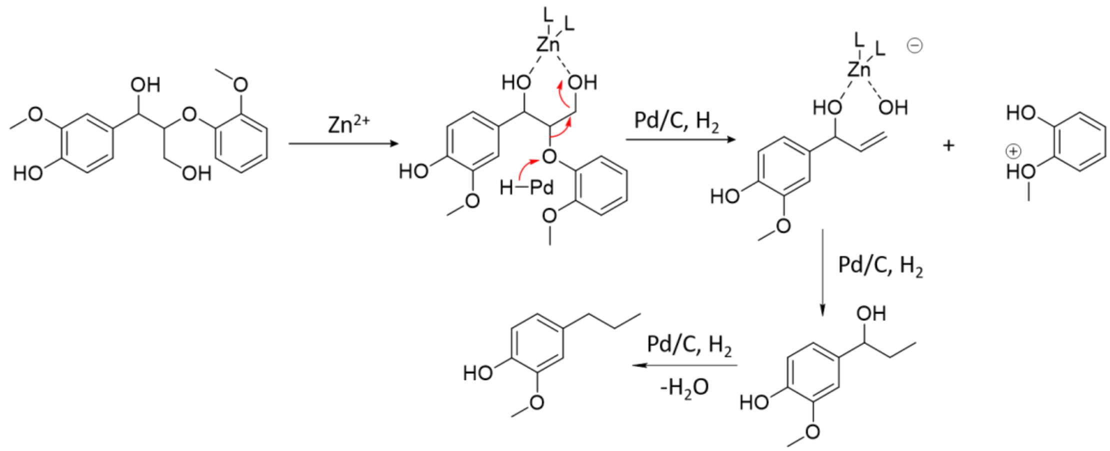

Scheme 1.5 Proposed mechanism for cleavage and HDO of β-O-4 ether linkage using Pd/C and Zn^{2+}. Reproduced from: Klein, I.; Marcum, C.; Kenttamaaa, H.; Abu-Omar, M. M. *Green Chem* **2016,** *18* (8), 2399-2405.

Another study investigated a prepared Pd-Zn bimetallic catalyst over carbon support for lignin valorization instead of a physical mixture of Pd/C and a zinc salt.[132] The molar ratio between Pd and Zn in the synthesized catalyst was 1:1. The Pd-Pd coordination was detected by the Pd K-edge extended x-ray absorption fine structure (EXAFS) analysis while Pd-Zn coordination was absent in the bimetallic catalyst. Thus, no Pd-Zn alloy nor direct interaction was created during the in-situ catalyst preparation. The zinc was hypothesized to have adsorbed onto the activated carbon via coordination to -OH groups on the carbon's surface. When the catalyst was heated to 225 °C with lignin substrate and methanol, the Zn^{2+} could be activated and released from the carbon surface to coordinate with hydroxyl groups of the lignin substrate. Therefore, the cleavage of lignin catalyzed by this Zn/Pd/C bimetallic catalyst would undergo the same reaction pathway as the physical mixture co-catalyst system. Compared to the physical mixture catalyst, the Zn/Pd/C catalyst showed similar activity and selectivity for poplar wood. 54% total yield of DHE and DMPP was observed. Meanwhile the solid carbohydrate residue containing 85% cellulose was recovered.[46]

1.4.2 Ruthenium

Ruthenium (Ru) has been widely used for biomass conversion. Similar to Pd, most of the active Ru catalysts are metallic ruthenium on porous support. Ru/C is one of the most used catalysts for lignin valorization. It exhibits the best selectivity for 4-ethylpehnol from lignin.[133]

Table 2. Comparison of Ru/C and Pd/C catalyzed RCF on birch wood

	Ru/C	Pd/C
Delignification (wt%)	85	90
Monomer yield (C%)	48	49
Dimer yield (C%)	13	15
DHE + DMPP selectivity (%)	75	4
PGOH + PSOH selectivity (%)	19	91
C5 carbohydrate retention (C%)	69	81
C6 carbohydrate retention (C%)	93	94

Table 1.2 Values are adapted from Van den Bosch, S.; Schutyser, W.; Koelewijn, S. F.; Renders, T.; Courtin, C. M.; Sels, B. F. *Chem Commun* **2015,** *51* (67), 13158-13161.

The Sels group contrasted Ru/C and Pd/C for lignin hydrogenolysis using birch wood as substrate.[134] The reactions were performed in methanol under hydrogen pressure. Ru/C gave comparable results to Pd/C, lignin conversion, total yield of monomers, and retention of carbohydrates fraction (Table 1.2). The striking difference was the selectivity of γ-OH. Pd/C gave primarily PG-OH and PS-OH with 91% total selectivity. In contrast, 75% of the phenolic monomers by Ru/C were DHE and DMPP. More -OH was removed by Ru/C indicating that it is a more efficient in catalyzing hydrogenolysis. Interestingly, the hydrogenolysis of lignin by Ru/C was found to be insignificantly affected by hydrogen pressure. As reported, when the Ru/C reaction was carried out under 1 bar N_2 in methanol, 40% yield of lignin monomers were still obtained. This result is attributed to the activity of Ru/C in catalyzing methanol reforming to produce in-situ hydrogen. In contrast, without added hydrogen, 4-ethylguaiacol and 4-

ethylsyringol became the major products in the Pd/C reaction. This finding was attributed to C-C hydrogenolysis by Pd/C through consecutive dehydrogenation/decarbonylation in the absence of hydrogen gas.[135] Overall, Ru/C is a good catalyst for reductive fractionation of lignin from biomass to make phenolic monomers (DHE and DMPP) without requiring added hydrogen. This could lower the cost and improve the safety and sustainability of lignin valorization.

Additional investigations from the Sels lab revealed further products arising from lignin including dimers and oligomers.[136] GPC and GC-MS analysis showed the phenolic monomers represent 50% yield of lignin carbon while another 18% fall into dimeric products. 2D HSQC NMR showed cleavage of all C-O ether bonds within the lignin network by Ru/C. However, Ru/C was ineffective in converting dimers and oligomers connected by C-C bond, Scheme 1.6 for example. Moreover, the free-orthro position on the G unit is active to form the 5-5 bond between two phenyl groups. The 5-5 bond is the most common and has the strongest BDE among all C-C interunit linkages in the lignin polymer.[77, 137] As a result, Ru/C does not achieve complete depolymerization of lignin because of native and non-native C-C bonds.

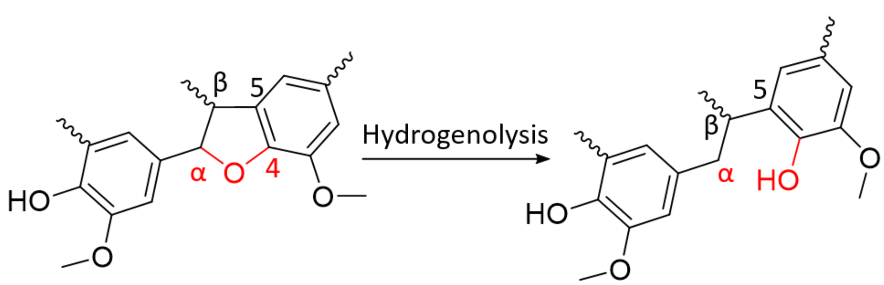

Scheme 1.6 Illustration of breaking α-O-4 unit on β-5 linkage. Reproduced from: Van den Bosch, S.; Schutyser, W.; Vanholme, R.; Driessen, T.; Koelewijn, S. F.; Renders, T.; De Meester, B.; Huijgen, W. J. J.; Dehaen, W.; Courtin, C. M.; Lagrain, B.; Boerjan, W.; Sels, B. F. *Energy & Environmental Science* **2015,** *8* (6), 1748-1763.

A modified ruthenium catalyst reported in 2019 may provide ways to overcome the conventional limit of incomplete C-C bond cleavage. Dong et al. introduced a mesoporous Ru/$NbOPO_4$ catalyst which gave excellent activity towards cleaving recalcitrant C-C interunit linkages in Kraft lignin.[137] Instead of making phenolic monomers, the monocyclic hydrocarbons including benzene, toluene, ethylbenzene, propylbenzene, and their corresponding cyclohexanes were obtained as the major products. This one-pot conversion was done in dodecane solvent with 5 bar H_2 at 310 ℃ over 40 hours. Under this condition, 68% selectivity to monocyclic arenes was achieved. In this Ru/$NbOPO_4$ catalyst, the abundant Brønsted acid sites on the phosphate-based support are possibly responsible for the superior C-C bond cleaving ability. Inelastic neutron scattering (INS) and DFT analysis indicated the acidic $NbOPO_4$ support shows stronger binding of phenyl structures than conventional Nb_2O_5 and other zeolitic materials. In cleaving the 5-5 bond, the biphenyl is first adsorbed on the $NbOPO_4$ support and undergoes partial hydrogenation. The BDE of the 5-5 bond is reduced by converting the stable sp^2-sp^2 to an active sp^2-sp^3 bond. After this step, the partially reduced 5-5 bond is broken through direct hydrogenolysis catalyzed by Ru particles. The design of this multifunctional ruthenium catalyst suggested a pathway for improved phenyl binding onto a catalyst with abundant acid sites to promote C-C interunit cleavage. Compared to the monometallic Ru/C catalyst, the products from this Ru/$NbOPO_4$ system are fully deoxygenated hydrocarbons. Although these are less valuable than phenolic monomers, C6-C9 hydrocarbons are potential drop-in fuels. The arene byproducts can be used as fuel additives or BTX replacements.[138] More studies on the catalyst design are necessary to tune the selectivity between hydrocarbons and monomeric phenols.

1.4.3 Earth-abundant Ni catalyst

Nickle (Ni) is an earth-abundant element and has shown promising performance in valorizing lignin into phenolic products. Compared with precious noble metal catalysts, the low-cost Ni catalyst is ecofriendly for large scale applications. Supported monometallic Ni/C catalyst has been studied extensively by our group with various biomass/lignin feedstock. An early study by

Klein et al. used amorphous Ni/C to catalyze lignin valorization in methanol at 200 °C starting from various woods, poplar, birch, and eucalyptus without added hydrogen.[36] Overall, birch performed best and gave DHE and DMPP as major products. It was also noted that Ni/C is active in reforming methanol to produce hydrogen in-situ.[139] Miscanthus, a grass biomass, was also investigated.[35] The one-pot RCF was carried out in methanol under hydrogen pressure at 225 ℃. Notably, besides DHE and DMPP, two molecules containing the methyl ferulate ester structure were observed (Figure 1.12). These two molecules originated from the unique ferulate/diferulate linkages that are present in grasses but absent from wood biomass. The total yield of the four lignin monomers was 69%. This higher yield indicates that lignin in grass species is potentially more accessible than in woody biomass. Besides, 61wt% of the starting miscanthus substrate was recovered as a solid residue. This solid residue was found to be carbohydrate rich, 56% cellulose and 21% xylan (monomer of hemicellulose). Moreover, this recovered polysaccharide pulp could be further converted to furfural and levulinic acid by a $FeCl_3$ catalyst. Because Ni/C exhibits the abilities to fractionate the native biomass and to depolymerize/upgrade lignin, it is another excellent catalyst for lignin-first processes.

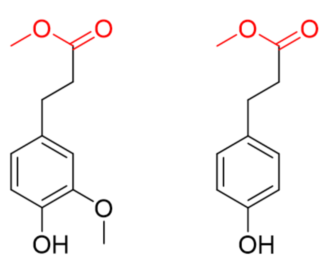

Figure 1.12 The unique methyl ferulate ester (labeled in red color) products only obtained from grassy lignin. Reproduced from: Luo, H.; Klein, I. M.; Jiang, Y.; Zhu, H. Y.; Liu, B. Y.; Kenttamaa, H. I.; Abu-Omar, M. M. *Acs Sustain Chem Eng* **2016,** *4* (4), 2316-2322.

In order to understand the ability of Ni/C to valorize technical lignin, Luo et al. studied several organosolv lignins from poplar wood.[5] The Ni/C was an effective catalyst for valorizing organosolv lignin to phenolic monomers with yields comparable to those observed from "lignin first" RCF processing. Genetically engineered poplar substrates were also used in this study. The gene modification tuned the content of S unit in the lignin network. Compared to wild-type poplar, one mutant contained higher content of S unit (high-S poplar) and another mutant had less S unit (low-S poplar). Interestingly, compared to the wild-type lignin the monomer yield obtained from high-S lignin was slightly improved. This was because the S unit, having two occupied ortho positions does not form 5-5 carbon linkages.

Taking the series of studies on Ni/C together, it has clearly been shown that Ni/C is a versatile catalyst for lignin valorization from biomass directly as well as from protected organosolv lignin. It is also an attractive catalyst because it can catalyze methanol reforming, thereby removing the requirement of added hydrogen.

1.4.4 Without an added transition-metal catalyst

Cheng and co-workers studied hydrogenolysis of organosolv lignin in ethanol/isopropanol medium under supercritical condition without the addition of a transition metal catalyst.[140] So far, no other studies have mentioned using supercritical alcohol mixtures for lignin depolymerization in the absence of an added catalyst. Organosolv lignins made from poplar biomass prepared by two different solvent treatments: methanol/sulfuric acid (MPL) and methanol/HCl (OPL) were employed as the feedstocks. Lignin depolymerization was performed under supercritical condition at 270 ℃ with 10 bar N_2 for 4 hours. In this study, isoeugenol and 4-propenyl syringol were obtained as the major products. Isopropanol acted as hydrogen-donor as evidenced by the formation of acetone in the product mixture. HSQC NMR of pre and post reaction mixtures showed significant disappearance of β-O-4 signal suggesting sufficient cleavage of C-O ether bonds while retaining β-5 and β- β signals. Therefore, C-C cross-links were not cleaved under supercritical conditions in EtOH/^{i}PrOH. The optimal ratio between the co-solvents was found to be 1:1 EtOH/^{i}PrOH, which gave 48% total yield of phenolic monomers. The yield of products and the selectivity for bond cleavages under these supercritical conditions were comparable to those observed with transition metal catalysts.[5, 134, 141] Notably, the mechanism of lignin depolymerization under supercritical conditions remains unclear. A study of the lignin β-O-4 linkage model compound showed no conversion under the same supercritical reaction conditions, suggesting that something in the lignin itself is essential for the reaction. Conversion of the model compound was only observed when a small amount of organosolv lignin or sodium chloride was added to the reaction mixture. Thus, the organosolv lignin itself appeared to serve as a catalyst to break β-O-4 bonds. It was suggested that minor ions or acids introduced along with the lignin from the organosolv treatment must be the actual catalyst(s) in this unique depolymerization/hydrogenolysis system.

In summary, the crucial activity of metal catalysts for lignin valorization is to catalyze hydrogenolysis of C-O and C-C bonds. Many carbon-supported monometallic catalysts are active toward cleavage of C-O ether linkages but leave C-C linkages intact. The recalcitrance of C-C bonds is attributed to their high BDEs. Thus, the C-C bonds in lignin limit the yields of phenolic monomers. Although the content of natural C-C interunit linkages in native lignin is relatively small, more C-C crosslinks form during the pulping of technical lignin and occur as side reactions along reductive catalytic upgrading. Additionally, the use of alcohol solvents is advantageous for lignin valorization because it prevents lignin re-condensation and can serve as a hydrogen donor eliminating the need for added hydrogen. Considering the future development of lignin valorization on a large industrial scale, technical lignin is a more desirable feedstock because it is more amenable to process intensification than raw biomass.

1.5 Upgrading of Lignin Derived Phenols

Lignin monomers are mainly methoxylated, hydroxylated, and alkylated benzenes. The highly functionalized structure makes them attractive developing applications. Taking advantage of these existing functional groups, lignin monomers can be further utilized as precursors for drug and biopolymer synthesis. For instance, Blondiaux et al. developed a 5-step synthesis from lignin-derived DHE to 3,4-dialkoxyanilines and alkyl propionates.[142] Aniline is a key molecule in the pharmaceutical industry. 3,4-dialkoxyanilines can be used as drop-in chemicals in the synthesis of anticancer drugs such as Gefitinib and Erlotinib.[143, 144] Jiang et al. synthesized polyphenol-furan thermoset polymers by using 4-methylcatechol, furfural, and 5-hydroxymethylfurfural (5-HMF) as the building blocks.[145] 4-methylcatechol can be obtained from reductive lignin valorization. 5-HMF and furfural are well-known platform chemicals from cellulose and hemicellulose, respectively.[146, 147] Thus, polyphenol-furan based thermosets is 100% renewable from lignocellulosic biomass. Besides organic synthesis, heterogeneous catalysis is another effective approach to increase the intrinsic value of lignin derived phenols. Hydrodeoxygenation (HDO) reactions catalyzed by transition metals can efficiently remove oxygen and retain the carbon structure to produce hydrocarbon fuels from lignin. The transformation of phenols to hydrocarbons increases the energy density and widens applications to larger fuel markets.

Zhang et al. recently published such a strategy using Ru on an acid support, $Ru(SO_4^{2-})/ZrO_2-CeO_2$, to catalyze HDO of lignin monomers into arenes, cyclic alkanes, and linear alkenes.[148] The lignin-based C6 to C9 hydrocarbons are within the range of carbon numbers in gasoline fuel. Utilization of lignin monomers for renewable biopolymer and biofuels has potential to reduce the demand on fossil energy and realize a more sustainable future. In this section we provide examples from our own work of lignin-derived biopolymers and biofuels.

1.5.1 Renewable thermoset plastics

Thermoset is a big family of crosslinked polymers such as phenolic and urea formaldehyde resins, unsaturated polyesters, and polyepoxides.[149] 20% of all commercial polymers are thermoset, of which, 70% is polyepoxide.[150] Generally, thermosetting plastics are synthesized in a liquid solution that irreversibly leads to solid material during the curing step. Heating and UV irradiation are commonly applied to promote cross-linking during thermoset synthesis. Because of the cross-linked structure, thermoset polymers exhibit outstanding mechanical properties, thermal stability, and solvent resistance compared to thermoplastics.[151]

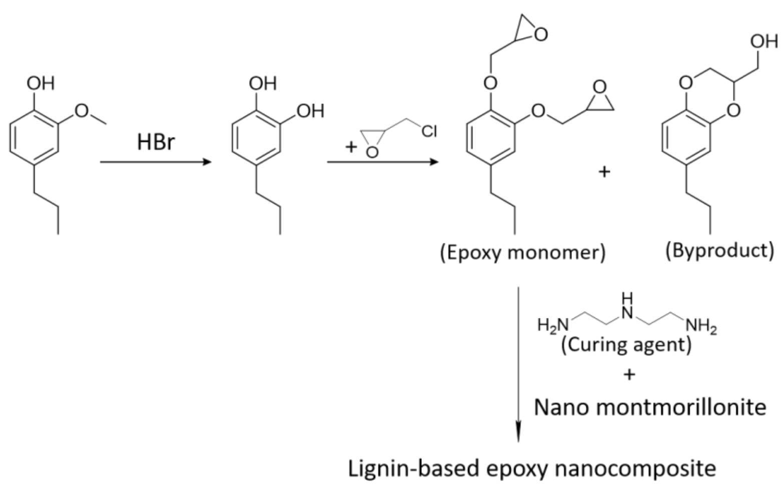

Scheme 1.7 Synthsis route of lignin-based epoxy nanocomposite. Reproduced from: Zhao, S.; Abu-Omar, M. M. *Biomacromolecules* **2015,** *16* (7), 2025-2031.

Zhao et al. introduced several pathways for making epoxy-based thermosetting plastics from lignin monomers (Scheme 1.7).[152] Monomers for making thermoset usually contain two to three hydroxyl groups, whereas the methoxy group limits the reactivity of lignin-based phenols such as DHE. To increase the content of hydroxyls, DHE was modified through ortho-demethylation to yield 4-propylcatechol (DHEO), which can be glycidylated with epichlorohydrin to generate a suitable epoxy monomer. With amine curing agents, lignin-based epoxy nanocomposites are made. More importantly, since lignin-derived monophenols have similar structures (Figure 1.3), this strategy can be applied to synthesize various types of lignin-based thermosets.

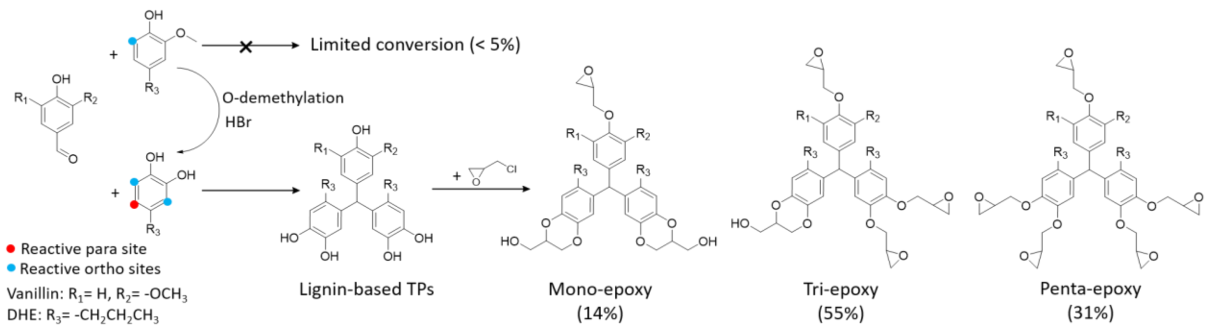

Scheme 1.8 Synthsis route of renewable TPs-epoxy from lignin derived aromatic aldehydre and phenols. Reproduced from: Zhao, S.; Abu-Omar, M. M. *Macromolecules* **2017,** *50* (9), 3573-3581.

Zhao et al. demonstrated in further studies the general applicability of this synthetic route.[151, 153] Scheme 1.8 illustrates an optimized strategy for making epoxy thermosets from two lignin monomers.[153] In this work, ortho-demethylation of DHE could activate its para and ortho sites. The activated catechol molecule can undergo condensation reactions with aldehydes to form triphenylmethane-type polyphenols (TPs). Vanillin, another lignin monomer was employed as the aldehyde precursor to produce a fully lignin-based TPs. According to the highly functioned TPs structure, five epoxides could be attached to its framework. The newly made TP-epoxy thermoset exhibited excellent storage modulus (12.3 GPa), glass transition temperature (167 °C), and thermal stability among other biobased epoxy thermosets.[154-156] The improved mechanical properties of the TP-epoxy thermoset are attributed to its rigid framework and high cross-link density.[157]

1.5.2 Bio-hydrocarbon fuels

Liquid hydrocarbons are the main energy sources consumed around the world. In 2019, Americans used 142 billion gallons of motor gasoline.[158] Gasoline on today's market is made from non-renewable fossil carbons. Production of gasoline from non-fossil energy sources will expand energy production in the future. Lignocellulose is by far the most abundant renewable carbon source. Biomass pyrolysis is a thermochemical process that has been developed to produce syngas and heavy oil for energy consumption.[159] The syngas (carbon monoxide and hydrogen gas) can be transformed by Fischer-Tropsch chemistry to produce liquid hydrocarbons.[160] However, typical pyrolysis requires high energy input and the synthesis of liquid hydrocarbons from syngas have low efficiency and the resulting bio-oils have undesirable chemical properties. Due to this dilemma, preparation of hydrocarbon fuels directly from biomass through low-energy cost, high efficiency, and simple processing is an attractive area of research.

Lignin derived C6 to C9 phenolic monomers are good precursors to generate biogasoline through HDO reactions. Lu and the co-workers introduced guaiacol conversion over Pd/TiO_2 catalyst to cyclohexane.[161] The HDO reaction was performed between 200-280 ℃ in n-dodecane solvent under 20 bar of hydrogen gas. In this study, several palladium catalysts were compared. Pd/C, for example, did not affect HDO and instead yielded 2-methoxycyclohexanol via ring hydrogenation. The TiO_2 support was necessary for C-O scission to induce HDO. It was also noted that the Pd/TiO_2 catalyst effectiveness in HDO reactions depended on the catalyst preparation temperature. For instance, the Pd/TiO_2 synthesized at 200 ℃ showed better conversion and higher selectivity for fully deoxygenated products than when it was prepared at 50 ℃. This was mainly because more Ti^{4+} was reduced to a lower oxidation state at higher temperatures. The partially reduced titanium exhibited stronger binding with oxygenated substrates. Although Pd/TiO_2 prepared at 500 ℃ still gave high selectivity toward the cyclohexane, conversion of guaiacol was reduced. This hindrance of catalyst activity was rationalized by more of the reduced TiO_x species migrated to Pd surface and suppressed H_2 adsorption. Therefore, Pd/TiO_2 prepared at 200 ℃ performed the best. However, some improvements were still necessary including the need for added hydrogen and use of alkane solvents.[162, 163]

A recent advance towards making C9 hydrocarbons as drop-in biofuel in water (a green solvent) was described by our group.[164] In this system, full deoxygenation was achieved by adding a small amount of methanol to serve as an in situ source of hydrogen. The HDO reaction was catalyzed by a physical mixture of Ru/C and Nb_2O_5. The preparation temperature of the Nb_2O_5 was key to preserving its acidity.[165] The mechanism of the co-catalyst system was elucidated through analysis of intermediates and isotope labeling experiments. Scheme 1.9 describes the proposed reaction steps for the conversion of DHE to propylcyclohexane (**1**), the green highlighted pathway. In the absence of Nb_2O_5 conversion to propylphenol and propylcyclohexanol was more prominent.[166] The stability of this co-catalyst system was demonstrated through multiple recycling tests.

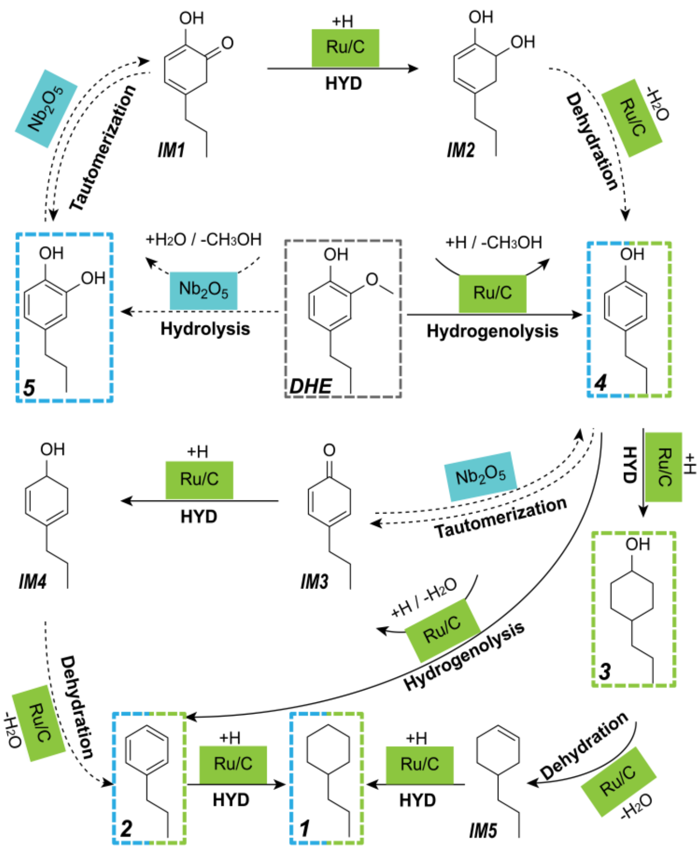

Scheme 1.9 Proposed sequence of mechanistic steps for conversion of DHE by the catalyst mixture Ru/C and Nb_2O_5. Steps catalyzed by Ru/C is lebaled in green color. The steps lebaled in blue color indicate function of Nb_2O_5. Reaction scheme was obtained from: Li, S.; Liu, B.; Truong, J.; Luo, Z.; Ford, P. C.; Abu-Omar, M. M. *Green Chem* **2020,** *22* (21), 7406-7416.

Besides the gasoline range hydrocarbons, the heavier fuel molecules such as jet fuel and biodiesel are also achievable from lignin. Wang et al. have studied a catalyst mixture of Ru/Al_2O_3 and acidic H^+-Y zeolite.[167] One advantage of their work was the use of lignin directly. This one-pot strategy combined lignin depolymerization and HDO for biofuel production. As well, water was used as solvent. The large-porous H^+-Y zeolite with abundant acid sites showed promising activity in catalyzing lignin depolymerization. Coupling the Ru/Al_2O_5 with the H^+-Y together did not only enhance the HDO reaction, but it also promoted the alkylation and dimerization reactions between monomers to yield higher carbon numbers. More than 80% conversion of lignin was achieved within a relatively short time (4 hours) at 250 ℃ with 85% selectivity for C12 – C18 hydrocarbons (jet fuel range). More importantly, the product distribution among the hydrocarbons was tunable by adjusting the catalyst amount and reaction temperature. For example, C6 – C11 cyclic hydrocarbons were the main product when only Ru/Al_2O_3 was used; and arenes were dominant when only H^+-Y acidic zeolite was used. Higher temperature promoted formation of non-cyclic alkanes with more than 18 carbons on average. Overall, the carbon efficiency of lignin conversion to hydrocarbons in this system was 38%, which compares well with other catalytic systems limited by 42-48 wt% conversion based on lignin.[168]

1.6 Conclusions and Further Perspectives

Lignin valorization can be achieved via catalytic reductive pathways either directly from the biomass itself, “lignin first” approach, or through catalytic depolymerization and upgrading of protected lignin such as organosolv. Both noble metal catalysts as well as earth-abundant catalysts such as nickel have been successful in these endeavors. Preservation of the lignin’s phenol monomer group can have advantages as these molecules can be used in making polymers, pharmaceutical molecules, or still be deoxygenated to make hydrocarbon biofuels. Biomass consumes CO_2 from the atmosphere. Thus, valorization of lignin enhances the carbon efficiency of biomass utilization. The intrinsic value of lignin is being recognized and realized. With more efficient methods and chemistries for lignin valorization, biomass use for renewable energy and chemicals will expand.

Despite impressive recent advances, lignin valorization to monomeric phenols and chemicals has been limited due to recalcitrant C-C bonds found in native lignin or formed via re-condensation during the lignin extraction process. Either reduction in C-C bond formation or new catalysts that can target specific C-C bonds without total pyrolysis are necessary. The use of hydrogen limits commercial utility for cost and safety reasons. Laboratory scale reactions have shown the use of alcohol solvents coupled with reforming catalysts can circumvent this limitation. However, the implication on cost as well as industrial practice of such a strategy remains to be vetted. Nevertheless, phenolic monomers that can be obtained from lignin have been used in making renewable plastics, chemicals used in drug syntheses, and hydrocarbon biofuels. In many instances, these chemistries have been demonstrated with commercial forms of the molecules from non-renewable carbon source rather than with the actual molecules coming from biomass processing. This presents a major challenge for separations and utilization of products derived directly from biomass or lignin samples.

1.7 Abbreviations

USD: United State dollars

C-O bond: Carbon-oxygen single bond

C-C bond: Carbon-carbon single bond

C=C bond: Carbon-carbon double bond

DHE: Dihydrogeneugenol

DHEO: 4-propylcatechol

DMPP: 2,6-Dimethoxy-4-propylphenol

PG-OH: Dihydroconiferyl alcohol

PS-OH: Dihydrosinapyl alcohol

PG-diol: 1-(4-Hydroxy-3-methoxyphenyl)propane-1,3-diol

FA/AA: Formic acid/acetic acid

5-HMF: 5-hydroxymethylfurfural

EtOH: Ethanol

^{i}PrOH: Isopropyl alcohol

TPs: triphenylmethane-type polyphenols

H unit: p-Hydroxyphenyl lignin unit

G unit: Guaiacyl lignin unit

S unit: Syringyl lignin unit

BTX: Benzene toluene xylene

High-S poplar: Poplar wood with higher content of syringyl lignin unit

Low-S poplar: Poplar wood with lower content of syringyl lignin unit

MPL: Organosolv lignin prepared from methanol/sulfuric acid treatment

OPL: Organosolv lignin prepared from methanol/hydrochloric acid treatment

2D HSQC NMR: Two-dimensional heteronuclear single quantum coherence nuclear magnetic resonance

^{13}C NMR: Carbon-13 nuclear magnetic resonance

SEM: Scanning electron microscopy

EXAFS: Extended x-ray absorption fine structure analysis

GPC: Gel permeation chromatography

GC-MS: Gas chromatography-mass spectrometry

INS: Inelastic neutron scattering

BDE: Bond dissociation energy

CDL: Catalytic depolymerization of lignin

RCF: Reductive catalytic fractionation

DFT: Density function theory

HDO: Hydrodeoxygenation

UV: Ultraviolet

GPa: Gigapascal, 1GPa = one billion pascals

1.8 References:

1. Lange, J. P., Lignocellulose conversion: an introduction to chemistry, process and economics. *Biofuel Bioprod Bior* **2007,** *1* (1), 39-48.

2. M. H. Langholtz, B. J. S., L. M. Eaton, 2016 Billion-Ton Report: Advancing Domestic Resources for a Thriving Bioeconomy. *U.S. Department of Energy. Oak Ridge National Laboratory* **2016,** *Volume 1: Economic Availability*.

3. (EIA), U. S. E. I. A. U.S. Energy Information Administration (EIA) U.S. Primary Energy Consumption by Energy Source, 2019. https://www.eia.gov/energyexplained/us-energy-facts/.

4. (EIA), U. S. E. I. A. U.S. Energy Information Administration (EIA), Annual Energy Review, 2009. https://www.eia.gov/totalenergy/data/annual/archive/038409.pdf.

5. Luo, H.; Abu-Omar, M. M., Lignin extraction and catalytic upgrading from genetically modified poplar. *Green Chem* **2018,** *20* (3), 745-753.

6. Jensen, C. U.; Guerrero, J. K. R.; Karatzos, S.; Olofsson, G.; Iversen, S. B., Fundamentals of Hydrofaction((TM)): Renewable crude oil from woody biomass. *Biomass Convers Bior* **2017,** *7* (4), 495-509.

7. Liu, Q. Q.; Luo, L.; Zheng, L. Q., Lignins: Biosynthesis and Biological Functions in Plants. *Int J Mol Sci* **2018,** *19* (2).

8. Bertella, S.; Luterbacher, J. S., Lignin Functionalization for the Production of Novel Materials. *Trends Chem* **2020,** *2* (5), 440-453.

9. Zheng, Y.; Zhang, R. H., Lignocellulosic Biomass Pretreatment for Bioethanol Production. *Energ Sci Eng Tech* **2009**, 1-48.

10. Waghmare, P. R.; Watharkar, A. D.; Jeon, B. H.; Govindwar, S. P., Bio-ethanol production from waste biomass of Pogonatherum crinitum phytoremediator: an eco-friendly strategy for renewable energy. *3 Biotech* **2018,** *8*.

11. Gnansounou, E.; Dauriat, A., Ethanol fuel from biomass: A review. *J Sci Ind Res India* **2005,** *64* (11), 809-821.

12. Busic, A.; Mardetko, N.; Kundas, S.; Morzak, G.; Belskaya, H.; Santek, M. I.; Komes, D.; Novak, S.; Santek, B., Bioethanol Production from Renewable Raw Materials and Its Separation and Purification: A Review. *Food Technol Biotech* **2018,** *56* (3), 289-311.

13. Bajwa, D. S.; Pourhashem, G.; Ullah, A. H.; Bajwa, S. G., A concise review of current lignin production, applications, products and their environmental impact. *Ind Crop Prod* **2019,** *139*.

14. Singh, R.; Prakash, A.; Dhiman, S. K.; Balagurumurthy, B.; Arora, A. K.; Puri, S. K.; Bhaskar, T., Hydrothermal conversion of lignin to substituted phenols and aromatic ethers. *Bioresource Technol* **2014,** *165*, 319-322.

15. Singh, S. K.; Ekhe, J. D., Towards effective lignin conversion: HZSM-5 catalyzed one-pot solvolytic depolymerization/hydrodeoxygenation of lignin into value added compounds. *Rsc Adv* **2014,** *4* (53), 27971-27978.

16. Zhao, C.; Xie, S. X.; Pu, Y. Q.; Zhang, R.; Huang, F.; Ragauskas, A. J.; Yuan, J. S., Synergistic enzymatic and microbial lignin conversion. *Green Chem* **2016,** *18* (5), 1306-1312.

17. Luo, Z. C.; Qin, S. F.; Chen, S.; Hui, Y.; Zhao, C. S., Selective conversion of lignin to ethylbenzene. *Green Chem* **2020,** *22* (6), 1842-1850.

18. Oregui-Bengoechea, M.; Miletic, N.; Hao, W. M.; Bjornerback, F.; Rosnes, M. H.; Garitaonandia, J. S.; Hedin, N.; Arias, P. L.; Barth, T., High-Performance Magnetic Activated

Carbon from Solid Waste from Lignin Conversion Processes. 2. Their Use as NiMo Catalyst Supports for Lignin Conversion. *Acs Sustain Chem Eng* **2017,** *5* (12), 11226-11237.

19. Ren, T. Y.; Qi, W.; Su, R. X.; He, Z. M., Promising Techniques for Depolymerization of Lignin into Value-added Chemicals. *Chemcatchem* **2019,** *11* (2), 639-654.

20. Huang, Y.; Duan, Y. J.; Qiu, S.; Wang, M.; Ju, C.; Cao, H.; Fang, Y. M.; Tan, T. W., Lignin-first biorefinery: a reusable catalyst for lignin depolymerization and application of lignin oil to jet fuel aromatics and polyurethane feedstock. *Sustain Energ Fuels* **2018,** *2* (3), 637-647.

21. Yang, H. B.; Zhang, X. M.; Luo, H.; Liu, B. Y.; Shiga, T. M.; Li, X.; Kim, J. I.; Rubinelli, P.; Overton, J. C.; Subramanyam, V.; Cooper, B. R.; Mo, H. P.; Abu-Omar, M. M.; Chapple, C.; Donohoe, B. S.; Makowski, L.; Mosier, N. S.; McCann, M. C.; Carpita, N. C.; Meilan, R., Overcoming cellulose recalcitrance in woody biomass for the lignin-first biorefinery. *Biotechnol Biofuels* **2019,** *12*.

22. Koranyi, T. I.; Fridrich, B.; Pineda, A.; Barta, K., Development of 'Lignin-First' Approaches for the Valorization of Lignocellulosic Biomass. *Molecules* **2020,** *25* (12).

23. Abu-Omar, M. M.; Barta, K.; Beckham, G. T.; Luterbacher, J.; Ralph, J.; Rinaldi, R.; Roman-Leshkov, Y.; Samec, J.; Sels, B.; Wang, F., Guidelines for performing lignin-first biorefining. *Energy & Environmental Science* **2020**.

24. Chakar, F. S.; Ragauskas, A. J., Review of current and future softwood kraft lignin process chemistry. *Ind Crop Prod* **2004,** *20* (2), 131-141.

25. Abdel Rahman, N.; Galiwango, E., Klason Method: An Effective Method for Isolation of Lignin Fractions from Date Palm Biomass Waste. *Journal of Food Process Engineering* **2018,** *57*, 46-58.

26. Başakçılardan Kabakcı, S.; Tanış, M. H., Pretreatment of lignocellulosic biomass at atmospheric conditions by using different organosolv liquors: a comparison of lignins. *Biomass Convers Bior* **2020**.

27. Nitsos, C.; Rova, U.; Christakopoulos, P., Organosolv Fractionation of Softwood Biomass for Biofuel and Biorefinery Applications. *Energies* **2018,** *11* (1).

28. Saraeian, A.; Aui, A.; Gao, Y.; Wright, M. M.; Foston, M.; Shanks, B. H., Evaluating lignin valorization via pyrolysis and vapor-phase hydrodeoxygenation for production of aromatics and alkenes. *Green Chem* **2020,** *22* (8), 2513-2525.

29. Chu, J. Y.; Jiang, W. K.; Wu, S. B., Depolymerization Characteristics during the Pyrolysis of Two Industrial Lignins. *Bioresources* **2017,** *12* (4), 7241-7254.

30. Lazaridis, P. A.; Fotopoulos, A. P.; Karakoulia, S. A.; Triantafyllidis, K. S., Catalytic Fast Pyrolysis of Kraft Lignin With Conventional, Mesoporous and Nanosized ZSM-5 Zeolite for the Production of Alkyl-Phenols and Aromatics. *Front Chem* **2018,** *6*.

31. Zhang, Z. L.; Zijlstra, D. S.; Lahive, C. W.; Deuss, P. J., Combined lignin defunctionalisation and synthesis gas formation by acceptorless dehydrogenative decarbonylation. *Green Chem* **2020,** *22* (12), 3791-3801.

32. Sricharoenchaikul, V., Assessment of black liquor gasification in supercritical water. *Bioresource Technol* **2009,** *100* (2), 638-643.

33. Gall, D. L.; Kontur, W. S.; Lan, W.; Kim, H.; Li, Y. D.; Ralph, J.; Donohue, T. J.; Noguera, D. R., In Vitro Enzymatic Depolymerization of Lignin with Release of Syringyl, Guaiacyl, and Tricin Units. *Appl Environ Microb* **2018,** *84* (3).

34. Lee, S.; Kang, M.; Bae, J. N.; Sohn, J. N.; Sung, B. H., Bacterial Valorization of Lignin: Strains, Enzymes, Conversion Pathways, Biosensors, and Perspectives. *Front Bioeng Biotech* **2019,** *7*.

35. Luo, H.; Klein, I. M.; Jiang, Y.; Zhu, H. Y.; Liu, B. Y.; Kenttamaa, H. I.; Abu-Omar, M. M., Total Utilization of Miscanthus Biomass, Lignin and Carbohydrates, Using Earth Abundant Nickel Catalyst. *Acs Sustain Chem Eng* **2016,** *4* (4), 2316-2322.

36. Klein, I.; Saha, B.; Abu-Omar, M. M., Lignin depolymerization over Ni/C catalyst in methanol, a continuation: effect of substrate and catalyst loading. *Catal Sci Technol* **2015,** *5* (6), 3242-3245.

37. Klein, I.; Marcum, C.; Kenttamaaa, H.; Abu-Omar, M. M., Mechanistic investigation of the Zn/Pd/C catalyzed cleavage and hydrodeoxygenation of lignin. *Green Chem* **2016,** *18* (8), 2399-2405.

38. Ma, R. S.; Guo, M.; Zhang, X., Selective Conversion of Biorefinery Lignin into Dicarboxylic Acids. *Chemsuschem* **2014,** *7* (2), 412-415.

39. Cherubini, F.; Stromman, A. H., Principles of Biorefining. *Biomass Biof Biochem* **2011**, 3-24.

40. Azadfar, M.; Gao, A. H.; Bule, M. V.; Chen, S. L., Structural characterization of lignin: A potential source of antioxidants guaiacol and 4-vinylguaiacol. *Int J Biol Macromol* **2015,** *75*, 58-66.

41. Shen, X. J.; Meng, Q. L.; Mei, Q. Q.; Liu, H. Z.; Yan, J.; Song, J. L.; Tan, D. X.; Chen, B. F.; Zhang, Z. R.; Yang, G. Y.; Han, B. X., Selective catalytic transformation of lignin with guaiacol as the only liquid product. *Chem Sci* **2020,** *11* (5), 1347-1352.

42. Sainsbury, P. D.; Hardiman, E. M.; Ahmad, M.; Otani, H.; Seghezzi, N.; Eltis, L. D.; Bugg, T. D. H., Breaking Down Lignin to High-Value Chemicals: The Conversion of Lignocellulose to Vanillin in a Gene Deletion Mutant of Rhodococcus jostii RHA1. *Acs Chem Biol* **2013,** *8* (10), 2151-2156.

43. Cheng, C. B.; Wang, J. Z.; Shen, D. K.; Xue, J. T.; Guan, S. P.; Gu, S.; Luo, K. H., Catalytic Oxidation of Lignin in Solvent Systems for Production of Renewable Chemicals: A Review. *Polymers-Basel* **2017,** *9* (6).

44. Araujo, J. D. P.; Grande, C. A.; Rodrigues, A. E., Structured packed bubble column reactor for continuous production of vanillin from Kraft lignin oxidation. *Catal Today* **2009,** *147*, S330-S335.

45. Fache, M.; Boutevin, B.; Caillol, S., Vanillin Production from Lignin and Its Use as a Renewable Chemical. *Acs Sustain Chem Eng* **2016,** *4* (1), 35-46.

46. Parsell, T.; Yohe, S.; Degenstein, J.; Jarrell, T.; Klein, I.; Gencer, E.; Hewetson, B.; Hurt, M.; Kim, J. I.; Choudhari, H.; Saha, B.; Meilan, R.; Mosier, N.; Ribeiro, F.; Delgass, W. N.; Chapple, C.; Kenttamaa, H. I.; Agrawal, R.; Abu-Omar, M. M., A synergistic biorefinery based on catalytic conversion of lignin prior to cellulose starting from lignocellulosic biomass. *Green Chem* **2015,** *17* (3), 1492-1499.

47. Ouyang, X. H.; Huang, X. M.; Zhu, J. D.; Boot, M. D.; Hensen, E. J. M., Catalytic Conversion of Lignin in Woody Biomass into Phenolic Monomers in Methanol/Water Mixtures without External Hydrogen. *Acs Sustain Chem Eng* **2019,** *7* (16), 13764-13773.

48. McVeigh, A.; Bouxin, F. P.; Jarvis, M. C.; Jackson, S. D., Catalytic depolymerisation of isolated lignin to fine chemicals: part 2-process optimisation. *Catal Sci Technol* **2016,** *6* (12), 4142-4150.

49. Huang, X. M.; Ludenhoff, J. M.; Dirks, M.; Ouyang, X. H.; Boot, M. D.; Hensen, E. J. M., Selective Production of Biobased Phenol from Lignocellulose-Derived Alkylmethoxyphenols. *Acs Catal* **2018,** *8* (12), 11184-11190.

50. Xu, Z. X.; Lei, P.; Zhai, R.; Wen, Z. Q.; Jin, M. J., Recent advances in lignin valorization with bacterial cultures: microorganisms, metabolic pathways, and bio-products. *Biotechnol Biofuels* **2019,** *12*.

51. Linger, J. G.; Vardon, D. R.; Guarnieri, M. T.; Karp, E. M.; Hunsinger, G. B.; Franden, M. A.; Johnson, C. W.; Chupka, G.; Strathmann, T. J.; Pienkos, P. T.; Beckham, G. T., Lignin valorization through integrated biological funneling and chemical catalysis. *P Natl Acad Sci USA* **2014,** *111* (33), 12013-12018.

52. Davis, K. M.; Rover, M.; Brown, R. C.; Bai, X. L.; Wen, Z. Y.; Jarboe, L. R., Recovery and Utilization of Lignin Monomers as Part of the Biorefinery Approach. *Energies* **2016,** *9* (10).

53. Renders, T.; Cooreman, E.; Van den Bosch, S.; Schutyser, W.; Koelewijn, S. F.; Vangeel, T.; Deneyer, A.; Van den Bossche, G.; Courtin, C. M.; Sels, B. F., Catalytic lignocellulose biorefining in n-butanol/water: a one-pot approach toward phenolics, polyols, and cellulose. *Green Chem* **2018,** *20* (20).

54. Karkas, M. D.; Matsuura, B. S.; Monos, T. M.; Magallanes, G.; Stephenson, C. R. J., Transition-metal catalyzed valorization of lignin: the key to a sustainable carbon-neutral future. *Org Biomol Chem* **2016,** *14* (6), 1853-1914.

55. Wang, H.; Tucker, M.; Ji, Y., Recent Development in Chemical Depolymerization of Lignin: A Review. *Journal of Applied Chemistry* **2013,** *2013*, 838645.

56. Li, H. L.; Song, G., Ru-Catalyzed Hydrogenolysis of Lignin: Base-Dependent Tunability of Monomeric Phenols and Mechanistic Study. *Acs Catal* **2019,** *9* (5), 4054-4064.

57. Galkin, M. V.; Smit, A. T.; Subbotina, E.; Artemenko, K. A.; Bergquist, J.; Huijgen, W. J. J.; Samec, J. S. M., Hydrogen-free catalytic fractionation of woody biomass. *Chemsuschem* **2016,** *9* (23), 3280-3287.

58. McCallum, C. S.; Strachan, N.; Bennett, S. C.; Forsythe, W. G.; Garrett, M. D.; Hardacre, C.; Morgan, K.; Sheldrake, G. N., Catalytic depolymerisation of suberin rich biomass with precious metal catalysts. *Green Chem* **2018,** *20* (12), 2702-2705.

59. Laskar, D. D.; Tucker, M. P.; Chen, X. W.; Helms, G. L.; Yang, B., Noble-metal catalyzed hydrodeoxygenation of biomass-derived lignin to aromatic hydrocarbons. *Green Chem* **2014,** *16* (2), 897-910.

60. Barrett, J. A.; Gao, Y.; Bernt, C. M.; Chui, M.; Tran, A. T.; Foston, M. B.; Ford, P. C., Enhancing Aromatic Production from Reductive Lignin Disassembly: in Situ O-Methylation of Phenolic Intermediates. *Acs Sustain Chem Eng* **2016,** *4* (12), 6877-6886.

61. Chui, M.; Metzker, G.; Bernt, C. M.; Tran, A. T.; Burtoloso, A. C. B.; Ford, P. C., Probing the Lignin Disassembly Pathways with Modified Catalysts Based on Cu-Doped Porous Metal Oxides. *Acs Sustain Chem Eng* **2017,** *5* (4), 3158-3169.

62. Zhai, Y. X.; Li, C.; Xu, G. Y.; Ma, Y. F.; Liu, X. H.; Zhang, Y., Depolymerization of lignin via a non-precious Ni-Fe alloy catalyst supported on activated carbon. *Green Chem* **2017,** *19* (8), 1895-1903.

63. Sturgeon, M. R.; O'Brien, M. H.; Ciesielski, P. N.; Katahira, R.; Kruger, J. S.; Chmely, S. C.; Hamlin, J.; Lawrence, K.; Hunsinger, G. B.; Foust, T. D.; Baldwin, R. M.;

Biddy, M. J.; Beckham, G. T., Lignin depolymerisation by nickel supported layered-double hydroxide catalysts. *Green Chem* **2014,** *16* (2), 824-835.

64. Patil, P. T.; Armbruster, U.; Richter, M.; Martin, A., Heterogeneously Catalyzed Hydroprocessing of Organosolv Lignin in Sub-and Supercritical Solvents. *Energ Fuel* **2011,** *25* (10), 4713-4722.

65. Rautiainen, S.; Di Francesco, D.; Katea, S. N.; Westin, G.; Tungasmita, D. N.; Samec, J. S. M., Lignin Valorization by Cobalt-Catalyzed Fractionation of Lignocellulose to Yield Monophenolic Compounds. *Chemsuschem* **2019,** *12* (2), 404-408.

66. Cheng, C. B.; Truong, J.; Barrett, J. A.; Shen, D. K.; Abu-Omar, M. M.; Ford, P. C., Hydrogenolysis of Organosolv Lignin in Ethanol/Isopropanol Media without Added Transition-Metal Catalyst. *Acs Sustain Chem Eng* **2020,** *8* (2), 1023-1030.

67. Edmunds, C. W.; Peralta, P.; Kelley, S. S.; Chiang, V. L.; Sharma-Shivappa, R. R.; Davis, M. F.; Harman-Ware, A. E.; Sykes, R. W.; Gjersing, E.; Cunningham, M. W.; Rottmann, W.; Miller, Z. D.; Peszlen, I., Characterization and enzymatic hydrolysis of wood from transgenic Pinus taeda engineered with syringyl lignin or reduced lignin content. *Cellulose* **2017,** *24* (4), 1901-1914.

68. Luo, H.; Abu-Omar, M. M., Chemicals From Lignin. In *Encyclopedia of Sustainable Technologies*, Abraham, M. A., Ed. Elsevier: Oxford, 2017; pp 573-585.

69. Patil, N. D.; Tanguy, N. R.; Yan, N., 3 - Lignin Interunit Linkages and Model Compounds. In *Lignin in Polymer Composites*, Faruk, O.; Sain, M., Eds. William Andrew Publishing: 2016; pp 27-47.

70. Zakzeski, J.; Bruijnincx, P. C. A.; Jongerius, A. L.; Weckhuysen, B. M., The Catalytic Valorization of Lignin for the Production of Renewable Chemicals. *Chem Rev* **2010,** *110* (6), 3552-3599.

71. Mei, Q.; Shen, X.; Liu, H.; Han, B., Selectively transform lignin into value-added chemicals. *Chinese Chemical Letters* **2019,** *30* (1), 15-24.

72. Uraki, Y.; Koda, K.; Yamada, T.; Oikawa, C.; Aso, T., Novel Functions of Non-Ionic, Amphiphilic Lignin Derivatives. *Acs Sym Ser* **2012,** *1107*, 243-+.

73. Galkin, M. V.; Samec, J. S. M., Lignin Valorization through Catalytic Lignocellulose Fractionation: A Fundamental Platform for the Future Biorefinery. *Chemsuschem* **2016,** *9* (13), 1544-1558.

74. Zhu, W. Z.; Theliander, H., Equilibrium of Lignin Precipitation. *16th International Symposium on Wood, Fiber and Pulping Chemistry, Proceedings, Vols I & Ii* **2011**, 195-199.

75. Vázquez, G.; Antorrena, G.; González, J.; Freire, S., The Influence of Pulping Conditions on the Structure of Acetosolv Eucalyptus Lignins. *Journal of Wood Chemistry and Technology* **1997,** *17* (1-2), 147-162.

76. Constant, S.; Wienk, H. L. J.; Frissen, A. E.; de Peinder, P.; Boelens, R.; van Es, D. S.; Grisel, R. J. H.; Weckhuysen, B. M.; Huijgen, W. J. J.; Gosselink, R. J. A.; Bruijnincx, P. C. A., New insights into the structure and composition of technical lignins: a comparative characterisation study. *Green Chem* **2016,** *18* (9), 2651-2665.

77. Rinaldi, R.; Jastrzebski, R.; Clough, M. T.; Ralph, J.; Kennema, M.; Bruijnincx, P. C. A.; Weckhuysen, B. M., Paving the Way for Lignin Valorisation: Recent Advances in Bioengineering, Biorefining and Catalysis. *Angew Chem Int Edit* **2016,** *55* (29), 8164-8215.

78. Lancefield, C. S.; Wienk, H. L. J.; Boelens, R.; Weckhuysen, B. M.; Bruijnincx, P. C. A., Identification of a diagnostic structural motif reveals a new reaction intermediate and condensation pathway in kraft lignin formation. *Chem Sci* **2018,** *9* (30), 6348-6360.

79. Giummarella, N.; Pylypchuk, I. V.; Sevastyanova, O.; Lawoko, M., New Structures in Eucalyptus Kraft Lignin with Complex Mechanistic Implications. *Acs Sustain Chem Eng* **2020,** *8* (29), 10983-10994.

80. Knudsen, J. N.; Jensen, P. A.; Lin, W. G.; Frandsen, F. J.; Dam-Johansen, K., Sulfur transformations during thermal conversion of herbaceous biomass. *Energ Fuel* **2004,** *18* (3), 810-819.

81. Rennenberg, H.; Huber, B.; Schroder, P.; Stahl, K.; Haunold, W.; Georgii, H. W.; Slovik, S.; Pfanz, H., Emission of Volatile Sulfur-Compounds from Spruce Trees. *Plant Physiol* **1990,** *92* (3), 560-564.

82. Saleh, S. B.; Flensborg, J. P.; Shoulaifar, T. K.; Sarossy, Z.; Hansen, B. B.; Egsgaard, H.; DeMartini, N.; Jensen, P. A.; Glarborg, P.; Dam-Johansen, K., Release of Chlorine and Sulfur during Biomass Torrefaction and Pyrolysis. *Energ Fuel* **2014,** *28* (6), 3738-3746.

83. Kai, D.; Tan, M. J.; Chee, P. L.; Chua, Y. K.; Yap, Y. L.; Loh, X. J., Towards lignin-based functional materials in a sustainable world. *Green Chem* **2016,** *18* (5), 1175-1200.

84. Inwood, J. P. W.; Pakzad, L.; Fatehi, P., Production of Sulfur Containing Kraft Lignin Products. *Bioresources* **2018,** *13* (1), 53-70.

85. Evdokimov, A. N.; Kurzin, A. V.; Fedorova, O. V.; Lukanin, P. V.; Kazakov, V. G.; Trifonova, A. D., Desulfurization of kraft lignin. *Wood Sci Technol* **2018,** *52* (4), 1165-1174.

86. Osada, M.; Hiyoshi, N.; Sato, O.; Arai, K.; Shirai, M., Reaction pathway for catalytic gasification of lignin in presence of sulfur in supercritical water. *Energ Fuel* **2007,** *21* (4), 1854-1858.

87. Agarwal, S.; Chowdari, R. K.; Hita, I.; Heeres, H. J., Experimental Studies on the Hydrotreatment of Kraft Lignin to Aromatics and Alkylphenolics Using Economically Viable Fe-Based Catalysts. *Acs Sustain Chem Eng* **2017,** *5* (3), 2668-2678.

88. Han, T.; Sophonrat, N.; Evangelopoulos, P.; Persson, H.; Yang, W. H.; Jonsson, P., Evolution of sulfur during fast pyrolysis of sulfonated Kraft lignin. *J Anal Appl Pyrol* **2018,** *133*, 162-168.

89. Vishtal, A.; Kraslawski, A., Challenges in Industrial Applications of Technical Lignins. *Bioresources* **2011,** *6* (3), 3547-3568.

90. Aro, T.; Fatehi, P., Production and Application of Lignosulfonates and Sulfonated Lignin. *Chemsuschem* **2017,** *10* (9), 1861-1877.

91. Zulfikar, M. A.; Wahyuningrum, D.; Lestari, S., Adsorption of Lignosulfonate Compound from Aqueous Solution onto Chitosan-Silica Beads. *Sep Sci Technol* **2013,** *48* (9), 1391-1401.

92. Flatt, R.; Schober, I., 7 - Superplasticizers and the rheology of concrete. In *Understanding the Rheology of Concrete*, Roussel, N., Ed. Woodhead Publishing: 2012; pp 144-208.

93. Matsushita, Y., Conversion of technical lignins to functional materials with retained polymeric properties. *J Wood Sci* **2015,** *61* (3), 230-250.

94. Yu, L. X.; Yu, J.; Mo, W. J.; Qin, Y. L.; Yang, D. J.; Qiu, X. Q., Etherification to improve the performance of lignosulfonate as dye dispersant. *Rsc Adv* **2016,** *6* (75), 70863-70869.

95. Yang, D. J.; Li, H. J.; Qin, Y. L.; Zhong, R. S.; Bai, M. X.; Qiu, X. Q., Structure and Properties of Sodium Lignosulfonate with Different Molecular Weight Used as Dye Dispersant. *J Disper Sci Technol* **2015,** *36* (4), 532-539.

96. Huang, C. X.; Ma, J. M.; Zhang, W. Y.; Huang, G.; Yong, Q., Preparation of Lignosulfonates from Biorefinery Lignins by Sulfomethylation and Their Application as a Water Reducer for Concrete. *Polymers-Basel* **2018,** *10* (8).

97. Kumar, A.; Anushree; Kumar, J.; Bhaskar, T., Utilization of lignin: A sustainable and eco-friendly approach. *Journal of the Energy Institute* **2020,** *93* (1), 235-271.

98. Mousavioun, P.; Doherty, W. O. S., Chemical and thermal properties of fractionated bagasse soda lignin. *Ind Crop Prod* **2010,** *31* (1), 52-58.

99. Schutyser, W.; Renders, T.; Van den Bossche, G.; Van den Bosch, S.; Koelewijn, S.-F.; Ennaert, T.; Sels, B., Catalysis in Lignocellulosic Biorefineries: The Case of Lignin Conversion: Applications in the Chemical Industry, Energy Development, and Environment Protection. 2017; pp 537-584.

100. Tanase-Opedal, M.; Espinosa, E.; Rodriguez, A.; Chinga-Carrasco, G., Lignin: A Biopolymer from Forestry Biomass for Biocomposites and 3D Printing. *Materials* **2019,** *12* (18).

101. Huang, X. M.; Atay, C.; Koranyi, T. I.; Boot, M. D.; Hensen, E. J. M., Role of Cu-Mg-Al Mixed Oxide Catalysts in Lignin Depolymerization in Supercritical Ethanol. *Acs Catal* **2015,** *5* (12), 7359-7370.

102. Baurhoo, B.; Ruiz-Feria, C. A.; Zhao, X., Purified lignin: Nutritional and health impacts on farm animals - A review. *Anim Feed Sci Tech* **2008,** *144* (3-4), 175-184.

103. Barta, K.; Matson, T. D.; Fettig, M. L.; Scott, S. L.; Iretskii, A. V.; Ford, P. C., Catalytic disassembly of an organosolv lignin via hydrogen transfer from supercritical methanol. *Green Chem* **2010,** *12* (9), 1640-1647.

104. Hochegger, M.; Cottyn-Boitte, B.; Cezard, L.; Schober, S.; Mittelbach, M., Influence of Ethanol Organosolv Pulping Conditions on Physicochemical Lignin Properties of European Larch. *Int J Chem Eng* **2019,** *2019*.

105. Sadeghifar, H.; Wells, T.; Le, R. K.; Sadeghifar, F.; Yuan, J. S.; Ragauskas, A. J., Fractionation of Organosolv Lignin Using Acetone:Water and Properties of the Obtained Fractions. *Acs Sustain Chem Eng* **2017,** *5* (1), 580-587.

106. Yu, O.; Yoo, C. G.; Kim, C. S.; Kim, K. H., Understanding the Effects of Ethylene Glycol-Assisted Biomass Fractionation Parameters on Lignin Characteristics Using a Full Factorial Design and Computational Modeling. *Acs Omega* **2019,** *4* (14), 16103-16110.

107. Saha, M.; Saynik, P. B.; Borah, A.; Malani, R. S.; Arya, P.; Shivangi; Moholkar, V. S., Dioxane-based extraction process for production of high quality lignin. *Bioresource Technology Reports* **2019,** *5*, 206-211.

108. Ľudmila, H.; Michal, J.; Andrea, k.; Alea, H. In *LIGNIN , POTENTIAL PRODUCTS AND THEIR MARKET VALUE*, 2015.

109. Wanmolee, W.; Laosiripojana, N.; Daorattanachai, P.; Moghaddam, L.; Rencoret, J.; del Rio, J. C.; Doherty, W. O. S., Catalytic Conversion of Organosolv Lignins to Phenolic Monomers in Different Organic Solvents and Effect of Operating Conditions on Yield with Methyl Isobutyl Ketone. *Acs Sustain Chem Eng* **2018,** *6* (3), 3010-3018.

110. Parto, S. G.; Jorgensen, E. K.; Christensen, J. M.; Pedersen, L. S.; Larsen, D. B.; Duus, J. O.; Jensen, A. D., Solvent assisted catalytic conversion of beech wood and organosolv lignin over NiMo/gamma-Al2O3. *Sustain Energ Fuels* **2020,** *4* (4), 1844-1854.

111. Wang, S. X.; Yang, L. P.; Stubbs, L. P.; Li, X.; He, C. B., Lignin-Derived Fused Electrospun Carbon Fibrous Mats as High Performance Anode Materials for Lithium Ion Batteries. *Acs Appl Mater Inter* **2013,** *5* (23), 12275-12282.

112. Rumpf, J.; Do, X. T.; Burger, R.; Monakhova, Y. B.; Schulze, M., Extraction of High-Purity Lignins via Catalyst-free Organosolv Pulping from Low-Input Crops. *Biomacromolecules* **2020,** *21* (5), 1929-1942.

113. Trubetskaya, A.; Lange, H.; Wittgens, B.; Brunsvik, A.; Crestini, C.; Rova, U.; Christakopoulos, P.; Leahy, J. J.; Matsakas, L., Structural and Thermal Characterization of Novel Organosolv Lignins from Wood and Herbaceous Sources. *Processes* **2020,** *8* (7).

114. de la Torre, M. J.; Moral, A.; Hernandez, M. D.; Cabeza, E.; Tijero, A., Organosolv lignin for biofuel. *Ind Crop Prod* **2013,** *45*, 58-63.

115. Akgul, M.; Kirci, H., An environmentally friendly organosolv (ethanol-water) pulping of poplar wood. *J Environ Biol* **2009,** *30* (5), 735-740.

116. Liu, F.; Liu, Q. Y.; Wang, A. Q.; Zhang, T., Direct Catalytic Hydrogenolysis of Kraft Lignin to Phenols in Choline-Derived Ionic Liquids. *Acs Sustain Chem Eng* **2016,** *4* (7), 3850-3856.

117. Hita, I.; Deuss, P. J.; Bonura, G.; Frusteri, F.; Heeres, H. J., Biobased chemicals from the catalytic depolymerization of Kraft lignin using supported noble metal-based catalysts. *Fuel Process Technol* **2018,** *179*, 143-153.

118. Huang, J.-b.; Wu, S.-b.; Cheng, H.; Lei, M.; Liang, J.-j.; Tong, H., Theoretical study of bond dissociation energies for lignin model compounds. *Journal of Fuel Chemistry and Technology* **2015,** *43* (4), 429-436.

119. Ma, Q. Z.; Liu, Q. Y.; Dou, X. M.; Li, W. Z.; Fan, W.; Liu, M. H., Depolymerization of Lignin to Produce Monophenols and Oligomers Using a Novel Ni/Ce-CNT Catalyst. *Bioresources* **2018,** *13* (4), 8024-8040.

120. Struven, J. O.; Meier, D., Hydrocracking of Organosolv Lignin in Subcritical Water to Useful Phenols Employing Various Raney Nickel Catalysts. *Acs Sustain Chem Eng* **2016,** *4* (7), 3712-3721.

121. Zhao, B.; Hu, Y.; Gao, J.; Zhao, G.; Ray, M. B.; Xu, C. C., Recent Advances in Hydroliquefaction of Biomass for Bio-oil Production Using In Situ Hydrogen Donors. *Ind Eng Chem Res* **2020,** *59* (39), 16987-17007.

122. Huang, X. M.; Koranyi, T. I.; Boot, M. D.; Hensen, E. J. M., Ethanol as capping agent and formaldehyde scavenger for efficient depolymerization of lignin to aromatics. *Green Chem* **2015,** *17* (11), 4941-4950.

123. Feng, J. F.; Yang, Z. Z.; Hse, C. Y.; Su, Q. L.; Wang, K.; Jiang, J. C.; Xu, J. M., In situ catalytic hydrogenation of model compounds and biomass-derived phenolic compounds for bio-oil upgrading. *Renew Energ* **2017,** *105*, 140-148.

124. Tekin, K.; Hao, N. J.; Karagoz, S.; Ragauskas, A. J., Ethanol: A Promising Green Solvent for the Deconstruction of Lignocellulose. *Chemsuschem* **2018,** *11* (20), 3559-3575.

125. Kim, K. H.; Kim, C. S., Recent Efforts to Prevent Undesirable Reactions From Fractionation to Depolymerization of Lignin: Toward Maximizing the Value From Lignin. *Front Energy Res* **2018,** *6*.

126. Huang, S. H.; Mahmood, N.; Tymchyshyn, M.; Yuan, Z. S.; Xu, C. B., Reductive de-polymerization of kraft lignin for chemicals and fuels using formic acid as an in-situ hydrogen source. *Bioresource Technol* **2014,** *171*, 95-102.

127. Ouyang, X. P.; Huang, X. Z.; Zhu, Y.; Qiu, X. Q., Ethanol-Enhanced Liquefaction of Lignin with Formic Acid as an in Situ Hydrogen Donor. *Energ Fuel* **2015,** *29* (9), 5835-5840.

128. Arakadiusz, G.; Monika, A.; Kinga, C., Bulk density of forest energy chips. *Ann. Warsaw Univ. Life Sci. – SGGW, Agricult* **2016,** *67*, 101-111.

129. Pandarus, V.; Beland, F.; Ciriminna, R.; Pagliaro, M., Selective Debenzylation of Benzyl Protected Groups with SiliaCat Pd(0) under Mild Conditions. *Chemcatchem* **2011,** *3* (7), 1146-1150.

130. Kim, J. K.; Lee, J. K.; Kang, K. H.; Song, J. C.; Song, I. K., Selective cleavage of C-O bond in benzyl phenyl ether to aromatics over Pd-Fe bimetallic catalyst supported on ordered mesoporous carbon. *Appl Catal a-Gen* **2015,** *498*, 142-149.

131. Lu, J. M.; Wang, M.; Zhang, X. C.; Heyden, A.; Wang, F., beta-O-4 Bond Cleavage Mechanism for Lignin Model Compounds over Pd Catalysts Identified by Combination of First-Principles Calculations and Experiments. *Acs Catal* **2016,** *6* (8), 5589-5598.

132. Parsell, T. H.; Owen, B. C.; Klein, I.; Jarrell, T. M.; Marcum, C. L.; Haupert, L. J.; Amundson, L. M.; Kenttamaa, H. I.; Ribeiro, F.; Miller, J. T.; Abu-Omar, M. M., Cleavage and hydrodeoxygenation (HDO) of C-O bonds relevant to lignin conversion using Pd/Zn synergistic catalysis. *Chem Sci* **2013,** *4* (2), 806-813.

133. Ye, Y. Y.; Zhang, Y.; Fan, J.; Chang, J., Selective production of 4-ethylphenolics from lignin via mild hydrogenolysis. *Bioresource Technol* **2012,** *118*, 648-651.

134. Van den Bosch, S.; Schutyser, W.; Koelewijn, S. F.; Renders, T.; Courtin, C. M.; Sels, B. F., Tuning the lignin oil OH-content with Ru and Pd catalysts during lignin hydrogenolysis on birch wood. *Chem Commun* **2015,** *51* (67), 13158-13161.

135. Davis, J. L.; Barteau, M. A., Decarbonylation and Decomposition Pathways of Alcohols on Pd(111). *Surf Sci* **1987,** *187* (2-3), 387-406.

136. Van den Bosch, S.; Schutyser, W.; Vanholme, R.; Driessen, T.; Koelewijn, S. F.; Renders, T.; De Meester, B.; Huijgen, W. J. J.; Dehaen, W.; Courtin, C. M.; Lagrain, B.; Boerjan, W.; Sels, B. F., Reductive lignocellulose fractionation into soluble lignin-derived phenolic monomers and dimers and processable carbohydrate pulps. *Energy & Environmental Science* **2015,** *8* (6), 1748-1763.

137. Dong, L.; Lin, L.; Han, X.; Si, X.; Liu, X.; Guo, Y.; Lu, F.; Rudić, S.; Parker, S. F.; Yang, S.; Wang, Y., Breaking the Limit of Lignin Monomer Production via Cleavage of Interunit Carbon–Carbon Linkages. *Chem-Us* **2019,** *5* (6), 1521-1536.

138. Hocking, M. B., 18 - Petroleum Refining. In *Handbook of Chemical Technology and Pollution Control (Third Edition)*, Hocking, M. B., Ed. Academic Press: San Diego, 2005; pp 593-636.

139. Song, Q.; Wang, F.; Cai, J.; Wang, Y.; Zhang, J.; Yu, W.; Xu, J., Lignin depolymerization (LDP) in alcohol over nickel-based catalysts via a fragmentation–hydrogenolysis process. *Energy & Environmental Science* **2013,** *6* (3), 994-1007.

140. Cheng, C. B.; Truong, J.; Barrett, J.; Shen, D. K.; Abu-Omar, M.; Ford, P., Efficient depolymerization of organosolv lignin in ethanol/iso-propanol media without catalyst. *Abstr Pap Am Chem S* **2019,** *258*.

141. Perras, F. A.; Luo, H.; Zhang, X. M.; Mosier, N. S.; Pruski, M.; Abu-Omar, M. M., Atomic-Level Structure Characterization of Biomass Pre- and Post-Lignin Treatment by Dynamic Nuclear Polarization-Enhanced Solid-State NMR. *J Phys Chem A* **2017,** *121* (3), 623-630.

142. Blondiaux, E.; Bomon, J.; Smolen, M.; Kaval, N.; Lemiere, F.; Sergeyev, S.; Diels, L.; Sels, B.; Maes, B. U. W., Bio-based Aromatic Amines from Lignin-Derived Monomers. *Acs Sustain Chem Eng* **2019,** *7* (7), 6906-6916.

143. Augustin, A.; Lamerz, J.; Meistermann, H.; Golling, S.; Scheiblich, S.; Hermann, J. C.; Duchateau-Nguyen, G.; Tzouros, M.; Avila, D. W.; Langen, H.; Essioux, L.; Klughammer, B., Quantitative Chemical Proteomics Profiling Differentiates Erlotinib from Gefitinib in EGFR Wild-Type Non-Small Cell Lung Carcinoma Cell Lines. *Mol Cancer Ther* **2013,** *12* (4), 520-529.

144. Zhang, Y. M.; Tortorella, M. D.; Liao, J. X.; Qin, X. C.; Chen, T. T.; Luo, J. F.; Guan, J. T.; Talley, J. J.; Tu, Z. C., Synthesis and Evaluation of Novel Erlotinib-NSAID Conjugates as More Comprehensive Anticancer Agents. *Acs Med Chem Lett* **2015,** *6* (10), 1086-1090.

145. Jiang, Y.; Ding, D. C.; Zhao, S.; Zhu, H. Y.; Kenttamaa, H. I.; Abu-Omar, M. M., Renewable thermoset polymers based on lignin and carbohydrate derived monomers. *Green Chem* **2018,** *20* (5), 1131-1138.

146. Zhang, X. M.; Murria, P.; Jiang, Y.; Xiao, W. H.; Kenttamaa, H. I.; Abu-Omar, M. M.; Mosier, N. S., Maleic acid and aluminum chloride catalyzed conversion of glucose to 5-(hydroxymethyl) furfural and levulinic acid in aqueous media. *Green Chem* **2016,** *18* (19), 5219-5229.

147. Jiang, Y.; Yang, L. N.; Bohn, C. M.; Li, G. N.; Han, D.; Mosier, N. S.; Miller, J. T.; Kenttamaa, H. I.; Abu-Omar, M. M., Speciation and kinetic study of iron promoted sugar conversion to 5-hydroxymethylfurfural (HMF) and levulinic acid (LA). *Org Chem Front* **2015,** *2* (10), 1388-1396.

148. Zhang, X.; Yan, H.; Zhu, L. J.; Li, T.; Wang, S. R., Hydrodeoxygenation of Lignin-Derived Monomers and Dimers over a Ru Supported Solid Super Acid Catalyst for Cycloalkane Production. *Adv Sustain Syst* **2020**.

149. Ng, F. F.; Couture, G.; Philippe, C.; Boutevin, B.; Caillol, S., Bio-Based Aromatic Epoxy Monomers for Thermoset Materials. *Molecules* **2017,** *22* (1).

150. Auvergne, R.; Caillol, S.; David, G.; Boutevin, B.; Pascault, J. P., Biobased Thermosetting Epoxy: Present and Future. *Chem Rev* **2014,** *114* (2), 1082-1115.

151. Zhao, S.; Abu-Omar, M. M., Catechol-Mediated Glycidylation toward Epoxy Vitrimers/Polymers with Tunable Properties. *Macromolecules* **2019,** *52* (10), 3646-3654.

152. Zhao, S.; Abu-Omar, M. M., Biobased Epoxy Nanocomposites Derived from Lignin-Based Monomers. *Biomacromolecules* **2015,** *16* (7), 2025-2031.

153. Zhao, S.; Abu-Omar, M. M., Renewable Thermoplastics Based on Lignin-Derived Polyphenols. *Macromolecules* **2017,** *50* (9), 3573-3581.

154. Fache, M.; Boutevin, B.; Caillol, S., Epoxy thermosets from model mixtures of the lignin-to-vanillin process. *Green Chem* **2016,** *18* (3), 712-725.

155. Shimasaki, T.; Yoshihara, S.; Shibata, M., Preparation and properties of biocomposites composed of sorbitol-based epoxy resin, pyrogallol-vanillin calixarene, and wood flour. *Polym Composite* **2012,** *33* (10), 1840-1847.

156. Hernandez, E. D.; Bassett, A. W.; Sadler, J. M.; La Scala, J. J.; Stanzione, J. F., Synthesis and Characterization of Bio-based Epoxy Resins Derived from Vanillyl Alcohol. *Acs Sustain Chem Eng* **2016,** *4* (8), 4328-4339.

157. Zhao, S.; Abu-Omar, M. M., Renewable Epoxy Networks Derived from Lignin-Based Monomers: Effect of Cross-Linking Density. *Acs Sustain Chem Eng* **2016,** *4* (11), 6082-6089.

158. (EIA), U. S. E. I. A. Gasoline Explained, Use of Gasoline. https://www.eia.gov/energyexplained/gasoline/use-of-gasoline.php.

159. Fahmy, T. Y. A.; Fahmy, Y.; Mobarak, F.; El-Sakhawy, M.; Abou-Zeid, R. E., Biomass pyrolysis: past, present, and future. *Environment, Development and Sustainability* **2020,** *22* (1), 17-32.

160. Revankar, S. T., Chapter Six - Chemical Energy Storage. In *Storage and Hybridization of Nuclear Energy*, Bindra, H.; Revankar, S., Eds. Academic Press: 2019; pp 177-227.

161. Lu, M. H.; Du, H.; Wei, B.; Zhu, J.; Li, M. S.; Shan, Y. H.; Song, C. S., Catalytic Hydrodeoxygenation of Guaiacol over Palladium Catalyst on Different Titania Supports. *Energ Fuel* **2017,** *31* (10), 10858-10865.

162. Wang, W. C.; Bai, C. J.; Thapaliya, N., The production of renewable transportation fuel through fed-batch and continuous deoxygenation of vegetable oil derived fatty acids over Pd/C catalyst. *Int J Energ Res* **2015,** *39* (8), 1083-1093.

163. Jin, W.; Pastor-Perez, L.; Villora-Pico, J. J.; Pastor-Blas, M. M.; Sepulveda-Escribano, A.; Gu, S.; Charisiou, N. D.; Papageridis, K.; Goula, M. A.; Reina, T. R., Catalytic Conversion of Palm Oil to Bio-Hydrogenated Diesel over Novel N-Doped Activated Carbon Supported Pt Nanoparticles. *Energies* **2020,** *13* (1).

164. Li, S.; Liu, B.; Truong, J.; Luo, Z.; Ford, P. C.; Abu-Omar, M. M., One-pot hydrodeoxygenation (HDO) of lignin monomers to C9 hydrocarbons co-catalysed by Ru/C and Nb2O5. *Green Chem* **2020,** *22* (21), 7406-7416.

165. Chan, X. J.; Pu, T. C.; Chen, X. Y.; James, A.; Lee, J.; Parise, J. B.; Kim, D. H.; Kim, T., Effect of niobium oxide phase on the furfuryl alcohol dehydration. *Catal Commun* **2017,** *97*, 65-69.

166. de Souza, P. M.; Rabelo-Neto, R. C.; Borges, L. E. P.; Jacobs, G.; Davis, B. H.; Sooknoi, T.; Resasco, D. E.; Noronha, F. B., Role of Keto Intermediates in the Hydrodeoxygenation of Phenol over Pd on Oxophilic Supports. *Acs Catal* **2015,** *5* (2), 1318-1329.

167. Wang, H. L.; Ruan, H.; Pei, H. S.; Wang, H. M.; Chen, X. W.; Tucker, M. P.; Cort, J. R.; Yang, B., Biomass-derived lignin to jet fuel range hydrocarbons via aqueous phase hydrodeoxygenation. *Green Chem* **2015,** *17* (12), 5131-5135.

168. Qin, S. F.; Li, B. L.; Luo, Z. C.; Zhao, C., The conversion of a high concentration of lignin to cyclic alkanes by introducing Pt/HAP into a Ni/ASA catalyst. *Green Chem* **2020,** *22* (9), 2901-2908.

Chapter 2. One-pot Hydrodeoxygenation (HDO) of Lignin Monomers to C9 Hydrocarbons Co-catalyzed by Ru/C and Nb_2O_5

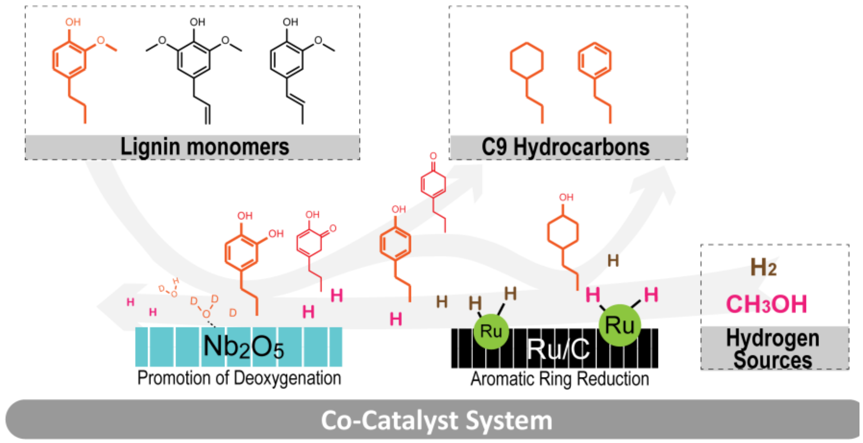

Figure 2.1 Illustration figure of Chapter 2.

2.1 Abstract

A physical mixture of Ru/C and Nb_2O_5 is an effective catalyst for upgrading lignin monomers under low H_2 pressure at 250 ℃ to give a clean cut of hydrocarbons appropriate for use as a liquid fuel. The reaction solvent is water with a small amount of methanol additive. The hydrodeoxygenation (HDO) was evaluated by using dihydroeugenol (DHE) as an exemplary model lignin monomer. Under optimized conditions, 100% conversion of DHE and very high selectivity to propyl cyclohexane (C9 hydrocarbon) was achieved. The Nb_2O_5 was prepared at low temperature (450 ℃) and was shown to contain acid sites that enhance the production of fully deoxygenated product. The methanol additive serves as hydrogen source for the Ru/C catalyzed reduction of the aromatic ring. In addition, when a substrate mixture of DHE, isoeugenol and 4-allylsyringol simulating lignin products was employed, 100% conversion to propyl cyclohexane (76%) and propyl benzene (24%) was observed, thereby suggesting the general applicability of this catalyst system for funneling lignin monomers into a clean slate of hydrocarbon liquid fuels.

This study sheds light on the function of each catalyst component and provides a simple and green utilization of biomass monomers as a feedstock for renewable hydrocarbon fuels.

Keywords: Lignin; Hydrodeoxygenation; Nb_2O_5; Biofuels

2.2 Introduction

Non-renewable fossil carbon has been the main resource to produce most chemicals and fuels for the past century; however, renewable alternatives are available. Lignocellulose is by far the most abundant renewable source of non-food-based carbon, and there is considerable interest in upgrading such biomass as a sustainable feedstock.[1-5] The lignin component of lignocellulose is the second most plentiful biopolymer in nature (after cellulose), has a high carbon content, and is (potentially) the largest renewable resource of aromatic chemicals and fuels.[5-9] However, it has an irregular structure with random linkages between monomeric components having different levels of oxygenation that is challenging to utilize chemically.[10] Due to this dilemma, pulp, and paper industries and biorefineries typically dispose of lignin by burning it. Thus, lignin is an attractive target for biomass valorization.

Lignin can be converted to bio-oil as a renewable liquid fuel.[11] However, bio-oils cannot be used in conventional gasoline and diesel fuel engines due to the high oxygen content [up to 60 weight % (wt %)] that makes them immiscible with petroleum-derived fuels.[12, 13] Thus, oxygen removal while maintaining the carbon structures has the potential to enhance the utilization of bio-oil as a transportation fuel.

Catalytic hydrodeoxygenation (HDO) can upgrade bio-oils. In most studies, HDO involves treatment at high temperatures (250-500 °C) with high pressure of H_2 (50-100 bar). The high pressures required may limit the scalability of the reaction and is a safety hazard.[14]

These obstacles encourage the research towards alternative approaches for phenolic upgrading under milder conditions.

The goal of the present study is to develop catalytic strategies that efficiently funnel lignin disassembly components into a narrowly defined product stream useful as a feedstock for the synthesis of aromatic chemicals (C6-C9 aromatic hydrocarbons) or as drop-in biofuels. Phenolics would be desirable for the former processes, while oxygen-free hydrocarbons that can replace fossil-carbon liquid fuels would serve the latter purpose.[15-17] In previous studies, various types of heterogeneous catalysts,[17-20] transition metal compounds (phosphides,[21-26] carbides,[24, 25] and nitrides[25, 27]), but mainly noble metals (Pt, Pd, Rh, Ru),[14, 15] have been used, but these require high temperature, and high pressure conditions. For example, Lu et al showed Pd/TiO_2 catalyst with the HDO/hydrogenation of guaiacol to cyclohexane, but this required 30 bar H_2 at 260 ℃.[28] Kim et al. reported that ruthenium on carbon (Ru/C) converted guaiacol to cyclohexanol with 60% selectivity using the H-donor 2-propanol without added H_2 at 200 ℃ for 5 h, but the HDO was only partial.[29]

The use of Niobium Oxide has primarily been studied to show its specific role involved in HDO. Shown in the studies of Wang et al., Nb_2O_5 was primarily used as a catalyst support for Ruthenium to form indane with and without the addition of CH_2Cl_2 as its primary solvent. The main function Nb_2O_5 partook was catalysing the intramolecular cyclization and hydrogenation of lignin oil.[7] Jiang et al., utilized Ni/Nb_2O_5 catalyst to produce value-added alcohols from lignin-derived phenols which exhibited selective HDO to give a total alcohol yield of 74%, but requires higher pressure (25 bar H_2).[8] Puurunen et al., used Pt/Nb_2O_5 to perform HDO on lignin monomer, 4-propylphenol under harsh temperature and pressure (350 °C, 20 bar H_2) to give a selectivity of 77% propylbenzene.[9] Rinaldi et al., studied Ni/Nb_2O_5 by tuning the acidic and hydrogenating properties of the catalyst to convert lignin to hydrocarbons at 91% yield under 15% catalyst loading and harsh conditions (200°C, 40 bar H_2).[30] Yang et al., reported Nb_2O_5 supported for Pd and Pt where they concluded HDO conversion of lignin to C_7-C_9 products at 42 and 64%, respectively.[18]

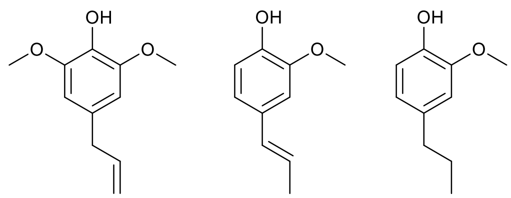

A B C

Figure 2.2 Structures of lignin monomer compounds: (A) 4-allyl-2,6-dimethoxyphenol (4-allysyringol), (B) isoeugenol, (C) 2-methoxy-4-propylphenol (dihydroeugenol, DHE)

Described here is the hydroprocessing of dihydroeugenol (DHE) in an aqueous medium using a physical mixture of two catalysts acting synergistically, one is Ru/C, the other is niobium pentoxide (Nb_2O_5). DHE was used as the primary model compound for testing the present catalytic system, since it includes the methoxy, hydroxy, and a propyl groups characteristic of the lignin monomers present in bio-oils (Figure 2.2). Nb_2O_5 is an air stable, water insoluble white solid that exhibits both strong Lewis and Brønsted acid sites.[31] It has proved to be an effective catalyst for hydration/dehydration, cracking, condensation, isomerization, and alkylation[32-35] as well as for HDO.[32-34, 36]

The dual catalyst system is effective in hydroprocessing DHE and several other lignin monomers under relatively mild conditions to produce hydrocarbons in high yields. We find that addition of small quantities of methanol (MeOH) as a co-reactant has a significant influence on the product distribution and offer evidence-based mechanistic insight. Furthermore, this system can be tuned to give high selectivity towards hydrocarbon products that can be employed as drop-in fuels.

2.3 Experimental

2.3.1 Reagents and feedstocks

All commercial chemicals were purchased and used as received. 2-Methoxy-4-propylphenol (≥99%), isoeugenol (98%), 2,2-biphenol (99%), and niobium(V) oxide (325 mesh, 99.9%) were purchased from Sigma-Aldrich. Dichloromethane (ACS reagent grade), methanol (ACS reagent grade), ethanol (200 Proof), and ethyl acetate (ACS reagent grade) were purchased from Fisher Chemical. Cetyltrimethyl ammonium bromide (CTAB, 98%) and n-dodecane (99%) were purchased from Alfa Aesar. Deuterium oxide (D, 99.9%), and methanol-d_4 (D, 99.8%) were purchased from Cambridge Isotope Laboratories Inc. Propyl benzene (98%) was purchased from Frontier Scientific. Para-cresol (cresylic acid) was purchased from Hercules Powder Company. Hydrochloric Acid (GR ACS) was purchased from EMD Millipore Corporation. Niobium (V) chloride (≥99%) was purchased from Strem Chemicals. Hydrogen gas (5.0 grade) and nitrogen (99.998%) were purchased from Praxair. Water used for reaction and sample preparation was obtained from a A10 Milli-Q water purification system by Millipore.

2.3.2 Catalyst preparation

Ru/C was obtained from Sigma-Aldrich with 5 wt% Ru loading and used as received. Nb_2O_5 was synthesized using a hydrothermal method according to a modified literature procedure.[35] Typically, a 20 mmol portion of the precursor $NbCl_5$ was dissolved in 20 mL ethanol with rigorous stirring for 10 min, then the solution was added to water solution of CTAB (1 g in 15 mL distilled water) dropwise. The mixed solution was then stirred for 0.5 h followed by adding 20 mL of aqueous HCl (pH 1) that was previously prepared by dissolving a specific amount of hydrochloric acid in water and stirring for another 1.5 h.

The resulting sol was then put into a Teflon-lined autoclave and aged at 160 ℃ for 24 h. Subsequently, the solid was separated and washed with distilled water and dried at 60 ℃ overnight. After that, the sample was ground and packed for calcination in air. A Thermolyne F6020 1200C Muffle furnace was used to calcinate the niobia sample. Ramping rate of the furnace was pre-set to 1 ℃/min. After 6h calcination at 450℃, the active Nb_2O_5 catalyst was collected at room temperature.

2.3.3 Catalyst characterization

***NH_3-Temperature Programmed Desorption (TPD)*:** To evaluate the acid sites on Nb_2O_5, NH_3-TPD was performed on a Micromeritics AutoChem 2920 instrument. A 200 mg sample of Nb_2O_5 was placed into a U-shaped quartz tube. This material was first pretreated by heating under flowing helium (25 cm^3/min) at 300 ℃ for 0.5 h. A mixture of NH_3 in He (1:9 v/v) was then passed through the tube at a flow rate of 15 cm^3/min at 25 ℃ for 1 h. After that, the sample was flushed with He (25 cm^3/min) at 100 ℃ for another hour. The TPD measurements were carried out over the temperature range 100-500 ℃ at ramp rate of 10 ℃ /min and the ammonia concentration in the effluent was monitored with filament thermal conductivity detector (TCD). The amount of desorbed ammonia was determined based on the integrated peak area.

X-ray Diffraction (XRD): The phase structure of Nb_2O_5 was analyzed by powder X-ray diffraction in the diffraction angle 2θ between 10^o and 80^o on a PANalytical X'Pert PRO X-ray diffractometer with Cu Kα1 radiation (45 kV and 40 mA, k = 1.5406 Å).

Scanning Electron Microscopy (SEM) and Transmission Electron Microscopy (TEM): The particle size and micro morphology of Nb_2O_5 were characterized by scanning electron microscopy (Hitachi SU-8010) at an acceleration voltage of 15 kV. The pore structure of

Nb_2O_5 was examined using high-resolution transmission electron microscopy (Tecnai G2 F20 S-TWIN) with the acceleration voltage of 200 kV.

X-ray Photoelectron Spectroscopy (XPS): The niobium oxidation state in the synthesized Nb_2O_5 catalyst was analyzed by X-ray photoelectron spectroscopy (Thermo Scientific K-Alpha+, USA) with a monochromatic radiation source Al Kα (12kV, 6mA, 72W). The wide scans were performed with 100 eV pass energy and 1 eV energy step, and the high resolution scans were performed with 30 eV pass energy and 0.1 eV step size. The C1s signal of adventitious carbon (284.8 eV) was used for energy calibration.

2.3.4 Catalytic reaction and product analysis

Reactions in Parr reactor: Batch reactions were carried out in a stainless steel 75 mL 6-series pressure reactor (Parr Instrument Company, 5000 series). The reactor vessel was equipped with magnetic stirring system. For a typical reaction, 0.1 g Ru/C and 0.2 g Nb_2O_5 were physically mixed in the vessel with 12 mL distilled water as solvent. To this were added substrate (0.2 mL) and MeOH (0.8 mL). The reactor was then sealed and purged with H_2 three times. Then, the reactor was filled with H_2 (6 bar). The reactor was heated to 250 ℃ and held at that temperature for a defined time (typically for 12 h). The stirring rate was kept at 700 rpm during the whole reaction period. Subsequently, the reactor was cooled to room temperature. The products in the liquid phase were extracted using ethyl acetate and the gas phase products were collected in a sealed gasbag for further analysis.

Catalyst recyclability test: The recycle experiments were performed in five successive runs with 1 mL DHE loading of each. A physical mixture of fresh Ru/C (0.1 g) and Nb_2O_5 (0.2 g) was employed in the first run. MeOH (1 mL) was then added with 12 mL distilled water as solvent to the reaction mixture in a 75 mL reactor vessel. The reactor was sealed and purged with H_2 three times. Then, the reactor was filled with 11 bar H_2 at room temperature. After that, the reactor was heated to 250 ℃ and held for 16 h with magnetic stirring at 700 rpm. After reaction, products in liquid phase were extracted using ethyl acetate. The catalyst was washed using ethanol and collected by centrifugation, then dried in a vacuum chamber for 24 h at room temperature. Prior to the next recycle run, the catalyst mixture was heated in an oven at 120 ℃ for 1 h. The following runs were performed with the same portion of this catalyst mixture collected from the previous run. Turnover number (TON) of each catalyst was calculated based on the total amount of C9 hydrocarbons, i.e. propyl benzene and propyl cyclohexane, produced after the fifth run to show the productivity of each catalyst. The TON was defined and calculated as follows:

$$TON = \frac{total\ moles\ of\ C9\ hydrocarbons\ by\ 5\ runs}{moles\ of\ catalyst}$$

GC-MS Analysis: A Hewlett-Packard 5890A gas chromatograph (GC) coupled to a Hewlett-Packard 5970B Mass Selective Detector (MSD) was used to identify the products qualitatively. A J&W DB-5 capillary column (30 m x 0.250 mm I.D. x 0.25 μm film thickness) was installed for analyte separation. Prior to the injection, the liquid sample was dissolved in ethyl acetate and filtered through a 0.2 micron PTFE syringe filter. The GC injector inlet was set to 280 ℃. The oven temperature was held at 50 ℃ for 2 min. Then the oven was heated to 300 ℃ at rate of 20 ℃ per min and held for 10 min. The MSD had a dedicated electron ionization (EI) source and a quadrupole mass analyzer. The mass range of detection was 40 to 550 m/z at a rate of 1.6 scans per second.

GC-FID Analysis: An Agilent 6890N gas chromatograph equipped with a flame ionization detector (FID) was used to quantify the reaction mixtures. A J&W DB-5 GC column (30 m x 0.250 mm I.D. x 0.25 μm film thickness) was selectively used for separation. The liquid products sample was first passed through a 0.2 micron PTFE syringe filter to remove solid particles, and then diluted to 25 mL in a volumetric flask. A 10 mM n-dodecane solution was pre-made as internal standard for GC quantification. The sample solution was mixed with internal standard (1:1 v/v) in a 2 mL Agilent GC vial. The sample was injected by autosampler. The inlet temperature was kept at 280 ℃ while the detector temperature was 310 ℃. The initial temperature of oven was 40 ℃ and held for 7 min. Then the oven was heated to 250 ℃ at ramp rate of 10 ℃/min and kept at the final temperature for 5 min. The split mode was used with the split ratio of 10:1. Helium was used as carrier gas at flow rate of 14 mL/min. The instrument was calibrated using the known samples of the products. The analytes were then identified according to their retention time. The quantification of each analyte was acquired from a calibration curve which represented the relationship between concentration versus the ratio of peak area over internal standard.

GC-TCD Analysis: Gas phase products were analyzed by GC-TCD. An Agilent 6890N (G1530N) gas chromatograph equipped with a thermal conductivity detector (TCD) and 30 m × 0.53 mm Fused Silica Carboxen 1010 capillary column was used. The detector was set to 250 ℃ with H_2 flow at 7 mL/min and air flow at 8 mL/min. The gas phase products were collected in RESTEK polypropylene combo valve gas sampling bag. For each measurement, the 50 μL gas sample was manually injected by a gastight syringe into the GC inlet at 245 ℃. The carrier gas, He, was set to 7 mL/min. The column was pre-heated to 35 ℃ and held for 5 min. Then the temperature ramped to 245 ℃ at the rate of 10 ℃/min and held for 10 min. Each gas analyte was identified by its retention time.

NMR Analysis: ^{1}H NMR was obtained by Varian Unity Inova 600 MHz spectrometer. The analyte was extracted by 700 μL $CDCl_3$ and packed in glass NMR tube for analysis. ^{2}H NMR was done by using Agilent 400-MR DDR2 400 MHz spectrometer. $CHCl_3$ with 10% $CDCl_3$ internal standard was used as the solvent for ^{2}H NMR analysis.

2.4 Results

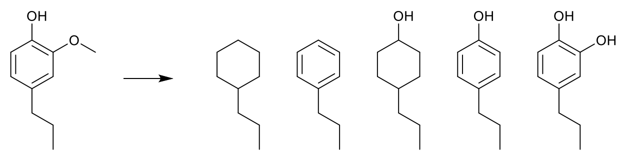

DHE *1* *2* *3* *4* *5*

Figure 2.3 DHE Conversion into five main products: propyl cyclohexane (1), propyl benzene (2), 4-propylcyclohexan-1-ol (3), 4-propylpheol (4), and 4-propylcatechol (5).

2.4.1 Optimization of dihydroeugenol (DHE) hydrodeoxygenation:

A typical HDO run involved heating a mixture of the model substrate DHE (0.20 mL) with the catalysts Ru/C (100 mg) and Nb_2O_5 (200 mg) added separately, water (12 mL) and a small amount of MeOH (0.8 mL) in a closed Parr® high pressure reactor that had been flushed with H_2 ($P(H_2)$ = 1 atm at room temperature, RT) then sealed. After a 12 h reaction at 250 ℃, the conversion of DHE was 95% (entry 3, Table 2.1) and of the five potential products shown in Figure 2.3, the fully deoxygenated hydrocarbons propyl cyclohexane (**1**) and propyl benzene (**2**) made up 64% of the product mixture. The balance was mostly the partially deoxygenated product 4-propylcyclohexanol (**3**). Thus, this catalyst mixture is a promising HDO system. The studies described here were designed to examine the effects of key variables such as MeOH concentration, H_2 pressure, and catalyst loading in order to define those features that may give the optimum selectivity toward desired product streams.

Table 1 illustrates the remarkable sensitivity of this system to the amount of methanol added as well as the cooperative requirement for both MeOH and H_2 to obtain the desired HDO products (**1**) and (**2**). For example, the reaction with no MeOH but with $P(H_2)$ = 6 bar (RT) (entry 1, Table 2.1) gave substantial conversion of DHE, but only ~7% of the fully deoxygenated hydrocarbons. In the absence of both H_2 and MeOH, no conversion was observed, and no products were detected (entry 5, Table 2.1).

Table 2.1 Performance comparison with different amounts of methanol.

Entry	MeOH (mL)	Conv. (%)	Product Distribution (%)				
			1	**2**	**3**	**4**	**5**
1[a]	0	82	3.3	3.5	80	13	-
2[b]	0.4	80	3.6	9.5	42	45	-
3[b]	0.8	95	42	22	34	2	-
4[b]	4	36	8	10	-	24	58
5[c]	0	0	-	-	-	-	-

Common conditions for each reaction: DHE 0.2 mL, Ru/C 100 mg, Nb_2O_5 200 mg, H_2O 12 mL, 250 ℃, 12 h. Unless noted otherwise, the reactor was first flushed with H_2. [a] Initial $P(H_2)$ at RT = 6 bar (5 bar, gauge). [b] Initial $P(H_2)$ at RT = 1 bar. [c] Purged with nitrogen, no added H_2.

Entries 2-4 in Table 2.1 compare the effect of changing the amount of MeOH added while holding $P(H_2)$ constant at 1 bar (RT). Under these conditions, the optimum amount of MeOH proved to be 0.8 mL. Surprisingly, raising the MeOH to 4 mL, only about one third the quantity of the aqueous cosolvent, suppressed both the conversion of DHE and the relative amount of HDO products.

Table 2.2 summarizes the product distributions found for DHE reactions for various $P(H_2)$ (RT) under typical conditions with 0.8 mL MeOH. In the absence of any externally added H_2 (entry 1, Table 2.2) there was about 64% conversion of DHE, but the only products were the phenol and cyclohexanol derivatives (**4**) and (**3**). The amount of conversion increases under increasing H_2 and is 100% when $P(H_2)$ is 6 bar or greater (entries 4-5, Table 2.2). More importantly, the yield of propyl cyclohexane (**1**) is 100%. Thus, the latter result requires addition of both MeOH and H_2 and the distribution of HDO products is a function of $P(H_2)$ with high selectivity occurring at a relatively low $P(H_2)$.

Table 2.2 Performance with different hydrogen pressures

Entry	$P(H_2)$ in bar [a]	Conv. (%)	Product Distribution (%)				
			1	**2**	**3**	**4**	**5**
1[b]	0	64	-	-	31	69	-
2[c]	1	95	42	22	34	2	-
3	2	98	53	17	27	3	-
4	6	100	100	-	-	-	-
5	11	100	100	-	-	-	-

Common conditions for each reaction: DHE 0.2 mL, Ru/C 100 mg, Nb_2O_5 200 mg, H_2O 12 mL, MeOH 0.8 mL, 250 °C, 12 h. Unless noted otherwise, the reactor was first flushed with H_2. [a] Initial $P(H_2)$ at RT. [b] Reactor purged with N_2 only, $P(N_2)$ = 1 atm at RT. [c] The same experiment as entry 3 in Table 1.

Table 2.3 summarizes experiments with different catalyst mixtures. Interestingly, when the reaction was examined with the addition of Nb_2O_5 alone, the material prepared in this laboratory proved to be much more active than that purchased from a commercial source. The XRD pattern, XPS analysis, SEM and TEM images of the synthesized Nb_2O_5 showed it to be an amorphous, mesoporous catalyst with the niobium in the +5 oxidation state (Supporting information (SI) Figures S-2.1 and S-2.2).

The principal reaction in the former case was hydrolysis of the DHE methoxy group to give catechol (**5**) (entry 1, Table 2.3) while little activity was seen with the commercial Nb_2O_5 (entry2, Table 2.3). One possible explanation may lie in the manner in which the two Nb_2O_5 samples were processed. The commercial sample had been calcined at 1000 °C while the Nb_2O_5 sample prepared in our laboratories and used for catalysis was calcined at 450 °C. Accordingly, we speculated that the higher temperature calcination may have diminished the number of acid sites on Nb_2O_5. This idea was tested by TPD studies of Nb_2O_5 samples that had been first dried and then exposed to ammonia. The amount of NH_3 was absorbed by the Nb_2O_5 sample calcined at 450 ℃ was 28 mmol per gram of Nb_2O_5 while an analogous sample prepared in this laboratory but calcined at 600 ℃ only absorbed and released about 2 mmol NH_3 per gram of the sample (SI Figure S-2.3). Furthermore, the commercial sample absorbed and desorbed essentially no NH_3. Thus, it is clear that higher temperature calcination strongly diminishes the number of acid sites on Nb_2O_5.

Table 2.3 Performance with different catalyst mixtures

Entry	Ru/C (mg)	Nb_2O_5 (mg)	Conv. (%)	Product Distribution (%)					P_{final} (bar)
				1	**2**	**3**	**4**	**5**	
1[a]	0	200	80	-	-	-	4	96	6
2[b]	0	200	-	-	-	-	-	-	6
3	100	0	96	7.7	8.2	82	2.1	-	14.5
4[c]	100	0	100	72	-	28	-	-	11.6
5[a, d]	100	200	100	100	-	-	-	-	11

Reaction condition: DHE 0.2 mL, H_2O 12 mL, methanol 0.8 mL, $P(H_2)$ = 6 bar, 250 ℃, 12 h. [a] Nb_2O_5 was custom prepared in this laboratory as described in the Experimental section. [b] commercial Nb_2O_5 calcined at 1000 ℃. [c] Ru/C was pre-treated in 12 mL H_2O under 10 bar H_2 at 200 ℃ for 2 h. [d] The same reaction as entry 4 in Table 2.

When Ru/C alone was used as a catalyst without pretreatment, the major product was propylcyclohexanol (**3**) although about only 8% each of the hydrocarbons (**1**) & (**2**) were formed (entry 3, Table 2.3). When the Ru/C was first pre-treated by heating under hydrogen to 200 ℃, the observed reactivity changed. The major product was propylcyclohexane (**1**) (72%) with the cyclohexanol (**3**) being the remainder (28%) (entry 4, Table 2.3). Unde r analogous conditions, the system to which both Ru/C (not activated with H_2) and Nb_2O_5 had been added gave 100% conversion to the propylcyclohexane product exclusively (entry 5, Table 2.3). Notably, when either form of Ru/C was present, the final pressure in the Parr reactor (after cooling to RT) was significantly higher than the initial P(H_2). This is apparently due to catalytic reforming of MeOH.

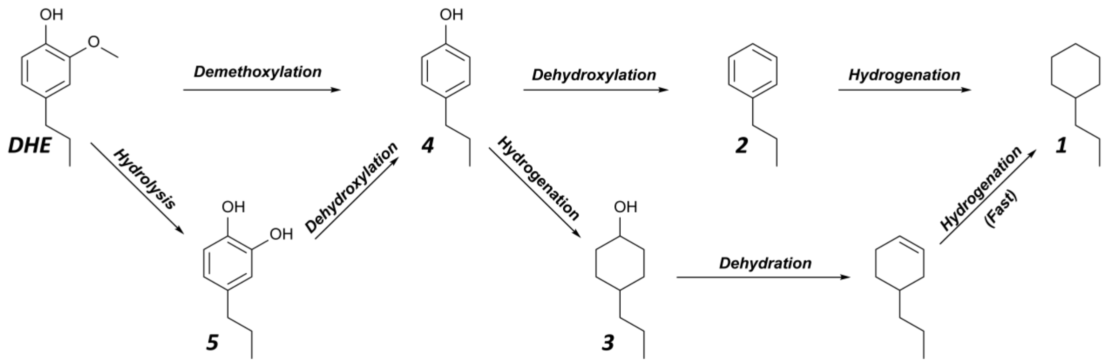

Scheme 2.1 Possible sequence of reactions leading from DHE to (1).

Thus, H_2-pretreated Ru/C can catalyze the HDO/ hydrogenation of DHE, although the reaction is more efficient when Nb_2O_5 is present. On the other hand, low T calcined Nb_2O_5 alone only catalyzed the conversion of DHE to the catechol (**5**), presumably the product of hydrolysis of the methoxy group.

The observation that the Ru/C catalyst is more active after pre-treatment suggested that the early stages of the reactions with the physically mixed catalyst would show an induction period while the Ru/C was being activated. This suggestion led to the experiments reported in Figure 2.4 and SI Table S-2.1 to examine the products formed by different catalyst combinations over an initial period of 2 h. The take-home lesson from Figure 3 is that, on this time scale, Ru/C alone displays modest activity (14% conversion), but the only product observed was the phenol (**4**), the result of HDO removal of the DHE methoxy group. With Nb_2O_5 alone, conversion was considerably higher, but the primary product was the catechol (**5**). The result with both catalysts illustrates the synergy of this mixture. Although the conversion was about the same as seen with Nb_2O_5 alone, products (**1**), (**2**) and (**3**) are also evident. Scheme 2.1 suggests a possible sequence of these transformations, with a principal role of the Nb_2O_5 being to catalyze the hydrolysis of the DHE methoxy group to form the catechol (**5**), although, surprisingly, a small amount of the phenol (**4**) was still formed with Nb_2O_5 alone.

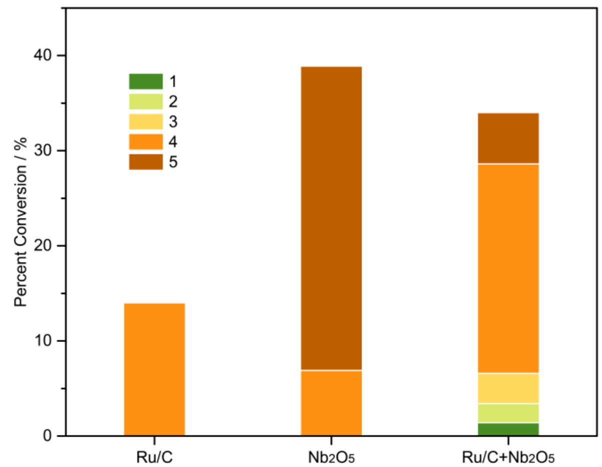

Figure 2.4 Graphic showing conversion (vertical axis) and product distribution after a 2 h reaction for a mixture of DHE (0.2 mL), H_2O (12 mL), MeOH (0.8 mL) under H_2 (6 bar) with Ru/C (100 mg), Nb_2O_5 (200 mg) or both at 250 °C.

Figure 2.5 illustrates the behavior of the mixed catalyst system as a function of reaction time. These data confirm the suspected induction period, during which the Ru/C catalyst is activated. After 4 h, all the DHE had been converted to products with 2/3 of the total being the hydrocarbons (**1**) & (**2**). By 8 h, all the products were (**1**) & (**2**) with propyl cyclohexane (**1**) representing an impressive 94 %, while after 12 h only a single product, (**1**), was evident (SI Table S-2.1). Formation of (**1**) requires HDO of both oxygen containing functional groups of DHE and the hydrogenation of the aromatic ring. Notably, the cyclohexanol (**3**) is observed as an intermediate that presumably undergoes HDO, but none of the direct product of DHE ring-hydrogenation 4 -propyl-2-methoxy-cyclohexanol was evident.

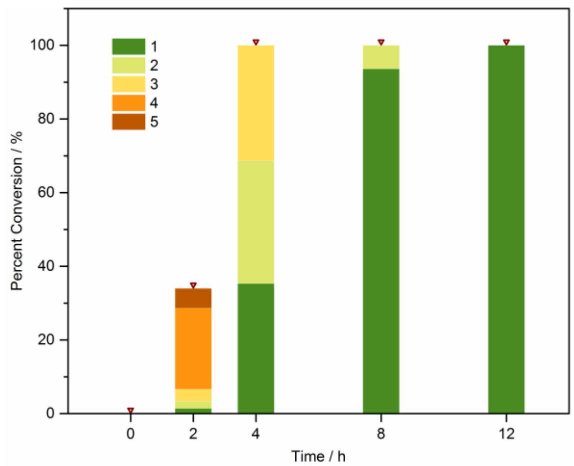

Figure 2.5 Graphic showing conversion (vertical axis) and product distribution after from 2h, 4h, 8h, 12h reaction for a mixture of DHE (0.2 mL), H_2O (12 mL), MeOH (0.8 mL) under H_2 (6 bar) with Ru/C (100 mg) and Nb_2O_5 (200 mg) at 250 °C.

2.4.2 Reactions of DHE with deuterated reactants

Table 2.4 Reaction performance in different isotopically labelled reactants

Entry	Water	Methanol	Hydrogen	Conv. (%)	Product Distribution (%)					P_{final} (bar)
					1	**2**	**3**	**4**	**5**	
1[a, b]	H_2O	MeOH	H_2 (1 bar)	80	3.6	9.5	42	45	-	8
2[b]	H_2O	MeOH	H_2 (1 bar)	95	42	22	34	2	-	11
3	D_2O	methanol-d_4	H_2 (1 bar)	54	-	-	-	66	34	6
4[c]	D_2O	methanol-d_4	H_2 (1 bar)	85	2.5	5.4	48	44	-	9.7
5	D_2O	MeOH	H_2 (1 bar)	81	1	3.1	11	82	2.3	9.1
6[b]	H_2O	MeOH	H_2 (6 bar)	100	100	-	-	-	-	11
7[d]	D_2O	methanol-d_4	H_2 (6 bar)	100	94	0.1	6.2	-	-	8.9
8	H_2O	MeOH	D_2 (6 bar)	100	61	21	16	2	-	9.6

Conditions: DHE 0.2 mL, Ru/C 100 mg, Nb_2O_5 200 mg, water 12 mL, methanol 0.8 mL unless noted, purged with H_2 and vented to give $P(H_2)$ = 1 bar, unless noted, 250 °C, 12 h reaction time, unless noted. [a] Methanol 0.4 mL.[b] Entry 1 and entry 2 are the same reactions as entry 2 and entry 3 in Table 1; entry 6 is the same reaction as entry 4 in Table 2. [c] Reaction time 24 h. [d] $P(H_2)$ = 6 bar.

Table 2.4 summarizes the conversion and products from analogous reactions of DHE in deuterated solvents. Notably, when both D_2O and methanol-d_4 were used instead of the perprotio analogues, there was a significant suppression both of the conversion and of the formation of the more reduced products (**1**), (**2**) and (**3**) with only (**4**) and (**5**) being found (entry 3, Table 2.4). Extending the reaction time to 24 h did increase production of (**1**), (**2**) & (**3**) with the cyclohexanol (**3**) and the phenol (**4**) now being the major products (entry 4, Table 2.4). The pattern was again different when the solvent mixture was D_2O with perprotio MeOH (entry 5, Table 2.4). The conversion was greater (81%) than when methanol-d4 was used (54%), and measurable amounts of (**1**), (**2**) & (**3**) were found, but the primary product was (**4**). Thus, isotope effects are evident in the product distributions from the deuteration of each solvent.

The DHE reaction with the two catalysts was also run in the D_2O/methanol-d_4 solvent with a higher $P(H_2)$ of 6 bar (entry 7, Table 2.4). As observed above (entry 6, Table 2.4), raising the hydrogen pressure substantially accelerated the reaction and improved the selectivity toward (**1**) to 94% in the deuterated medium.

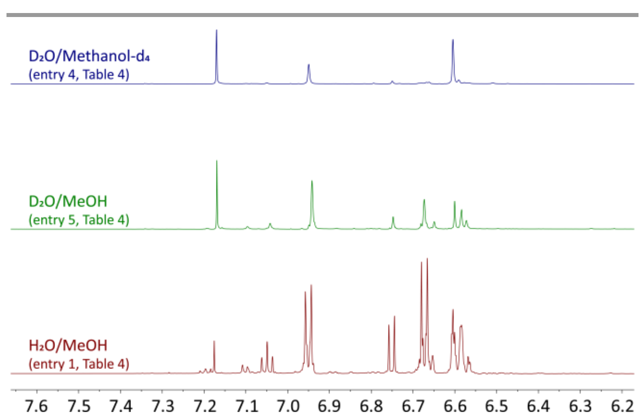

Figure 2.6 ^{1}H NMR in the aromatic region of the products obtained after DHE reactions in D_2O/methanol-d_4 (top, entry 4 in Table 2.4) D_2O/MeOH (middle, entry 5 in Table 4) and H_2O/MeOH (bottom, entry 1 in Table 2.4)

Figure 2.6 displays the aromatic regions of the ^{1}H NMR spectra of products isolated after reactions in H_2O/MeOH (entry 1, Table 2.4), D_2O/methanol-d4 (entry 4, Table 2.4) and D_2O/MeOH (entry 5, Table 2.4). SI Figure S-2.4 displays the aliphatic regions of these spectra.

A particularly meaningful comparison is between the spectra of entries 1 and 4 in Table 2.4 since the product distributions for these are very similar with (**4**) being the primary aromatic product in each case. Simple inspection of these spectra shows that considerable exchange of the aromatic protons with the solvents accompanies the transformation of DHE to the phenolic product (**4**). Their similar patterns in the aliphatic region indicate the deuterated reactants and solvent have little influence on the exchange of alkyl protons. The ^{2}H NMR spectrum of the product mixture from entry 4 in Table 2.4 confirms the introduction of both aromatic and aliphatic hydrogens from the deuterated solvent (SI Figure S-2.5).

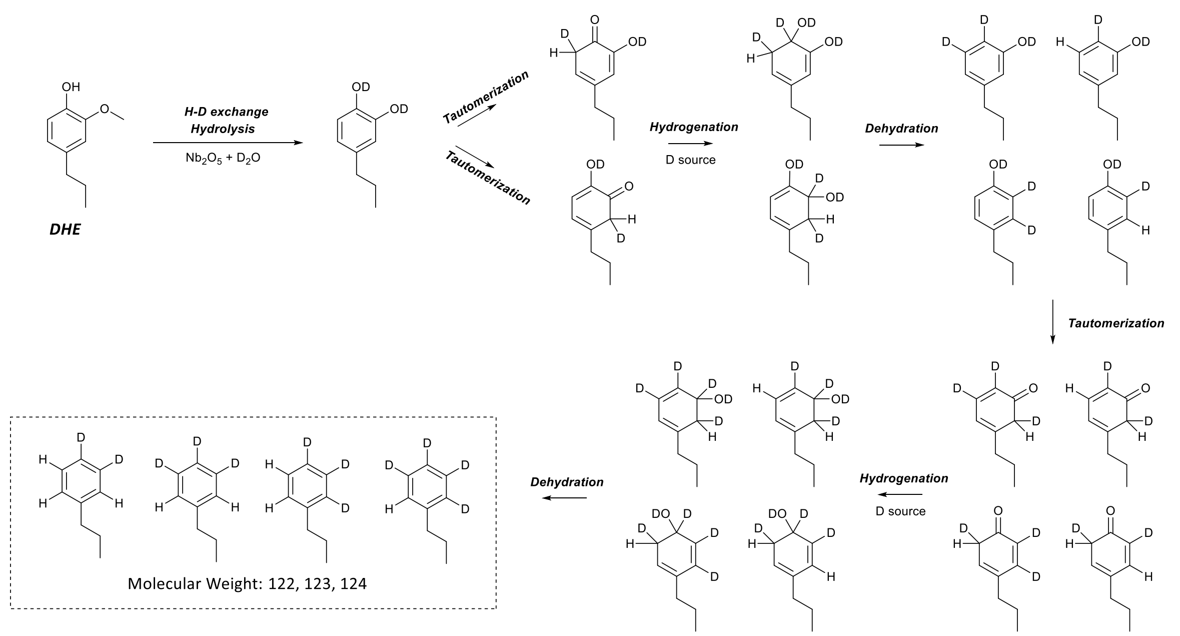

Scheme 2.2 Hypothetical pathways for exchange of aromatic protons with solvent. H-D exchange reaction is very fast in water.

The same conclusion can be drawn from the mass spectrum (obtained by GC-MS analysis) of product (**2**) formed by reaction in D_2O/methanol-d_4 (entry 4, Table 2.4). The parent MS peak for propylbenzene should appear at mass 120, but the major peak in this region of the MS spectrum (SI Figure S-2.6) appeared at M /e 123, again indicating that H/D exchange of the aromatic ring occurred prior to ring hydrogenation. Scheme 2.2 offers a plausible pathway for such exchange via tautomerization of the catechol product (**4**) formed by hydrolysis of the DHE methoxy group.

The proposed catechol tautomerization mechanism was tested by carrying out the reaction of p-cresol with Nb_2O_5 with D_2O under 6 bar H_2 at 250 ℃ for 12 h. No HDO of this substrate was observed, but inspection of the aromatic region ^2H NMR and mass spectrum of the recovered p-cresol (SI Figure S-2.7) showed that there had been considerable hydrogen exchange with the solvent, as would be expected via tautomerization as illustrated in Scheme 2.2.

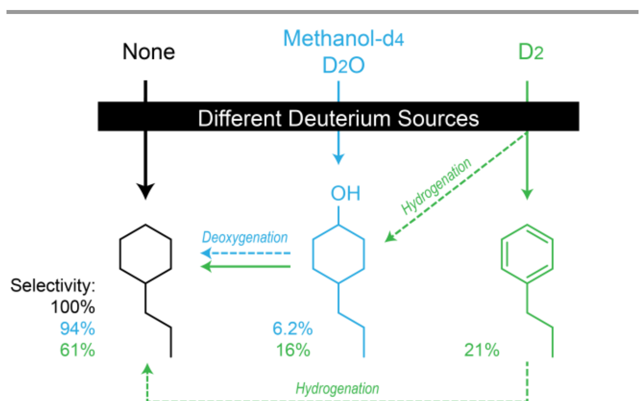

Scheme 2.3 The apparent roles of different hydrogen sources.

Table 2.4 also lists the DHE reaction run with the two catalysts in the H_2O/MeOH solvent with D_2 at a pressure of 6 bar (entry 8, Table 2.4). In this case, the yield of (**1**) was only 61% as opposed to the 100% selectivity seen under comparable conditions with H_2 (entry 6, Table 2.4). Products (**2**) (21%) and (**3**) (16%) made up the bulk of the other products. Thus, there is a substantial kinetic isotope effect on the HDO and aromatic ring reduction reactions upon replacing H_2 with D_2. The ^2H NMR spectrum of the product mixture shows deuterium in the aliphatic region corresponding to (**1**) and (**3**) and no deuterium in the aromatic region (SI Figure

S-2.8), consistent with dihydrogen (H_2/D_2) as the source of aromatic hydrogenation. Scheme 2.3 outlines the various pathways indicated by these isotope effects.

2.4.3 Catalyst recyclability and stability test

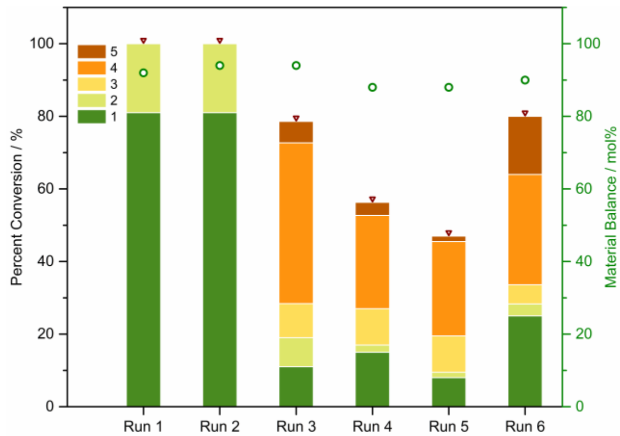

Figure 2.7 Performance of catalyst reusability. The catalyst mixture was washed twice using ethanol, dried in vacuum chamber at RT for 24 h, and heated in oven at 120 ℃ for 1 h prior to the next run. For Run 4, catalyst was calcinated under N_2 at 450 ℃ for another 45 min before use. For Run 5, catalyst was reduced under H_2 (5 %)/Ar at 350 ℃ for 3 h before use. For run 6, fresh Nb_2O_5 0.1 g was added to the recovered catalyst (0.2 g remained after run 5). The height of the bar represents the amount of conversion while the small circle represents the material balance of recovered reactant and products which averaged ~91% after workup.

The recyclability of the Ru/C and Nb_2O_5 mixture for DHE conversion was tested in five successive runs (Figure 2.7 and SI Table S-2.2). An optimized reaction condition with higher substrate loading (1 mL DHE) and longer reaction time (16 h) was applied to understand the performance of this catalyst mixture. Within the first two runs, 12.5 mmol DHE was fully converted to products (**1**) (81%) and (**2**) (19%) (Runs 1 and 2, Figure 2.7 and SI Table S-2.2). The conversion of DHE decreased significantly to 78.6%, for run 3. Attempts to reactivate the catalyst mixture by calcining at 450 ℃ (run 4) or heating under H_2 (run 5) were unsuccessful with conversion dropping to 56%, and 47%, respectively. Thus, the catalyst mixture became less active toward HDO reactions after the second recycle given that propyl phenol (**4**) was the main product in the last three runs. Overall, the catalyst mixture was able to catalyze the reaction of 15.06 mmol DHE to fully deoxygenated products (**1**) and (**2**) during the first five runs. Notably, the addition of fresh Nb_2O_5 (0.1 g) led to a marked increase in conversion (80%) and yield of hydrocarbon products. For the six runs the material balance of recovered reactant and products averaged 91±3 mol%.

The calculated TON for hydrocarbon production for the first 5 runs was 301 based on the ruthenium (0.05 mmol) or 20 based on the Nb_2O_5 (0.75 mmol) initially present.

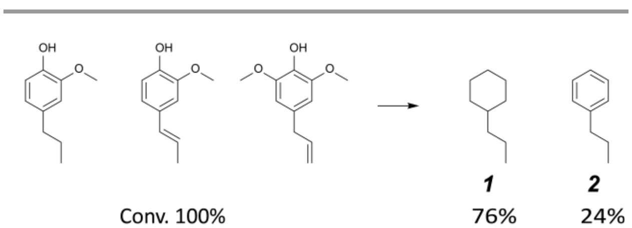

Figure 2.8 The reaction with a mixture of monolignols: dihydoeugenol (DHE), isoeugenol and 4-allylsyringol. Conditions: 70 µL of each substrate, Ru/C (100 mg), Nb_2O_5 (200 mg), H_2O (12 mL), MeOH (1.2 mL), $P(H_2)$ = 11 bar, 250 ℃, 12 h reaction time.

2.4.4 Application to a mixture of lignin monomers.

DHE, isoeugenol, and 4-allylsyringol are among the most common lignin monomers. When a mixture of these three substrates (70 µL of each) was subjected to the standard procedure for 12 h, the only products were the hydrocarbons (**1**) (76%) and (**2**) (24%) according to GC analysis (Figure 2.8). Since a 100% yield of (**1**) can be achieved with an extended reaction time, this system offers a viable new strategy for funnelling the multiple monolignols from lignin disassembly into a much simpler mixture of C9 alkanes.

2.5 Discussion

Reported are batch reactor studies addressing the hydrodeoxygenation (HDO) of the lignin monomer dihydroeugenol to the hydrocarbons propyl cyclohexane (**1**) and propyl benzene

(**2**). This transformation is affected by a Ru/C and Nb_2O_5 co-catalyst mixture under H_2 in an aqueous medium containing a small amount of methanol additive. The key observations are:

(a) MeOH serves as a secondary hydrogen donor that promotes HDO under lower H_2 pressures compared to current methods.[37-41] The overall reaction appears optimal with a H_2O/MeOH ratio ~15 and H_2 pressures of 1-6 bar. The increased pressure after the reaction and the presence of CO_2 in the gas phase (SI Figure S-2.9) are consistent with methanol being reformed in the presence of Ru/C.

(b) The Nb_2O_5 is primarily active in the conversion of DHE to 4-propylcatechol (**5**), presumably by hydrolysis of the methoxy group.[42] The Nb_2O_5 prepared in this laboratory and calcined at 450 °C was much more active than a commercial sample that was apparently calcined at a much higher temperature.[43] The difference was attributed to the much greater number of acid sites on the former material as shown by NH_3-TPD test (Figure S-2.1).[44]

(c) Ru/C catalyzes HDO of (**5**) and the subsequently formed intermediates 4-propylcyclohexan-1-ol (**3**) and 4-propylphenol (**4**), and hydrogenation of the aromatic ring.[45, 46] The Ru/C is more effective after pre-treatment by heating under H_2. While Ru/C alone can catalyze HDO of DHE to products (**1**)-(**4**), the synergistic activity of the two-catalyst system is more efficient and selective, toward as much as 100% conversion and selectivity to propylcyclohexane (**1**).

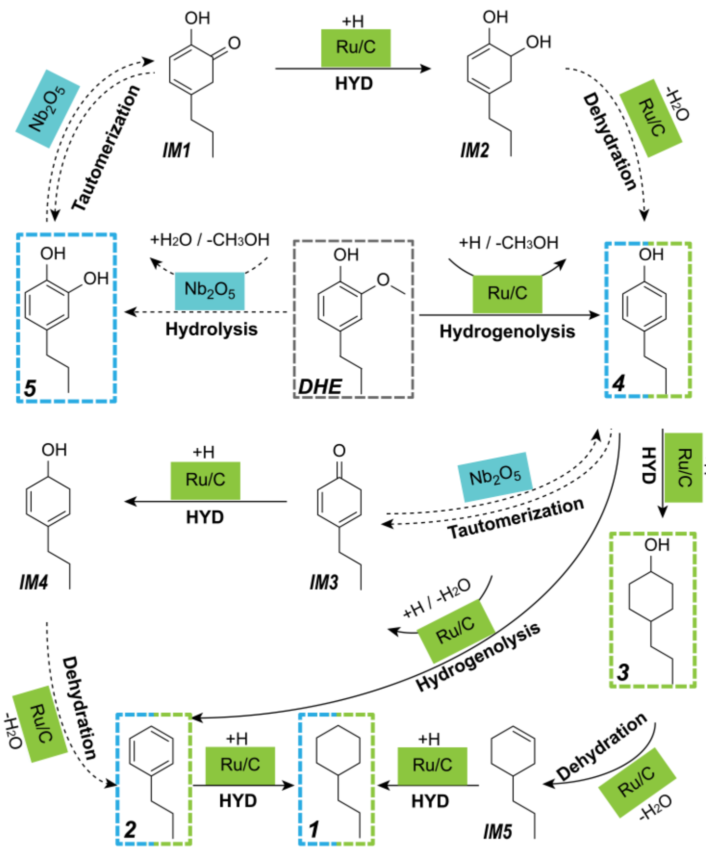

Scheme 2.4 A proposed sequence of mechanistic steps for conversion of DHE by the catalyst mixture Ru/C and Nb_2O_5 in a H_2O/MeOH medium under H_2. Hydrogenation is abbreviated as "HYD".

Scheme 2.4 outlines the likely sequence of catalyzed reactions leading to the potential products. Conversion of DHE is initiated into two pathways by each catalyst. The proposed mechanism of Ru/C catalyzed HDO is, highlighted in green colour with solid arrows in Scheme 2.4). This is based on the observed production of (**1**)-(**4**) with Ru/C alone

(Entries 3 and 4, Table 2.3, and Figure 2.5). The deoxygenated products can be obtained through hydrogenolysis, dehydration, and hydrogenation reactions.

The reactions labelled with dash lines and blue colour in Scheme 4 describe proposed pathways via intermediates (**IM1**)-(**IM4**) facilitated by activated Nb_2O_5 and based upon the observations of 4-propylcatechol (**5**) formation in the initial stage (entry 1, Table 2.3, and Figure 2.4). Key steps in this mechanism are Nb_2O_5 catalyzed tautomerizations of (**4**) and (**5**) to give carbonyl species (**IM1** & **IM3**) followed by activated Ru/C catalyzed hydrogenation to give a cyclic diene alcohols (**IM2**, **IM4**), that upon dehydration are rearomatized to (**2**) and (**4**), respectively.[47] Support for the tautomerization steps was the observation that Nb_2O_5 alone catalyzes the deuteration of the aromatic C-H groups with solvent D_2O as demonstrated by ^{2}H NMR and MS experiments (Figure S-2.5 and Scheme S-2.1). Notably, even though this reaction was run under H_2, no HDO of p-cresol occurred in the absence of Ru/C. Therefore, all the dehydration reactions should be primarily catalyzed by Ru/C. This point was verified by examining the reactions of a mixture of propyl cyclohexanol (**3**) and 2-methoxy-4-propylcyclohexanol with either Ru/C or Nb_2O_5 alone under the standard conditions (SI Table S-2.3). In the former case, nearly 100% conversion to propyl cyclohexane (**1**) was achieved: however, with Nb_2O_5 alone, conversion was 62% with only 14.5% selectivity towards (**1**) and the remaining products were not identified.

The reactions with deuterated solvents (D_2O, methanol-d_4) and with D_2 summarized in Table 4 provide further insight into the HDO/hydrogenation mechanism(s). Strong isotope effects on the product are observed upon using D_2O and methanol-d_4. These are particularly evident in the Ru/C catalyzed HDO steps of (**5**) → (**4**) as well as (**4** & **3**) → (**1**

& **2**). What's more, the final pressure in the reactor is lower when using methanol-d_4. An isotope effect was also evident when D_2 (6 bar) replaced H_2 (6 bar) in a reaction with the H_2O/MeOH medium. In this case, the principal isotope effect was some decrease in ring hydrogenation further supporting the view that MeOH and H_2 supply reducing equivalents at distinctly different stages of the reaction.

The stability and reusability tests show this co-catalyst system to be recyclable and stable during the first 32 h in producing a clean cut of C9 hydrocarbons and excellent material balance of isolated products >90%. The catalyst system displayed decreasing activity in the second, third and fourth recycles (Run 3, 4, and 5 in Figure 2.7), although propyl cyclohexane was consistently produced in each case. Notably, adding fresh Nb_2O_5 to the system (Run 6, Figure 2.7) partially restored the activity in terms of the production of (**1**), although the product distribution did not match that of a completely fresh catalyst. Thus, a continuous feeding of fresh Nb_2O_5 after the first recycle could improve the total yield of hydrocarbons and maximize the usability of Ru/C catalyst. Ongoing studies will address strategies to minimize catalyst deactivation pathways.

Lastly, subjecting a simulated bio-oil mixture of lignin monomers to the catalyst system optimal for the conversion of DHE, gave a mixture of just the hydrocarbons (**1**) and (**2**). Thus, this system provides the opportunity to funnel complex bio-oil mixtures primarily composed of oxygenated lignins to simple C9 hydrocarbons more compatible with applications as liquid transportation fuels.

2.6 References:

1. Barta, K.; Ford, P. C., Catalytic Conversion of Nonfood Woody Biomass Solids to Organic Liquids. *Accounts Chem Res* **2014,** *47* (5), 1503-1512.

2. Tuck, C. O.; Perez, E.; Horvath, I. T.; Sheldon, R. A.; Poliakoff, M., Valorization of Biomass: Deriving More Value from Waste. *Science* **2012,** *337* (6095), 695-699.

3. Huber, G. W.; Iborra, S.; Corma, A., Synthesis of transportation fuels from biomass: Chemistry, catalysts, and engineering. *Chem Rev* **2006,** *106* (9), 4044-4098.

4. Li, C. Z.; Zhao, X. C.; Wang, A. Q.; Huber, G. W.; Zhang, T., Catalytic Transformation of Lignin for the Production of Chemicals and Fuels. *Chem Rev* **2015,** *115* (21), 11559-11624.

5. Gallezot, P., Conversion of biomass to selected chemical products. *Chem Soc Rev* **2012,** *41* (4), 1538-1558.

6. Hari, T. K.; Yaakob, Z.; Binitha, N. N., Aviation biofuel from renewable resources: Routes, opportunities and challenges. *Renew Sust Energ Rev* **2015,** *42*, 1234-1244.

7. Xin, Y.; Jing, Y. X.; Dong, L.; Liu, X. H.; Guo, Y.; Wang, Y. Q., Selective production of indane and its derivatives from lignin over a modified niobium-based catalyst. *Chem Commun* **2019,** *55* (63), 9391-9394.

8. Song, W. J.; He, Y. Y.; Lai, S. T.; Lai, W. K.; Yi, X. D.; Yang, W. M.; Jiang, X. M., Selective hydrodeoxygenation of lignin phenols to alcohols in the aqueous phase over a hierarchical Nb2O5-supported Ni catalyst. *Green Chem* **2020,** *22* (5), 1662-1670.

9. Mäkelä, E.; González Escobedo, J. L.; Neuvonen, J.; Lahtinen, J.; Lindblad, M.; Lassi, U.; Karinen, R.; Puurunen, R. L., Liquid-phase Hydrodeoxygenation of 4-Propylphenol to Propylbenzene: Reducible Supports for Pt Catalysts. *Chemcatchem* **2020**.

10. Kim, H.; Ralph, J., Solution-state 2D NMR of ball-milled plant cell wall gels in DMSO-d(6)/pyridine-d(5). *Org Biomol Chem* **2010,** *8* (3), 576-591.

11. Jafarian, S.; Tavasoli, A.; Nikkhah, H., Catalytic hydrotreating of pyro-oil derived from green microalgae spirulina the (Arthrospira) plantensis over NiMo catalysts impregnated over a novel hybrid support. *Int J Hydrogen Energ* **2019,** *44* (36), 19855-19867.

12. Elliott, D. C., Historical developments in hydroprocessing bio-oils. *Energ Fuel* **2007,** *21* (3), 1792-1815.

13. Ramesh, A.; Tamizhdurai, P.; Mangesh, V. L.; Palanichamy, K.; Gopinath, S.; Sureshkumar, K.; Shanthi, K., Mg/SiO2-Al2O3 supported nickel catalysts for the production of naphthenic hydrocarbon fuel by hydro-de-oxygenation of eugenol. *Int J Hydrogen Energ* **2019,** *44* (47), 25607-25620.

14. Karatzos, S.; van Dyk, J. S.; McMillan, J. D.; Saddler, J., Drop-in biofuel production via conventional (lipid/fatty acid) and advanced (biomass) routes. Part I. *Biofuel Bioprod Bior* **2017,** *11* (2), 344-362.

15. Arun, N.; Sharma, R. V.; Dalai, A. K., Green diesel synthesis by hydrodeoxygenation of bio-based feedstocks: Strategies for catalyst design and development. *Renew Sust Energ Rev* **2015,** *48*, 240-255.

16. Zhang, J. J.; Zhao, C., A new approach for bio-jet fuel generation from palm oil and limonene in the absence of hydrogen. *Chem Commun* **2015,** *51* (97), 17249-17252.

17. Ramesh, A.; Tamizhdurai, P.; Suthagar, K.; Sureshkumar, K.; Theres, G. S.; Shanthi, K., Intrinsic role of pH in altering catalyst properties of NiMoP over alumino-silicate for the vapour phase hydrodeoxygenation of methyl heptanoate. *New J Chem* **2019,** *43* (8), 3545-3555.

18. Dong, L.; Shao, Y.; Han, X.; Liu, X. H.; Xia, Q. N.; Parker, S. F.; Cheng, Y. Q.; Daemen, L. L.; Ramirez-Cuesta, A. J.; Wang, Y. Q.; Yang, S. H., Comparison of two multifunctional catalysts [M/Nb2O5 (M = Pd, Pt)] for one-pot hydrodeoxygenation of lignin. *Catal Sci Technol* **2018,** *8* (23), 6129-6136.

19. Jin, S. H.; Guan, W. X.; Tsang, C. W.; Yan, D. Y. S.; Chan, C. Y.; Liang, C. H., Enhanced Hydroconversion of Lignin-Derived Oxygen-Containing Compounds Over Bulk Nickel Catalysts Though Nb2O5 Modification. *Catal Lett* **2017,** *147* (8), 2215-2224.

20. Teles, C. A.; de Souza, P. M.; Rabelo-Neto, R. C.; Griffin, M. B.; Mukarakate, C.; Orton, K. A.; Resasco, D. E.; Noronha, F. B., Catalytic upgrading of biomass pyrolysis vapors and model compounds using niobia supported Pd catalyst. *Appl Catal B-Environ* **2018,** *238*, 38-50.

21. Zarchin, R.; Rabaev, M.; Vidruk-Nehemya, R.; Landau, M. V.; Herskowitz, M., Hydroprocessing of soybean oil on nickel-phosphide supported catalysts. *Fuel* **2015,** *139*, 684-691.

22. He, Z.; Wang, X., Hydrodeoxygenation of model compounds and catalytic systems for pyrolysis bio-oils upgrading. *Catalysis for Sustainable Energy* **2012,** *1*.

23. Ding, L. N.; Wang, A. Q.; Zheng, M. Y.; Zhang, T., Selective Transformation of Cellulose into Sorbitol by Using a Bifunctional Nickel Phosphide Catalyst. *Chemsuschem* **2010,** *3* (7), 818-821.

24. Wang, H. L.; Yan, S. L.; Salley, S. O.; Ng, K. Y. S., Support effects on hydrotreating of soybean oil over NiMo carbide catalyst. *Fuel* **2013,** *111*, 81-87.

25. Alexander, A. M.; Hargreaves, J. S. J., Alternative catalytic materials: carbides, nitrides, phosphides and amorphous boron alloys. *Chem Soc Rev* **2010,** *39* (11), 4388-4401.

26. Li, K. L.; Wang, R. J.; Chen, J. X., Hydrodeoxygenation of Anisole over Silica-Supported Ni2P, MoP, and NiMoP Catalysts. *Energ Fuel* **2011,** *25* (3), 854-863.

27. Zhong, X.; Jiang, Y.; Chen, X. L.; Wang, L.; Zhuang, G. L.; Li, X. N.; Wang, J. G., Integrating cobalt phosphide and cobalt nitride-embedded nitrogen-rich nanocarbons: high-performance bifunctional electrocatalysts for oxygen reduction and evolution. *J Mater Chem A* **2016,** *4* (27), 10575-10584.

28. Lu, M. H.; Du, H.; Wei, B.; Zhu, J.; Li, M. S.; Shan, Y. H.; Song, C. S., Catalytic Hydrodeoxygenation of Guaiacol over Palladium Catalyst on Different Titania Supports. *Energ Fuel* **2017,** *31* (10), 10858-10865.

29. Kim, M.; Ha, J. M.; Lee, K. Y.; Jae, J., Catalytic transfer hydrogenation/hydrogenolysis of guaiacol to cyclohexane over bimetallic RuRe/C catalysts. *Catal Commun* **2016,** *86*, 113-118.

30. Leal, G. F.; Lima, S.; Graca, I.; Carrer, H.; Barrett, D. H.; Teixeira-Neto, E.; Curvelo, A. A. S.; Rodella, C. B.; Rinaldi, R., Design of Nickel Supported on Water-Tolerant Nb2O5 Catalysts for the Hydrotreating of Lignin Streams Obtained from Lignin-First Biorefining. *Iscience* **2019,** *15*, 467-+.

31. Nowak, I.; Ziolek, M., Niobium compounds: Preparation, characterization, and application in heterogeneous catalysis. *Chem Rev* **1999,** *99* (12), 3603-3624.

32. Alharbi, W.; Kozhevnikova, E. F.; Kozhevnikov, I. V., Dehydration of Methanol to Dimethyl Ether over Heteropoly Acid Catalysts: The Relationship between Reaction Rate and Catalyst Acid Strength. *Acs Catal* **2015,** *5* (12), 7186-7193.

33. Guo, T. Y.; Li, X. C.; Liu, X. H.; Guo, Y.; Wang, Y. Q., Catalytic Transformation of Lignocellulosic Biomass into Arenes, 5-Hydroxymethylfurfural, and Furfural. *Chemsuschem* **2018,** *11* (16), 2758-2765.

34. Jehng, J. M.; Wachs, I. E., The Molecular-Structures and Reactivity of Supported Niobium Oxide Catalysts. *Catalysis Today, Vol 8, No 1* **1990**, 37-55.

35. Xia, Q. N.; Cuan, Q.; Liu, X. H.; Gong, X. Q.; Lu, G. Z.; Wang, Y. Q., Pd/NbOPO4 Multifunctional Catalyst for the Direct Production of Liquid Alkanes from Aldol Adducts of Furans. *Angew Chem Int Edit* **2014,** *53* (37), 9755-9760.

36. Ziolek, M.; Sobczak, I., The role of niobium component in heterogeneous catalysts. *Catal Today* **2017,** *285*, 211-225.

37. Roldugina, E. A.; Naranov, E. R.; Maximov, A. L.; Karakhanov, E. A., Hydrodeoxygenation of guaiacol as a model compound of bio-oil in methanol over mesoporous noble metal catalysts. *Appl Catal a-Gen* **2018,** *553*, 24-35.

38. Wang, X.; Zhu, S. H.; Wang, S.; He, Y.; Liu, Y.; Wang, J. G.; Fan, W. B.; Lv, Y. K., Low temperature hydrodeoxygenation of guaiacol into cyclohexane over Ni/SiO2 catalyst combined with H beta zeolite. *Rsc Adv* **2019,** *9* (7), 3868-3876.

39. Yu, M. J.; Park, S. H.; Jeon, J. K.; Ryu, C.; Sohn, J. M.; Kim, S. C.; Park, Y. K., Hydrodeoxygenation of Guaiacol Over Pt/Al-SBA-15 Catalysts. *J Nanosci Nanotechno* **2015,** *15* (1), 527-531.

40. Lee, H.; Kim, H.; Yu, M. J.; Ko, C. H.; Jeon, J. K.; Jae, J.; Park, S. H.; Jung, S. C.; Park, Y. K., Catalytic Hydrodeoxygenation of Bio-oil Model Compounds over Pt/HY Catalyst. *Sci Rep-Uk* **2016,** *6*.

41. Heroguel, F.; Nguyen, X. T.; Luterbacher, J. S., Catalyst Support and Solvent Effects during Lignin Depolymerization and Hydrodeoxygenation. *Acs Sustain Chem Eng* **2019,** *7* (20), 16952-16958.

42. Dong, L.; Xin, Y.; Liu, X. H.; Guo, Y.; Pao, C. W.; Chen, J. L.; Wang, Y. Q., Selective hydrodeoxygenation of lignin oil to valuable phenolics over Au/Nb2O5 in water. *Green Chem* **2019,** *21* (11), 3081-3090.

43. Chan, X. J.; Pu, T. C.; Chen, X. Y.; James, A.; Lee, J.; Parise, J. B.; Kim, D. H.; Kim, T., Effect of niobium oxide phase on the furfuryl alcohol dehydration. *Catal Commun* **2017,** *97*, 65-69.

44. Lebarbier, V.; Houalla, M.; Onfroy, T., New insights into the development of Bronsted acidity of niobic acid. *Catal Today* **2012,** *192* (1), 123-129.

45. Michel, C.; Gallezot, P., Why Is Ruthenium an Efficient Catalyst for the Aqueous-Phase Hydrogenation of Biosourced Carbonyl Compounds? *Acs Catal* **2015,** *5* (7), 4130-4132.

46. Duong, N. N.; Aruho, D.; Wang, B.; Resasco, D. E., Hydrodeoxygenation of anisole over different Rh surfaces. *Chinese J Catal* **2019,** *40* (11), 1721-1730.

47. de Souza, P. M.; Rabelo-Neto, R. C.; Borges, L. E. P.; Jacobs, G.; Davis, B. H.; Sooknoi, T.; Resasco, D. E.; Noronha, F. B., Role of Keto Intermediates in the Hydrodeoxygenation of Phenol over Pd on Oxophilic Supports. *Acs Catal* **2015,** *5* (2), 1318-1329.

2.7 Supporting Information

Contents

Figure S-2.2 SEM (a) and TEM (b) images of Nb_2O_5 catalyst.

Figure S-2.3 NH_3-TPD profile of different Nb_2O_5 catlaysts.

Figure S-2.4 ^{1}H NMR in the aliphatic region of the products obtained after DHE reactions in D_2O/methanol-d_4, D_2O/MeOH and H_2O/MeOH.

Figure S-2.5 ^{2}H NMR spectrum of products obtained from the reaction of DHE in D_2O and methanol-d_4.

Figure S-2.6 GC-MS of propyl benzene obtained as a product from the reaction of DHE in D_2O and methanol-d_4.

Figure S-2.7 ^{2}H NMR spectra and GC-MS of p-cresol after reaction with Nb_2O_5 in D_2O.

Figure S-2.8 ^{2}H NMR spectrum of the products from the catalyzed reaction of DHE with D_2 in H_2O and MeOH.

Figure S-2.9 GC-TCD analysis of a typical reaction in the co-catalyst system.

Schemes: 1

Scheme S-2.1 The mechanism of p-cresol reacting with Nb_2O_5 in D_2O.

2.7.1 Tables

Table S-2.1 Time profile of co-catalyst system

Entry	Time (h)	Conv. (%)	Product Distribution (%)				
			1	**2**	**3**	**4**	**5**
1[a]	2	14	-	-	-	100	-
2[b]	2	41	-	-	-	18	82
3	2	36	4	5.9	9.4	65	16
4	4	100	35	33	31	-	-
5	8	100	94	6.4	-	-	-
6[c]	12	100	100	-	-	-	-

Reaction condition: DHE 0.2 mL, Ru/C 100 mg, Nb_2O_5 200 mg, H_2O 12 mL, methanol 0.8 mL, P(H_2) = 6 bar, 250 °C, 12h. [a] Reaction with Ru/C only. [b] Reaction with Nb_2O_5 only. [C] The same experiment as entry 4 in Table 2.

Table S-2.2 Catalyst recyclability test

Run	Conv. (%)	Product Distribution (%)					Material balance (mol%)
		1	**2**	**3**	**4**	**5**	
1	100	81	19	-	-	-	92
2	100	81	19	-	-	-	94
3	78.6	14	10	12	56	8	94
4[a]	56.3	27	4	18	46	6	88
5[b]	47	17	3	21	55	3	88
6[c]	80	31	4	7	38	20	90

Reaction condition: DHE 1 mL, Ru/C 100 mg, Nb_2O_5 200 mg, H_2O 12 mL, methanol 1 mL, $P(H_2)$ = 6 bar, 250 ℃, 16 h. Unless noted, the catalyst was washed using ethanol twice, dried in vacuum chamber at room temperature for 24 h and in oven at 120 ℃ for 1 h before using for next run. [a] Catalyst was calcinated under N_2 at 450 ℃ for another 45 min before use. [b] Catalyst was reduced under H_2(5%)/Ar at 350 ℃ for another 3 h before use. [c] Fresh Nb_2O_5 0.1 g was added into the reused catalyst mixture (0.2 g left after five runs) for the Run 6.

Table S-2.3 Reaction with cyclohexanol feedstock over Ru/C or Nb_2O_5 alone.

Entry	Substrate	Conv. (%)	Product Distribution (%)	
			1	**other**
1	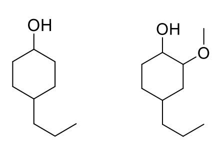	99	100	0
2		62	14.5	85.5

Reaction condition: propyl cyclohexanol and 2-methoxy-4-propycyclohexanol mixture (1:1) 0.4 mL, Ru/C 100 mg (entry 1) or Nb_2O_5 200 mg (entry 2), H_2O 12 mL, methanol 0.8 mL, initial $P(H_2)$ = 6 bar, 250 ℃, 12 h.

2.7.2 Figures

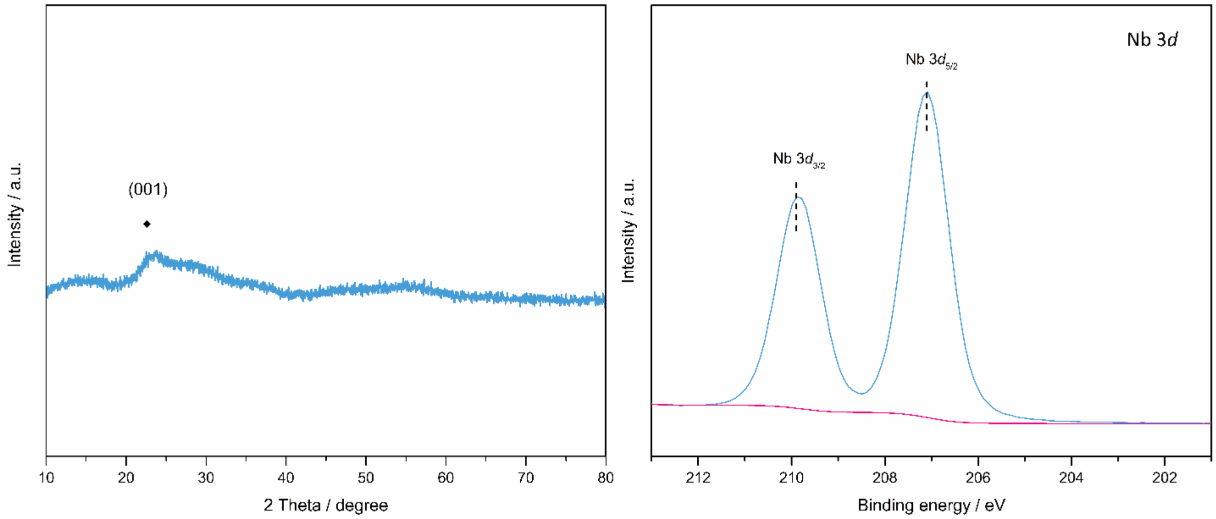

Figure S-2.1 XRD pattern (left) and XPS analysis (right) of Nb_2O_5 catalyst. According to XRD pattern of Nb_2O_5 (left), only one broad diffraction peak located at about 22.7^o is observed, which corresponds to the facet (001). No sharp peak is observed, which suggests that the synthesized Nb_2O_5 has the amorphous structure. XPS analysis was also performed to obtain the oxidation state (right). The catalyst shows the typical Nb 3$d_{3/2}$ (209.9 eV) and Nb 3$d_{5/2}$ (207.1 eV) peaks of Nb^{5+}.[1] No other peaks were obtained.

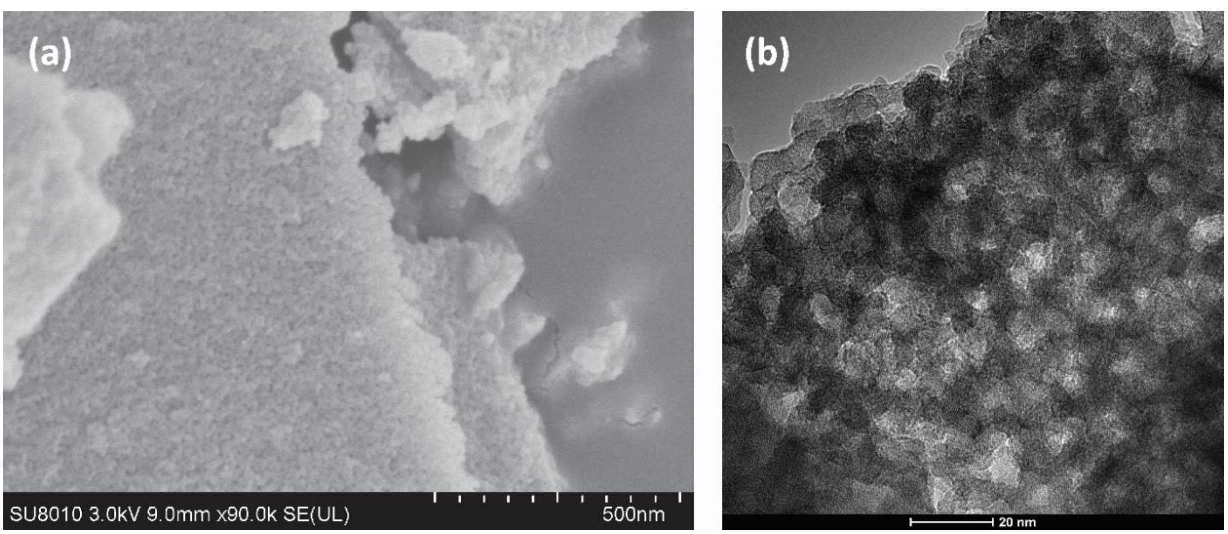

Figure S-2.2 SEM (a) and TEM (b) images of Nb_2O_5 catalyst. According to the SEM image, the bulk-shape particles of synthesized Nb_2O_5 are not the crystalline form. Numerous pores are evenly distributed on the top and cross section of the catalyst evenly. From the TEM image, the inner pores of Nb_2O_5 can be observed more clearly. The pores are not regular but has relatively consistent pore size that is around 5 nm. Combining with the XRD result, the synthesized Nb_2O_5 is an amorphous mesoporous solid.

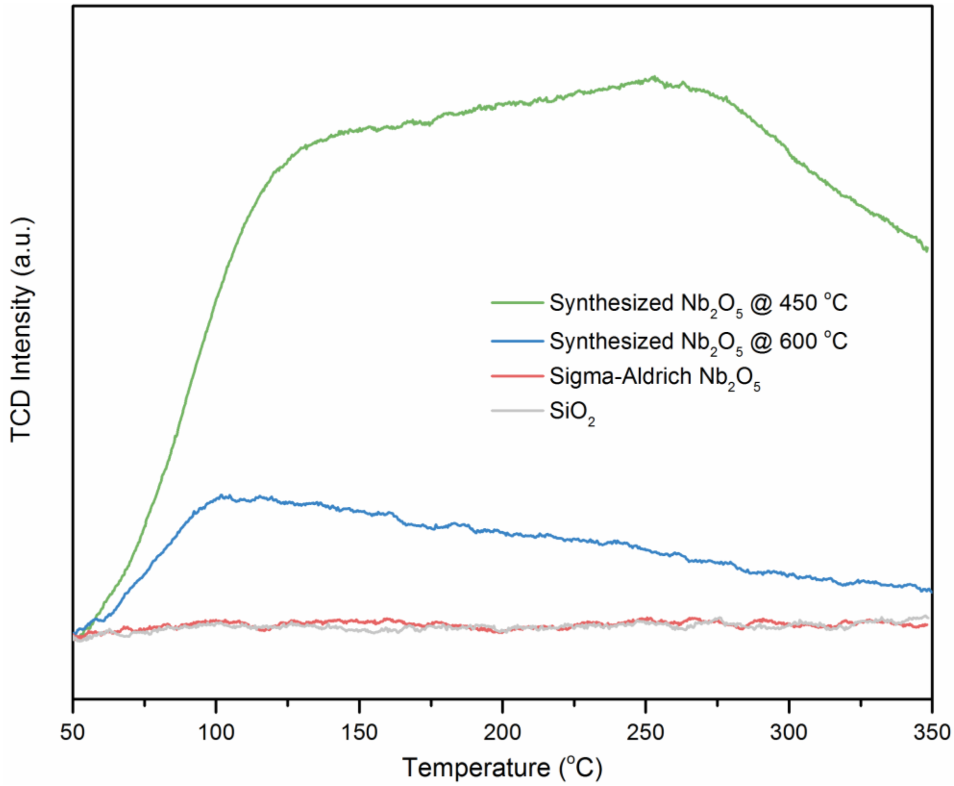

Figure S-2.3 NH_3-TPD profiles of different Nb_2O_5 catalysts. The Nb_2O_5 was prepared by using niobium (V) chloride and CTAB in a Teflon lined autoclave and calcinated at 450 °C and 600 °C, respectively. Nb_2O_5 purchased from Sigma-Aldrich used as is. SiO_2 has no acid sites and was analyzed for comparison. 0.2600 g Nb_2O_5 prepared at 450°C, 0.1964 g Nb_2O_5 prepared at 600°C, 0.2210 g purchased Nb_2O_5, and 0.2173 g SiO_2 samples were loaded for NH_3-TPD analysis. The ammonia adsorption was determined in term of mmol of NH_3 per gram of loaded sample.

The acid property of Nb_2O_5 catalyst is sensitive to the calcination temperature. According to the figure, Nb_2O_5 calcinated at 450 °C adsorbs the largest amount of ammonia among other samples which indicates the 450 °C Nb_2O_5 has the most abundant acid sites. When the calcination temperature increased to 600 °C, the acid sites reduced dramatically. And the purchased Nb_2O_5 from Sigma-Aldrich has been reported to be calcinated at 1000 °C almost has no acid sites comparing to SiO_2.[2] According to our results, abundant acid sites of Nb_2O_5 are vital to our HDO reactions. From entries 1 and 2 in Table 3, Nb_2O_5 calcinated at 450 °C promotes the hydrolysis to catechol (**5**) and dehydroxylation to phenol (**4**) but the purchased Nb_2O_5 shows no activity.

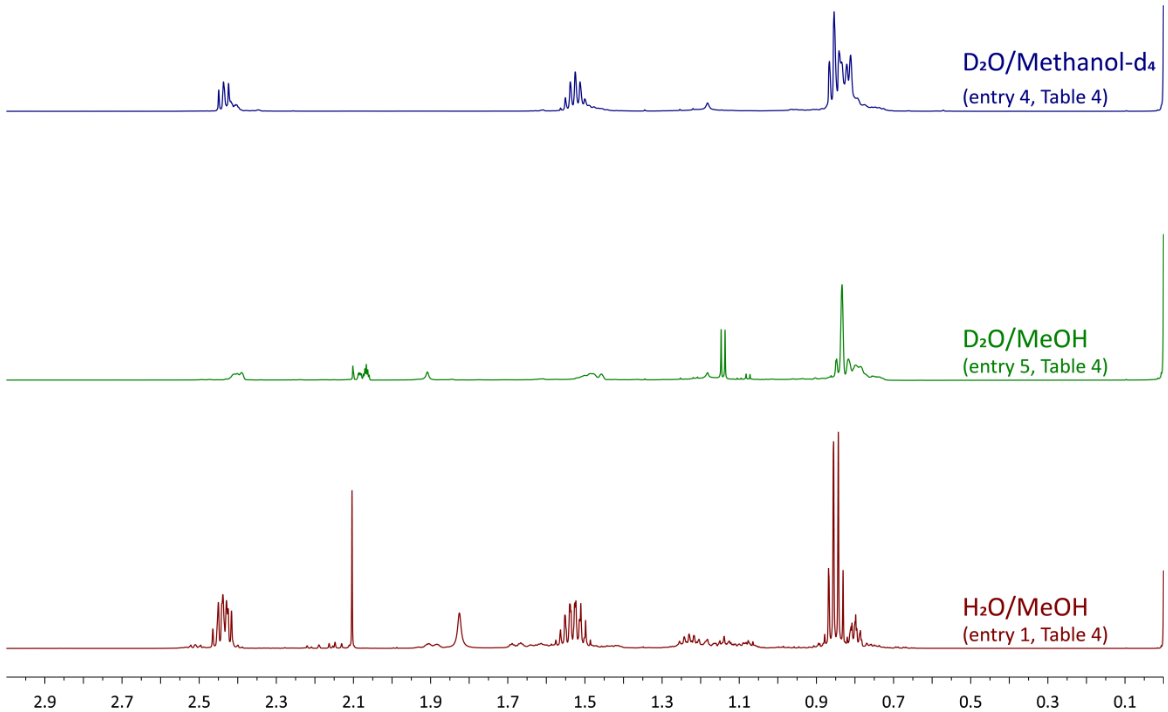

Figure S-2.4 ^{1}H NMR in the aliphatic region of the products obtained after DHE reactions in D_2O/methanol-d_4 (top, entry 4 in Table 4) D_2O/MeOH (middle, entry 5 in Table 4) and H_2O/MeOH (bottom, entry 2 in Table 4). Conditions: DHE 0.2 mL, Ru/C 100 mg, Nb_2O_5 200 mg, water 12 mL, methanol 0.8 mL, purged with H_2 and vented to P(H_2) = 1 bar, 250 °C, 12 h reaction time. For the entry 4 in Table 4 (top), the reaction time was 24 h; for the entry 1 in Table 4 (bottom), 0.4 mL MeOH was used.

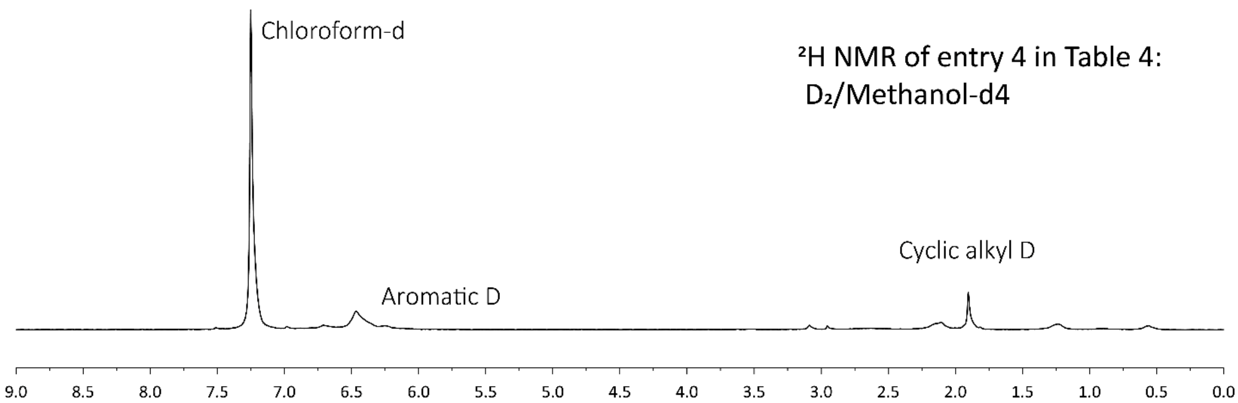

Figure S-2.5 ^2H NMR spectrum of products obtained from the reaction of DHE in D_2O and methanol-d_4. Conditions: DHE 0.2 mL, Ru/C 100 mg, Nb_2O_5 200 mg, D_2O 12 mL, methanol-d_4 0.8 mL, purged with H_2 and vented to $P(H_2)$ = 1 bar, 250 °C, 24 h reaction time.

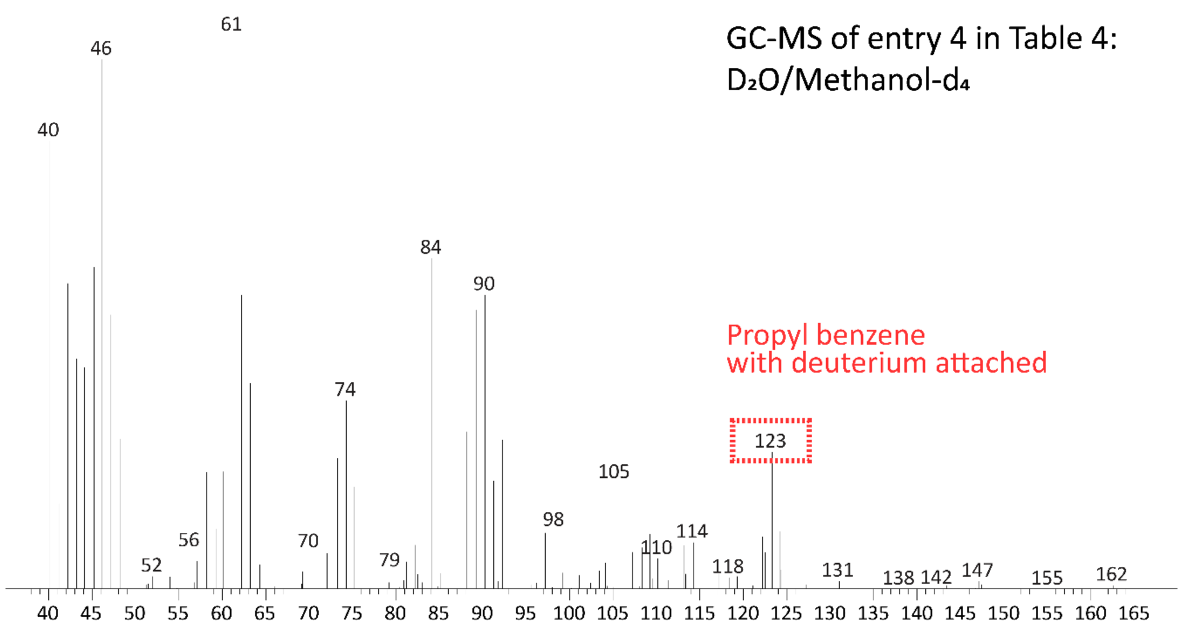

Figure S-2.6 GC-MS of propyl benzene obtained from the reaction of DHE in D_2O and methanol-d_4. Conditions: DHE 0.2 mL, Ru/C 100 mg, Nb_2O_5 200 mg, D_2O 12 mL, methanol-d_4 0.8 mL, purged with H_2 and vented to $P(H_2)$ = 1 bar, 250 °C, 24 h reaction time.

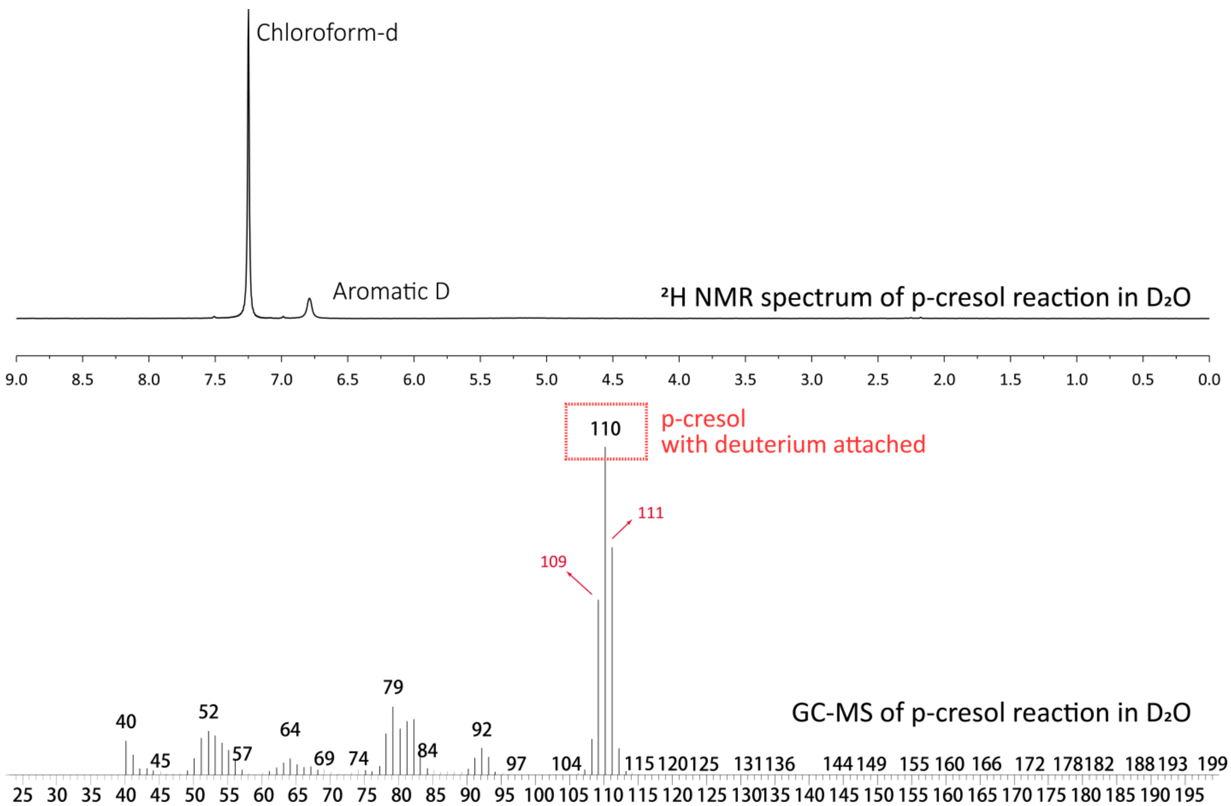

Figure S-2.7 ^{2}H NMR (above) and GC-MS (bottom) spectra of p-cresol after reaction with Nb_2O_5 in D_2O. Conditions: p-cresol 0.2 mL, Nb_2O_5 200 mg, D_2O 12 mL, $P(H_2)$ = 6 bar, 250 °C, 12 h reaction time. No HDO product was observed after reaction. However, the molecular weight of p-cresol was detected to be M/e 109, 110, and 111 by GC-MS. This suggests that up to three aromatic hydrogens on p-cresol exchanged with the solvent D_2O during the reaction. The aromatic deuteriums detected upon recording the ^{2}H NMR spectrum of the p-cresol after reaction, can be explained by the tautomerization mechanism (Scheme S-1).

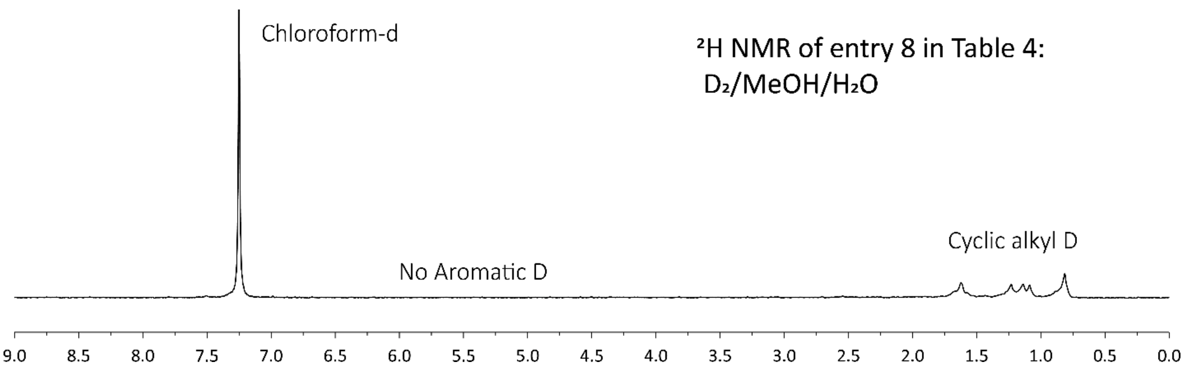

Figure S-2.8 ^{2}H NMR spectrum of the products from the catalyzed reaction of DHE with D_2 in H_2O and MeOH. Conditions: DHE 0.2 mL, Ru/C 100 mg, Nb_2O_5 200 mg, H_2O 12 mL, MeOH 0.8 mL, P(D_2) at RT = 6 bar, 250 ℃, 24 h reaction time.

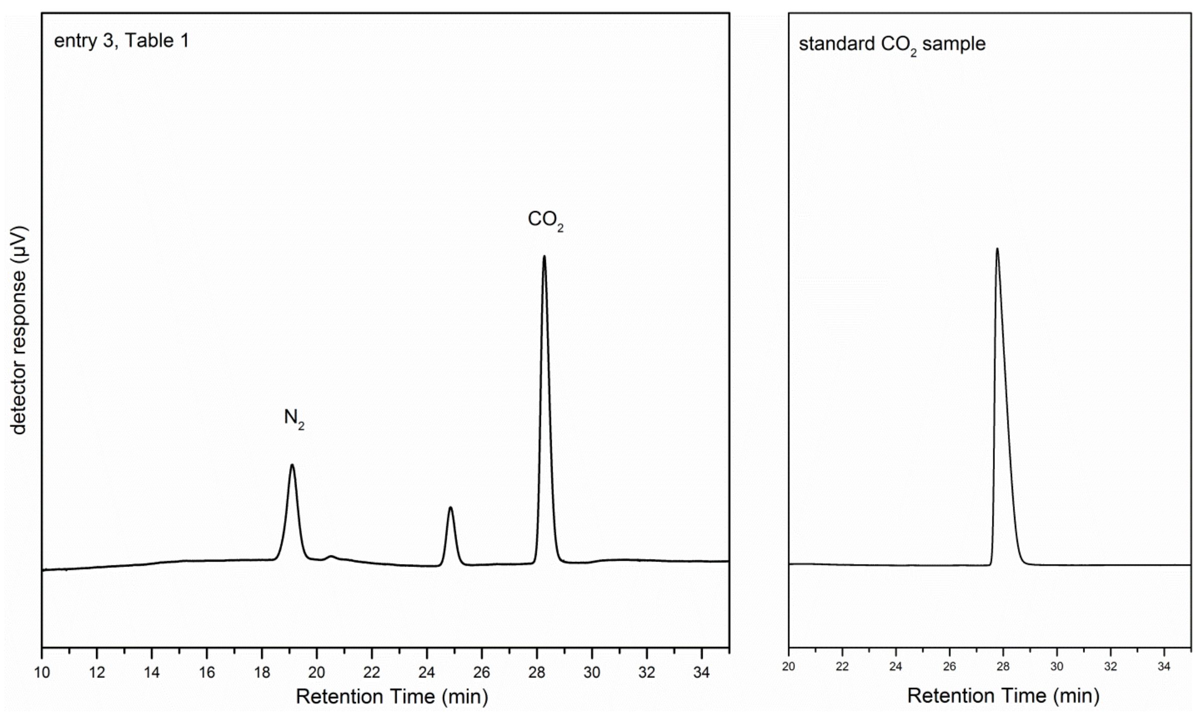

Figure S-2.9 GC-TCD analysis of a typical reaction in the co-catalyst system (entry 3, Table 1). The gas phase products were collected after reaction (left). A standard CO_2 sample was obtained and analyzed for peak assignment by its retention time at 28.2 to 28. 5 min (right). Reaction condition: DHE 0.2 mL, Ru/C 100 mg, Nb_2O_5 200 mg, H_2O 12 mL, methanol 0.8 mL, P(H_2) = 1 bar, 250 ℃, 12 h. CO_2 gas was detected as the main product in gas phase after the HDO reaction. It was evident that catalytic reforming of methanol occurs in this co-catalyst system.

2.7.3 Scheme

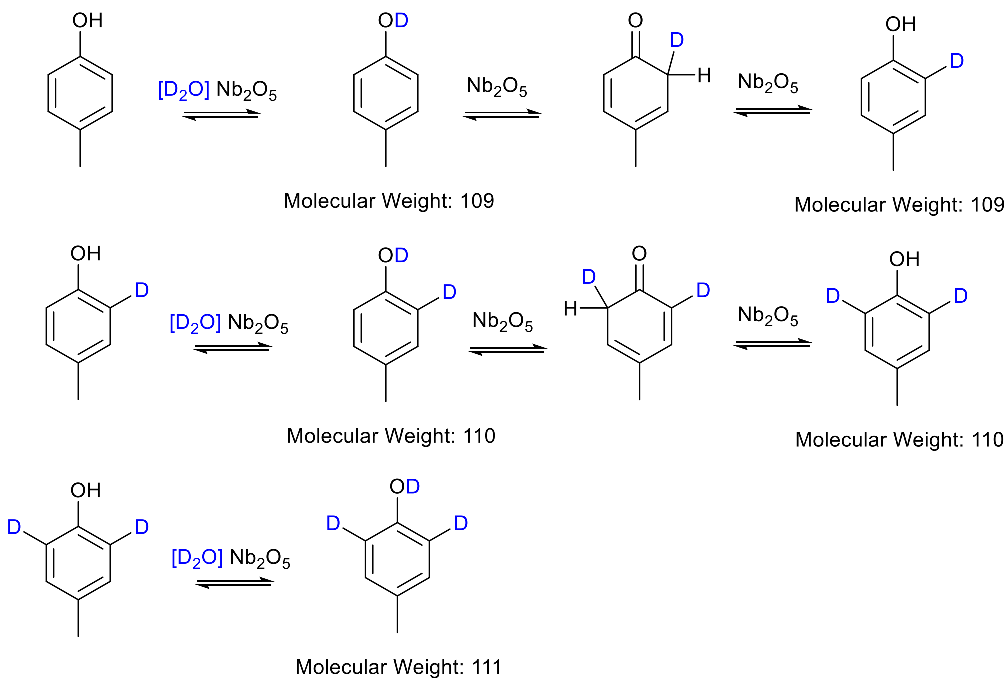

Scheme S-2.1 The mechanism of p-cresol reaction with Nb_2O_5 in D_2O. The deuterium from D_2O could transfer to aromatic ring through tautomerization catalyzed by Nb_2O_5. This Scheme shows the possible structures and molecular weight of p-cresol after isotopic reaction with Nb_2O_5 in D_2O in agreement with the GC/MS and ^{2}H NMR results.

2.7.4 References

1. Özer, N.; Rubin, M. D.; Lampert, C. M., Optical and electrochemical characteristics of niobium oxide films prepared by sol-gel process and magnetron sputtering A comparison. *Solar Energy Materials and Solar Cells* **1996,** *40* (4), 285-296.

2. Chan, X. J.; Pu, T. C.; Chen, X. Y.; James, A.; Lee, J.; Parise, J. B.; Kim, D. H.; Kim, T., Effect of niobium oxide phase on the furfuryl alcohol dehydration. *Catal Commun* **2017,** *97*, 65-69.

Chapter 3. Catalytic Conversion of Activated Carbon Purified Lignin Derived Phenolics to 4-Propylcyclohexanol under Mild Condition

3.1 Abstract

Propylcyclohexanols can be achieved from Ru/C catalyzed conversion of lignin monomers under H_2 pressure at low temperature 140 ℃. Under optimized conditions, dihydroeugenol (DHE), a model compound of lignin monomer, is 100 % converted to equal amount of 4-propylcyclohexanol and 2-methoxy-4-propylcyclohexanol in a solvent-free system. The applicability of this catalytic system is demonstrated by funneling a substrate mixture of DHE, isoeugenol, and 4-allylsyringol simulating bio-oil into two propylcyclohexanol products. In the case of upgrading real lignin derived bio-oil, its complex components deactivate Ru/C and prevent the formation of propylcyclohexanol products. This obstacle is addressed in this work by applying a simple purification treatment with activated carbon. By which, it illustrates the catalyst deactivation attributes to the presence of sulfur and lignin biopolymer residues in bio-oil. Thus, we have been able to show that a combination of both catalytic conversion and purification strategy enables the utilization of biomass derived bio-oil directly as a renewable source for propylcyclohexanol production.

3.2 Introduction

Lignin, a polymer of oxygenated aromatics, is the most abundant source of renewable phenolics from nature.[1, 3-7] 20 million tons of lignin is grown through photosynthesis every year, and it contributes to 10-25 % of natural biomass.[8, 9] As a promising material, it has been widely researched to be utilized in many ways. Methods such as pyrolysis,[10-12] catalytic conversion,[1, 3, 13, 14] and enzymatic degradation[15-17] have been studied to break lignin into its monomers, a mixture of small phenols with methoxy groups and short alkyl chains, also known as bio-oil. Bio-oil is an important feedstock for energy products[18] and renewable plastics.[19] Among the above three methods, metal-catalyzed depolymerization of lignin is well known for its highest efficiency. We have reported an earth-abundant metal, nickel, to be one of the desired metals for catalyzing native lignin into a mixture of mainly 4-propylguaiacol (DHE), 4-propylsyringol (DMPP), and their propenyl forms.[3, 20] Herein, upgrading the Ni-catalyzed propylphenols will provide further advances into utilizing the bio-oil feedstocks to the next-step chemicals and complete a route from natural biomass to value-added products.

The goal of this study is to develop a further utilization method of lignin derived propylphenols to 4-propylcyclohexanol. Propylcyclohexanols have many industrial uses. They are known as useful intermediates and additives in the fragrance industry.[21] Their hydroxyl group can be easily oxidized to form propylcyclohexanone which makes it a potential intermediate for making new nylon polymers.[22-24] 4-propylcyclohexanol can be achieved from propylphenol through hydrogenation of the aromatic ring. However, in the case of using bio-oil as a feedstock, the specific 4-propylcyclohexanol cannot be achieved by a simple hydrogenation. Due to one or two methoxy groups in the ortho positions of propylphenol, a deoxygenation reaction must be selectively preformed between the aromatic carbon and methoxy oxygen.

By far, the existed studies have shown the hydrodeoxygenation (HDO) reactions with transition metals (Co, Ni, Ru, Pd, and Zr etc.), organic solvents (n-dodecane, hexadecane, and isooctane etc.), and hydrogen pressure (> 10 bar) at elevated temperature (> 200 °C) are efficient for converting propylphenols to propylcyclohexanol.[4, 25-29] For example, Schutyser et al reported using DHE in hexadecane solvent with high nickel loading (65 wt% Ni) on silica/alumina catalyst gives 85 % yield of propylcyclohexanol at 250 ℃ under 10 bar hydrogen atmosphere.[26] Xu et al showed their RuZrLa-2 catalyst is active for catalyzing DMPP to propylcyclohexanol (86.9 % yield) at 200 ℃ with 40 bar hydrogen pressure.[4] However, using high-boiling organic solvents increases the difficulty of product separation. The high temperature may also limit the scalability of the reaction and is not energy-saving. Therefore, the milder condition with low-boiling solvent, or even a neat reaction is more desirable for upgrading propylphenols.

Here, we studied Ru/C catalyzed DHE to propylcyclohexanol at 140 ℃. Although, this mild condition is effective to convert DHE to 4-propylcyclohexanol (**1**) and 2-methoxy-4-propylcyclohexanol (**2**) without using any solvent, adding small amount of methanol (0.25 mL to 20 g DHE) plays a crucial role in avoiding formation of by-products. More importantly, even though there are some studies that have provided promising yield of propylcyclohexanol, but due to the complexity of natural biomass, the use of actual lignin bio-oil as the feedstock to make propylcyclohexanol has not been realized until now.[30-32] In this contribution, we describe a purification strategy that successfully promotes the upgrading of lignin bio-oil made from Poplar wood to propylcyclohexanols (**1**) and (**2**), and we delineate the culprits in the bio-oil causing catalyst inhibition/deactivation . Last but not least, the unreacted lignin biopolymer residue is recycled in our purification treatment.

3.3 Experimental

Materials. All commercial chemicals were purchased and used as is. 2-methoxy-4-propylphenol (≥ 99 %), isoeugenol (98 %), acetic acid (≥ 99.7 %)), activated carbon (100 mesh), and ruthenium on carbon (5 wt% loading) were purchased from Sigma-Aldrich. Acetone (ACS Reagent Grade), ethyl acetate (ACS Reagent Grade), methanol (ACS Reagent Grade), methylene chloride (DCM, High-resolution Gas Chromatography Grade), and pyridine-d_5 (≥ 99.5 % atom % D) were purchased from Fisher Chemical. 4-ally-2,6-dimethoxyphenol (98 %) and n-dodecane (99 %) were purchased from Alfa Aesar. 4-propylcyclohexanol (cis- and trans-mixture > 98 %) was purchased from Tokyo Chemical Industry Co., LTD (TCI). Dimethyl sulfoxide-d_6 was purchased from Cambridge Isotope Laboratories Inc. Ultra-pure hydrogen gas (5.0 Grade) was purchase from Praxair. Deionized water was obtained from A10 Milli-Q water purification system by Millipore.

Poplar dry woody biomass was obtained from the ACE Hardware Lumberyard, Santa Barbara, CA. Lignin was extracted from Poplar shavings by organosolv method.[1] Organosolv lignin (OPL) was further depolymerized into lignin monomers by Ni/C catalyst. The bio-oil obtained from catalytic depolymerization of lignin (CDL) and the preparation of Ni/C catalyst were reported in our previous work.[3]

Purification of Biomass Products. The purification process was done in a stainless-steel pressurized vessel equipped with magnetic stirring system (Parr Instrument Company, 5000 series). 1 g CDL mixture was first dissolved in 30mL methanol and then mixed with 3.5 g activated carbon (100 mesh) into a 75 mL reactor vessel. The mixture was constantly stirred by a magnetic glass stir bar at 700 rpm. The reactor vessel was then sealed and purged three times with 5.0 grade hydrogen. 10 bar hydrogen was charged into the vessel after the purge cycles. The vessel was then heated to 100 ℃ and held for 12 hours in heating jacket. The heating process was controlled automatically by a programmable controller box (Parr Instrument Company). After the heating period, vessel was cooled to room temperature with continuous stirring. Once the vessel was cooled, remaining gas pressure was vented. The carbon-methanol mixture was then transferred by washing with 50 mL methanol into a 100 mL Buchner funnel with glass frit plate.

The Buchner funnel was connected to vacuum. The solid phase was separated and collected by vacuum filtration. The methanol filtrate was stored in a 500 mL round bottom flask. 50 mL DI water was used to wash the solid. The aqueous wash solution was collected for ICP analysis. The remaining solid was dried under vacuum for four hours. Then the dry solid was transferred into another 500 mL round bottom flask with 200 mL acetone. The mixture was stirred with magnetic stir bar while refluxing at 60 ℃ for two hours. The solid was separated again by vacuum filtration in Buchner funnel and washed slowly by another 100mL acetone. The total 300 mL acetone filtrate was combined to the previous methanol filtrate. The acetone and methanol solvents of the combined filtrate were removed by a rotavapor (Buchi Corporation V-100 series). The remaining neat liquid containing organic CDL products were stored for further reactions. After processing the solid with acetone, the remaining solid was stirred and refluxed again in 100 mL DCM at 40 ℃ for one hour. After that, the mixture was transferred to Buchner funnel immediately at 40 ℃ for vacuum filtration. Another portion of 100 mL DCM was used to wash the remaining solid. The DCM filtrate was then collected for further NMR analysis.

Catalytic Reactions. The catalytic conversion was carried out in a pressurized batch reactor (Parr Instrument Company, 5000 series). A portion of 2 g starting material was physically mixed with 10 wt% Ru/C (0.2 g, 5 wt% Ru loading on activated carbon) and employed to 20 mL methanol in a 75 mL stainless-steel reactor vessel. A magnetic glass stir bar was used to stir the reaction mixture. The reactor vessel was then sealed and placed into heating jacket. A magnetic stirring system was equipped with the heating jacket and the stirring rate was preset to 700 rpm for the whole reaction period. The vessel was purged three times with 5.0 Grade hydrogen gas. After that, 35 bar H_2 was charged and sealed into the vessel at room temperature. The reaction mixture was then heated to 140 ℃ and held for 4 hours. After the reaction, the vessel was removed from heating jacket and cooled to room temperature. Prior to collecting the products mixture, the remaining gas was vented. The products and solid catalyst were washed from reactor vessel by using 250 mL methanol and passed through a filter paper with pore size of 11 μm (Whatman 150 mm) to remove solid catalyst from the products mixture. The liquid filtrate was then stored in a 500 mL round bottom flask for GC-FID and GC-MS analysis. The neat DHE reaction was carried out with the same condition using 20 g DHE but only 0.25 mL methanol was added.

GC-FID Analysis. Methanol solvent was removed from the liquid filtrate of catalytic reaction by using rotavapor. The neat organic products were diluted in ethyl acetate in 50 mL volumetric flask. 10 mM n-dodecane in ethyl acetate solution was prepared as internal standard. 500 μL products solution mixed with 500 μL internal standard solution and filtered through 0.2 micron PTFE syringe filter into a 2 mL Agilent GC vial with screw cap for GC analysis. Agilent 6890N gas chromatographer equipped with flame ionization detector (FID) was used to quantify the products. J&W DB-5 column (30 m x 0.250 mm I.D. x 0.25 μL film thickness) was installed to separate the analytes. Prior to sample injection, the inlet temperature was set to 310 ℃ and its total flow was at 14.0 mL/min. Helium was used as the carrier gas and the GC was set to split mode with 10:1 split ratio. The initial oven temperature was equilibrated at 35 ℃ for three minutes. The ramping rate was set at 15 ℃/min to warm the oven to 310 ℃ after the equilibrium. The FID detector was kept at 310 ℃ during the whole measurement. For each run of analysis, 2 μL analyte solution was injected by autosampler. Each product molecule was identified according to its retention time which was pre-determined by using the commercial standards. The quantification of each analyte was calculated based on a calibration curve. The calibration curve was made according to the function of the concentrations and the ratios of peak area between analyte versus the internal standard.

GC-MS Analysis. The products were identified by mass spectrometer. 0.2 g neat products mixture was dissolved in 25 mL ethyl acetate. Then the sample solution was filtered through 0.2-micron PTFE syringe filter. 1 μL sample solution was then manually injected into a Hewlett-Packard 5890A GC. The injector was set to 280 ℃ while the initial oven temperature was at 50 ℃. Then the oven was heated to 300 ℃ at rate of 20 ℃/min. During the ramping period, each analyte molecule was separated by GC column (J&W DB-5 column, 30 m x 0.250 mm I.D. x 0.25 μL film thickness) and carried by helium gas into a Hewlett-Packard 5970B Mass Selective Detector (MSD). The MSD was equipped with dedicated electron ionization (EI) source and a quadrupole mass analyzer. The mass range of detection was set from 40 to 550 m/z at rate of 1.6 scans per second.

ICP Analysis. Inductively Coupled Plasma (ICP) Spectrometer was used to analyze the elements in water filtrate collected during the purification process. iCAP 6300 ICP (Thermo Scientific) was used for this analysis. Sample uptake rate was pre-set to 1.5 mL/min and the carrier gas flow being 0.5 L/min. The Burgener Teflon Mira Mist nebulizer and radical view torch with 13 mm viewing height and 1150 W RF power were equipped to this ICP. The water sample was placed into a 50 mL centrifuge tube (Falcon), then the aqueous solution was directly pumped into the ICP instrument for analysis. A portion of clean DI water and a portion of DI water collected by washing fresh activated carbon were also used as control samples for comparison.

NMR Analysis. A Bruker AVANCE500 (500 MHz) spectrometer was used for HSQC analysis of DCM filtrate from the purification process. For a typical HSQC sample preparation, DCM solvent was first removed by rotavapor, and then the remaining solid was dried under vacuum at room temperature for 12 hours. After that, the dried brown lignin solid was collected and dissolved in a 700 μL DMSO-d_6: pyridine-d_5 5:1 (v/v) co-solvent mixture. The spectrometer operated at 500.13 and 125.77 MHz for ^{1}H and ^{13}C nuclei. The 2D-HSQC spectra were then acquired by an echo-antiecho experiment called HSQCETGP.

3.4 Results and Discussion

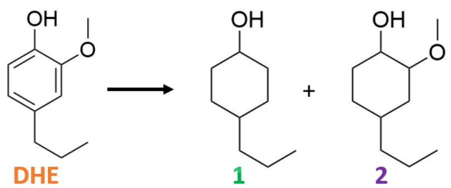

Scheme 3.1 DHE Conversion to two main products: 4-propylcyclohexanol (**1**) and 2-methoxy-4-propylcyclohexanol (**2**)

Ruthenium had been reported to be one of the ideal metals in heterogeneous catalysis, especially in catalyzing biomass derivatives into value-added chemicals.[26, 32-37] Ruthenium loaded onto activated carbon (Ru/C) is known for its ability highlighted in hydrodeoxygenation, thermo stability, recyclability, and commercial accessibility in large quantities. Hence, Ru/C was chosen to study the catalytic conversion of lignin monomers to propylcyclohexanol (**1**) and 2-methoxy-4-propylcyclohexanol (**2**) (Scheme 3.1). DHE, one of the major lignin monomers was studied as the model compound.

3.4.1 Optimization of reaction conditions

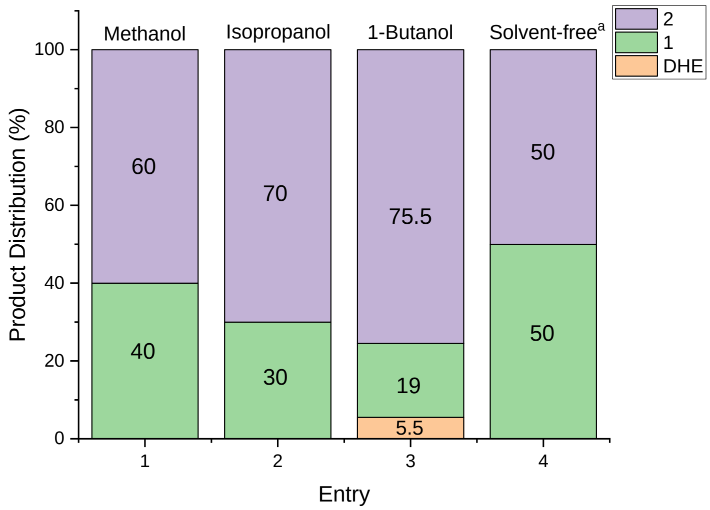

Figure 3.1 Product distribution of (1) and (2) (by mass) in different low-boiling alcohol solvents. Common condition for each reaction: DHE 2 g, Ru/C 0.2 g, alcohol solvent 20 mL, initial H_2 35 bar, 140 ℃, 4 h. (a) Entry 1 was done with 20 g DHE, 2 g Ru/C, and 0.25 mL methanol, initial H_2 was 50 bar for 1 hour reaction at 140 °C, then cooled to room temperature to add another 50 bar H_2 then held at 140℃ for another 1 hour, repeated for 4 times to 4 hours in total.

The choice of solvent is important for a catalytic system. Investigations of using low-boiling point alcohols and solvent-free reactions were done to understand the impact attributed to solvent (Figure 3.1). Figure 3.1 illustrates that DHE can be converted to (**1**) and (**2**) at 140 ℃ within 4 hours in alcohols medium. Although a higher reaction temperature could potentially accelerate the kinetics (Entries 1-4, SI, Figure S-3.1), surprisingly, raising the temperature above 160 ℃ suppressed both the conversion of DHE and the formation of products (Entries 5 and 6, Figure S-3.1). Therefore, in case of using alcohol solvent, temperature between 140-160 ℃ is desirable. The amount of Ru/C was also examined and summarized in supporting information (SI) Figure S-3.2. Although the 100 % conversion of DHE is still achieved with less catalyst in 4 hours, the product distribution varies by 10 %. Entries 1-4 in Figure S-3.2 show 10 wt% of Ru/C is optimal to achieve (**1**).

Entries 1-3 in Figure 3.1 indicate the selectivity of (**1**) and (**2**) at different polarities of the alcohol solvents. Thus, the more polar methanol improves hydrogenolysis reaction for methoxy removal while the less polar 1-butanol promotes more hydrogenation on the aromatic ring. Entry 4 in Figure 3.1 shows the product distribution of the neat reaction (solvent-free). Without using any alcohol solvent, DHE is fully converted to (**1**) and (**2**) equally. However, the product mixture was initially observed becoming yellow-greenish in color. The formation of this colored byproduct was found to be easily inhibited by adding a very small amount of methanol (0.25 mL methanol to 20 g DHE) to the reaction mixture. This phenomenon suggests, besides being a solvent, methanol also plays an important role in protecting this catalytic conversion of DHE. Overall, the success of the neat reaction suggests the upgrading of phenolics can be done in a greener way with a more favorable selectivity to (**1**) than in solvent.

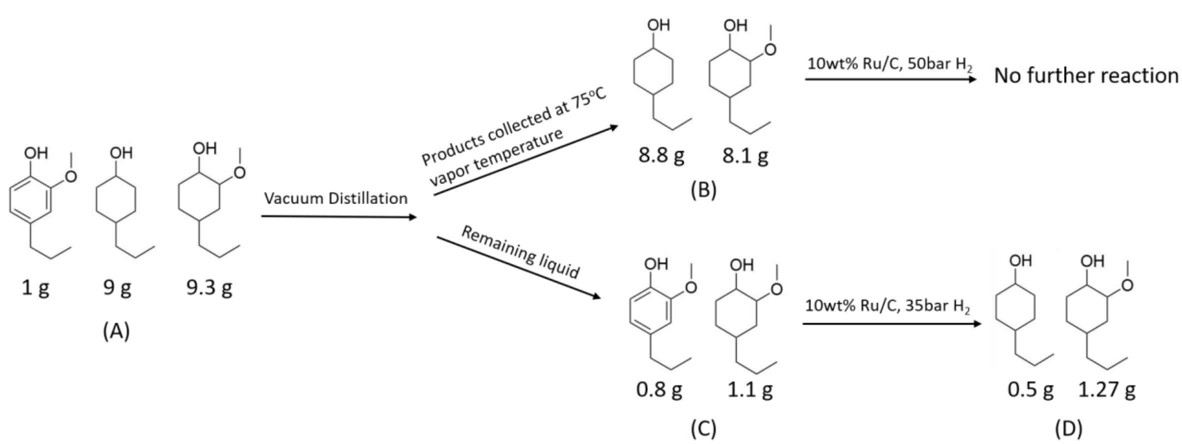

Figure 3.2 Sequences of neat reactions. (A) Product mixture of a reaction starting with DHE 20 g, Ru/C 2 g, and initial H_2 50 bar, held at 140℃ for 1 hour and cooled to room temperature to add another 50 bar H_2, repeated three times; (B) Distillate collected by vacuum distillation at 75 ℃ vapor temperature and combined with fresh Ru/C 1.7g, initial H_2 50 bar and repeated the heating and cooling steps till 4 hours at 140 ℃ in total; (C) The remaining product mixture after vacuum distillation; (D) Product mixture of using (C) as the starting material with fresh Ru/C 0.2 g and 35 bar H_2 held at 140 ℃ for 4 hours.

3.4.2 Mechanism

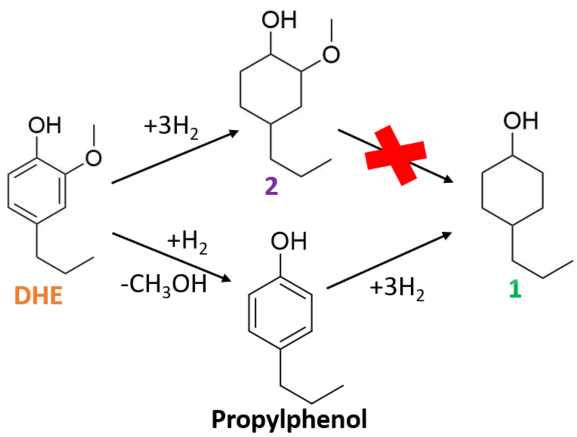

Scheme 3.2 Possible reaction mechanism for conversion of DHE catalyzed by Ru/C at 140 °C.

Described in Figure 3.2 are product mixtures of neat reactions as well as the mass balances. Mixture (A) in Figure 3.2 was obtained from a solvent-free reaction starting with 20 g DHE. The reaction was quenched before it went to completion. By performing vacuum distillation, mixture (A) was separated into two fractions, (B) and (C). Products (**1**) and (**2**) maintained the same proportions after the second run of reaction with mixture (B) and fresh Ru/C while the remaining DHE in mixture (C) was converted further into (**1**) and (**2**). Accordingly, we hypothesized that the demethoxylation must be performed prior to the saturation of the aromatic ring. This result was consistent with the conclusion drawn from longer reaction time in methanol solvent (SI, Figure S-3.3), which showed no conversion of (**2**) into (**1**) after 16-hour reaction. Scheme 3.2 outlines the possible mechanism for this Ru/C catalyzed reaction from DHE to (**1**) and (**2**). In the presence of hydrogen gas, DHE is simply reduced to (**2**) via hydrogenation reaction which stabilizes the methoxy group on the cyclohexane ring. Thus (**2**) does not convert to (**1**) under our reaction conditions. The demethoxylation of (**2**) requires higher temperature (200-300 ℃) to overcome the activation boundaries for C(sp^3)-O cleavage.[4, 26] On the other hand, demethoxylation is favorable for C(sp^2)-O of DHE at low temperature (140 ℃) and produces propylpehnol as an intermediate. Then the propylphenol is rapidly reduced to (**1**). No 4-propylcatechol was detected and the lack of acid sites on carbon support suggest the demethoxylation of DHE into catechol (via hydrolysis) in this study is less likely.[38, 39] Lastly, taking mixtures (B) and (D) together accounts for 93 % of the mass balance of the starting 20 g DHE.

3.4.3 Application to lignin derived monomer mixtures, simulated lignin bio-oil

A mixture of DHE, isoeugenol, and 4-allylsyringol was obtained from commercial standards to simulate a bio-oil mixture of lignin monomers. This simulated bio-oil was fully converted to (**1**) and (**2**) (Figure 3.3). Thus, this mild system provides the opportunity to funnel multiple lignin monomers into propylcyclohexanols **1** and **2**.

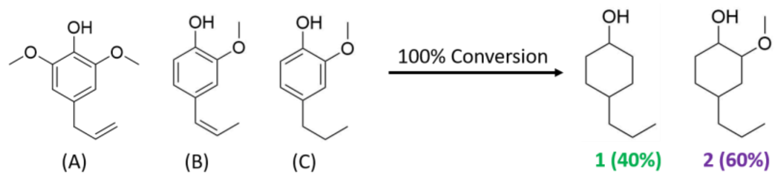

Figure 3.3. Reaction of simulated bio-oil mixture: 0.7 g of each (A) 4-allylsyringol, (B) isoeugenol, and (C) DHE with Ru/C 0.2 g and H_2 35 bar in 20 mL methanol solvent at 140 °C for 4 hours.

Notably, when actual lignin bio-oil containing DMPP, isoeugenol, and DHE (obtained from CDL reaction of Poplar biomass) was used, products **1** and **2** were not observed. This outcome could be a result of catalyst deactivation caused by the complexity of the bio-oil mixture, potentially containing more than 400 minor components.[40] For example, sulfur is ubiquitous in raw biomass and well known for its poisoning and deactivating Ru/C.[41] Sulfur can be accumulated through processing biomass into bio-oil. Besides, deposition attributed to the viscous unreacted lignin biopolymers and oligomers on catalyst surface could also play a role in suppressing the reaction by preventing contact between monomeric substrates and active sites.[42]

Therefore, a purification treatment should be done to remove catalyst poisons and promote the utilization of actual lignin bio-oil.

3.4.5 Purification strategy

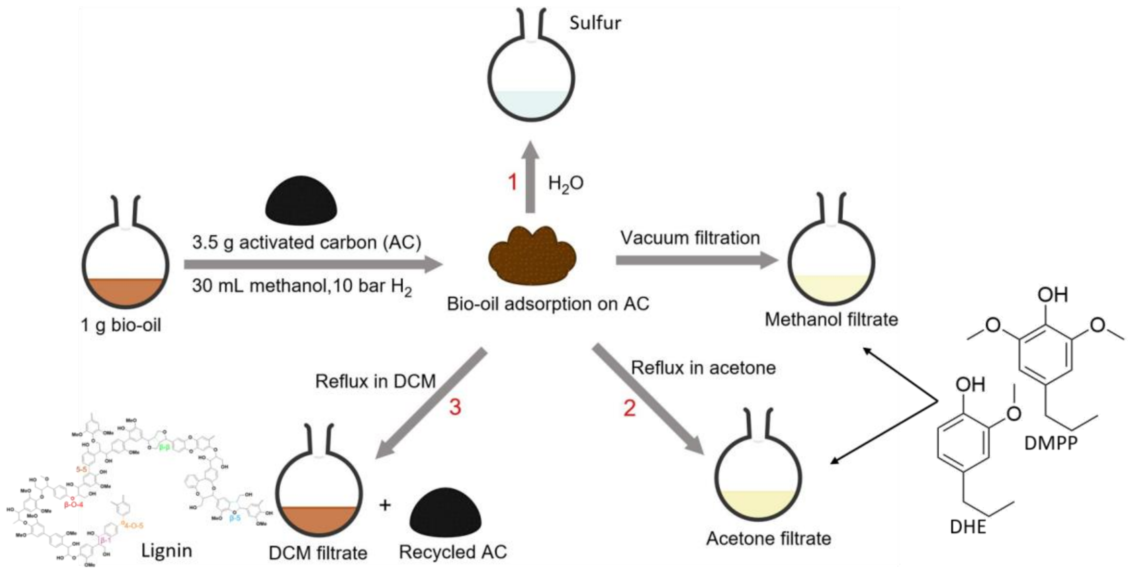

Figure 3.4 Activated carbon purification treatment for bio-oil obtained from lignin of Poplar biomass.

Figure 3.4 outlines our three-step purification method of using activated carbon (AC) to adsorb the bio-oil and release/fractionate different components. A similar strategy of using AC as the purification agent has been previously studied for adsorption of arsenics.[43] In this work, the raw bio-oil after CDL is a viscous liquid of dark brown color. To 1 g of lignin bio-oil 3.5 g AC in methanol was added and the mixture held at 100 ℃ for 12 hours, the bio-oil adsorption onto the AC was indicated by the disappearance of brown color in the methanol solution. After vacuum filtration, light-yellow methanol filtrate was collected which gave DHE and DMPP as the major solutes. 10 bar hydrogen pressure was necessary to create a pressurized system and retained methanol in liquid phase at 100 ℃. Moreover, isoeugenol was converted to DHE during purification. This observation suggests hydrogenation of the side chain C=C of isoeugenol. Follow route 1 in Figure 3.4, AC with adsorbed bio-oil was first washed with water. Although the aqueous wash solution appeared clear, ICP analysis showed sulfur in the aqueous filtrate (SI, Figure S-3.4). Described in route 2 of Figure 3.4 is a reflux treatment of the sulfur-free AC mixture in acetone. Collected in the light-yellow acetone filtrate was another portion of DHE and DMPP from the raw bio-oil. Route 3 in Figure 3.4 shows reflux of the remaining AC solid in methylene chloride (DCM). Brown colored DCM solution was collected after this treatment. After evaporation of DCM, a brown solid was collected. 2D HSQC NMR analysis of this brown solid product indicated typical lignin linkages (Figure 3.5). Thus, the brown solid recovered in DCM is suggested to be unreacted lignin and thereby it can be recycled for further upgrading CDL reaction. Notably, the recovered AC after performing route 3 was reusable for more than two cycles of this purification treatment without doing additional reactivation to the AC.

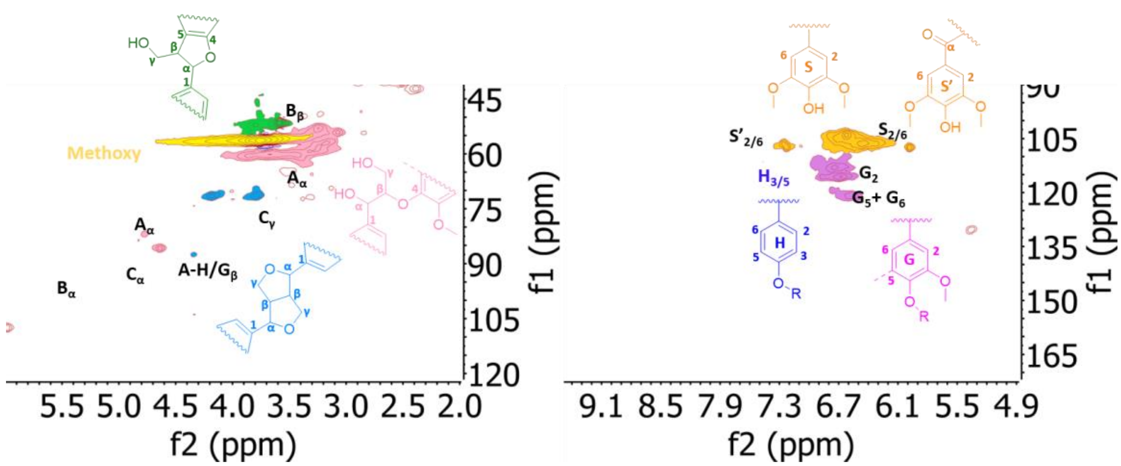

Figure 3.5 2D ^1H-^{13}C HSQC spectra of recovered brown solid (lignin) from the DCM filtrate (route 3 in Figure 3.4). The left spectra show the aliphatic side chain region, in which, β-5 linkage (green), methoxy (yellow), β-o-4 linkage (pink), and β- β linkage (blue) are assigned. The right spectra depict the aromatic region where the S and S' lignin (orange), G lignin (purple), and H lignin (indigo) are detected. All assignments were determined according to the

After performing the AC purification, DHE and DMPP collected in methanol and acetone fractions were combined and converted to propylcyclohexanols (**1**) and (**2**). Figure S-3.5 in SI summarizes the mass balance of purifying bio-oil and upgrading clean monomers to (**1**) and (**2**). AC purification recovered 81 % by mass of the starting phenolics in the methanol and acetone fractions. 0.63 g of (**1**) and (**2**) were produced from the recovered phenolics by the mild conversion with Ru/C which was about 91 % yield by mass of purified phenolics and 73 % yield by mass of the starting phenolics in the raw lignin bio-oil. Therefore, the reasons for inhibiting upgrading actual lignin bio-oil are concluded to be catalyst deactivation caused by the sulfur content and lignin biopolymer residue in the bio-oil mixture.

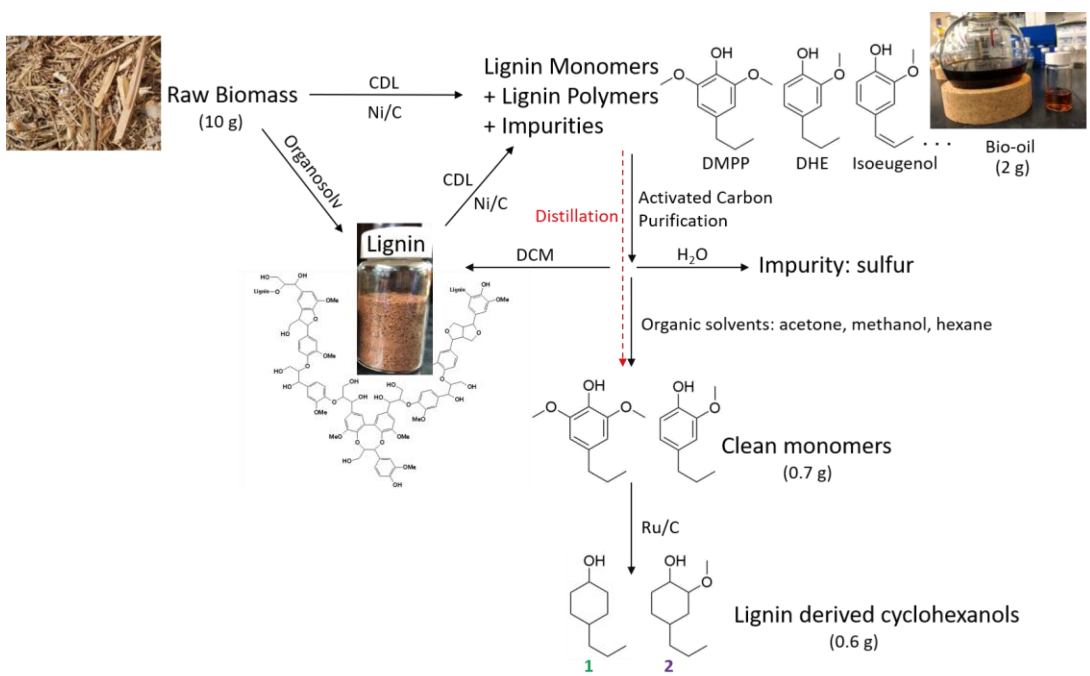

Figure 3.6 Bio-oil processing sequence to (**1**) and (**2**)

Figure 3.6 outlines an overview of processing biomass as feedstock to (**1**) and (**2**). Typically, lignin in raw biomass can be directly converted to bio-oil (dark brown liquid) by Ni/C catalyzed CDL reaction.[3] On the other hand, lignin (brown solid) can also be first isolated by an organosolv method prior to CDL reaction leading to the same bio-oil.[1] Purification by activated carbon is the key step of this process. Activated carbon has large surface area which allows the components of bio-oil depositing on its surface and sequentially releasing different components into different fractions. The sulfur impurity is removed by water and the unreacted lignin biopolymer is recycled in DCM. By which, the deactivation of Ru/C is avoided. Therefore, the purified lignin monomers collected in organic solvents can be eventually converted to (**1**) and (**2**). Interestingly, the isoeugenol is reduced to DHE during the purification under small amount of hydrogen pressure. Even though performing a direct fractional distillation (labelled in red color) of the bio-oil can also isolate a clean mixture of phenolic compounds. However, the elevated temperature for distilling those high-boiling phenolics could drive self-condensation of lignin and lignin derivatives and result in an inactive form of bio-oil that becomes quite recalcitrant towards upgrading.[44] Thus, the fractional distillation is less favorable in collecting clean lignin monomers and recycling lignin biopolymer from bio-oil.

3.5 Conclusion

In summary, our study provides a new route of utilizing lignin derivatives into useful chemicals through hydrogenolysis and hydrogenation reactions under mild conditions and without requiring a solvent. DHE and DMPP with Ru/C react in neat conditions and produce selectively propylcyclohexanols (**1**) and (**2**); addition of a small amount of methanol (1.25 % v/v) protects the reaction from colored byproducts. The solvent effect suggests the less polar alcohol solvents lead to ring hydrogenation favoring (**2**) while polar alcohols such as methanol and neat reactions improve the yield of propylcyclohexanol (**1**). Moreover, selectivity to (**2**) can also be tuned by using less amount of Ru/C. Our mechanistic study indicates the hydrogenation of the aromatic ring stabilizes the attached methoxy group and under our conditions $C(sp^3)$-O cleavage is less favored in comparison to $C(sp^2)$-O. Thus, the formation of (**1**) is only achieved through hydrogenolysis of the methoxy group on DHE first to 4-propylphenol, followed by ring hydrogenation. Although many studies have reported success in upgrading lignin model compounds, our AC purification treatment realizes a more practical route to utilize native lignin monomers from actual lignin bio-oil into value-added products. What's more, the purification illustrates the sulfur and lignin biopolymer could be the reason of Ru/C deactivation and preventing the upgradability of actual bio-oil. The highlight of this treatment is not only purifying the bio-oil mixtures, but also recycling the unreacted lignin biopolymer from CDL mixture. More importantly, our success in upgrading lignin bio-oil from Poplar biomass to (**1**) and (**2**) provides the opportunity for utilizing many lignocellulosic derivatives to wide purposes.

3.6 References:

1. Cheng, C. B.; Truong, J.; Barrett, J. A.; Shen, D. K.; Abu-Omar, M. M.; Ford, P. C., Hydrogenolysis of Organosolv Lignin in Ethanol/Isopropanol Media without Added Transition-Metal Catalyst. *Acs Sustain Chem Eng* **2020,** *8* (2), 1023-1030.

2. Sette, M.; Wechselberger, R.; Crestini, C., Elucidation of Lignin Structure by Quantitative 2D NMR. *Chem-Eur J* **2011,** *17* (34), 9529-9535.

3. Luo, H.; Klein, I. M.; Jiang, Y.; Zhu, H. Y.; Liu, B. Y.; Kenttamaa, H. I.; Abu-Omar, M. M., Total Utilization of Miscanthus Biomass, Lignin and Carbohydrates, Using Earth Abundant Nickel Catalyst. *Acs Sustain Chem Eng* **2016,** *4* (4), 2316-2322.

4. Xu, G. Y.; Guo, J. H.; Qu, Y. C.; Zhang, Y.; Fu, Y.; Guo, Q. X., Selective hydrodeoxygenation of lignin-derived phenols to alkyl cyclohexanols over a Ru-solid base bifunctional catalyst. *Green Chem* **2016,** *18* (20), 5510-5517.

5. Maki-Aryela, P.; Murzin, D. Y., Hydrodeoxygenation of Lignin-Derived Phenols: From Fundamental Studies towards Industrial Applications. *Catalysts* **2017,** *7* (9).

6. Li, C. Z.; Zhao, X. C.; Wang, A. Q.; Huber, G. W.; Zhang, T., Catalytic Transformation of Lignin for the Production of Chemicals and Fuels. *Chem Rev* **2015,** *115* (21), 11559-11624.

7. Huang, X. M.; Ludenhoff, J. M.; Dirks, M.; Ouyang, X. H.; Boot, M. D.; Hensen, E. J. M., Selective Production of Biobased Phenol from Lignocellulose-Derived Alkylmethoxyphenols. *Acs Catal* **2018,** *8* (12), 11184-11190.

8. Watkins, D.; Hosur, M. N. M.; Tcherbi-Narteh, A.; Jeelani, S., Extraction and characterization of lignin from different biomass resources. *J Mater Res Technol* **2015,** *4* (1), 26-32.

9. Vanholme, R.; Demedts, B.; Morreel, K.; Ralph, J.; Boerjan, W., Lignin Biosynthesis and Structure. *Plant Physiol* **2010,** *153* (3), 895-905.

10. Shen, D. K.; Gu, S.; Luo, K. H.; Wang, S. R.; Fang, M. X., The pyrolytic degradation of wood-derived lignin from pulping process. *Bioresource Technol* **2010,** *101* (15), 6136-6146.

11. Collard, F. X.; Blin, J., A review on pyrolysis of biomass constituents: Mechanisms and composition of the products obtained from the conversion of cellulose, hemicelluloses and lignin. *Renew Sust Energ Rev* **2014,** *38*, 594-608.

12. Yang, H. P.; Yan, R.; Chen, H. P.; Lee, D. H.; Zheng, C. G., Characteristics of hemicellulose, cellulose and lignin pyrolysis. *Fuel* **2007,** *86* (12-13), 1781-1788.

13. Hita, I.; Deuss, P. J.; Bonura, G.; Frusteri, F.; Heeres, H. J., Biobased chemicals from the catalytic depolymerization of Kraft lignin using supported noble metal-based catalysts. *Fuel Process Technol* **2018,** *179*, 143-153.

14. Huang, X. M.; Atay, C.; Zhu, J. D.; Palstra, S. W. L.; Koranyi, T. I.; Boot, M. N.; Hensen, E. J. M., Catalytic Depolymerization of Lignin and Woody Biomass in Supercritical Ethanol: Influence of Reaction Temperature and Feedstock. *Acs Sustain Chem Eng* **2017,** *5* (11), 10864-10874.

15. Xu, Z. X.; Lei, P.; Zhai, R.; Wen, Z. Q.; Jin, M. J., Recent advances in lignin valorization with bacterial cultures: microorganisms, metabolic pathways, and bio-products. *Biotechnol Biofuels* **2019,** *12*.

16. Fuchs, G.; Boll, M.; Heider, J., Microbial degradation of aromatic compounds - from one strategy to four. *Nat Rev Microbiol* **2011,** *9* (11), 803-816.

17. Bugg, T. D. H.; Ahmad, M.; Hardiman, E. M.; Singh, R., The emerging role for bacteria in lignin degradation and bio-product formation. *Curr Opin Biotech* **2011,** *22* (3), 394-400.

18. Zhang, W.; Chen, J. Z.; Liu, R. L.; Wang, S. P.; Chen, L. M.; Li, K. G., Hydrodeoxygenation of Lignin-Derived Phenolic Monomers and Dimers to Alkane Fuels over Bifunctional Zeolite-Supported Metal Catalysts. *Acs Sustain Chem Eng* **2014,** *2* (4), 683-691.

19. Zhao, S.; Huang, X. N.; Whelton, A. J.; Abu-Omar, M. M., Renewable Epoxy Thermosets from Fully Lignin-Derived Triphenols. *Acs Sustain Chem Eng* **2018,** *6* (6), 7600-7608.

20. Luo, H.; Abu-Omar, M. M., Lignin extraction and catalytic upgrading from genetically modified poplar. *Green Chem* **2018,** *20* (3), 745-753.

21. Hiyoshi, N.; Sato, O.; Yamaguchi, A.; Rode, C. V.; Shirai, M., Kinetic analysis of 4-isopropylphenol hydrogenation over activated carbon-supported rhodium catalysts in supercritical carbon dioxide solvent. *Green Chem* **2012,** *14* (3), 633-638.

22. Zhang, J. S.; Lu, Y. C.; Wang, K.; Luo, G. S., Novel One-Step Synthesis Process from Cyclohexanone to Caprolactam in Trifluoroacetic Acid. *Ind Eng Chem Res* **2013,** *52* (19), 6377-6381.

23. Thomas, J. M.; Raja, R., Design of a "green" one-step catalytic production of epsilon-caprolactam (precursor of nylon-6). *P Natl Acad Sci USA* **2005,** *102* (39), 13732-13736.

24. Kumar, R.; Shah, S.; Das, P. P.; Bhabavanbhai, G. G.; Al Fatesh, A.; Chowdhury, B., An overview of caprolactam synthesis. *Catal Rev* **2019,** *61* (4), 516-594.

25. Nakagawa, Y.; Ishikawa, M.; Tamura, M.; Tomishige, K., Selective production of cyclohexanol and methanol from guaiacol over Ru catalyst combined with MgO. *Green Chem* **2014,** *16* (4), 2197-2203.

26. Schutyser, W.; Van den Bossche, G.; Raaffels, A.; Van den Bosch, S.; Koelewijn, S. F.; Renders, T.; Sels, B. F., Selective Conversion of Lignin-Derivable 4-Alkylguaiacols to 4-Alkylcyclohexanols over Noble and Non-Noble-Metal Catalysts. *Acs Sustain Chem Eng* **2016,** *4* (10), 5336-5346.

27. Liu, X. H.; Jia, W. D.; Xu, G. Y.; Zhang, Y.; Fu, Y., Selective Hydrodeoxygenation of Lignin-Derived Phenols to Cyclohexanols over Co-Based Catalysts. *Acs Sustain Chem Eng* **2017,** *5* (10), 8594-8601.

28. Liu, X. H.; Xu, L. J.; Xu, G. Y.; Jia, W. D.; Ma, Y. F.; Zhang, Y., Selective Hydrodeoxygenation of Lignin-Derived Phenols to Cyclohexanols or Cyclohexanes over Magnetic CoNx@NC Catalysts under Mild Conditions. *Acs Catal* **2016,** *6* (11), 7611-7620.

29. Heroguel, F.; Nguyen, X. T.; Luterbacher, J. S., Catalyst Support and Solvent Effects during Lignin Depolymerization and Hydrodeoxygenation. *Acs Sustain Chem Eng* **2019,** *7* (20), 16952-16958.

30. Balan, V., Current challenges in commercially producing biofuels from lignocellulosic biomass. *ISRN Biotechnol* **2014,** *2014*, 463074.

31. Kumar, A.; Anushree; Kumar, J.; Bhaskar, T., Utilization of lignin: A sustainable and eco-friendly approach. *Journal of the Energy Institute* **2020,** *93* (1), 235-271.

32. Stummann, M. Z.; Hansen, A. B.; Hansen, L. P.; Davidsen, B.; Rasmussen, S. B.; Wiwel, P.; Gabrielsen, J.; Jensen, P. A.; Jensen, A. D.; Hoj, M., Catalytic Hydropyrolysis of Biomass Using Molybdenum Sulfide Based Catalyst. Effect of Promoters. *Energ Fuel* **2019,** *33* (2), 1302-1313.

33. Jones, D. R.; Iqbal, S.; Miedziak, P. J.; Morgan, D. J.; Edwards, J. K.; He, Q.; Hutchings, G. J., Selective Hydrogenation of Levulinic Acid Using Ru/C Catalysts Prepared by Sol-Immobilisation. *Top Catal* **2018,** *61* (9-11), 833-843.

34. Vriamont, C. E. J. J.; Chen, T. Y.; Romain, C.; Corbett, P.; Manageracharath, P.; Peet, J.; Conifer, C. M.; Hallett, J. P.; Britovsek, G. J. P., From Lignin to Chemicals: Hydrogenation of Lignin Models and Mechanistic Insights into Hydrodeoxygenation via Low-Temperature C-O Bond Cleavage. *Acs Catal* **2019,** *9* (3), 2345-2354.

35. Selva, M.; Gottardo, M.; Perosa, A., Upgrade of Biomass-Derived Levulinic Acid via Ru/C-Catalyzed Hydrogenation to gamma-Valerolactone in Aqueous-Organic-Ionic Liquids Multiphase Systems. *Acs Sustain Chem Eng* **2013,** *1* (1), 180-189.

36. Liu, Y.; Chen, L. G.; Wang, T. J.; Zhang, Q.; Wang, C. G.; Yan, J. Y.; Ma, L. L., One-Pot Catalytic Conversion of Raw Lignocellulosic Biomass into Gasoline Alkanes and Chemicals over LiTaMoO6 and Ru/C in Aqueous Phosphoric Acid. *Acs Sustain Chem Eng* **2015,** *3* (8), 1745-1755.

37. Guo, X. C.; Guan, J.; Li, B.; Wang, X. C.; Mu, X. D.; Liu, H. Z., Conversion of biomass-derived sorbitol to glycols over carbon-materials supported Ru-based catalysts. *Sci Rep-Uk* **2015,** *5*.

38. Dong, L.; Xin, Y.; Liu, X. H.; Guo, Y.; Pao, C. W.; Chen, J. L.; Wang, Y. Q., Selective hydrodeoxygenation of lignin oil to valuable phenolics over Au/Nb2O5 in water. *Green Chem* **2019,** *21* (11), 3081-3090.

39. de Souza, P. M.; Rabelo-Neto, R. C.; Borges, L. E. P.; Jacobs, G.; Davis, B. H.; Sooknoi, T.; Resasco, D. E.; Noronha, F. B., Role of Keto Intermediates in the Hydrodeoxygenation of Phenol over Pd on Oxophilic Supports. *Acs Catal* **2015,** *5* (2), 1318-1329.

40. Ruddy, D. A.; Schaidle, J. A.; Ferrell, J. R.; Wang, J.; Moens, L.; Hensley, J. E., Recent advances in heterogeneous catalysts for bio-oil upgrading via "ex situ catalytic fast pyrolysis": catalyst development through the study of model compounds. *Green Chem* **2014,** *16* (2), 454-490.

41. Dreher, M.; Steib, M.; Nachtegaal, M.; Wambach, J.; Vogel, F., On-Stream Regeneration of a Sulfur-Poisoned Ruthenium-Carbon Catalyst Under Hydrothermal Gasification Conditions. *Chemcatchem* **2014,** *6* (2), 626-633.

42. Kouris, P. D.; Huang, X. M.; Boot, M. D.; Hensen, E. J. M., Scaling-Up Catalytic Depolymerisation of Lignin: Performance Criteria for Industrial Operation. *Top Catal* **2018,** *61* (18-19), 1901-1911.

43. Chuang, C. L.; Fan, M.; Xu, M.; Brown, R. C.; Sung, S.; Saha, B.; Huang, C. P., Adsorption of arsenic(V) by activated carbon prepared from oat hulls. *Chemosphere* **2005,** *61* (4), 478-483.

44. Shuai, L.; Saha, B., Towards high-yield lignin monomer production. *Green Chem* **2017,** *19* (16), 3752-3758.

45. Matilainen, R.; Tummavuori, J., Determination of sulfur in fertilizers by inductively coupled plasma-atomic emission spectrometry: Spectral and interelement effects at various wavelengths. *J Aoac Int* **1996,** *79* (5), 1026-1035.

3.7 Supporting Information

Contents

Figures: 5

3.7.1 Figures

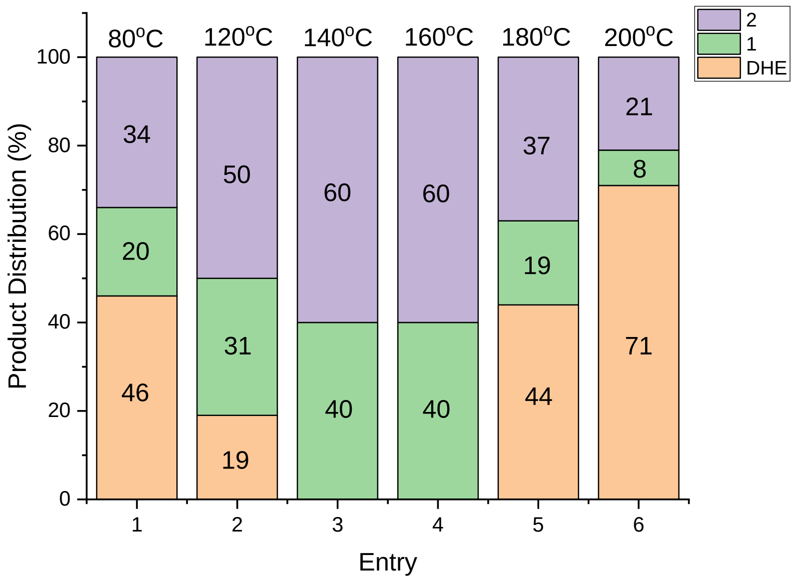

Figure S-3.1 Temperature profile of the DHE conversion catalyzed by Ru/C to (**1**) and (**2**). Reaction condition: DHE 2 g, Ru/C 0.2 g, methanol 20 mL, H_2 35 bar, 4 hours at various reaction temperatures.

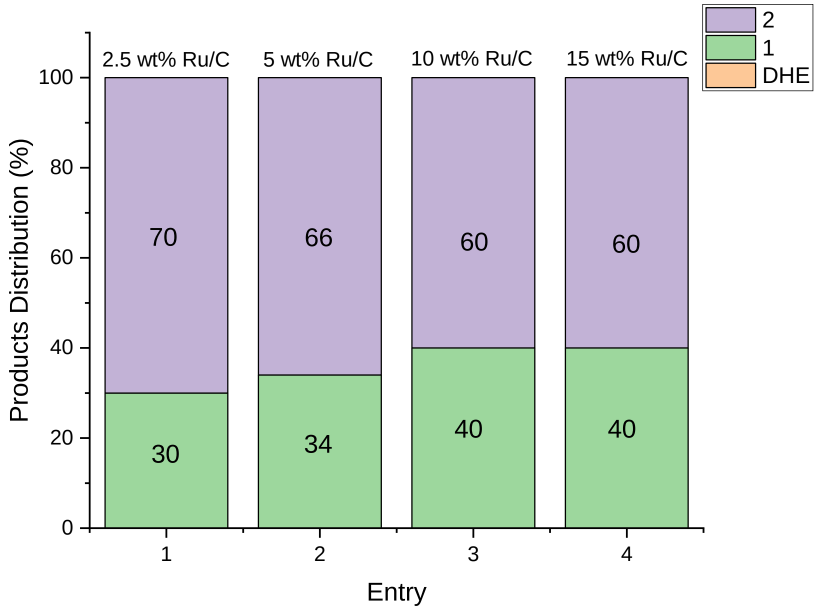

Figure S-3.2 DHE conversion catalyzed by Ru/C to (**1**) and (**2**) with different amount of catalyst. Reaction condition: DHE 2 g, methanol 20 mL, H_2 35 bar, 4 hours at 140 ℃.

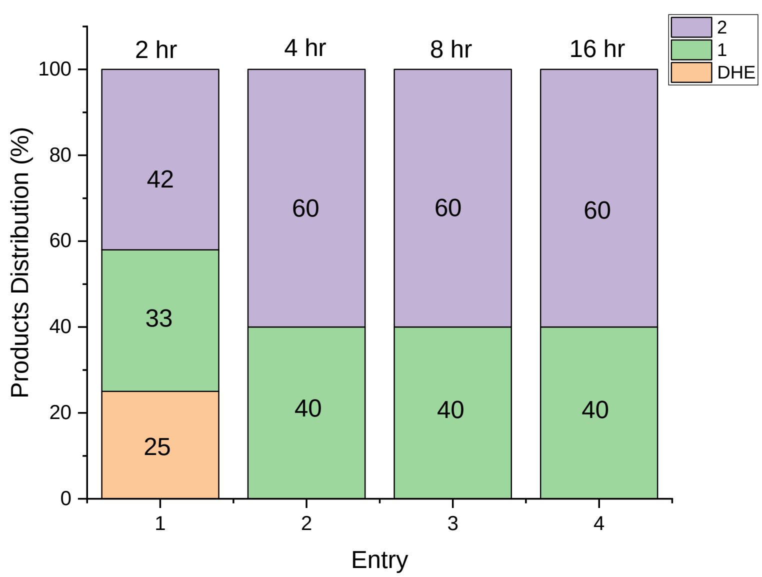

Figure S-3.3 DHE conversion catalyzed by Ru/C to (**1**) and (**2**) at different reaction time. Reaction condition: DHE 2 g, Ru/C 0.2 g, methanol 20 mL, H_2 35 bar at 140 ℃ held for 2, 4, 8, and 16 hours of reaction time.

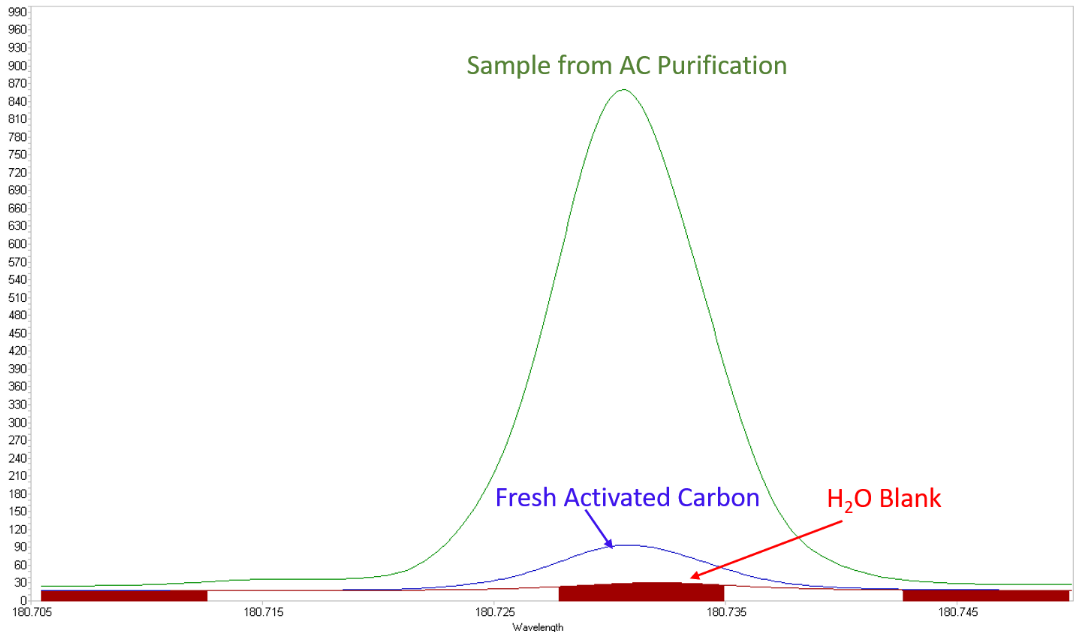

Figure S-3.4 ICP analysis of water sample from AC purification treatment.

Figure S-3.4 compares the ICP spectra of three aqueous samples. Peak labeled in red color shows the blank link of injecting pure water in ICP. The blank line also indicates there is no sulfur detection in clean water. The peak labeled in blue color illustrates the very small sulfur measurement from a sample of 3.5 g fresh activated carbon washed by 50 mL clean water. The sulfur component of bio-oil acquired from AC purification treatment is shown in the green colored peak. Activated carbon used for AC purification was 3.5 g and water used to wash sulfur after the adsorption of bio-oil on AC surface was 50 mL. The large green peak shows the evidence of sulfur content removed from AC purification is significant. The peak assignment for sulfur at 180.731 nm is based on the specific ICP instrument calibration and literature result.[1]

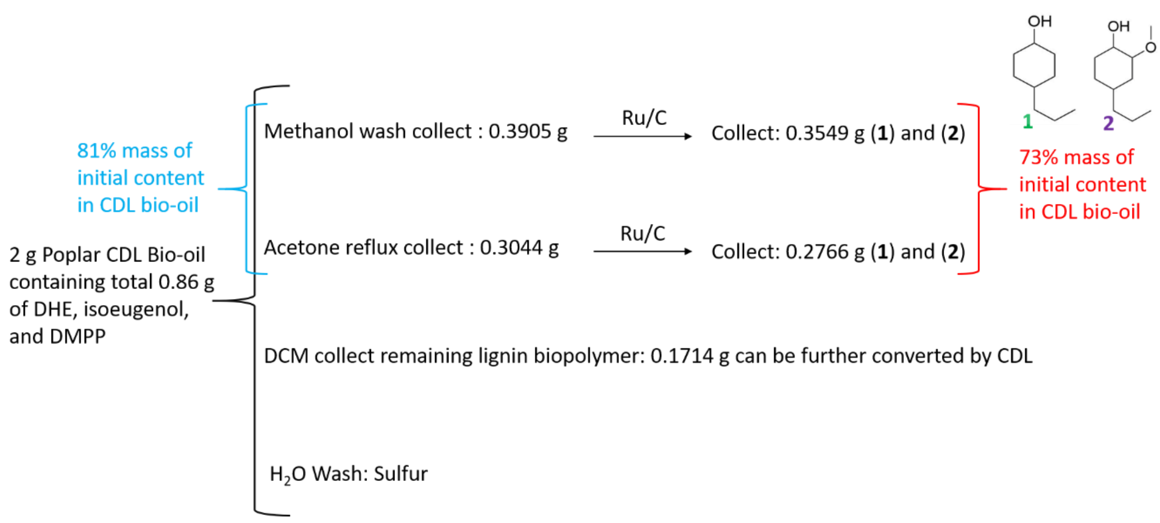

Figure S-3.5 Mass balance of bio-oil processed by AC purification treatment to product (**1**) and (**2**).

2 g bio-oil was obtained from CDL reaction of Poplar biomass. The total content of DHE, isoeugenol, and DMPP was analyzed being 0.86 g by HPLC which the method has been previously reported.[2] The 2 g bio-oil was purified by using AC treatment in 2 portions, 1 g bio-oil with 3.5 g AC of each portion. The propylphenols collected in methanol solvent was 0.3905 g while it collected by refluxing in acetone was 0.3044 g in total. Then the propylphenols isolated in different solvents were reacted in two separated reactions with the same condition. A 4-hour reaction at 140 ℃ with 10 wt% Ru/C, 20 mL methanol, and 35 bar H_2 was applied to convert the recovered propylphenols to (**1**) and (**2**).

3.7.2 References

1. Matilainen, R.; Tummavuori, J., Determination of sulfur in fertilizers by inductively coupled plasma-atomic emission spectrometry: Spectral and interelement effects at various wavelengths. *J Aoac Int* **1996,** *79* (5), 1026-1035.
2. Luo, H.; Klein, I. M.; Jiang, Y.; Zhu, H. Y.; Liu, B. Y.; Kenttamaa, H. I.; Abu-Omar, M. M., Total Utilization of Miscanthus Biomass, Lignin and Carbohydrates, Using Earth Abundant Nickel Catalyst. *Acs Sustain Chem Eng* **2016,** *4* (4), 2316-2322.

Chapter 4. Stepwise Kinetic Study of Glucose Conversion to EG and PG over Ru/C-AMT Co-catalysts System

4.1 Abstract

The combination of Ru/C and ammonium metatungstate (AMT) constitute a bifunctional catalyst system for ethylene glycol (EG) and propylene glycol (PG) production from glucose under hydrogen atmosphere at elevated temperature (240 ℃). Herein, the kinetic details and effect of each catalyst component are described. The kinetics of the three-phase reaction revealed the Ru/C is activated at moderate temperature (120 ℃) and glucose is initially hydrogenated to sorbitol following first-order kinetics. This hydrogenation process is not mass transfer limited at pressure ≥ 450 psi. 10 wt% of Ru/C showed the best catalyst efficiency. Sorbitol is then converted to smaller aldose and polyols through first order hydrogenolysis at elevated temperature (≥ 200 ℃). Ru/C shows activity towards C-C bond cleavage to polyols at a temperature ≥ 200 ℃. AMT requires higher temperature (≥ 185 ℃) to activate and it plays an important role in converting aldose intermediates. EG is immediately produced by C2-C4 cleavage of sorbitol. C4 intermediates are determined to be erythrose and erythritol. Further C-C cleavage of these intermediates gives PG and additional EG. Moreover, deposition of soluble AMT is observed, and it modifies Ru/C and results in a slower degradation of sorbitol and higher EG formation. Since AMT's role impacts selectivity for EG, the ratio of EG and PG can be adjusted from 2:1 to 100:1 by controlling the amount of AMT. 10 wt% Ru/C with 5 wt% of AMT provides an optimal reaction condition, at which glucose and intermediate sorbitol reach the highest conversion toward EG and PG formation with the highest reaction rate. A comprehensive reaction mechanism is described for Ru/C-AMT catalysis for making EG and PG from glucose. Kinetic modeling is developed to fit experimental data and provide elementary rate constants.

4.2 Introduction

Much attention has been given to converting lignocellulosic feedstocks into bioenergy, new materials, and value-added chemicals.[1-11] Cellulose is the largest component (> 50%) of lignocellulosic biomass.[12-13] Glucose is the monomeric unit of cellulose. Development of catalytic conversion of glucose to value-added chemicals and the understanding of reaction mechanisms and kinetics will result in advancing cellulose valorization in renewable applications.

Glucose has wide spectrum of products by either upgradation,[14-15] or degradation.[16-21] The two important derivatives from glucose, ethylene glycol (EG) and propylene glycol (PG) have high annual consumptions.[12, 22-26] An ultimate goal of cellulose valorization is to use glucose as a sustainable resource to produce EG and PG and substitute their conventional production from petrochemicals. Hydrothermal condition with heterogeneous catalysts is promising for glucose conversion among other methods. Noble metals and earth abundant metals, such as Ru,[12, 26-27] W,[28-30] Pt,[12] Ni,[27, 31] and Cu[32] respectively, are active for converting glucose to EG and PG. The combination of ruthenium on activated carbon support (Ru/C) and ammonia metatungstate hydrate (AMT) gives in outstanding yield and selectivity in aqueous mixture under hydrogen pressure. Up to 60% of EG yield can be obtained with 80% of total polyol yield.[12] Herein, understanding the mechanistic and kinetic details of this Ru/C – AMT co-catalysts with the tri-phase system is essential for cellulose valorization.

The mechanism of converting glucose to EG and PG is still not well-understood. Two major pathways have been proposed. They are distinguished based on C-C bond cleavage and the resulting intermediates. One involves Ru/C catalyzed aldose and ketose epimerization to their stereoisomers through Lobry de Bruyn-Alberda van Ekenstein reaction.[33-34] By which, glucose is first partially isomerized to fructose, and followed by direct C-C cleavage via retro-aldol condensation to generate intermediate aldehydes, such as erythrose, glycerolaldehyde, and glycolaldehyde.[35] Then the erythrose can be further fragmented to two units of glycolaldehyde. The glycerolaldehyde is reduced to PG and glycerol by Ru/C while glycolaldehyde is reduced to EG through hydrogenation. In the second mechanism sorbitol is converted to diols, which is consistent with the observation of sorbitol during catalysis.[27] Ru/C is both an efficient hydrogenation catalyst as well as a good hydrogenolysis catalyst.[34] Thus, the reaction pathway through sorbitol became more plausible. Instead of stereoisomerization, glucose is first reduced to sorbitol by Ru/C through hydrogenation. Sorbitol is subsequently cleaved by hydrogenolysis to generate the same series of aldehyde intermediates as those proposed for the direct C-C cleavage pathway of glucose. However, the hydrogenolysis leads to another point of contention, retro-aldol condensation versus decarbonylation.[34, 36-37] Although this question cannot be fully answered, the release of carbon monoxide supports C-C cleavage through decarbonylation.

Glucose conversion under heterogeneous catalysis is commonly conducted under harsh conditions such that the proposed intermediates are also unstable. As a result the kinetics and catalyst performance are difficult to determine. Therefore, the reaction setup should be defined to study the catalysis of glucose. In general, there are two kinds of reaction setup. One is a continuous flow reactor and the other one is a fixed batch reactor. Zhao et al.[12] introduced the advantages of using a continuous reactor, but it is still limited by the low energy efficiency, residence time, and mass transfer effect between the substrates and catalyst. Compared to the continuous reactor, although the yield and selectivity of EG are not significantly improved with the use of batch reactors, the batch system equipped with fast stirring and higher pressure can minimize mass transfer effects between both solid-liquid and liquid-gas phases. Therefore, it is more advantageous to use a batch reactor system to study the catalysis and kinetics of converting glucose to diols. Glucose in both setups requires elevated temperature (above 150 ℃) and pressure (above 400 psi) to promote catalyst activation and glucose conversion. To study the kinetics, a pressurized sampler was utilized to sample from the tri-phase reaction mixture in situ and minimize hydrogen pressure and solid catalyst losses. The hot liquid samples are cooled immediately to quench the reaction and to archive its instantaneous composition of glucose, intermediates, and diol products.

To obtain the kinetic details and understand the mechanism, we defined a batch reactor system to study the physical mixture of the co-catalyst system with physically mixed Ru/C and AMT in aqueous glucose solution under hydrogen pressure and coupled with magnetic stirring at constant rate of 700 rpm. After an investigation of reaction temperature from 90 ℃ to 240 ℃, our findings indicated Ru/C was activated at 120 ℃ in the presence of hydrogen. At this stage, while maintained above 225 psi gauge pressure, hydrogen had no impact on reaction rates. AMT was observed to be activated above 185 ℃ and became homogeneous tungsten bronze (H_xWO_3).[38] The different activation temperature allowed us to study the two catalysts separately to understand their respective functions as well as their combined benefits. In this work, the catalytic conversion of glucose was studied under two distinct conditions, under mild temperatures (120 – 180 ℃) and elevated temperatures (185 – 240 ℃). Hydrogen pressure, substrate concentration, and catalysts ratio were evaluated as factors to understand their influences on the mechanism, diol selectivity, and reaction kinetics. Experimental kinetic data was obtained under different controls and fitted with kinetic models. A plausible mechanism is proposed based on intermediates, products distribution, and kinetic dependencies.

4.3 Experimental Section

4.3.1 Reaction setup and auto sampling

The batch reaction was carried in 100mL stainless steel pressure vessel designed by Parr Instrument Company. The pressure vessel was equipped with a mechanical impeller stirrer, sampling dip tube, and a Parr 4848 reactor controller. Ru/C and AMT were physically mixed and employed to 50 mL of glucose aqueous solution in reactor vessel. The vessel was sealed and purged 4 times by 5.0 grade hydrogen gas. The hydrogen pressure was then adjusted and charged into the vessel. The reaction mixture was heated and stirred automatically by the programmed controller system to desired temperature. The mechanical impeller was set at 800 rpm stirring rate. The kinetics samples were taken by using the Parr 4878 automated liquid sampler once the reaction mixture reached the setting temperature. The auto-sampler was purged and pressurized with nitrogen gas. It created a 50 – 100 psi higher than the pressure in reaction vessel at working temperature. A 1mL liquid sample was taken through a dipping tube for each measurement at a recorded reaction time. The dipping tube was equipped with a fine filter to minimize the loss of solid catalyst from reaction mixture. The hot liquid sample was fast cooled by circling through cooling pipes to quench the reaction immediately. Then the cold liquid sample was ejected out from the cooling pipes by a small nitrogen pressure. Liquid samples were collected and sealed in 10 mL glass tube for further analysis. The auto-sampler was cleaned by purging three times of high-pressure nitrogen gas between each sampling.

4.3.2 Identification and quantification methods

The liquid sample was filtered through a 0.2 microns PTFE syringe filter to remove insoluble particles. A 500 micro liters of filtrate was mixed with internal standard by 1:1 volume ratio in an Agilent screw cap vial for HPLC analysis. A 10 mM tert-butanol aqueous solution was pre-made as the HPLC internal standard. Agilent 1260 Infinity HPLC system was used to analyze the composition of the liquid sample. An Agilent Hi-Plex H column (300 x 7.7 mm) was selected to separate sugar alcohols in this work. A 5 mM sulfuric acid aqueous solution was prepared as mobile phase and flowed through the column at rate of 0.6000 mL/min. The column was set to 70 ℃ at its working condition. Refractive index detector (RID) was used for sample analysis. The electronic signal was automatically transformed into chromatography spectrum by Agilent HPLC control program. The retention time of each possible product at the described HPLC condition was first determined by the pure commercial standard. Then the composing analytes were qualitatively identified according to their retention time. Quantification of each analyte was determined based on a calibration curve which represented the function of analyte concentration versus peak area ratio between analyte and internal standard. The calibration curve was pre-made and followed the same sample preparation steps and HPLC condition by using various concentrations of commercial standard of each analyte and the 10 mM tert-butanol aqueous solution. Additionally, an Agilent Hi-Plex Ca column was also used to distinguish glucose, fructose, sorbitol, and mannitol at the same HPLC working condition as described above.

TGA and NH_3-TPD analysis were also performed to determine the AMT and organic substrates deposition on Ru/C. TGA analysis showed the evidence of organic substrates was adsorbed on Ru/C by measuring the weight loss. Ru/C from different reactions were collected and dried under vacuum for 12 hours. A portion of 10mg Ru/C sample was placed in a platinum pan and loaded to a Discovery Thermogravimetric Analyzer. The percentage of weight loss was recorded after a temperature scanning from 40 ℃ to 600 ℃ at 20 ℃/min ramping rate.

NH_3-TPD was done by Micromeritics AutoChem 2920 instrument. A portion of 100 mg Ru/C sample was placed into a U-shaped, flow thru, quartz sample tube. Prior to measurements, the catalyst was pretreated in He (25 cm^3/min) at 500 ℃ for 0.5 hours. A mixture of NH_3 in He

(10%) was passed (15 cm^3/min) at 25 ℃ for 1 hour. Then, the sample was, subsequently flushed with He (25 cm^3/min) at 100 ℃ for another hour. The TPD measurements were carried out in the range 100-800 ℃ at a heating rate of 10 ℃/min. Ammonia concentration in the effluent was monitored with filament thermal conductivity detector. The amount of desorbed ammonia was determined based on the integrated area under the peak.

The gas phase of reaction mixture was analyzed by using Residual Gas Analyzer (RGA). Gas phase samples were collected after each reaction while the whole system was cooled to room temperature. Samples were vent from reaction vessel and collected in gas sampling bags. 100 micro liters of gas sample were then injected to RGA by gas-tight syringe. Analytes were identified by directly reading the molecular weight (m/Z) signals from RGA.

4.3.3 Data processing and computational modeling

The first order experimental rate constant, k_{obs}, was determined by fitting the exponential function into the curve of the analyte concentration (mM) versus time (s). The obtained k_{obs} was then used in computational modeling. The computational work was performed based on the function of rate expressions derived from proposed kinetic models (KS4-1, KS4-2).

4.3.4 Materials

All commercial chemicals were purchased and used as is. Ammonium metatungstate hydrate (99.99%), D-mannitol (≥98%), D-sorbitol (99%), 1,3-butanediol (≥99%), ethylene glycol (99.8%), tert-butanol (≥99.5%), glycolaldehyde (99%), erythrose (75%), ruthenium (III) chloride (99.98%), zirconium (IV) oxide, and ruthenium on carbon (5wt% Ru loading) were purchased from Sigma Aldrich. According to the merchant report, commercial Ru/C was synthesized and analyzed to have 900 m^2/g surface area and 19 microns particle size on average. No further catalyst characterization and pretreatment had been done before use in this work. D-glucose (99%) was purchased from Alfa Aesar. D-fructose (99%) was purchased from Acros Organics. Glycerol (99%) was purchased from Fisher Chemical. 1,4-butanediol (99%) was purchased from Spectrum. 1000 ppm ruthenium in 10% (V/V) HCl was purchased from Inorganic Ventures. The 5.0 grade hydrogen gas and nitrogen (99.998%) were purchased from Praxair. Water used for reaction and sample preparation was obtained from a A10 Milli-Q water purification system by Millipore.

Ru (5 wt%) supported on ZrO_2 was prepared by wet impregnation method. Ruthenium chloride precursor (0.0980 g) ($RuCl_3$, Aldrich) taken in beaker containing 10 mL of distilled water. This solution was added to 0.950 g of ZrO_2. It was mixed thoroughly and dried at 80 ℃ using a rotary evaporator. The solid obtained was recovered and dried at 110 ℃ for 4 hours in an electric oven. In specific case, Ru/ZrO_2 material was calcined at 400 ℃ for 3 hours. In other cases, catalysts were reduced under flow of hydrogen (50 mL/min) at 400 ℃ for 3 hours.

4.4 Results and Discussion

4.4.1 Hydrogenation of glucose to sorbitol

4.4.1.1 Catalyst dependence

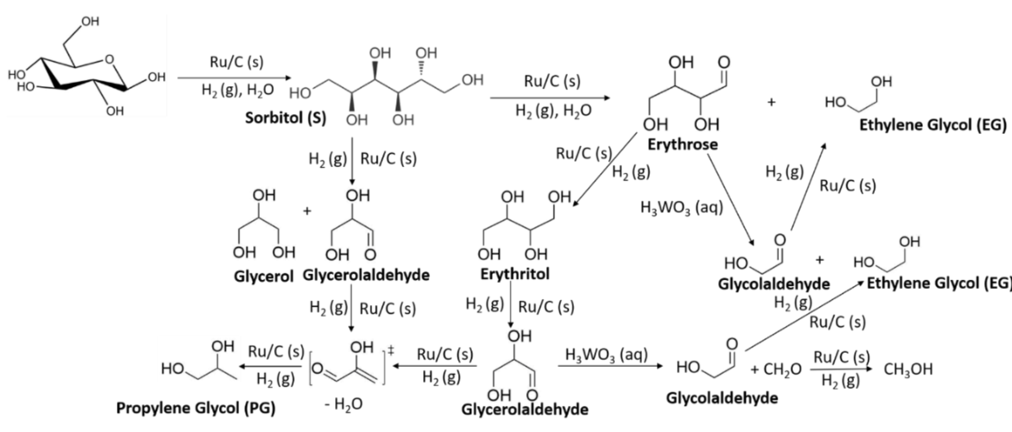

Scheme 4.1 Proposed mechanism scheme of glucose conversion through sorbitol to EG and PG catalyzed by Ru/C and AMT under hydrogen at 240 ℃.

By summarizing the literature and our experimental results from the detection of products and intermediates, Scheme 4.1 illustrates our proposed mechanism of Ru/C and AMT catalyzed glucose conversion to EG and PG. The overall mechanism can be divided into two stages: (1) hydrogenation of glucose to sorbitol, and (2) the hydrogenolysis of sorbitol to cleave carbon-carbon bonds into smaller intermediates and products. By which, we first observed the glucose was fully converted into sorbitol rapidly during this catalytic process. The C-C cleavage and subsequent reactions occurred mainly after catalyst activation at higher temperature. EG product was detected concurrently with erythritol once the reaction reached the hydrogenolysis temperature. Thus, we propose the first step of the hydrogenolysis is C2-C4 cleavage to give EG (C2 product) and erythrose (C4 intermediate). However, glycerol was also detected during the reaction and the formation of PG was not observed initially. Therefore, we concluded there were also some C3-C3 hydrogenolysis decomposed sorbitol to glycerol and glycerolaldehyde (C3 intermediates). After that, the C3 intermediates were converted to PG. Meanwhile, the further conversion of erythritol could either undergo C2-C2 hydrogenolysis to EG or C3-C1 hydrogenolysis to PG. In this work, the reaction kinetics was studied according to this proposed mechanism. More details of the reaction mechanism and the experimental results of the reaction pathways will be provided and discussed below.

To investigate the hydrogenation of glucose in this system (Scheme 4.1), a series of reactions at different temperatures were conducted (Figure S-4.1). Hydrogenation product sorbitol was detected at 97% yield, and Ru/C catalyst only showed activity of hydrogenation between 120 ℃ to 180 ℃. As a result, 120 ℃ was selected as the reaction temperature to study the conversion of glucose to sorbitol by Ru/C. Different amount of catalyst was loaded into the reaction mixture from 2.2 wt% to 40 wt%. Interestingly, a negative trend between the observed rate constant (k_{obs}) with increasing amount of catalyst loading were observed when more than 10 wt% Ru/C was used (Figure 4.1).

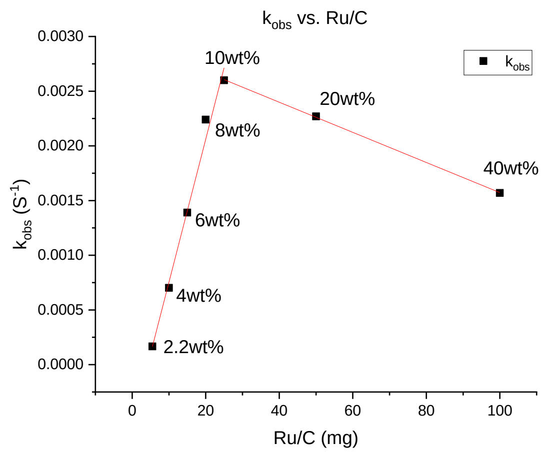

Figure 4.1. K_{obs} of glucose conversion dependence on Ru/C. (Condition: 28 mM glucose aqueous solution 50 mL, 2.2 wt% - 40 wt% Ru/C, 450 psi H_2, 240 °C)

Ru/C (wt%)	**AC/G (wt)**	**Ru/G (wt)**	**K_{obs} (S^{-1})**
2.2	0.0209	0.0011	1.67×10^{-4}
4	0.038	0.002	7.02×10^{-4}
6	0.057	0.003	1.39×10^{-3}
8	0.076	0.004	2.24×10^{-3}
10	0.095	0.005	2.56×10^{-3}
20	0.19	0.01	2.27×10^{-3}
40	0.38	0.02	1.57×10^{-3}

Table 4.1 K_{obs} of glucose conversion with various amount of Ru/C catalyst. Mass of activated carbon (AC) and ruthenium metal were determined based on the loading of ruthenium on support. The amount (mg) of Ru/C was contributed by 5% ruthenium and 95% activated carbon.

When the catalyst loading is increased, the ratio between activated carbon and glucose substrate increased as well and more significantly than the ratio between Ru and glucose (Figure 4.2).

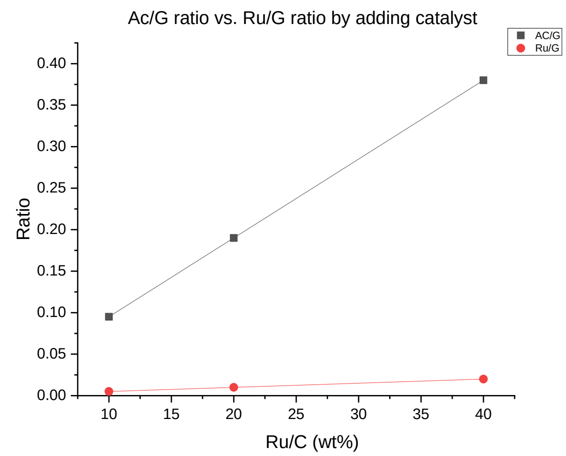

Figure 4.2 Ratio of carbon-glucose and ruthenium-glucose at different amount of catalyst loading. Ac: activated carbon, G: glucose.

According to this phenomenon, our hypothesis was the adsorption of substrate on excess catalyst support (activated carbon) slows down glucose conversion to sorbitol because less glucose is available for reaction on Ru sites (Figure S-4.2, Table S-4.1). This process is summarized as the following hypothesized equations (HEq) 1-3. By which, the HEq.1 states the glucose that is sufficiently adsorbed the Ru active sites which can be further converted to sorbitol and released from Ru site to reaction medium in HEq.2. In contrast, the HEq.3 represents the glucose is adsorbed on the excess carbon surface which is not immediately converted by Ru sites and thus slows the reaction rate.

Glucose + Ru/C → Glucose-Ru/C ------ HEq.1

Glucose-Ru/C → Ru/C + Sorbitol ------ HEq.2

Glucose + Ru/C → Ru/C-Glucose ------ HEq.3

Therefore, catalyst loading from 2.2 wt% to 10 wt% (Figure 4.1) resulted in a linear increase in k_{obs} indicating first order dependence on catalyst and in this range the additional amount of activated carbon did not impact the kinetics of glucose hydrogenation .

4.4.1.2 Hydrogen dependence and mass transfer effect

The hydrogen gas pressure was another important parameter to be evaluated for its effect on the kinetics. A sequence of reactions was performed with 10 wt% Ru/C loading and 5 different initial H_2 pressures: 225, 450, 550, 650, and 750 psi. A significant increase of k_{obs} was detected when the H_2 loading was increased from 225 to 450 psi (Figure 4.3 and Table 4.2). However, k_{obs} values remained constant over H_2 pressure from 450 to 750 psi (Figure 4.3, Table 4.2).

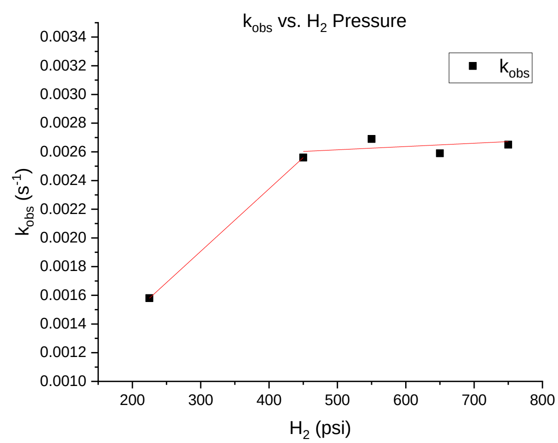

Figure 4.3 K_{obs} of glucose conversion dependence on H_2. (Condition: 28mM glucose aqueous solution 50mL, 25mg Ru/C, 225psi – 750psi H_2, 240℃)

H_{2i} (psi)	$K_{obs\text{-}G}$ (S^{-1})
225	$1.58x10^{-3}$
450	$2.56x10^{-3}$
550	$2.69x10^{-3}$
650	$2.96x10^{-3}$
750	$2.65x10^{-3}$

Table 4.2 K_{obs} of glucose conversion with various amount of initial hydrogen pressure recorded at room temperature.

Table 4.2 summarizes k_{obs} at different H_2 pressures. By which, it suggested the conversion of glucose to sorbitol is independent of hydrogen pressure > 450 psi. Moreover, this finding also indicated the gas phase hydrogen above 450 psi created a nearly constant soluble hydrogen ([H]) in liquid phase which was enough accessible for hydrogenation reaction and thus overcame the mass transfer effect between the gas phase and catalyst active sites. Besides, different amount of initial glucose concentrations was tested. Concentration of glucose also showed negligible impact on the observed reaction rate constant (Figure S-4.3, Table S-4.2). Therefore, we concluded there was no mass transfer effect in both gas-liquid and liquid-solid phases in our defined batch reactor system.

4.4.1.3 Kinetic model

Assumption of a four-step process was made for hydrogenation of glucose on Ru/C catalyst surface (Kinetic Model KS4-1), which included (1) glucose adsorption on catalyst surface, (2) catalyst activation by hydrogen ([H]), (3) irreversible hydrogenation of glucose, and (4) sorbitol desorption from catalyst surface. An expression was derived to describe this four-step process (Eq. 1) with steady state approximation. Since no mass transfer effect and zero-order dependence on hydrogen pressure (> 450 psi) were determined, the constant [H] was estimated by Henry's law.

$$\frac{d[\mathrm{s}]}{dt} = \frac{k_{1f}k_{2f}k_{3f}[G][Ru][H_2]}{(k_{2r} + k_{3f})(k_{1r}+k_{2f}[H_2])} - k_{4r}[\mathrm{S}][\mathrm{Ru}] \quad \text{------ Eq. 1}$$

The sorbitol term in Eq. 1, k_{4r}[S][Ru], demonstrates that as the sorbitol concentration in liquid phase increases the conversion rate slows down by affecting the equilibrium between sorbitol adsorption and desorption from the catalyst surface. A higher [S] would reduce the reaction rate by shifting the equilibrium to sorbitol adsorption. More sorbitol would occupy the surface of catalyst and reduced accessibility of active sites for glucose. With this assumption, two sequences of control experiments were done with adding different amount of sorbitol at the beginning of reaction, and different starting ratios of sorbitol and glucose vs. Ru/C. Very small change of k_{obs} was observed with different amount of sorbitol added (Figure S-4.4, Table S-4.3). This finding suggested the effect by sorbitol concentration was negligible to the whole kinetic process. Therefore, the desorption of sorbitol from catalyst surface is more favorable than its adsorption. Furthermore, this simplifies the rate expression into Eq. 2, which was advanced for computational modeling (Figure 4.4, Table 4.3).

$$\therefore k_{obs} \cong \frac{k_{1f}k_{2f}k_{3f}[Ru][H_2]}{(k_{2r} + k_{3f})(k_{1r}+k_{2f}[H_2])} \quad \text{------ Eq. 2}$$

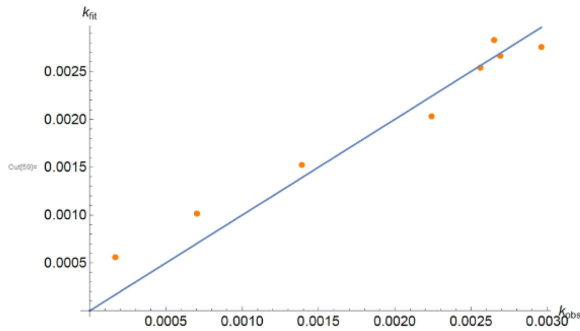

	Estimate	Standard Error	T-Statistic	P-Value
K_{1f}	21.6396	4.55	4.67	0.0176
K_{1r}	0.17063	0.296	0.576	0.605
K_{2f}	23.0312	0.002	10.5	1.91E-12
K_{2r}	10.0539	3.56	2.83	0.0664
K_{3f}	17.5910	2.03	8.65	0.00325

Figure 4.4 Experimental k_{obs} fitted with kinetics model.

Table 4.3 Estimated rate constant with standard error, T-statistic, and P-values.

In comparison with the simulated result (blue line on Figure 4), our experimental values (orange dots on Figure 4.4), k_{obs} were well dispersed around k_{fit} curve, which indicated the overall hydrogenation of glucose over Ru/C in this batch system follows first-order kinetics. Table 4.3 summarizes the fitted rate constants based on the kinetic model. The very small estimated k_{1r} suggested the adsorption of glucose was favorable, and can be considered irreversible. The values of k_{1f} and k_{2f} were estimated to be larger than k_{3f} which indicated the rate-determine step was the hydrogenation step where the glucose was reduced after the binding to the active sites of catalyst (SI, KS4-1 Step 3). Although k_{4f} and k_{4r} could not be estimated in this study, control experiments with initial sorbitol addition suggested the sorbitol adsorption on Ru/C was not favorable. Thereby, k_{4r} was expected to be a much smaller value than k_{4f}.

4.4.2 Sorbitol hydrogenolysis to ethylene glycol and propylene glycol

4.4.2.1 Catalyst behavior

To understand the C-C cleavage step, a control reaction of glucose, Ru/C, and AMT was first brought up to 185℃, at this point both Ru/C and AMT would be activated under hydrogen pressure (Figure S-4.5). Over 85% of glucose was converted into sorbitol within five minutes during the heating up period. Once the mixture reached 185 ℃, the clear colorless solution turned into light yellow within 2 minutes and all glucose was converted, but sorbitol accumulated, and its concentration stayed steady as the reactor temperature reached 185 ℃. This phenomenon suggested the major starting substrate for the following hydrogenolysis steps was sorbitol.

However, previous studies introduced the tungsten catalyst as more active towards C-C bonds in aldose (glucose) than saturated polyols (sorbitol).[38,39] Thus, a sequence of reactions was performed to understand the role of the tungsten catalyst (AMT) and Ru/C in the sorbitol conversion to diols. First, a mixture of 28 mM sorbitol and 10 wt% of AMT was heated to 240 ℃ under 850 psi hydrogen. Without Ru/C, no reaction was observed (Figure S-4.6). In contrast, a mixture of 28 mM sorbitol with 10 wt% of Ru/C was investigated under the same condition and 100% conversion of sorbitol was observed with an observed first-order rate constant k_{obs} of 1.24×10^{-3} s^{-1} (Figure S-4.7). Meanwhile, first order formation of EG and PG were also observed and the product distribution between those two was about 2:1 (Figure S-4.8). Lastly, with both AMT and Ru/C (10 wt% of each), sorbitol under the same condition was converted slower than with Ru/C alone but produced EG with much higher selectivity (Table 4.4).

Trials	K_{obs-S} x10^{-4} (S^{-1})	K_{obs-EG} x10^{-5} (S^{-1})	K_{obs-PG} x10^{-5} (S^{-1})	S Conversion (%)	EG : PG
2.5wt% Ru/C, 5wt% AMT, 850psi H_2	1.90	3.20	3.72	54	5.6 : 1
5wt% Ru/C, 5wt% AMT, 850psi H_2	2.35	4.67	7.14	68	3.7 : 1
10wt% Ru/C, 5wt% AMT, 850psi H_2	3.82	12.7	11.8	91	1.65 : 1
10wt% Ru/C, 10wt% AMT, 850psi H_2	1.81	3.07	6.70	58	37 : 1
10wt% Ru/C, 20wt% AMT, 850psi H_2	1.78	1.97	4.67	58	115 : 1
10wt% Ru/C, 5wt% AMT, 450psi H_2	3.81	5.72	15.2	84	5.5 : 1
10wt% Ru/C, 5wt% AMT, 650psi H_2	3.73	6.83	15.6	83	4.4 : 1
10wt% Ru/ZrO_2, 5wt% AMT, 850psi H_2	2.13	7.3	6.1	60	28 : 1

Table 4.4 Experimental rate constant, sorbitol conversion, and product distribution at Ru/C-AMT bi-catalyst system. Sorbitol conversion and EG:PG was recorded at 5000 seconds of reaction period. Reaction condition: 28 mL sorbitol aqueous solution 50 mL, Ru/C, AMT, H2, 240 °C.

Interestingly, although the conversion of sorbitol was lowered to 58% when the co-catalyst of AMT and Ru/C was employed, product selectivity was improved. The ratio of EG:PG was 37:1. This finding suggested the EG formation was favorable with the addition of AMT. Even though EG formation was improved for the co-catalyst system, the observed rate constant of was slower by an order of magnitude compared to Ru/C alone (Table 4.4). In total, our experimental results are consistent with the hydrogenolysis of sorbitol being initiated by Ru/C to form unsaturated aldose and aldehyde intermediates. And AMT catalyzes further C-C cleavage of the aldose and aldehyde intermediates to produce EG. However, with addition of AMT to the reaction mixture, the overall reaction rate of sorbitol hydrogenolysis was decreased. Thus, there must be some interaction between AMT and Ru/C modifying the catalyst and affecting the overall reaction kinetics.

4.4.2.2 Ru/C only system

The catalytic conversion of sorbitol with the two catalysts mixture was more complicated than the step of glucose hydrogenation (Scheme 4.1). Not only because it had multiple reaction pathways, and intermediates, but also interactions between the two catalysts were observed. To understand the function of each catalyst clearly for both sorbitol decomposition and EG formation, control experiments with solo catalyst were first performed to study the factors that could influence the reaction kinetics. Since the AMT was observed to have no activity in catalyzing sorbitol but still affecting the rate of sorbitol hydrogenolysis, and meanwhile Ru/C could catalyze sorbitol to EG and PG by itself, a study of the solo dependence on Ru/C for sorbitol hydrogenolysis was undertaken. The Ru/C catalyzed hydrogenolysis for C-C cleavage occurred only above 220 ℃. A sequence of experiments with different Ru/C loading, 2.5 wt%, 5 wt%, and 10 wt%, were investigated under 450 psi hydrogen pressure at 240 ℃. As a result, sorbitol disappearance and the products formation were both observed with first order dependence on Ru/C loading.

Trials	$K_{obs\text{-}S}$ x10^{-4} (S^{-1})	$K_{obs\text{-}EG}$ x10^{-5} (S^{-1})	$K_{obs\text{-}PG}$ x10^{-5} (S^{-1})	S Conversion (%)	EG : PG
2.5wt% Ru/C, 450psi H_2	2.35	3.04	1.29	68	2.0 : 1
5wt% Ru/C, 450psi H_2	3.52	6.66	2.76	81	1.2 : 1
10wt% Ru/C, 450psi H_2	6.83	9.27	4.92	98	2.1 : 1
10wt% Ru/C, 650psi H_2	8.16	24.8	15.7	100	1.2 : 1
10wt% Ru/C, 850psi H_2	12.4	32.1	22.7	100	1.8 : 1

Table 4.5 Experimental rate constant, sorbitol conversion, and product distribution at Ru/C solo system. Sorbitol conversion and EG:PG was recorded at 5000 second of reaction period. (Condition: 28mL sorbitol aqueous solution 50mL, Ru/C, H2, 240℃)

Table 4.5 summarizes the measured kinetics data of sorbitol conversion by Ru/C solo catalyst trials. It indicates the complete conversion of sorbitol was reached at10 wt% of Ru/C loading. We hypothesized the sorbitol degradation would follow substrate-adsorption and product-desorption steps on catalyst surface. However, compared to the catalytic hydrogenation of glucose under the same reaction condition, sorbitol required longer times to the react. This could be because the adsorption of sorbitol from liquid phase onto the Ru/C surface was not favorable and thus reduced the rate of reaction. This phenomenon of unfavorable sorbitol adsorption onto Ru/C catalyst was consistent with what we have concluded above. In case of starting from glucose, the generated sorbitol could possibly undergo an inner-surface transfer to the active sites of hydrogenolysis on Ru/C, and this resulted a faster overall reaction rate.

The effect of hydrogen pressure was also studied in this Ru/C solo system and the kinetics data obtained with different hydrogen pressure summarized in Table 4.5. Within the hydrogen pressure from 450 to 850 psi (gauge), first order dependence on hydrogen was observed (Figure S-4.9). According to the proposed mechanism in Scheme 4.1, the last step prior to EG and PG formation is a Ru/C catalyzed hydrogenation of C_2 (glycolaldehyde) and C_3 aldehyde intermediates, which we had concluded the hydrogenation process was zero order dependence on hydrogen in our batch reactor system when hydrogen pressure was above 450 psi. The first order dependence on hydrogen suggested the C-C cleavage is accelerated by higher hydrogen pressure, (Figure S-4.10).

4.4.2.3 Co-catalyst system

As we determined, the AMT only catalyzed the reaction with aldose and aldehyde intermediates in this system. However, the unstable aldehyde intermediates were not detectable in our in situ sampling.

Various ratios of AMT:Ru/C were investigated with 28 mM sorbitol solution at 240 ℃. A critical point was found at mass ratio of 0.5:1 which had 12.5 mg AMT and 25 mg Ru/C charged into the co-catalyst system. 91% of sorbitol conversion was observed with an observed rate constant of $3.82 \times 10^{-4}\ s^{-1}$ (Table 4.4). As summarized in Table 4.4, increasing the Ru/C loading from 2.5 wt% to 10 wt% significantly increased the reaction rate. Meanwhile, when the AMT loading was increased from 0 to 5 wt% it decreased the reaction rate when compared to the Ru/C solo reaction. Interestingly, although the AMT slowed the overall reaction, with 10 wt% and 20 wt% of AMT had no impact on further reduction of the reaction rate. By which the observed rate constant of sorbitol decomposition was determined to be around $1.80 \times 10^{-4}\ s^{-1}$ when more than 5 wt% of AMT was used. Besides, when the catalysts ratio was 1:1 (10 wt% of each catalyst), the product distribution of EG:PG was obtained as 37:1, while lower AMT loading by half (AMT:Ru/C at 0.5:1) gave the EG and PG ratio as 1.65 : 1 (Table 4.4). Moreover, in comparison with Ru/C solo system, EG formation was improved with use of AMT, but production of PG was inhibited with use of more than 5 wt% AMT. Although high AMT content (>10 wt%) would result in more selective EG formation, the lower ratio of AMT gave nearly twice of the total product yield. In total, 10 wt% Ru/C and 5 wt% AMT was determined as the most efficient combination for this co-catalyst system (Figure S-4.11). A higher AMT loading may be used if only EG is desired, with 20 wt% AMT, EG:PG = 115:1.

Although the use of AMT affected the reaction rate and products distribution, AMT did not change the kinetics dependencies of the reaction. The slower reaction rate observed for sorbitol hydrogenolysis suggested that the Ru/C must be modified by AMT. To understand the interactions between AMT and Ru/C, several analyses of the catalysts were performed. While AMT was activated, it became homogeneous in the reaction solution.[12] We hypothesized the homogeneous tungsten species were possibly adsorbed to the Ru/C surface. Since the contact between the substrate and ruthenium had been discussed to affect the kinetics, therefore the slower sorbitol conversion could attribute to the competition between AMT and sorbitol adsorption on Ru/C surface. To understand this, ruthenium catalyst on zirconia with smaller surface area (Ru(5%)/ZrO_2, < 300 m^2/g) were synthesized to simulate the reduced catalyst surface area after AMT deposition onto Ru/C. The less surface area of catalyst support provides a less contact between substrate and active sites. 25 mg Ru/ZrO_2 was charged into 28 mM sorbitol aqueous solution with 12.5 mg AMT. The reaction was heated to 240 ℃ under 850 psi hydrogen pressure. The k_{obs} was measured as $2.13x10^{-4}$ s^{-1} which is nearly 2x less than using the same equivalent Ru/C (Table 4.4). This confirmed the poor accessibility of substrate to catalyst resulted in slower sorbitol conversion. To detect the adsorbed AMT on Ru/C and determine if it was competing with the substrate adsorption, thermal desorption measurement (NH_3-TPD) and thermogravimetric analysis (TGA) were conducted. Known AMT's higher acidity compared to Ru/C, NH_3-TPD was used to observe the existence of tungsten species on Ru/C (Figure S-4.12, Table S-4.4), by which a higher acidity would be observed when AMT was adsorbed on Ru/C. As a result, the spent Ru/C catalyst was recovered from the co-catalyst system and it gave 1.4 mmol/g of NH_3 adsorption compared to 0.90 mmol/g for fresh Ru/C. The higher NH_3 adsorption indicated the spent Ru/C catalyst became more acidic than the starting Ru/C catalyst. Therefore, the NH_3-TPD analysis is consistent with our hypothesis of increased acidity due to AMT deposition onto the Ru/C catalyst. On the other hand, TGA test was performed for a further confirmation of the occupancy of tungsten, by which the adsorbed AMT would lower the adsorption of sorbitol or other intermediates on Ru/C. Figure S-4.13 and Table S-4.5 illustrate the spent Ru/C versus Ru/C solo reaction gave 17% and 22.5% weight loss, respectively. This result is consistent with lowered substrate adsorption on Ru/C by addition of AMT. Therefore, the slower hydrogenolysis of sorbitol hydrogenolysis was mainly because of the deposition of tungsten species onto Ru/C inhibiting sorbitol access.

4.4.2.4 Co-catalyst kinetic model

Scheme 4.2 describes the proposed stepwise reaction pathways of converting glucose into EG and PG with the co-catalyst system (Ru + W). The overall mechanism contains multiple steps. Different intermediates are involved. However, for the kinetics data analysis , a simplified mechanism of the whole process is needed.

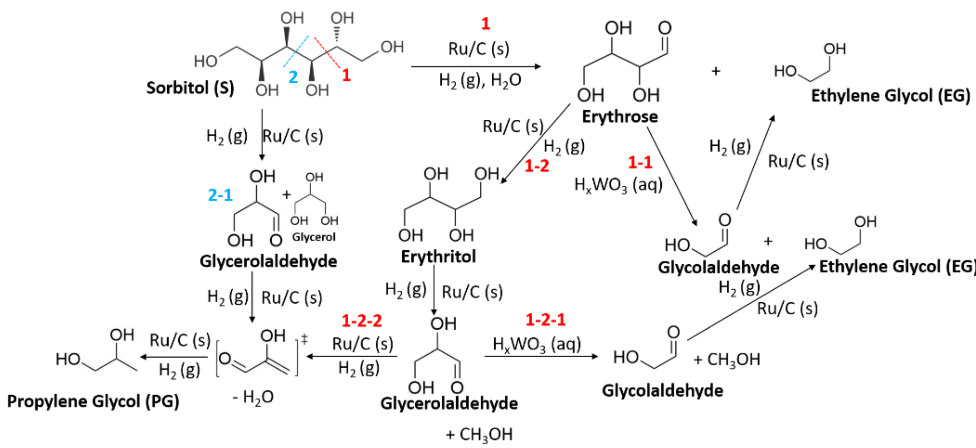

Scheme 4.2 Reaction scheme of sorbitol conversion to EG and PG through various intermediates.

According to Scheme 4.2, the formation of PG is mainly through the pathway 2-1 and 1-2-2. These two pathways are catalyzed by Ru/C. As a result, 2-1 and 1-2-2 could be combined and the determined k_{obs} of PG formation represent the rate constants of both pathways. EG formation is dependent on AMT, herein pathways 1-1 and 1-2-1 could be combined for the best estimation of kinetic parameters. A significant amount of erythritol was detected as an intermediate during the reaction. Thus, route 1 was proposed in which the Ru/C catalyzed hydrogenolysis produces erythrose and EG from sorbitol. Subsequently erythrose is either reduced over Ru/C to form erythritol, or erythrose is converted over tungsten to glycolaldehyde and EG through pathway 1-1. Therefore, k_{obs} determined by EG formation stems from the complex pathways of 1, 1-1, and 1-2-1. With these assumptions, a simplified reaction scheme is proposed in Scheme 4.3.

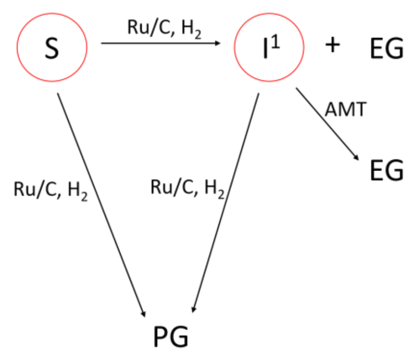

Scheme 4.3 Simplified scheme for computational modeling. I^1: intermediate of the direct sorbitol conversion by Ru/C catalyzed hydrogenolysis.

The rate expressions for sorbitol conversion and EG, PG formation could be derived based on this simplified model (Eqs 3-6 and Kinetic Model KS4-2).

$$\frac{d[S]}{dt} = -k_{1f}RH[S] - k_{2f}RH[S] \text{ ------ Eq. 3}$$
$$\frac{d[I]}{dt} = k_{1f}RH[S] - k_{3f}RH[I] - k_{4f}A[I] = 0 \text{ ------ Eq. 4}$$
$$\frac{d[P]}{dt} = 2k_{2f}RH[S] + k_{3f}RH[I] \text{ ------ Eq. 5}$$
$$\frac{d[E]}{dt} = k_{1f}RH[S] + k_{4f}A[I] \text{ ------ Eq. 6}$$

By solving for intermediate [I], the rate expressions were further transformed into a function in terms of sorbitol (Eq #7-#9 and Kinetic Model KS4-2).

$$S(t) = a_0 \exp[\alpha t] \text{ ------ Eq. 7}$$

$$P(t) = \frac{a_0}{\alpha}\beta \exp[\alpha t] + b_1 \text{ ------ Eq. 8}$$

$$E(t) = \frac{a_0}{\alpha}\gamma \exp[\alpha t] + c_1 \text{ ------ Eq. 9}$$

The Greek letters α, β, and γ represent observed rate constant for sorbitol, PG, and EG respectively. The computational fitting was accomplished by applying the observed rate constants back to Eq. 3-6.

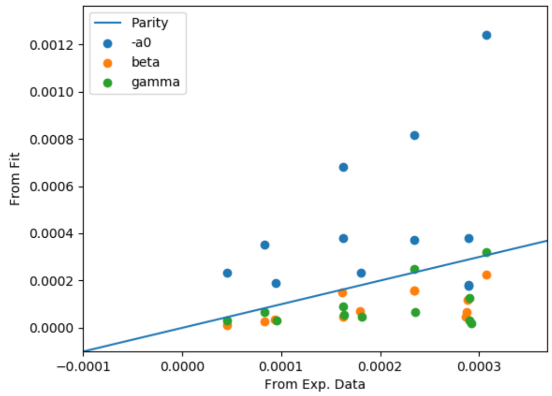

Figure 4.5 Experimental kinetic parameters (Table S-4.6) of sorbitol conversion and EG, PG formation at various reaction conditions fitted with computational model.

Figure 4.5 compares the computed kinetic data (blue line?) versus experimental results (dots). The estimation of rate constant k_1 through k_4 was acquired based on a quasi-Newton method, Broyden Fletcher Goldfarb Shanno algorithm (BFGS). The k_1 was estimated to be (1.3$\pm$0.5) x10^{-5} $mM^{-2}s^{-1}$. The unit of k_1 in this estimation is third-order rate constant which was attributed to taking the amount of Ru/C and soluble [H] into account. However, using number of active sites on Ru/C instead of using the amount of reagents (in unit of moles) of Ru/C could give a better estimation. k_2 was computed to be (2$\pm$1) x10^{-5} $mM^{-2}s^{-1}$. The large error obtained in the k_2 estimation was because of the complexity of PG formation though erythritol pathways. In contrast, the lower uncertainty in k_1 estimation suggested the EG was the major product from both Ru/C catalyzed hydrogenolysis of sorbitol and AMT catalyzed aldehyde conversion, and thus experimental k_{obs} measured by EG formation were well represented in the experimental reaction kinetics. k_1 could help to estimate k_4 to be a much larger value than k_1 indicating pathway 1-1 over AMT is fast and the rate determining step is C-C cleavage through hydrogenolysis. Moreover, this also explains the phenomenon that EG was detected immediately once the reaction reached the catalyst activation temperature, but PG formation was delayed. However, k_3 and k_4 were estimated with large errors due to the complexity of the other undetected intermediates, not much information is reflected on these steps from experimental measurements.

4.5 Conclusion

In this work, we studied the kinetics of the tri-phasic catalytic conversion of glucose over Ru/C and AMT in a fixed batch reactor system. The well fitted experimental results indicated glucose conversion in our system followed first order kinetics. Substrate consumption and product formation over the heterogeneous catalyst was through adsorption-desorption steps, and thus the mathematical expression described well glucose conversion. Sorbitol formation at mild temperature (120 – 180 ℃), and the absence of fructose, indicated the reaction was initiated by the hydrogenation reaction of glucose, instead of isomerization or direct glucose hydrogenolysis/scission. AMT catalyzed the cracking of aldose at above 180 ℃. The addition of AMT improved the formation of EG, but the homogenous tungsten species reduced the contact between substrates and Ru/C and herein resulted in a slower reaction rate of the co-catalyst system. The absence of carbon monoxide in the gas phase supported sorbitol degradation through retro-aldol condensation, rather than decarbonylation. The computed rate constants also suggested the hydrogenolysis of sorbitol was the rate determining step in this reaction. While evaluating the factors impacting reaction kinetics, our findings indicated that excess of carbon support inhibited glucose conversion. Thereby, we concluded 10 wt% Ru/C and 5wt% AMT loading was desirable. Although hydrogen pressure >450 psi had no influence on sorbitol formation within the Ru/C catalyzed hydrogenation of glucose, a higher pressure was ideal for sorbitol hydrogenolysis (C-C cleavage). The rate constants of sorbitol conversion to C_2-C_4 and C_3-C_3 were estimated according to a simplified kinetics model, yielding estimated rate constants of EG was (1.29$\pm$0.54) x10^{-5} $mM^{-2}S^{-1}$ and PG was (2.14$\pm$1.05) x10^{-5} $mM^{-2}S^{-1}$, respectively.

4.6 References:

1. Alvarez, J.; Amutio, M.; Lopez, G.; Santamaria, L.; Bilbao, J.; Olazar, M., Improving bio-oil properties through the fast co-pyrolysis of lignocellulosic biomass and waste tyres. *Waste Manag* **2019,** *85*, 385-395.

2. Amirjalayer, S.; Fuchs, H.; Marx, D., Understanding the Mechanocatalytic Conversion of Biomass: A Low-Energy One-Step Reaction Mechanism by Applying Mechanical Force. *Angew Chem Int Ed Engl* **2019,** *58* (16), 5232-5235.

3. Arias, K. S.; Climent, M. J.; Corma, A.; Iborra, S., Biomass-derived chemicals: synthesis of biodegradable surfactant ether molecules from hydroxymethylfurfural. *ChemSusChem* **2014,** *7* (1), 210-20.

4. Bi, Z.; Lai, B.; Zhao, Y.; Yan, L., Fast Disassembly of Lignocellulosic Biomass to Lignin and Sugars by Molten Salt Hydrate at Low Temperature for Overall Biorefinery. *ACS Omega* **2018,** *3* (3), 2984-2993.

5. Blanpain, A.; Clark, J. H.; Farmer, T. J.; Guo, Y.; Ingram, I. D. V.; Kendrick, J. E.; Lawrenson, S. B.; North, M.; Rodgers, G.; Whitwood, A. C., Rapid Ring-Opening Metathesis Polymerization of Monomers Obtained from Biomass-Derived Furfuryl Amines and Maleic Anhydride. *ChemSusChem* **2019**.

6. Chen, X.; Li, S.; Liu, Z.; Chen, Y.; Yang, H.; Wang, X.; Che, Q.; Chen, W.; Chen, H., Pyrolysis characteristics of lignocellulosic biomass components in the presence of CaO. *Bioresour Technol* **2019,** *287*, 121493.

7. Jansen, E.; Jongbloed, L. S.; Tromp, D. S.; Lutz, M.; de Bruin, B.; Elsevier, C. J., Ligand effects on the hydrogenation of biomass-inspired substrates with bifunctional Ru, Ir, and Rh complexes. *ChemSusChem* **2013,** *6* (9), 1737-44.

8. Jha, A.; Naidu, A. B.; Abdelkhalik, A. M., Transition metal-free one-pot cascade synthesis of 7-oxa-2-azatricyclo[7.4.0.0(2,6)]trideca-1(9),10,12-trien-3-ones from biomass-derived levulinic acid under mild conditions. *Org Biomol Chem* **2013,** *11* (43), 7559-65.

9. Luo, H.; Klein, I. M.; Jiang, Y.; Zhu, H. Y.; Liu, B. Y.; Kenttamaa, H. I.; Abu-Omar, M. M., Total Utilization of Miscanthus Biomass, Lignin and Carbohydrates, Using Earth Abundant Nickel Catalyst. *Acs Sustain Chem Eng* **2016,** *4* (4), 2316-2322.

10. Nitsos, C. K.; Lazaridis, P. A.; Mach-Aigner, A.; Matis, K. A.; Triantafyllidis, K. S., Enhancing Lignocellulosic Biomass Hydrolysis by Hydrothermal Pretreatment, Extraction of Surface Lignin, Wet Milling and Production of Cellulolytic Enzymes. *ChemSusChem* **2019,** *12* (6), 1179-1195.

11. Zhang, B.; Shi, J.; Ding, C.; Chong, R.; Zhang, B.; Wang, Z.; Li, A.; Liang, Z.; Liao, S.; Li, C., Conversion of Biomass Derivatives to Electricity in Photo Fuel Cells using Undoped and Tungsten-doped Bismuth Vanadate Photoanodes. *ChemSusChem* **2015,** *8* (23), 4049-55.

12. Zhao, G. H.; Zheng, M. Y.; Zhang, J. Y.; Wang, A. Q.; Zhang, T., Catalytic Conversion of Concentrated Glucose to Ethylene Glycol with Semicontinuous Reaction System. *Ind Eng Chem Res* **2013,** *52* (28), 9566-9572.

13. Fukuoka, A.; Dhepe, P. L., Catalytic conversion of cellulose into sugar alcohols. *Angew Chem Int Edit* **2006,** *45* (31), 5161-5163.

14. Felder, S.; Noel, A.; Wooley, K., Ring-opening polymerization of a 5-membered ring glucose carbonate, toward biocompatible degradable polymeric materials. *Abstr Pap Am Chem S* **2015,** *250*.

15. Gregory, G. L.; Kociok-Kohn, G.; Buchard, A., Polymers from sugars and CO2: ring-opening polymerisation and copolymerisation of cyclic carbonates derived from 2-deoxy-D-ribose. *Polym Chem-Uk* **2017,** *8* (13), 2093-2104.

16. Kanie, Y.; Akiyama, K.; Iwamoto, M., Reaction pathways of glucose and fructose on Pt nanoparticles in subcritical water under a hydrogen atmosphere. *Catal Today* **2011,** *178* (1), 58-63.

17. Dutta, S.; De, S.; Patra, A. K.; Sasidharan, M.; Bhaumik, A.; Saha, B., Microwave assisted rapid conversion of carbohydrates into 5-hydroxymethylfurfural catalyzed by mesoporous TiO2 nanoparticles. *Appl Catal a-Gen* **2011,** *409*, 133-139.

18. Peng, L. C.; Lin, L.; Li, H.; Yang, Q. L., Conversion of carbohydrates biomass into levulinate esters using heterogeneous catalysts. *Appl Energ* **2011,** *88* (12), 4590-4596.

19. Ran, M. F.; Liu, Y.; Chu, W.; Borgna, A., Enhanced Conversion of Cellobiose to Sugar Alcohols by Controlled Dispersion of Ruthenium Nanoparticles Inside Carbon Nanotube Channels. *Catal Lett* **2013,** *143* (11), 1139-1144.

20. Hu, L.; Zhao, G.; Tang, X.; Wu, Z.; Xu, J. X.; Lin, L.; Liu, S. J., Catalytic conversion of carbohydrates into 5-hydroxymethylfurfural over cellulose-derived carbonaceous catalyst in ionic liquid. *Bioresource Technol* **2013,** *148*, 501-507.

21. Bayu, A.; Guan, G. Q.; Karnjanakom, S.; Hao, X. G.; Kusakabe, K.; Abudula, A., Catalytic synthesis of levulinic acid and formic acid from glucose in choline chloride aqueous solution. *Chemistryselect* **2016,** *1* (2), 180-188.

22. Yue, H. R.; Zhao, Y. J.; Ma, X. B.; Gong, J. L., Ethylene glycol: properties, synthesis, and applications. *Chem Soc Rev* **2012,** *41* (11), 4218-4244.

23. Xu, L. L.; Huo, Z. B.; Fu, J.; Jin, F. M., Highly efficient conversion of biomass-derived glycolide to ethylene glycol over CuO in water. *Chem Commun* **2014,** *50* (45), 6009-6012.

24. Pang, J. F.; Zheng, M. Y.; Sun, R. Y.; Song, L.; Wang, A. Q.; Wang, X. D.; Zhang, T., Catalytic conversion of cellulosic biomass to ethylene glycol: Effects of inorganic impurities in biomass. *Bioresource Technol* **2015,** *175*, 424-429.

25. Choomwattana, C.; Chaianong, A.; Kiatkittipong, W.; Kongpanna, P.; Quitain, A. T.; Assabumrungrat, S., Process integration of dimethyl carbonate and ethylene glycol production from biomass and heat exchanger network design. *Chem Eng Process* **2016,** *107*, 80-93.

26. Romero, A.; Cantero, D. A.; Nieto-Marquez, A.; Martinez, C.; Alonso, E.; Cocero, M. J., Supercritical water hydrolysis of cellulosic biomass as effective pretreatment to catalytic production of hexitols and ethylene glycol over Ru/MCM-48. *Green Chem* **2016,** *18* (14), 4051-4062.

27. Tan, Z. C.; Miao, G.; Liu, C.; Luo, H.; Bao, L. W.; Kong, L. Z.; Sun, Y. H., Catalytic conversion of glucose into alkanediols over nickel-based catalysts: a mechanism study. *Rsc Adv* **2016,** *6* (67), 62747-62753.

28. Wang, H.; Guo, Y. G.; Zheng, D.; Han, J. Y., Direct incorporation of tungsten into ordered mesoporous alumina and enhanced selectivity for converting cellulose to ethylene glycol. *J Porous Mat* **2015,** *22* (4), 919-925.

29. Ribeiro, L. S.; Orfao, J. J. M.; Pereira, M. F. R., Insights into the effect of the catalytic functions on selective production of ethylene glycol from lignocellulosic biomass over carbon supported ruthenium and tungsten catalysts. *Bioresource Technol* **2018,** *263*, 402-409.

30. Li, N. X.; Ji, Z. X.; Wei, L. F.; Zheng, Y.; Shen, Q. H.; Ma, Q. H.; Tan, M. L.; Zhan, M. M.; Zhou, J. C., Effect of the surface acid sites of tungsten trioxide for highly selective hydrogenation of cellulose to ethylene glycol. *Bioresource Technol* **2018,** *264*, 58-65.

31. Ji, N.; Zhang, T.; Zheng, M. Y.; Wang, A. Q.; Wang, H.; Wang, X. D.; Chen, J. G. G., Direct Catalytic Conversion of Cellulose into Ethylene Glycol Using Nickel-Promoted Tungsten Carbide Catalysts. *Angew Chem Int Edit* **2008,** *47* (44), 8510-8513.

32. Jin, X.; Thapa, P. S.; Subramaniam, B.; Chaudhari, R. V., Kinetic Modeling of Sorbitol Hydrogenolysis over Bimetallic RuRe/C Catalyst. *Acs Sustain Chem Eng* **2016,** *4* (11), 6037-6047.

33. Delidovich, I.; Leonhard, K.; Palkovits, R., Cellulose and hemicellulose valorisation: an integrated challenge of catalysis and reaction engineering. *Energ Environ Sci* **2014,** *7* (9), 2803-2830.

34. Hausoul, P. J. C.; Beine, A. K.; Neghadar, L.; Palkovits, R., Kinetics study of the Ru/C-catalysed hydrogenolysis of polyols - insight into the interactions with the metal surface. *Catal Sci Technol* **2017,** *7* (1), 56-63.

35. Zhang, J. Y.; Hou, B. L.; Wang, A. Q.; Li, Z. L.; Wang, H.; Zhang, T., Kinetic Study of Retro-Aldol Condensation of Glucose to Glycolaldehyde with Ammonium Metatungstate as the Catalyst. *Aiche J* **2014,** *60* (11), 3804-3813.

36. Sohounloue, D. K.; Montassier, C.; Barbier, J., Catalytic Hydrogenolysis of Sorbitol. *React Kinet Catal L* **1983,** *22* (3-4), 391-397.

37. Deutsch, K. L.; Lahr, D. G.; Shanks, B. H., Probing the ruthenium-catalyzed higher polyol hydrogenolysis reaction through the use of stereoisomers. *Green Chem* **2012,** *14* (6), 1635-1642.

38. Liu, G. X.; Wang, S. N.; Nie, Y. T.; Sun, X. H.; Zhang, Y. H.; Tang, Y., Electrostatic-induced synthesis of tungsten bronze nanostructures with excellent photo-to-thermal conversion behavior. *J Mater Chem A* **2013,** *1* (35), 10120-10129.

39. Wang, A.Q.; Zhang, T., One-Pot Conversion of Cellulose to Ethylene Glycol with Multifunctional Tungsten-Based Catalysts. *Accounts of Chemical Research* **2013**, 46 (7), 1377-1386.

4.7 Supporting Information

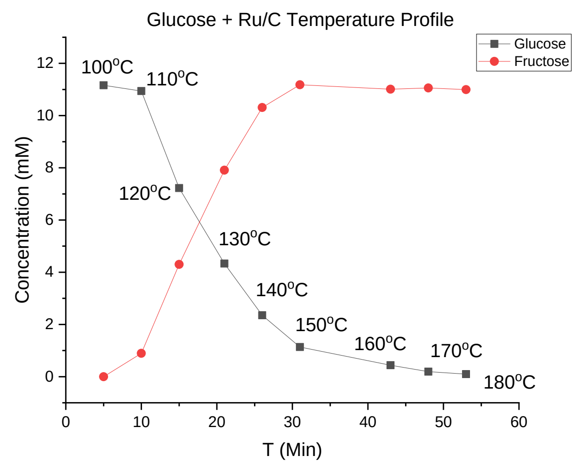

Figure S-4.1. Determination of activation temperature of Ru/C for glucose conversion. Reaction condition: 12mM aqueous glucose solution, 10wt% Ru/C, 450psi H_2, scanning temperature range from 100 to 180℃ by taking samples every 5 minutes.

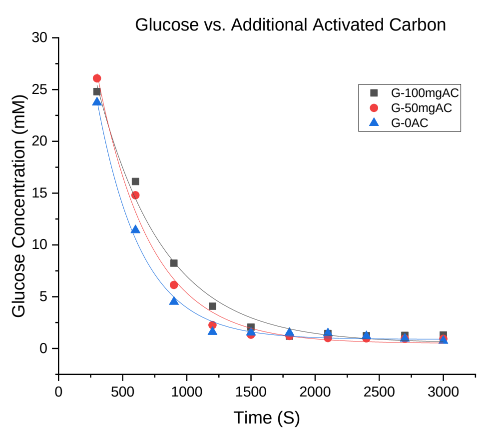

Figure S-4.2 Influence of additional activated carbon on glucose conversion. Reaction condition: 28mM glucose aqueous solution 50mL, 25mg Ru/C, 0mg – 100mg activated carbon (AC), 450psi H_2, 120℃.

AC (mg)	K_{obs-G} (S^{-1})
0	$2.89x10^{-3}$
50	$2.40x10^{-3}$
100	$1.93x10^{-3}$

Table S-4.1 K_{obs} measured by glucose conversion at different amount of additional activated carbon. Reaction condition: 28mM glucose aqueous solution 50mL, 25mg Ru/C, 0mg – 100mg activated carbon (AC), 450psi H_2, 120℃.

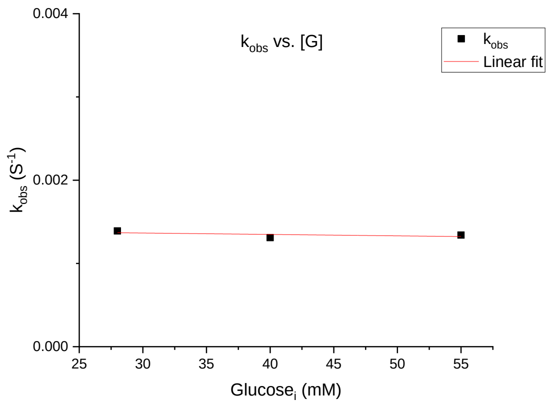

Figure S-4.3 K_{obs} dependence of initial glucose concentration measured by glucose conversion. (Condition: 28mM – 56mM glucose aqueous solution 50mL, 15mg Ru/C, 450psi H_2, 120℃)

$Glucose_i$ (mM)	Ru/C (mg)	$K_{obs-G/Ru}$ (S^{-1})
28	15	$1.39x10^{-3}$
40	15	$1.31x10^{-3}$
55	15	$1.34x10^{-4}$

Table S-4.2 K_{obs} measured by glucose conversion at different initial glucose concentration. (Condition: 28mM – 56mM glucose aqueous solution 50mL, 15mg Ru/C, 450psi H_2, 120℃)

Kinetic Model KS4-1:

1. G + Ru ⇋ G·Ru with rate constant k_{1f} and k_{1r}
2. G·Ru + H_2 ⇋ G·Ru* with rate constant k_{2f} and k_{2r}
3. G·Ru* → S·Ru with rate constant k_{3f}
4. S·Ru ⇋ S + Ru with rate constant k_{4f} and k_{4r}

$$\frac{d[G\cdot Ru]}{dt} = k_{1f}[G][Ru] - k_{1r}[G\cdot Ru] - k_{2f}[G\cdot Ru][H_2] = 0$$

$$\therefore [G\cdot Ru] = \frac{k_{1f}}{k_{1r}+k_{2f}[H_2]}[G][Ru] \quad \text{----- Eq.1}$$

$$\frac{d[G\cdot Ru^*]}{dt} = k_{2f}[G\cdot Ru][H_2] \quad \text{----- Eq. 2}$$

Eq.1 + Eq. 2

$$\therefore \frac{d[G\cdot Ru^*]}{dt} = \frac{k_{1f}[G][Ru][H_2]}{k_{1r}+k_{2f}[H_2]} \quad \text{------ Eq. 3}$$

$$\frac{d[G\cdot Ru^*]}{dt} = k_{2f}[G\cdot Ru][H_2] - k_{2r}[G\cdot Ru^*] - k_{3f}[G\cdot Ru^*] = 0$$

$$\therefore k_{2f}[G\cdot Ru][H_2] = (k_{2r} + k_{3f})\,[G\cdot Ru^*] \quad \text{----- Eq. 4}$$

Take Eq.4 into Eq.3

$$\therefore [G\cdot Ru^*] = \frac{k_{1f}k_{2f}[G][Ru][H_2]}{(k_{2r} + k_{3f})(k_{1r}+k_{2f}[H_2])} \quad \text{----- Eq. 5}$$

$$\frac{d[S\cdot Ru]}{dt} = k_{3f}[G\cdot Ru^*] - k_{4f}[S\cdot Ru] = 0$$

$$\therefore [S\cdot Ru] = \frac{k_{3f}[G\cdot Ru^*]}{k_{4f}} \quad \text{----- Eq.6}$$

Take Eq.6 and Eq.5 together

$$\therefore [S\cdot Ru] = \frac{k_{1f}k_{2f}k_{3f}[G][Ru][H_2]}{k_{4f}(k_{2r} + k_{3f})(k_{1r}+k_{2f}[H_2])} \quad \text{----- Eq. 7}$$

$$\frac{d[s]}{dt} = k_{4f}[S^{\cdot}Ru] - k_{4r}[S][Ru]$$

Take Eq.7 together

$$\therefore \frac{d[s]}{dt} = \frac{k_{1f}k_{2f}k_{3f}[G][Ru][H_2]}{(k_{2r}+k_{3f})(k_{1r}+k_{2f}[H_2])} - k_{4r}[S][Ru] \quad \text{----- Eq.8}$$

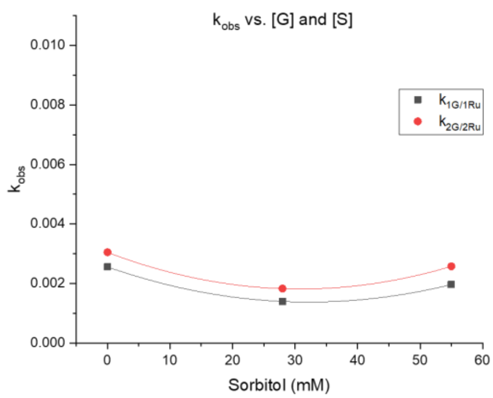

Glucose$_i$ (mM)	Sorbitol (mM)	$K_{obs\text{-}G/Ru}$ (S^{-1})
28	0	2.56×10^{-3}
28	28	1.41×10^{-3}
28	56	1.97×10^{-3}
56	0	3.05×10^{-3}
56	28	1.83×10^{-3}
56	56	2.58×10^{-3}

Figure S-4.4 & **Table S-4.3** K_{obs} dependence of sorbitol concentration with different initial concentration of glucose at the same weight percentage of Ru/C loading (10wt%). (Conditions: 28mM, 56mM glucose aqueous solution with 0mM, 28mM, 56mM sorbitol 50mL, 10wt% Ru/C according to glucose, 450psi H_2 120℃)

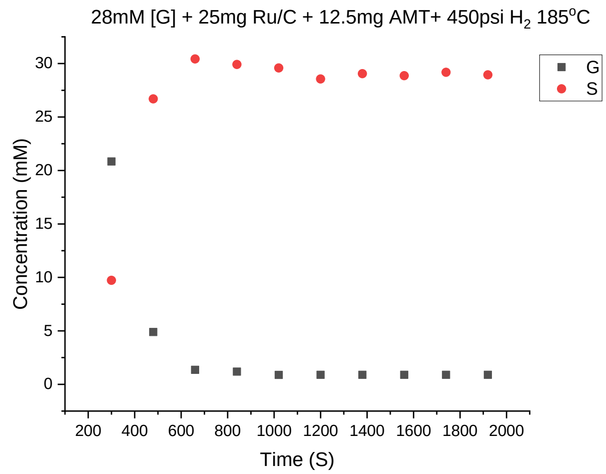

Figure S-4.5 Glucose conversion and sorbitol formation during reactor heating up process. (Condition: 28mM glucose aqueous solution 50 mL, 25mg Ru/C, 12.5 mg AMT, 450 psi H_2, 120 ℃)

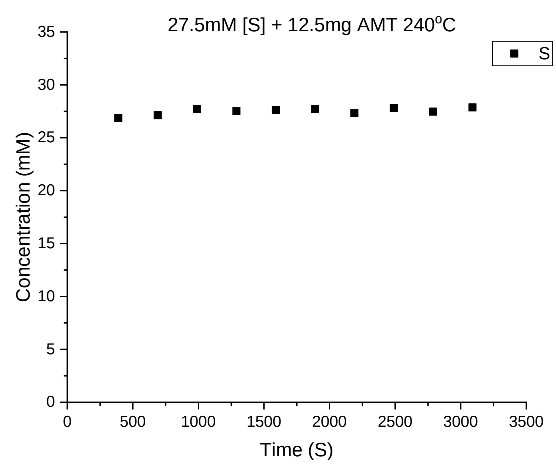

Figure S-4.6 Sorbitol conversion in case of using AMT solo catalyst. (Condition: 27.5 mM sorbitol aqueous solution 50 mL, 12.5 mg AMT, 450 psi H_2, 240 ℃)

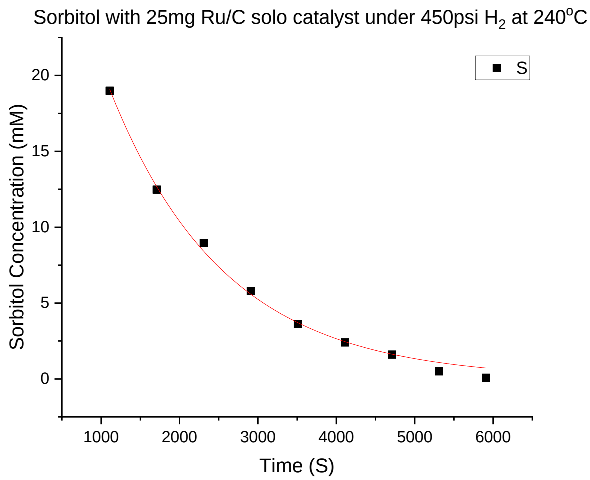

Figure S-4.7 Sorbitol conversion in case of using Ru/C solo catalyst. (Condition: 27.5 mM sorbitol aqueous solution 50 mL, 25 mg Ru/C, 450 psi H_2, 240 ℃)

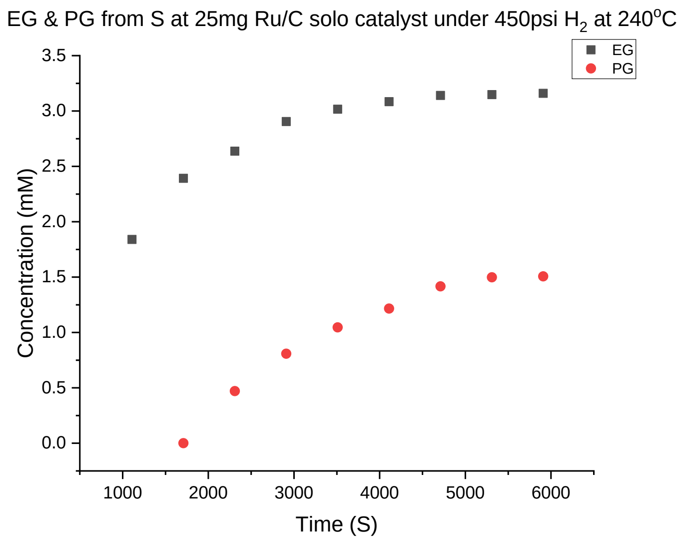

Figure S-4.8 First order behavior of EG and PG formation from sorbitol in case of Ru/C solo catalyst. (Condition: 28 mM sorbitol aqueous solution 50 mL, 25 mg Ru/C, 450 psi H_2, 240 ℃)

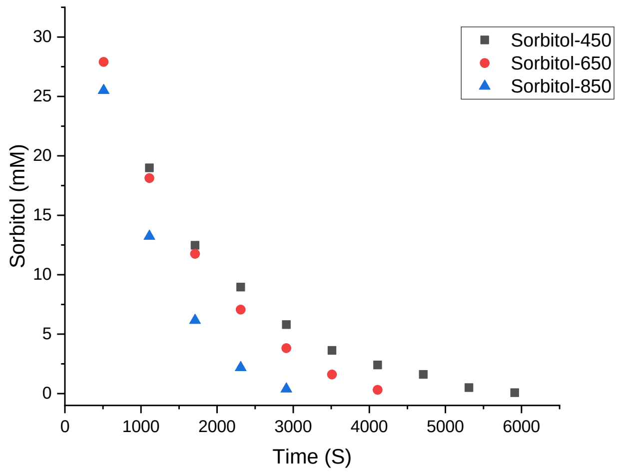

Figure S-4.9 Dependence of initial hydrogen pressure on sorbitol conversion in case of Ru/C solo catalyst. (Condition: 28 mM sorbitol aqueous solution 50 mL, 25 mg Ru/C, 450 psi – 850 psi H_2, 240 ℃)

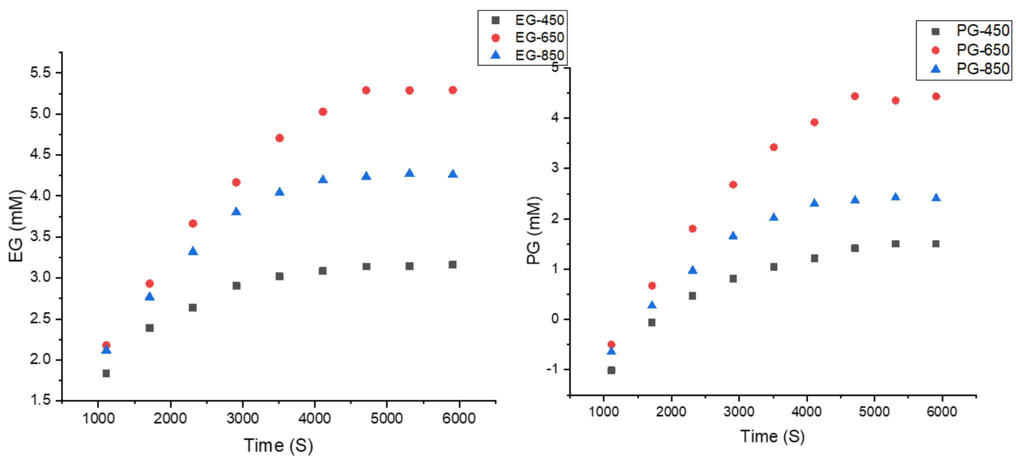

Figure S-4.10 Dependence of initial hydrogen pressure on EG and PG formation from sorbitol in case of Ru/C solo catalyst. (Condition: 28mM sorbitol aqueous solution 50 mL, 25 mg Ru/C, 450 psi – 850 psi H_2, 240 ℃)

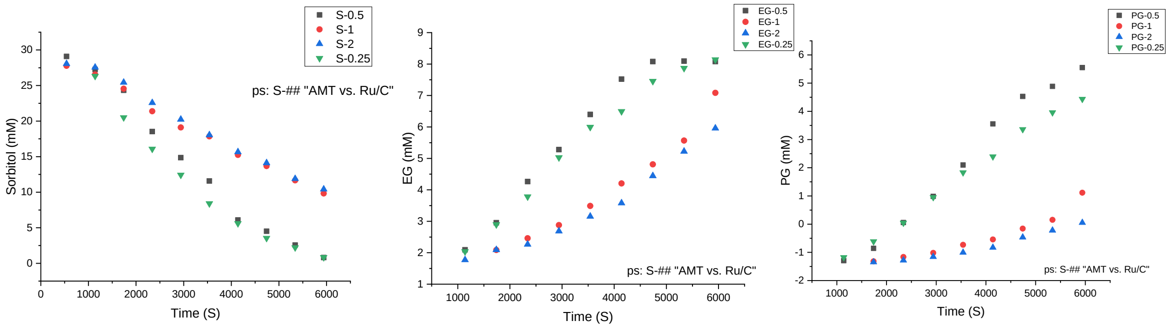

Figure S-4.11 AMT dependence on sorbitol conversion and EG, PG formation. (Condition: 28 mM sorbitol aqueous solution 50 mL, Ru/C, AMT, 850 psi H_2, 240 ℃)

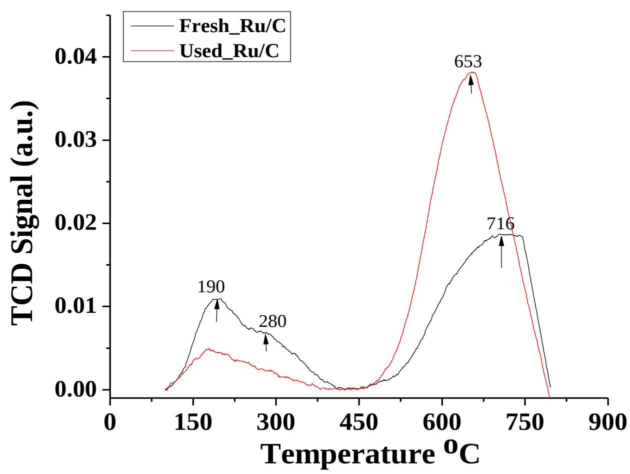

Figure S-4.12 NH_3-TPD results of fresh and used Ru/C. Peaks in region of 150 ℃ - 300 ℃ indicated acidity changes on activated carbon support. Peaks in region of 500 ℃ - 800 ℃ indicated acidity changes on ruthenium metal.

Ru/C Catalyst	NH_3 (mmol/g)
Fresh	0.899
Used	1.394

Table S-4.4 NH_3 adsorption measured by NH_3-TPD of different Ru/C samples. Used Ru/C samples were collected from reaction condition: 28 mM sorbitol aqueous solution 50 mL, 10 wt% Ru/C, 5 wt% AMT, 850 psi H_2, 240 ℃, 5000 seconds.

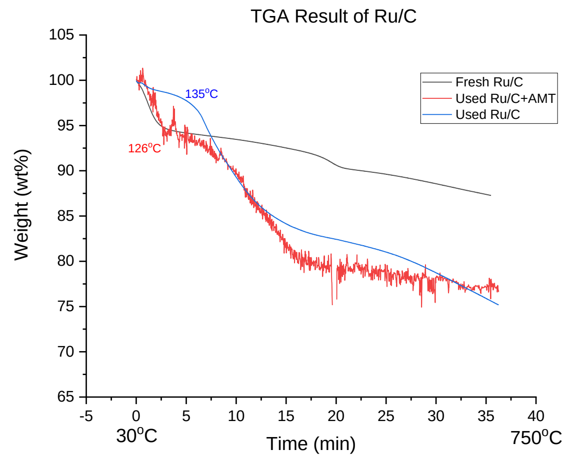

Figure S-4.13 TGA spectrum of fresh and used Ru/C samples in temperature range of 30 ℃ - 750 ℃.

	Fresh Ru/C	Ru/C +AMT	Used Ru/C
Weight lost (wt%)	13	17	22.5

Table S-4.5 Weight loss (wt%) of different Ru/C samples measured by TGA. Used Ru/C + AMT was collected from reaction condition: 28 mM sorbitol aqueous solution 50 mL, 10 wt% Ru/C, 5 wt% AMT, 850 psi H_2, 240 ℃, 5000 seconds. Used Ru/C was collected from reaction condition: 28m M sorbitol aqueous solution 50 mL, 10 wt% Ru/C, 850 psi H_2, 240 ℃, 5000 seconds.

Kinetic Model KS4-2. For Ruthenium concentration R, hydrogen concentration H, and AMT concentration A. Hydrogen is assumed to be in large excess, as in prior steps.

$$\frac{d[S]}{dt} = -k_{1f}RH[S] - k_{2f}RH[S] \text{ ------ Eq. 3}$$
$$\frac{d[I]}{dt} = k_{1f}RH[S] - k_{3f}RH[I] - k_{4f}A[I] = 0 \text{ ------ Eq. 4}$$
$$\frac{d[P]}{dt} = 2k_{2f}RH[S] + k_{3f}RH[I] \text{ ------ Eq. 5}$$
$$\frac{d[E]}{dt} = k_{1f}RH[S] + k_{4f}A[I] \text{ ------ Eq. 6}$$

From Eq3. – 6. The [I] intermediate can be solved and resulted:

$$\frac{d[S]}{dt} = -(k_{1f} + k_{2f})RH[S] = \alpha[S]$$

$$\frac{d[P]}{dt} = \left(2k_{2f} + \frac{k_{1f}k_{3f}RH}{k_{4f}A + k_{3f}RH}\right)RH[S] = \beta[S]$$

$$\frac{d[E]}{dt} = k_{1f}\left(1 + \frac{k_{4f}A}{k_{4f}A + k_{3f}RH}\right)RH[S] = \gamma[S]$$

Simplified form of [S], [E], and [P] as:

$$S(t) = a_0 \exp[\alpha t]$$

$$P(t) = b_0 \exp[\alpha t] + b_1$$

$$E(t) = c_0 \exp[\alpha t] + c_1$$

Notably, all growth/decay follows the same time constant a_1.

The b_0 and c_0 constants are related to the step rate constants via:

$$b_0 = \frac{a_0}{\alpha}\beta, \quad c_0 = \frac{a_0}{\alpha}\gamma$$

β and γ are combinations of rate constants found by solving the system.

This preserves the correct sign: $b_0 < 0$, but $\beta > 0$

The procedure of computational estimation of kinetic models follows the steps:

1. Perform a rough (global) minimization via differential evolution.
2. Refine that guess with BFGS.
3. The values of a_0, b_0, and c_0 were summarized in the Table S-4.6.

Trials	a_0	b_0	c_0
2.5wt% Ru/C, 450psi H_2	3.131976185260018042e+01	-1.716559450403492892e+00	-4.056027662905104414e+00
5wt% Ru/C, 450psi H_2	3.481841750940597535e+01	-2.735829112183947309e+00	-6.589070018332206402e+00
10wt% Ru/C, 450psi H_2	4.072915301253477338e+01	-2.932060269027001898e+00	-5.529015077627058794e+00
10wt% Ru/C, 650psi H_2	4.327301650797204502e+01	-8.348470305511606071e+00	-1.312660285105961933e+01
10wt% Ru/C, 850psi H_2	4.870555452727766266e+01	-8.917025236135369681e+00	-1.259718874055196558e+01
2.5wt% Ru/C, 5wt% AMT, 850psi H_2	3.663066742987538760e+01	-7.196900298581483391e+00	-6.187658584587810040e+00
5wt% Ru/C, 5wt% AMT, 850psi H_2	3.708453118364056422e+01	-1.125201142786525743e+01	-7.369030652667779790e+00
10wt% Ru/C, 5wt% AMT, 850psi H_2	4.019981839518772659e+01	-1.241748787605101434e+01	-1.340583606599472333e+01
10wt% Ru/C, 10wt% AMT, 850psi H_2	3.198134413790045372e+01	-1.185447242650822375e+01	-5.435913759076769658e+00
10wt% Ru/C, 20wt% AMT, 850psi H_2	3.283519923699459042e+01	-8.598875636791156296e+00	-3.628598676415227597e+00
10wt% Ru/C, 5wt% AMT, 450psi H_2	4.030412381463631277e+01	-1.610587256928132049e+01	-6.046246272152998813e+00
10wt% Ru/C, 5wt% AMT, 650psi H_2	4.259107512404994367e+01	-1.787304357980998049e+01	-7.801911665418534092e+00

Table S-4.6 The a_0, b_0, and c_0 values acquired by plotting experimental concentration of sorbitol, EG, and PG versus time.

Chapter 5. Catalytic Conversion of Delignified Biomass Residue to Diols with Ru/C and AMT Co-catalysts

5.1 Abstract

Cellulose is one of the major components in biomass. It is the largest renewable carbon resource from nature. Utilization of cellulose from native biomass to produce value-added chemicals brings a lot of benefits for the sustainable future. Cellulose from Poplar wood can be extracted from several biomass pretreatments. Catalytic depolymerization of lignin reactions (CDL) selectively remove lignin from biomass and leave the intact cellulose and hemicellulose as solid residue. On the other hand, organosolv treatments can separate the fractions of biomass into clean cut lignin, cellulose, and hemicellulose derivatives. In this work, the cellulose obtained from genetically modified Poplar biomass with different pretreatments were studied to produce ethylene glycol (EG) with other diols, such as propylene glycol (PG), 1,2-butanediol (12BD), and 2,3-butanediol (23BD). The maximum yield of EG was 47% obtained from the cellulose prepared by acetone treated high-S Poplar biomass. The acetone treated organosolv method also gave the best purity of cellulose which had an average content of cellulose above 82%. The optimal condition of cellulose conversion was determined to be10 wt% equivalent amounts of Ru/C and AMT (each) co-catalysts at 240 ℃ under 5 MPa gauge pressure of hydrogen for 1.5 hours.

5.2 Introduction

Biomass has drawn a lot of efforts to study its valorization in recent years.[1-3] According to its clean and renewable characteristics, biomass has been concerned as an ideal substitute of petrochemicals for future production of sustainable fuels and chemicals. In general, biomass has three major components, known as cellulose (40-60%), hemicellulose (20-40%), and lignin (10-

25%).[4] Nowadays, the "lignin first" biomass valorization is mainly using the value of lignin while the secondary generation biorefinery is mainly making low-value products such as ethanol from carbohydrates (cellulose and hemicellulose). Therefore, the use of carbohydrates for making value-added products is necessary to enlarge the profits of biomass valorization.

Ethylene glycol (EG) has high values, and it plays important roles in many industries. The conventional production of EG was mainly from the fossils in petrochemical industries. Fossil is unrenewable source and use of fossil also generates a lot of pollutions. Thus, the recent studies are looking for a greener and more sustainable production of EG. By which, it has proven the EG can be produced by decomposition of the most abundant natural polymer, cellulose, with heterogeneous catalysts.[5] There are several studies focusing on the conversion of glucose and microcrystalline cellulose to various value-added products including EG.[6, 7] However, there are still few studies on the direct catalytic conversion of the cellulose from real biomass into EG. Using the raw carbohydrate residues from biomass as feedstock would be extremely meaningful to understand the durability of performing catalysis with natural polymer and to evaluate the application of biomass valorization for EG production.

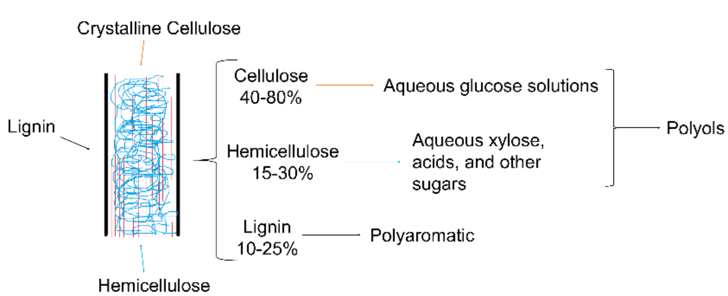

Figure 5.1 General structure and components of woody biomass.

Figure 5.1 displays a general configuration and composition of woody biomass.[8] Each portion of the biomass could be utilized in different ways for different chemicals. Cellulose and hemicellulose are renewable polysaccharides in nature while lignin is the most abundant aromatic biopolymers from biomass.[9] In this work, we aimed the study on making EG and other value-added polyol products from cellulose and hemicellulose. In the native form of biomass, cellulose is bonded with lignin and intercrossed by hemicellulose. Therefore, lignin could prevent the conversion of carbohydrates.[10] In order to obtain a clean cut of carbohydrates from biomass, methods for lignin removal have been developed.[11] Catalytic depolymerization of lignin (CDL) has been reported as one of the lignin removal methods. By which, the catalyst used in CDL catalysis selectively catalyzes lignin depolymerization into monomers that are dissolved and extracted by organic solvents.[12, 13] Meanwhile, the CDL catalysts leave the carbohydrates intact in its original chemical and physical form. Hao et al. studied a nickel catalyst on carbon support (Ni/C) was an efficient catalyst for CDL reaction. By which, the Ni/C selective depolymerized lignin Miscanthus biomass into its aromatic monomers but left the carbohydrates as solid residue.[12] Moreover, Hao et al. also showed their leftover carbohydrates was upgradable with Lewis acids to produce higher value products, such as furfural. On the other hand, organosolv method is another approach to remove lignin from biomass and generate a clean-cut carbohydrates.[14, 15] In a typical organosolv treatment, the lignin biopolymer is soluble in organic solvent while the cellulose is not. Thus, the dissolved lignin can be extracted in organic filtrates and leave the cellulose as solid residue. Abdelkafi et al developed an organosolv treatment by using acetic acid coupled with formic acid.[14] Among them, not only the lignin was removed, but also cellulose and hemicellulose were successfully isolated into two different fractions. Therefore, the organosolv method separates the three major biomass components into different fractions with high quality. The clean-cut cellulose obtained from organosolv methods is potentially an ideal feedstock for further utilizations into high-value products.

After the removal of lignin, conversion of cellulose to valuable chemicals could be catalyzed by using heterogeneous catalysts.[16] Transition metals, such as Ni[16], Pd[17], Pt[18], W[19], and Ru[20], were reported to be the most efficient catalysts for catalyzing the hydrogenolysis of cellulose to break its carbon back bone and the hydrogenation of unsaturated aldehyde intermediates to diols. For instance, the monometallic catalyst system with Ni, Pt, Ru, and Pd could give 40% yield of diols with a conversion of 63.5% cellulose.[19] Interestingly, Zhang et al. reported their total yield of diols was only 2.2% while using tungsten (W) in a monometallic catalyst system.[20] Although the yield of diols was low, the conversion of cellulose was 100% with W catalyst. Therefore, Zhang et al. concluded the W should have great ability in depolymerization of cellulose by cleaving the carbon-oxygen linkages (C-O cleavage), but W was not functionalized in catalyzing the carbon bond cleavage (C-C cleavage) to produce small diols. Thus, a transition metal coupled with W for a co-catalyst system was proposed. By which, the cellulose would be more rapidly depolymerized by W into its monomeric form. After that, the other metal species would catalyze the hydrogenolysis of cellulose monomers, such as glucose or other equivalent six carbon intermediates, into the diols. By doing this, the monomeric form of cellulose could be easier and more selectively converted into EG. For instance, Yan et al. introduced their co-catalyst system with Ru nanoparticles gave 100% conversion of cellulose and 61.7% was EG.[20] According to the previous studies, Ru was one of the most promising catalysts for hydrogenolysis and hydrogenation reaction. Ru catalysts have been widely used in industrial productions.[21-23] Therefore, a co-catalyst system with use of Ru and W could be an efficient catalyst system for cellulose conversion and EG formation. Zhao et al. studied the Ru-W co-catalyst system with glucose and gave EG yield at 61%.[24] In order to provide a sufficient tungsten species for depolymerization of cellulose, water soluble ammonium metatungstate hydrate (AMT) [25] was selectively used in this study with Ru/C to promote EG production from cellulose.

Poplar is one of the fast-growing biomasses and widely grown within northern temperate zone on Earth. Most of Poplar trees are consumed in making paper, furniture, and raw woodwares.[15] Thus, using cellulose from Poplar woody biomass as feedstock to produce EG is attractive. Our lab have previously introduced several contributions of using poplar biomass as feedstocks for chemical productions.[13, 15, 26] These studies focused on the catalytic conversions of lignin with both CDL and organosolv methods. However, the intact cellulose residues from our previous work were not used. Due to the under-developed catalysis of CDL and organosolv cellulose residues, here we report a continuous study to understand the heterogeneous catalysis of different cellulose residues for EG production.

In this work, an optimized condition with Ru/C-AMT co-catalyst system was developed to convert cellulose from gene modified Poplar woody biomass (High S, Low S, and wild type)[15] into diol products. Ethylene glycol (EG), propylene glycol (PG), 1,2-butandiol (12BD), and 2,3-butandiol (23BD) were detected as the major products giving a total yield of 55%. The maximum yield of EG was 47%. Besides, some minor polyols, such as sorbitol and glycerol were also observed in the product mixture.

5.3 Experimental Section

5.3.1 Materials

Catalyst Ru/C and ammonium metatungstate hydrate (AMT) were purchased from Sigma-Aldrich. Ni/C catalyst was prepared by the incipient wetness impregnation method.[27] The wild type Popular raw biomass was obtained from Purdue University and milled to a fine particle size of 40 mesh by using a Mini Wiley Mill (Thomas Scientific, Swedesboro, NJ). High-S Poplar was provided by Drs. Clint Chapple and Richard Meilan from Purdue University.[15] Low-S Poplar was provided by the U.S. Department of Energy BES project (0012846). The contents of the intact biomass are summarized in the Table S5-1. Tert-butyl alcohol was purchased from Sigma-Aldrich as internal standards for quantification analysis. Water was obtained from Milli-Q Academic A10 water purification system (EMD Millipore Co.). All chemicals were used without further purification.

5.3.2 Pretreatment of raw biomass

CDL cellulose was collected from solid residue after catalytic depolymerization of lignin (CDL) with raw biomass.[12] CDL reaction was performed in a 75 mL stainless steel vessel of batch Parr reactor (Parr Instrument Co., MRS 5000). Ni/C catalyst was synthesized based on reported literature method.[14] 15 wt% Ni/C was loaded to a 325 mesh microporous catalyst cage placing in the vessel. Then 45mL methanol, 1 g raw biomass, and 3.5 MPa hydrogen were added at room temperature. The whole CDL reaction took 12 hours at 225 ℃. Cellulose remained as solid residue after CDL was washed with 200 mL methanol and dried under vacuum.

Cellulose from organic solvent method (Organosolv cellulose) was isolated following the steps were previously reported.[14] Formic acid coupled with acetic acid and acetone were the two types of organic solvent investigated in this work (details of the organosolv methods are mention in the supporting information). Organosolv cellulose collected from each type was washed with large amount of water to remove organic solvent and dried under vacuum.

5.3.3 Conversion of biomass cellulose to diols

Reactions in heterogeneous system were performed in stainless steel batch Parr reactor (Parr Instrument Co., MRS 5000). 0.5 g of biomass cellulose, 10 wt% Ru/C catalyst, 10 wt% AMT, 40 mL water, and a glass shielded magnetic stair bar were added to a 75 mL stainless steel vessel. The loaded vessel was well sealed and purged with UHP grade hydrogen gas for 4 times to remove air. Then the vessel was pressurized to 50 bar by hydrogen gas at 20 ℃ and heated to 240 ℃. The reaction was conducting at 240 ℃ and holding for 2 h at 600 rpm stirring rate. After reaction, the vessel was cooled to room temperature in air. The heterogeneous mixture was separated by using filter paper. Ru/C, unreacted biomass cellulose, and impurities were remaining in solid phase and washed with 250 mL water. Polyols were collected in aqueous phase after filtration. The aqueous phase was concentrated to 25 mL in volumetric flask after extra water solvent was removed by using rotavapor (Buchi V100). 500 μL 10 mM tert-Butyl alcohol as internal standard was added to 500 μL aqueous sample and filtered with 0.2 μm PTFE syringe filter before injecting to HPLC.

5.3.4 Acid hydrolysis of biomass cellulose

The composition analysis of biomass cellulose was based on a standard acid hydrolysis method reported by NREL. 0.3 g biomass cellulose and 3 mL 72% sulfuric acid were added to a 100 mL pressure tube. Then the pressure tube was heated to 30 ℃ in water bath on a thermo shaker with shaking speed at 150 rpm for 1 h. Glass rod was inserted to pressure tube. The mixture was well stirred by using glass rod every 10 min. After shaking, glass rod was removed and 87 mL water was added to the mixture. Then the pressure tube was well sealed and transferred to a liquid mode autoclave. The mixture was heated to 121 ℃ for 1 h in autoclave. 1 mL liquid sample from final mixture was obtained from pressure tube and added to 10 mL water. 400 μL 10 mM tert-butyl alcohol as internal standard was added to 600 μL diluted sample and filtered with 0.2 μm

PTFE syringe filter before injecting to HPLC (Agilent HPLC 1260). Examples of acid hydrolysis and HPLC spectra are described in supporting information and Figure S-5.1.

5.3.5 Analytical methods

The liquid polyol samples and acid hydrolysis samples were analyzed with liquid chromatography (Agilent HPLC 1260). The analyte was identified and quantified by retention time and peak area ratio to internal standard. The HPLC was operating with a H-column at 70 ℃, a refractive index detector (RID), and 5mM sulfuric acid as mobile phase with flowing rate of 0.6 mL/min. The remaining solid from biomass cellulose conversion reactions was dried in air and weighed to analyze the remaining residue. An example of HPLC spectra for product measurement is displayed in Figure S-5.2.

5.4 Results and Discussion

5.4.1 Catalyst loading

To date, most articles published on the catalytic conversions to make EG with monometallic catalyst, such as Ni, Pt, Pd, Ir, and Ru are still mainly focused on the use of commercial clean standard glucose and/or cellulose.[24] In contrast, the bimetallic co-catalysts system is more active for decomposing raw cellulose and biomass feedstocks to EG and other diols.[19] Ru/C-AMT has been reported as one of the most effective combinations of catalysts for glucose degradation. Therefore, the amount of catalyst loading of each species as weight percentage (wt%) of biomass feedstock should be investigated to obtain an optimal conversion.

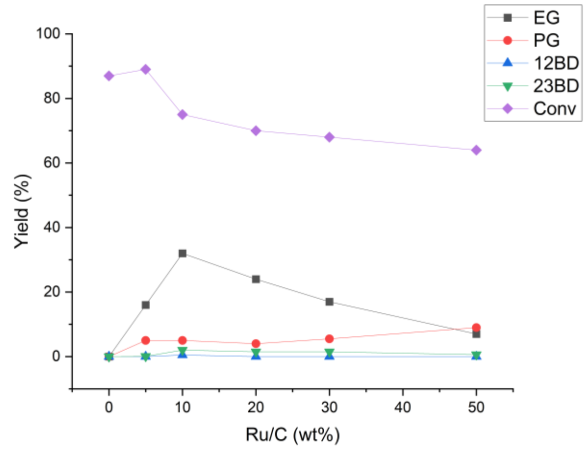

Figure 5.2 Conversion of WT Poplar cellulose pretreated by acetone. Reaction conditions: Organosolv WT cellulose 0.5 g; 25 mg AMT; 0 g (0 wt%), 25 mg (5 wt%), 50 mg (10 wt%), 100 mg (20%), 150 mg (30 wt%), 200 mg (40 wt%), and 250 mg (50 wt%) Ru/AC; 40 mL H_2O; 240℃; 1.5 hour. Conversion was calculated based on the weight difference between the total amount of feedstock cellulose and catalysts solid versus the solid residue after reaction. Yield was calculated based on the weight of product divided by the weight of feedstock.

In this study, many types of cellulose obtained from different biomass treatments were used as feedstock for EG production. Among those, cellulose collected from wild type Poplar biomass processed by organosolv treatment in acetone was selected to study the catalyst loading. Figure 5.2 illustrates the results of cellulose conversion and diols formation with different Ru/C loading. Although the cellulose was decomposed with 5 wt% addition of AMT, there was no product detected without adding Ru/C. Thus, the Ru/C catalyst was essential for the diols' formation.

According to the results summarized in Figure 5.2, it indicated more cellulose was converted into liquid products and gave fewer solid residues when AMT was the only catalyst or with equal amount of Ru/C (5 wt% of each). In contrast, with increasing addition of Ru/C (> 10 wt%), more solid residues were collected at the end of reaction. Regarding the yield of EG, its maximum production was observed when 10 wt% of Ru/C and 5 wt% of AMT were used. Interestingly, when increasing the Ru/C loading above 30 wt%, PG formation was increased. PG became the major product when 50 wt% of Ru/C loading was used. Taking the results together, 10 wt% of Ru/C with 5 wt% of AMT was optimal which gave the maximum 40% total yield and 80% selectivity toward EG formation.

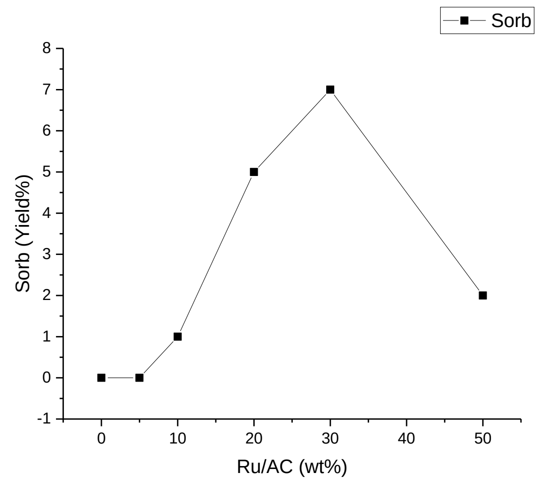

Figure 5.3 Sorbitol yield with different amount of Ru/C.

Sorbitol as the initial intermediate was also detected and quantified during the reaction. Figure 5.3 summarizes the formation of sorbitol from the conversion of cellulose from wild type Poplar biomass. The yield of sorbitol was increased when more Ru/C was used for the reaction. However, the sorbitol started decreasing when more than 30 wt% of Ru/C was used. Scheme 5.1 illustrates the reaction pathway of sorbitol formation from cellulose and further conversion of sorbitol to diols.[28] By which, the cellulose polymer was first decomposed to its monomer glucose at elevated temperature by AMT. Then glucose intermediates underwent two reaction pathways. Glucose could be directly decomposed by AMT to smaller aldose or aldehydes and followed by hydrogenolysis reaction catalyzed by Ru/C to diols (Scheme 5.1, black arrow). On the other hand, with excess amount of Ru/C than AMT, other reaction pathways became competitive with the AMT catalyzed C-C cleavage. Instead, the Ru/C catalyzed hydrogenation reduced glucose to sorbitol. However, AMT alone showed no activity in catalyzing the polyols for C-C cleavages (as discussed in Chapter 4). Therefore, when more than 5 wt% of Ru/C was loaded, more sorbitol was detected. Nevertheless, Ru/C could also catalyze the hydrogenolysis to decompose sorbitol directly. Thus, when more than 30 wt% of Ru/C was used, less sorbitol was detected due to its further reaction with Ru/C (Scheme 5.1, red arrow).

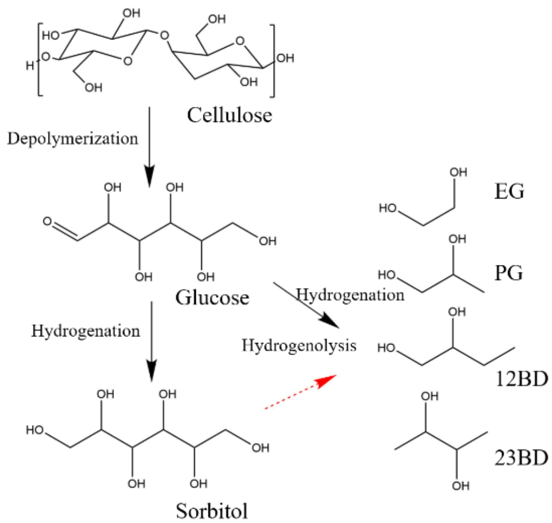

Scheme 5.1 Reaction pathway from cellulose to diols.

Taking Figures 5.2 and 5.3 together suggest EG was selectively produced by AMT. carbon-carbon bond cleavage catalyzed by AMT with aldose were dominant through C2-C4 (six carbon intermediates, such as glucose) and C2-C2 (four carbon intermediates, such as erythrose) cleavages toward EG formation. In contrast, the Ru/C catalyzed hydrogenolysis could cleave both C2-C4 and C3-C3 breakage of sorbitol and thus more PG was observed when increasing Ru/C loading.

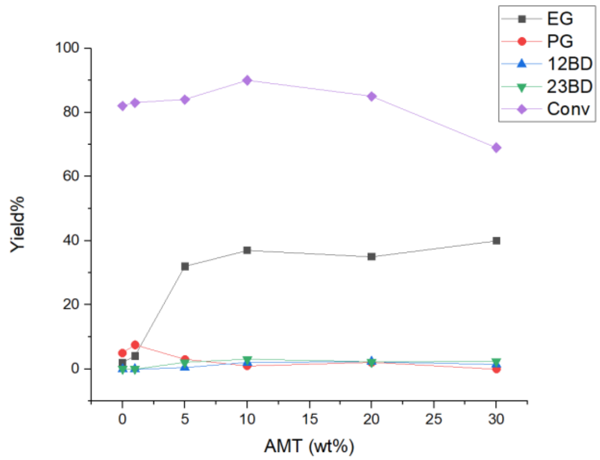

Figure 5.4 Conversion of WT Poplar cellulose pretreated by acetone with different amount of AMT loading. Reaction conditions: Organosolv WT cellulose 0.5 g; 50 mg Ru/AC; 0 g (0 wt%), 5 mg (1 wt%), 25 mg (5 wt%), 50 mg (10 wt%), 100 mg (20%), and 150 mg (30 wt) AMT; 40 mL H_2O; 240°C; 1.5 hour. Conversion was calculated based on the weight difference between the total amount of feedstock cellulose and catalysts solid versus the solid residue after reaction. Yield was calculated based on the weight of product divided by the weight of feedstock.

EG formation over the variation of AMT loading is displayed in Figure 5.4. In this case, 10 wt% AMT with 10 wt% Ru/C resulted in the least amount of solid residues (90% conversion) and the highest yield of EG (37%). It is notable that when even without AMT added, 10 wt% Ru/C still gave 7% yield of diols. Adding a small amount of AMT (5 wt%) improved EG yield by 16 times higher than without AMT. Hence, AMT greatly enhanced the catalytic conversion of cellulose decomposition and EG formation. Although excess amount of AMT (30 wt% loading) could slightly improve EG yield to 40%, it also generated more solid residues by the end of reaction. The solid residues could be coke, which may result from the higher acidity by adding more AMT to the reaction. Therefore, more than 10 wt% of AMT gave negative impact on the conversion of cellulose and EG selectivity. Moreover, significant PG formation was observed when AMT loading was low. When increasing the AMT loading, the production of PG was inhibited. Therefore, this also suggests that AMT modified the carbon-carbonbond cleavage. By which, the C2-C4 and C2-C2 were more selective with AMT. Taking Figures 5.2 and 5.4

together, the reaction pathway leading to the production of PG from cellulose was dependent on Ru/C.

5.4.2 Reaction time profile

To obtain an ideal reaction for cellulose conversion, other reaction parameters were also studied. For instance, the reaction temperature, gauge pressure of hydrogen, and reaction time. Tai et al. had investigated the effect of reaction temperature for cellulose conversion to EG.[29] Their results indicated the highest EG yield at 60% could be obtained at 240 ℃. Besides, hydrogen pressure was also investigated from 4 MPa to 6 MPa with relevant yield of EG and other diols. By which, 5 MPa hydrogen gauge pressure had been reported as the most efficient pressure for EG with a yield of 60%.[24] However, there was a lack of studies on the time profile to monitor cellulose conversion to EG. Especially for cellulose derived from biomass which usually have other contaminants. For instance, the acid insoluble lignin, protein, ash, and inorganic salts were identified in the cellulose residue after CDL and organosolv treatments.[30] Thus, in general the conversions of organosolv and CDL cellulose require longer reaction time but give lower yield of EG than using glucose or commercial cellulose as feedstock.

Figure 5.5 summarizes the time profile of cellulose conversion and EG formation. Highest yield of EG was detected from a 10 min reaction affording good yield as high as 44%. However, the conversion of cellulose was only 32% at 10 min and thus the overall amount of EG was small. With a longer reaction to 2 hours, the cellulose conversion was up to 90% while the EG formation was slightly reduced to 30%. Therefore, an optimal reaction time for cellulose conversion should be between 1 hour to 2 hours to balance the overall conversion and product yield. When the reaction time was longer than 2 hours, the total yield of diols was decreased. Our hypothesis is that some dimerization or polymerization reaction could happen between the diols at the reaction temperature (240 °C) and thus it lowers the yield of monomeric diols. For instance, Ru may also be a dehydrogenation catalyst that converts the diols and polyols to the more reactive aldehydes. Thus, aldol condensation could happen between the reactive aldehydes and lead to formation of byproducts. Compare the results with the study from Zhang et al. which indicated 50 min was sufficient for converting > 95% commercial microcrystalline cellulose and cellobiose to EG,[31] cellulose made from poplar biomass in this work indeed required longer reaction time.

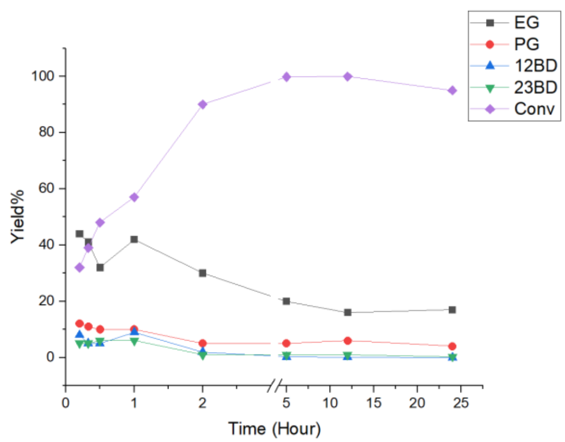

Figure 5.5 Time profile of conversion of WT Poplar cellulose pretreated by acetone. Reaction conditions: Organosolv WT cellulose 0.5 g; 25 mg AMT; 50 mg Ru/AC; 40 mL H_2O; 240℃; 10 min, 20 min, 30 min, 1 hr, 2 hr, 5 hr, 12 hr, and 24 hr. Conversion was calculated based on the weight difference between the total amount of feedstock cellulose and catalysts solid versus the solid residue after reaction. Yield was calculated based on the weight of product divided by the weight of feedstock.

5.4.3 EG production from different cellulose

Table 5.1. Cellulose content from different treatments of poplar biomass

Biomass type	Pretreatment methods			
	Acetone	FA/AA	CDL	Raw
WT	82%	69%	62%	43%
Low S	88%	70%	60%	45%
High S	80%	66%	66%	45%

Table 5.1 Cellulose content in different type of Poplar biomass. The cellulose content was measured according to the standard acid hydrolysis method provided by NREL. The details of acid hydrolysis method are introduced in the supporting information and Appendix i.

The content of cellulose was analyzed by doing acid hydrolysis according to NREL standard procedure (Appendix i). During the acid hydrolysis, all cellulose was converted to glucose by acid and the quantification of glucose represented the amount of cellulose in biomass sample.

Table 5.1 summarizes the cellulose content determined from different biomass treatments. Among these, the organosolv method with acetone gave the best purity of cellulose which nearly 88% of the residue recovered from low-S Poplar was cellulose. The cellulose content was low in the FA/AA treatment due to the presence of organic acids was mainly extracting the acid soluble lignin and left the acid insoluble lignin behind. Meanwhile, the acids also converted the cellulose and hemicellulose into furfural (FF) and hydroxymethylfurfural (HMF) under organosolv conditions at 110 ℃.[32] In contrast, the CDL treatment could only decompose lignin and removed the lignin monomers by washing with methanol. Therefore, the CDL treatment did not separate hemicellulose and cellulose into two portions and thus the presence of hemicellulose decreased the content of cellulose. However, the polymer unit (xylose or xylan) of hemicellulose has 5 carbon backbone which could potentially give an improved PG yield. The content of cellulose in raw biomass was analyzed and provided by NREL which had been summarized in Table S-5.1.

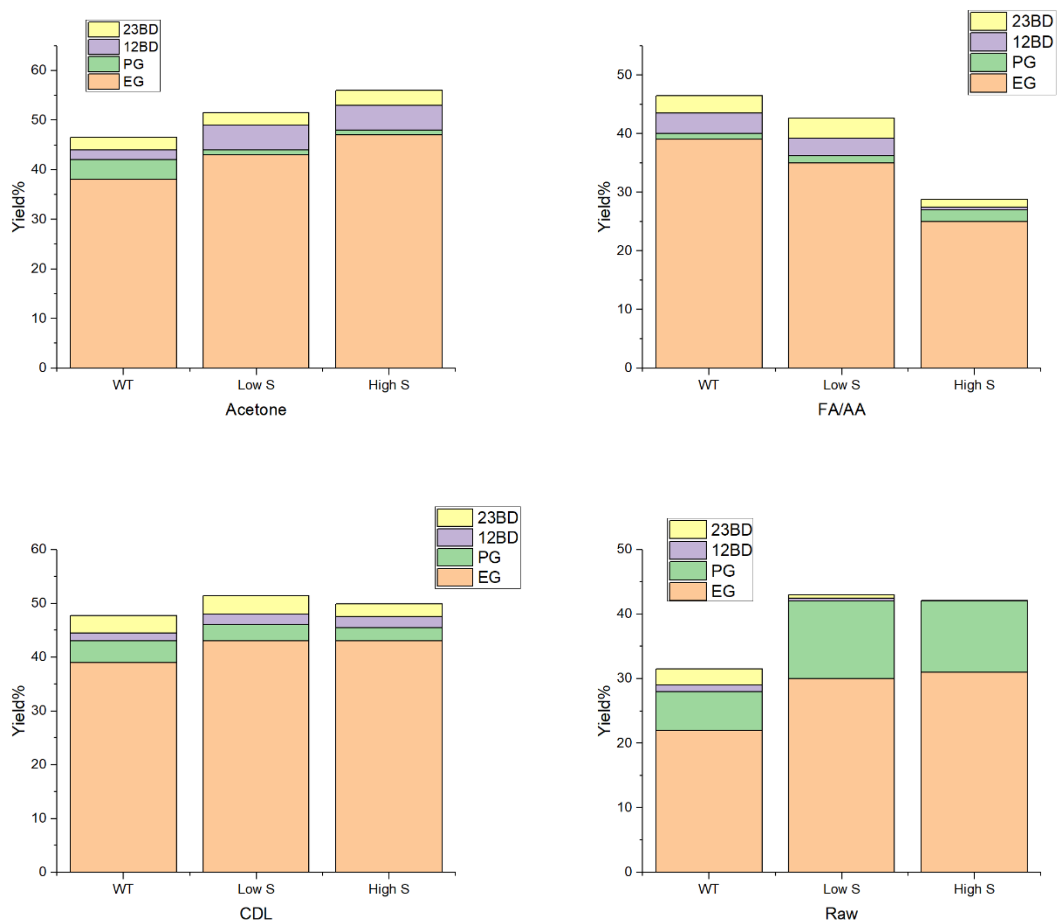

Figure 5.6 Diols yield of different Poplar biomass derived cellulose at optimized condition. Reaction conditions: Poplar biomass 0.5 g; 50 mg AMT; 50 mg Ru/AC; 40 mL H_2O; 240℃; 1.5 hr.

The yield of diols from different types of cellulose are summarized in 4 charts and displayed in Figure 5.6. In this study, among all types of the cellulose feedstock, the maximum yield of diols was obtained by using the cellulose from high-S Poplar treated with acetone organosolv method. By which, the yield of EG was 47% with 5% 12BD and 3% 23BD. The overall conversion of high-S acetone cellulose was 98%. Moreover, the yield of byproducts glycerol and sorbitol were determined around 1%. Figure S-5.3 illustrates an example of mass balance by using high-S acetone treated cellulose for EG production which shows 73.5 wt% of the feedstock cellulose were converted into the diol products. The maximum yield of EG from FA/AA and CDL cellulose and raw biomass were 39%, 43%, and 31%, respectively. Taking the cellulose retention into consideration (Table 5.1), it suggested the higher purity of cellulose which had less contaminations would give a better yield of diols.

The other diols, such as 12BD and 23 BD are also valuable products obtained from cellulose conversion. Interestingly, cellulose obtained from organosolv treatment (both acetone and FA/AA) gave higher yield of 12BD and 23BD, except from high-S FA/AA treated cellulose. In contrast, the CDL cellulose and raw biomass gave less 12BD and 23BD products. Instead, PG production from CDL cellulose and raw biomass were higher than the organosolv cellulose. This phenomenon is because in both CDL and raw biomass there is significant hemicellulose present, which yields PG through C2-C3 cleavage of xylose/xylitol. Therefore, the higher yield of PG produced from CDL cellulose and raw biomass were because of the higher content of hemicellulose along with cellulose.

5.5 Conclusion

In this study, we investigated the catalytic conversion of poplar cellulose produced from different pretreatments to EG over the Ru/C and AMT co-catalysts system. Our results indicated the depolymerization of cellulose was catalyzed by AMT, reduction of glucose to sorbitol over Ru/C, and subsequent hydrogenolysis to EG by both Ru/C and AMT. AMT improved the selectivity for EG formation. An optimized catalyst loading has been determined as 10 wt% for each of the Ru/C and AMT. To balance the overall cellulose conversion between the yield of EG, 1.5 – 2 hours reaction time at 240 ℃ was desirable. After screening organosolv methods and the CDL treatment, our findings indicated the organosolv treatment with acetone resulted in the best quality of cellulose. Regarding the cellulose from different genetically modified Poplar biomasses, the cellulose obtained from high-S poplar with acetone treatment gave the best yield of EG at 47 % with 98% conversion. In the case of PG production, both low-S and high-S raw poplar wood are suitablefeedstock.

5.6 References:

1. Luterbacher, J. S.; Rand, J. M.; Alonso, D. M.; Han, J.; Youngquist, J. T.; Maravelias, C. T.; Pfleger, B. F.; Dumesic, J. A., Nonenzymatic Sugar Production from Biomass Using Biomass-Derived gamma-Valerolactone. *Science* **2014,** *343* (6168), 277-280.

2. Huber, G. W.; Iborra, S.; Corma, A., Synthesis of transportation fuels from biomass: Chemistry, catalysts, and engineering. *Chem Rev* **2006,** *106* (9), 4044-4098.

3. Luo, C.; Wang, S. A.; Liu, H. C., Cellulose conversion into polyols catalyzed by reversibly formed acids and supported ruthenium clusters in hot water. *Angew Chem Int Edit* **2007,** *46* (40), 7636-7639.

4. Yang, H. P.; Yan, R.; Chen, H. P.; Zheng, C. G.; Lee, D. H.; Liang, D. T., In-depth investigation of biomass pyrolysis based on three major components: Hemicellulose, cellulose and lignin. *Energ Fuel* **2006,** *20* (1), 388-393.

5. Xi, J.; Ding, D.; Shao, Y.; Liu, X.; Lu, G.; Wang, Y., Production of Ethylene Glycol and Its Monoether Derivative from Cellulose. *ACS Sustainable Chemistry & Engineering* **2014,** *2* (10), 2355-2362.

6. Zhang, Y. R.; Li, N.; Li, M. F.; Fan, Y. M., Highly efficient conversion of microcrystalline cellulose to 5-hydroxymethyl furfural in a homogeneous reaction system. *Rsc Adv* **2016,** *6* (26), 21347-21351.

7. Rinaldi, R.; Palkovits, R.; Schuth, F., Depolymerization of Cellulose Using Solid Catalysts in Ionic Liquids. *Angew Chem Int Edit* **2008,** *47* (42), 8047-8050.

8. Barta, K.; Ford, P. C., Catalytic Conversion of Nonfood Woody Biomass Solids to Organic Liquids. *Accounts Chem Res* **2014,** *47* (5), 1503-1512.

9. Zakzeski, J.; Jongerius, A. L.; Bruijnincx, P. C. A.; Weckhuysen, B. M., Catalytic Lignin Valorization Process for the Production of Aromatic Chemicals and Hydrogen. *Chemsuschem* **2012,** *5* (8), 1602-1609.

10. Wang, A. Q.; Zhang, T., One-Pot Conversion of Cellulose to Ethylene Glycol with Multifunctional Tungsten-Based Catalysts. *Accounts Chem Res* **2013,** *46* (7), 1377-1386.

11. Yan, N.; Zhao, C.; Dyson, P. J.; Wang, C.; Liu, L. T.; Kou, Y., Selective Degradation of Wood Lignin over Noble-Metal Catalysts in a Two-Step Process. *Chemsuschem* **2008,** *1* (7), 626-629.

12. Luo, H.; Klein, I. M.; Jiang, Y.; Zhu, H. Y.; Liu, B. Y.; Kenttamaa, H. I.; Abu-Omar, M. M., Total Utilization of Miscanthus Biomass, Lignin and Carbohydrates, Using Earth Abundant Nickel Catalyst. *ACS Sustainable Chemistry & Engineering* **2016,** *4* (4), 2316-2322.

13. Klein, I.; Saha, B.; Abu-Omar, M. M., Lignin depolymerization over Ni/C catalyst in methanol, a continuation: effect of substrate and catalyst loading. *Catal Sci Technol* **2015,** *5* (6), 3242-3245.

14. Abdelkafi, F.; Ammar, H.; Rousseau, B.; Tessier, M.; El Gharbi, R.; Fradet, A., Structural Analysis of Alfa Grass (Stipa tenacissima L.) Lignin Obtained by Acetic Acid/Formic Acid Delignification. *Biomacromolecules* **2011,** *12* (11), 3895-3902.

15. Luo, H.; Abu-Omar, M. M., Lignin extraction and catalytic upgrading from genetically modified poplar. *Green Chem* **2018,** *20* (3), 745-753.

16. Fabicovicova, K.; Malter, O.; Lucas, M.; Claus, P., Hydrogenolysis of cellulose to valuable chemicals over activated carbon supported mono- and bimetallic nickel/tungsten catalysts. *Green Chem* **2014,** *16* (7), 3580-3588.

17. Grilc, M.; Likozar, B.; Levec, J., Hydrodeoxygenation and hydrocracking of solvolysed lignocellulosic biomass by oxide, reduced and sulphide form of NiMo, Ni, Mo and Pd catalysts. *Appl Catal B-Environ* **2014,** *150*, 275-287.

18. Fukuoka, A.; Dhepe, P. L., Catalytic conversion of cellulose into sugar alcohols. *Angew Chem Int Edit* **2006,** *45* (31), 5161-5163.

19. Zheng, M. Y.; Wang, A. Q.; Ji, N.; Pang, J. F.; Wang, X. D.; Zhang, T., Transition Metal-Tungsten Bimetallic Catalysts for the Conversion of Cellulose into Ethylene Glycol. *Chemsuschem* **2010,** *3* (1), 63-66.

20. Yan, N.; Zhao, C.; Luo, C.; Dyson, P. J.; Liu, H. C.; Kou, Y., One-step conversion of cellobiose to C-6-alcohols using a ruthenium nanocluster catalyst. *J Am Chem Soc* **2006,** *128* (27), 8714-8715.

21. Dhepe, P. L.; Fukuoka, A., Cellulose Conversion under Heterogeneous Catalysis. *Chemsuschem* **2008,** *1* (12), 969-975.

22. Deng, W. P.; Tan, X. S.; Fang, W. H.; Zhang, Q. H.; Wang, Y., Conversion of Cellulose into Sorbitol over Carbon Nanotube-Supported Ruthenium Catalyst. *Catal Lett* **2009,** *133* (1-2), 167-174.

23. Wang, H. J.; Zhu, L. L.; Peng, S.; Peng, F.; Yu, H.; Yang, J., High efficient conversion of cellulose to polyols with Ru/CNTs as catalyst. *Renew Energ* **2012,** *37* (1), 192-196.

24. Zhao, G. H.; Zheng, M. Y.; Zhang, J. Y.; Wang, A. Q.; Zhang, T., Catalytic Conversion of Concentrated Glucose to Ethylene Glycol with Semicontinuous Reaction System. *Ind Eng Chem Res* **2013,** *52* (28), 9566-9572.

25. Tai, Z. J.; Zhang, J. Y.; Wang, A. Q.; Pang, J. F.; Zheng, M. Y.; Zhang, T., Catalytic Conversion of Cellulose to Ethylene Glycol over a Low-Cost Binary Catalyst of Raney Ni and Tungstic Acid. *Chemsuschem* **2013,** *6* (4), 652-658.

26. Klein, I.; Marcum, C.; Kenttamaaa, H.; Abu-Omar, M. M., Mechanistic investigation of the Zn/Pd/C catalyzed cleavage and hydrodeoxygenation of lignin. *Green Chem* **2016,** *18* (8), 2399-2405.

27. Song, Q.; Wang, F.; Cai, J. Y.; Wang, Y. H.; Zhang, J. J.; Yu, W. Q.; Xu, J., Lignin depolymerization (LDP) in alcohol over nickel-based catalysts via a fragmentation-hydrogenolysis process. *Energ Environ Sci* **2013,** *6* (3), 994-1007.

28. Manaenkov, O. V.; Mann, J. J.; Kislitza, O. V.; Losovyj, Y.; Stein, B. D.; Morgan, D. G.; Pink, M.; Lependina, O. L.; Shifrina, Z. B.; Matveeva, V. G.; Sulman, E. M.; Bronstein, L. M., Ru-Containing Magnetically Recoverable Catalysts: A Sustainable Pathway from Cellulose to Ethylene and Propylene Glycols. *Acs Appl Mater Inter* **2016,** *8* (33), 21285-21293.

29. Tai, Z. J.; Zhang, J. Y.; Wang, A. Q.; Zheng, M. Y.; Zhang, T., Temperature-controlled phase-transfer catalysis for ethylene glycol production from cellulose. *Chem Commun* **2012,** *48* (56), 7052-7054.

30. Rambo, M. K. D.; Schmidt, F. L.; Ferreira, M. M. C., Analysis of the lignocellulosic components of biomass residues for biorefinery opportunities. *Talanta* **2015,** *144*, 696-703.

31. Zhang, K.; Wu, S. B.; Yang, H.; Yin, H. M.; Li, G., Catalytic conversion of cellulose for efficient ethylene glycol production and insights into the reaction pathways. *Rsc Adv* **2016,** *6* (81), 77499-77506.

32. Cai, C. L.; Liu, Q. Y.; Tan, J.; Wang, T. J.; Zhang, Q.; Ma, L. L., Conversion of Cellulose to 5-Hydroxymethylfurfural using Inorganic Acidic Catalysts in the Presence of Pressurized Water Steam. *Bioresources* **2017,** *12* (1), 1201-1215.

5.7 Supporting Information

CDL pretreatment

Ni catalyst preparation. 5.5 g nickel nitrate hexahydrate (Sigma-aldrich) was first dissolved in 16 mL deionized water in beaker and stirred for 30 minutes till no solid left in mixture. This resulted a clear green solution. Then transfer the solution to a 50 mL burette and wash beaker three times with deionized water and add washing solution to burette to ensure all nickel nitrate was collected. 10 g activated carbon was placed in a 150 mL beaker with a glass rod inserted. Slowly add nickel nitrate solution dropwise to AC carbon while the AC carbon was stirring by glass rod at the same time to ensure a fine dispersion of nickel on AC carbon. The dispersion took about one hour with stirring. After all nickel nitrate solution was add to AC carbon, 2 mL deionized water was added to wash burette then slowly dispersed on AC carbon with stirring.

The AC carbon with nickel nitrate dispersed then placed in a fume hood overnight to dry the AC carbon in room temperature. Then transfer Ni/AC to 120℃ oven for 12 hours deep dry. The oven-dried Ni/AC was finally reduced under flowing nitrogen with rate 60-80 mL/min at 450℃ for 2 hours with a heating rate from 20℃ to 450 ℃ in 60 minutes.

CDL reaction and cellulose collection. The heterogeneous catalytic reaction was performed in a 75 mL stainless steel vessel in Parr MRS 5000 batch reactor system. 0.15 g Ni/AC catalyst was first added to a catalyst cage which the microporous cage had a passing size of 325 mesh. The loaded cage was placing in the middle of vessel on hood. The cage with catalyst was first washed twice with 45 mL HPLC grade methanol. After washing the catalyst, 1.0 g of 40 mesh dry raw Poplar biomass with 45 mL HPLC grade methanol and a glass-shield magnetic stir bar were added to the vessel and well-sealed. Using UHP grade hydrogen for 5 times purging at pressure of 3.5 MPa. After the vessel was purged, then add 3.5 MPa UHP grade hydrogen to pressurize the vessel. The vessel was then heated to 225℃ for 12 hours. After the reaction, the solid phase was collected by filtration. The lignin was removed into liquid phase in methanol. The filtered solid residue was washed by HPLC grade methanol 4 times and 60 mL for each time. Dry the solid residue in fume hood for two days. The dry solid finally collected was the lignin removed CDL biomass.

Organosolv treatments

Treatment with acetic acid with formic acid (FA/AA). The FA/AA solvent was first prepared by FA/AA/water in volume ratio of 50/30/20. Then 30 g of 40 mesh dry raw Proplar biomass was combined with 300 mL FA/AA solvent in a 1 L round bottom flask. The mixture was then transferred to oil bath in fume hood. There was a two-step heating process. First, heated the mixture to 60℃ for 60 minutes. Then the temperature was quickly increased to 110℃ for 3 hours. After reaction, the mixture was cooled to room temperature. The solid phase was collected by filtration and washed by 3 portions of 200 mL 0.5 N acetic acid at 60℃ for 30 minutes. Then the solid was dried in fume hood for two days. The solid fraction was the cellulose portion isolated from raw Poplar biomass. Lignin and hemicellulose was extracted into acidic liquid phase.

Treatment with acetone. 2 g of 40 mesh dry raw Poplar biomass was add to 75 mL stainless steel vessel in Parr MRS 5000 batch reactor system. 20 mL acetone was then added to the vessel following by 1:20 solid: liquid ratio. The reaction was catalyzed by 20 mL 0.045 N sulfuric acid and 4 mL 37% formaldehyde. A glass-shield magnetic stir bar was also added to the vessel. The vessel was well-sealed and purged by UHP grade nitrogen gas for 5 times. The vessel was then heated up to 160℃ for 30 minutes under 1.2 MPa nitrogen pressure. After reaction, solid phase was collected by filtration and washed 3 times by 20 mL acetone for each. Lignin and hemicellulose were extracted into liquid. The remaining solid was cellulose fraction. Left the cellulose fraction in fume hood for two days to dry.

Analysis of cellulose content and diols

HPLC details. The analyte with internal standard was added to a 2 mL LC vial before injecting to HPLC. The analyte was identified by retention time. The quantification analysis was based on the peak area of each analyte and the area ratio between analyte and internal standard.

Glucose peak with 10 mM tert-butyl alcohol as shown below Figure S-5.1.

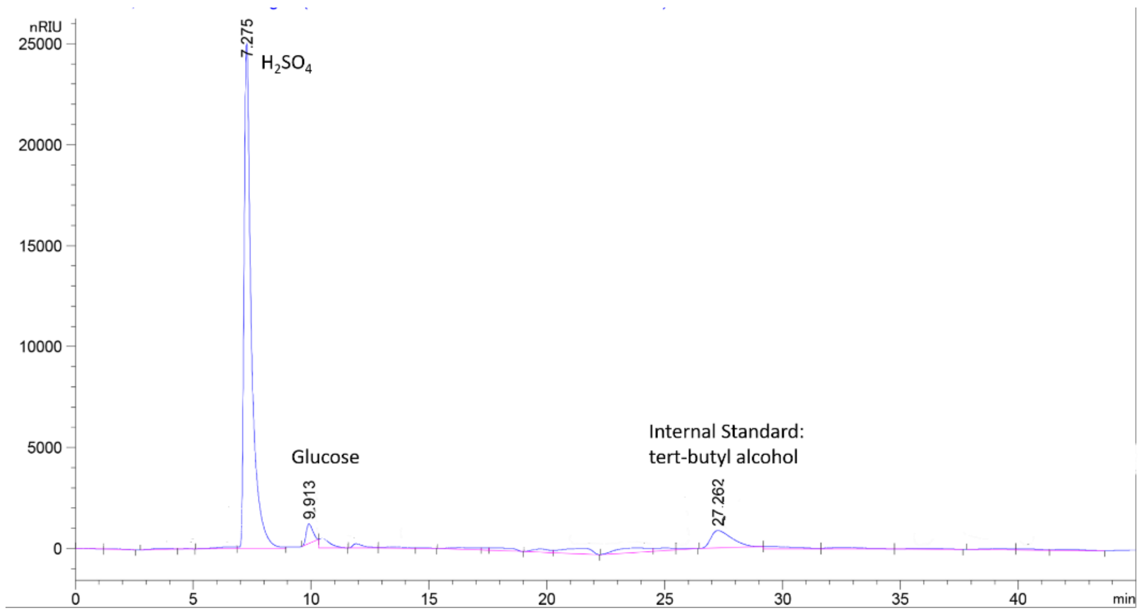

Figure S-5.1 HPLC result of glucose for analysis of cellulose content.

HPLC peak of diols as shown in Figure S-5.2

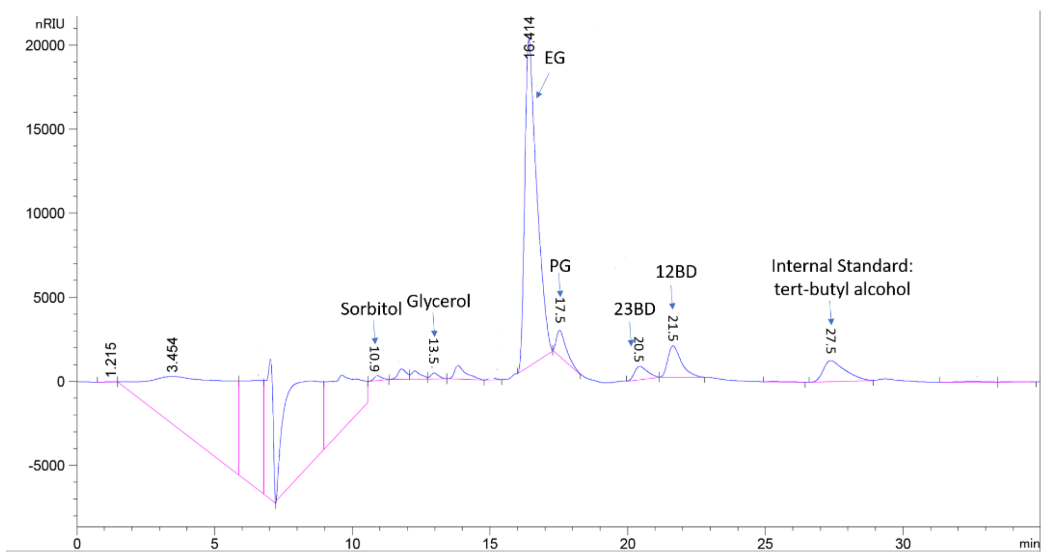

Figure S5-2. HPLC result of diols.

Mass balance of the diols' formation from cellulose by high-S Poplar treated by acetone organosolv method.

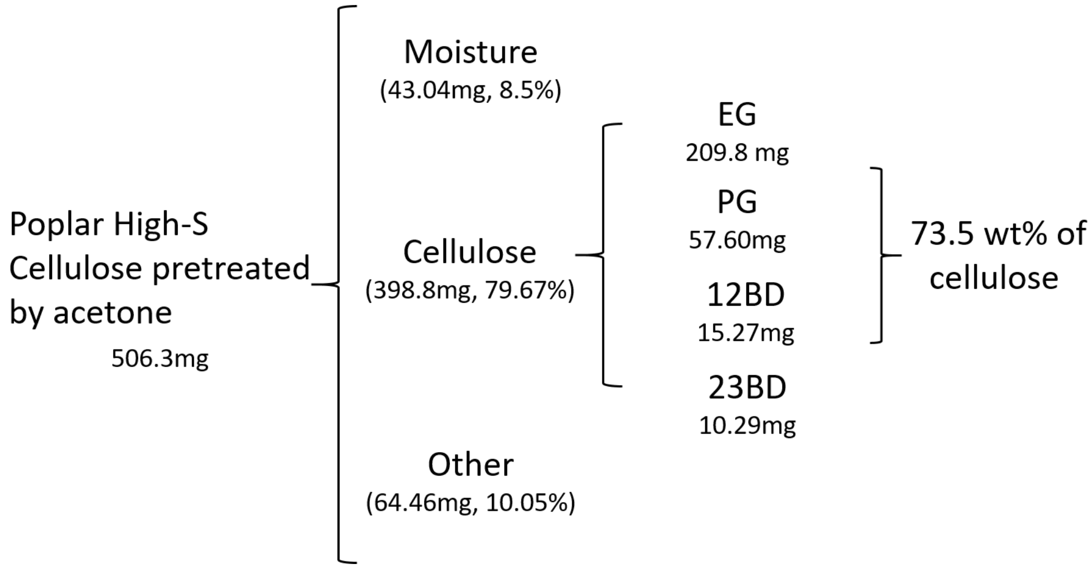

Figure S-5.3 The mass balance of cellulose from acetone treated High S Poplar biomass.

Content of Poplar cellulose in raw biomass measured by NERL. Table S-5.1

	Wild Type	High S	Low S
Glucan	43.40%	44.49%	44.54%
Xylan	21.20%	21.48%	20.97%
Arabinan	0	0	0
Acetyl	1.80%	1.87%	1.79%
Acid Insoluble Lignin	15.46%	16.67%	16.78%
Acid Soluble lignin	5.90%	5.62%	4.64%
Ash	0.70%	0.49%	0.53%
Glucose	0.99%	0	0.69%
Xylose	0.79%	0	0.36%
Arabinose	0	0	0
Acetic Acid	0	0	0
Water Extractives	5.41%	0.31%	4.29%
Ethanol Extractives	2.43%	3.94%	3.64%
Mass Balance	98.07%	94.88%	98.24%

Appendix i: Determination of Cellulose and Hemicellulose Content in Solid Biomass

Reagents:

(1) Dry biomass samples (40mesh particle size), (2) High purity standards: Glucose, Xylose, and 10mM tert-butyl alcohol, (3) MilliQ water, (4) 72% w/w Sulfuric acid, (5) 5mM Sulfuric acid, (6) Sodium bicarbonate

Materials:

(1) 100mL Glass pressure tubes and caps, (2) 30cm x 0.5cm Glass stir rod, (3) 10.00mL Volumetric automated pipettor and pipettor tips, (4) 100.0mL Graduated cylinder, (5) Autoclavable pressure tube rack, (6) Autoclavable plastic tray, (7) 3mL Plastic syringe, (8) 0.2 micron syringe filter, (9)1L Beaker

Instruments:

(1) Precision shaking water bath (SWB15), (2) Liquid Autoclave, (3) Agilent 1260 Infinity HPLC, (4) Agilent Hi-Plex H HPLC column, (5) Agilent 2mL HPLC vial

Procedures:

Sample Treatment (Acid Hydrolysis)[1]:

1. Place 100mL glass pressure tubes and caps in 60^{o}C oven overnight. Cool the tubes and caps to room temperature prior to use.
2. Prepare shaking water bath to 30^{o}C at 150 rpm shaking rate.
3. Exactly weigh 0.3000g of dry biomass and transfer into 100mL glass pressure tube.
4. Exactly measure 3.00mL 72% w/w sulfuric acid by 10.00mL volumetric automated pipettor and transfer into 100mL glass pressure tube.
5. Insert glass stir rod into the pressure tube and mix the dry biomass evenly with 72% w/w sulfuric acid. The mixture will turn into dark brown color immediately. Leave the glass rod inserted in the pressure tube.
6. Place the pressure tube into the 30^{o}C shaking water bath in tube rack vertically at 150 rpm shaking rate for 1 hour. Stir the mixture with glass rod every 10 minutes to ensure the biomass is fully reacted with sulfuric acid.
7. Place the pressure tube in autoclavable tube rack. Add 84.0mL MilliQ water to the mixture and rinse the glass stir rod. Remove glass rod and seal the pressure tube.
8. Transfer the sealed pressure tube and autoclavable tube rack on an autoclavable tray. Fill the tray with 500mL DI water.
9. Place the tray in autoclave. Choose liquid setting for 1 hour at 121^{o}C. After the completion of the autoclave cycle, allow the mixture to cool to room temperature.

Sugar Analyze[2,3]:

1. Cellulose and Hemicellulose will be converted into glucose and xylose during the above treatment. Filter the liquid portion out of the pressure tube through 0.2 micron syringe filter.
2. Exactly measure 1.00mL filtrate and dispense in 10.00mL MilliQ water.
3. Exactly measure 1.00mL from the diluted filtrate made above and mix with 1.00mL 10mM tert-butyl alcohol into a 2mL HPLC vial. Seal and label the vial.
4. Prepare a series of calibration standards containing different concentrations of glucose and xylose. Each calibration standard is made by 1.00mL of analyte solution mixed with 1.00mL of 10mM tert-butyl alcohol solution in 2mL HPLC vial.
5. Set HPLC conditions to a sugar method: 5mM sulfuric acid mobile phase at 0.6000mL/min flow rate, Hi-Plex H column heated to 70^{o}C, and refractive index detector (RID) at 35^{o}C. Each measurement takes 35 minutes HPLC run time.
6. Under this HPLC condition, glucose is determined at 9.6-9.8 minutes by retention time while xylose is at 10.5-10.6 minutes. Tert-butyl alcohol is used as internal standard for quantitative analysis which is at 27.8-28.1 minutes.
7. Calculate the amount of analyte by calibration curve which is made by ratio between peak areas of analyte and internal standard (tert-butyl alcohol) versus concentration.

Waste Treatment:

1. Collect the waste mixture into a 1L beaker.
2. Slowly add sodium bicarbonate while stirring the mixture with glass rod till no bubbling observed.
3. Transfer the neutralized waste into a proper waste container.

Calculations:

HPLC Calibration Curve:

1. Integrate the peak area of each concentration of the calibration standard analyte and the peak area of 10mM tert-butyl alcohol at each measurement.
2. Use the peak area of tert-butyl alcohol as denominator to acquire the ratio of peak area between standard analyte and internal standard.
3. The calibration curve f(X) can be plot by setting each standard concentration in unit of mM as y-axis and each relevant ratio of peak area as x-axis, $f(X) = aX + b$.
4. Integrate the peak area of the analyte from biomass sample and acquire its peak area ratio X_i with internal standard (repeat Step 1 and 2).
5. The concentration of analyte in unit of mM, [Glucose] and [Xylose], from biomass sample can be calculated by calibration curve $f(X_i) = aX_i + b$.
6. The amount of glucose and xylose in grams (g) can be calculated by:
   $m_{Glucose} = ([Glucose] * 2 * 11 * 87 * 10^{-6})$ *mol* * 180 *g/mol*

m_{Xylose} = ([Xylose] * 2 * 11 * 87 * 10^{-6}) *mol* * 150 *g/mol*

7. Glucose represents the cellulose in biomass sample while xylose represents the hemicellulose. The exact amount of cellulose and hemicellulose can be calculated by the mass conversion between glucose versus glucan and xylose versus xylan:
   $m_{Cellulose} = m_{Glucose} * \frac{162\ g/mol}{180\ g/mol}$
   $m_{Hemicellulose} = m_{Xylose} * \frac{132\ g/mol}{150\ g/mol}$
8. The content of cellulose and hemicellulose in biomass sample can be calculated:
   $\%Cellulose = \frac{m_{Cellulose}}{0.3000} * 100\%$
   $\%Hemicellulose = \frac{m_{Hemicellulose}}{0.3000} * 100\%$
9. The total sugar content in biomass sample can be calculated:
   $\%Sugar \cong \%Cellulose + \%Hemicellulose$

Reference:

1. Sluiter, A., Hames, B., Ruiz, R., Scarlata, C., Sluiter, J., Templeton, D., Crocker, D. *Laboratory Analytical Procedure: Determination of Structural Carbohydrates and Lignin in Biomass*. National Renewable Energy Laboratory (NREL). 2012
2. ASTM E1758-01. *Standard Test Method for Determination of Carbohydrates in Biomass by High Performance Liquid Chromatography*. ASTM International, West Conshohocken, PA, 2015
3. Mahood, S. A., Cable, D. E. *The chemistry of wood*. J. Ind. Eng. Chem. 1922, 14 (10), 933–934.

Appendix ii: Determination of Acid Soluble (ASL) and Insoluble Lignin (AIL) Content in Solid Biomass

Reagents:

(1) Dry biomass samples (40mesh particle size), (2) MilliQ water, (3) 72% w/w Sulfuric acid, (4) Warm DI water (40-45°C)

Materials:

(1) 100mL Glass pressure tubes and caps, (2) 30cm x 0.5cm Glass stir rod, (3) 10.00mL Volumetric automated pipettor and pipettor tips, (4) 100.0mL Graduated cylinder, (5) Autoclavable pressure tube rack, (6) Autoclavable plastic tray, (7) 3mL Plastic syringe, (8) 0.2 micron syringe filter, (9) 250mL Filtration Flask, (10) Filtering crucible, (11) 250mL Volumetric flask, (12) UV-Vis cuvette with 1 cm pathlength

Instruments:

(1) Precision shaking water bath (SWB15), (2) Liquid Autoclave, (3) Temperature programable muffle furnace, (4) Desiccator, (5) 105°C Oven, (6) UV-Vis Spectrophotometer

Procedures:

Biomass Treatment (Acid Hydrolysis)[1,2]:

10. Place 100mL glass pressure tubes and caps in 60°C oven overnight. Cool the tubes and caps to room temperature prior to use.
11. Prepare shaking water bath to 30°C at 150 rpm shaking rate.
12. Exactly weigh 0.3000g of dry biomass and transfer into 100mL glass pressure tube.
13. Exactly measure 3.00mL 72% w/w sulfuric acid by 10.00mL volumetric automated pipettor and transfer into 100mL glass pressure tube.
14. Insert glass stir rod into the pressure tube and mix the dry biomass evenly with 72% w/w sulfuric acid. The mixture will turn into dark brown color immediately. Leave the glass rod inserted in the pressure tube.
15. Place the pressure tube into the 30°C shaking water bath in tube rack vertically at 150 rpm shaking rate for 1 hour. Stir the mixture with glass rod every 10 minutes to ensure the biomass is fully reacted with sulfuric acid.
16. Place the pressure tube in autoclavable tube rack. Add 84.0mL MilliQ water to the mixture and rinse the glass stir rod. Remove glass rod and seal the pressure tube.
17. Transfer the sealed pressure tube and autoclavable tube rack on an autoclavable tray. Fill the tray with 500mL DI water.
18. Place the tray in autoclave. Choose liquid setting for 1 hour at 121°C. After the completion of the autoclave cycle, allow the mixture to cool to room temperature.

Acid Insoluble Lignin (AIL) Measurement[1]:

1. Put filtering crucible in muffle furnace at 575°C for 12 hours.
2. Allow the crucible cool down to 105°C. Remove the crucible from furnace and transfer into a desiccator.
3. After 30 minutes cooling down period in desiccator, exactly measure the weight of crucible three times. Take the average of the three measurement as the exact weight of crucible, $m_{Crucible1}$.
4. Put the crucible back to muffle furnace for another 4 hours at 575°C and allow it cool down to 105°C. Then remove the crucible from furnace and transfer into desiccator for another 30 minutes.
5. After 30 minutes cooling down period in desiccator, exactly measure the weight of crucible three times. Take the average of the three measurement as the exact weight of the crucible, $m_{Crucible2}$.
6. Compare the two averaged weight of crucible, $m_{Crucible1}$ and $m_{Crucible2}$, if the difference is less than 0.0003g, then the crucible is ready for the further use to analyze acid insoluble lignin (AIL). If the difference is greater than 0.0003g, then repeat step 3 to 4 till the difference is less 0.0003g.
7. Turn on the vacuum condensation trap 1 hour prior to the vacuum filtration.
8. Vacuum filter the solid residue from the pressure tube by using filtering crucible. Use 50.0mL hot DI water to rinse the pressure tube and wash the solid residue in crucible.
9. Collect the solid residue with crucible for AIL analysis. Capture the filtrate in filtration flask and save for acid soluble lignin (ASL) analysis.
10. Transfer the crucible with solid residue left in together into a 105°C oven and dry for 12 hours.
11. After 12 hours in oven, remove the crucible with solid residue and transfer into desiccator for 30 minutes to let them cool down.
12. Measure the weight of crucible with solid residue and record as $m_{Crucible+SolidResidue1}$.
13. Put the crucible with solid residue back to 105°C oven for another 4 hours. Then transfer them to desiccator to cool down for 30 minutes. After cooling down, measure the weight of crucible with solid residue and record as $m_{Crucible+SolidResidue2}$.
14. Compare the two measurements, $m_{Crucible+SolidResidue1}$ and $m_{Crucible+SolidResidue2}$, if the difference is less than 0.0003g, then the crucible and solid residue are ready for further analysis. If the difference is greater than 0.0003g, then repeat step 13 and 14 till the weight difference is less than 0.0003g.
15. Place the crucible with solid residue in the muffle furnace. Set the furnace ramping program as: (1) ramp from room temperature to 105°C, (2) hold at 105°C for 12 minutes, (3) ramp to 250°C at 10°C/min, (4) hold at 250°C for 30 minutes, (5) ramp to 575°C at 20°C/min, (6) hold at 575°C for 16 hours, (7) cool down to 105°C, (8) hold at 105°C till the crucible and solid residue are removed. During this heating process, all the acid insoluble lignin, wax, and protein burnt out. The left grey solid is ash[3].
16. Remove the crucible and solid residue from furnace and transfer into desiccator for 30 minutes to let them cool down.
17. Weigh the crucible and ash residue together and record the weight $m_{Crucible+Ash1}$.

18. Put the crucible and ash residue back to furnace and heat to 575°C holding for 4 hours. Then Allow them cool down to 105°C. After that, transfer the crucible and ash residue into desiccator for 30 minutes. Measure the weight after 30 minutes and record as $m_{Crucible+Ash2}$.
19. Compare the two measurements, $m_{Crucible+Ash1}$ and $m_{Crucible+Ash2}$, if the difference is less than 0.0003g, then the value is acceptable for further calculation. If the difference is greater than 0.0003g, then repeat step 18 till the difference is less than 0.0003g.

Acid Soluble Lignin (ASL) Measurement[1]:

1. Use DI water as background on UV-Vis spectrophotometer before analyzing ASL from biomass sample.
2. Dilute the filtrate which has been filtered and saved from pressure tube in a 250mL volumetric flask with DI water.
3. Obtain 1mL liquid sample from the dilution in a UV-Vis cuvette.
4. Measure and record the absorbance of the liquid sample at appropriate wavelength, UV_{abs}.

Calculations:

Acid Insoluble Lignin (AIL) Content:

1. Calculate the weight of solid residue after autoclave cycles in unit of gram:
   $m_{Residue} = \frac{m_{Crucible+Solid\ Residue\ 1} + m_{Crucible+Solid\ Residue\ 2}}{2} - \frac{m_{Crucible\ 1} + m_{Crucible\ 2}}{2}$
2. Calculate the weight of acid insoluble lignin in unit of gram:
   $m_{AIL} = m_{Residue} - (\frac{m_{Crucible+Ash\ 1} + m_{Crucible+Ash\ 2}}{2} - \frac{m_{Crucible\ 1} + m_{Crucible\ 2}}{2}) - m_{Protein}$
   The $m_{Protein}$ can be determined by an NREL procedure[1,4]. However, this measurement is only necessary for biomass has significant amount of protein.
   Thus: $m_{AIL} \cong m_{Residue} - (\frac{m_{Crucible+Ash\ 1} + m_{Crucible+Ash\ 2}}{2} - \frac{m_{Crucible\ 1} + m_{Crucible\ 2}}{2})$

Acid Soluble Lignin (ASL) Content:

1. Calculate the weight of acid soluble lignin in unit of gram:
   $m_{ASL} = \frac{UV_{abs}}{\varepsilon * 1\ cm} * 250\ mL * 10^{-3}\ mL^{-1}$
   The ε has a unit of *L/g*cm*. Its values were determined and reported by NREL[1].

Biomass	Lambda max (nm)	ε (L/g*cm)	Lambda max (nm)	ε (L/g*cm)
Pinus Radiata	198	25	240	12
Bagasse	198	40	240	25
Corn Stover	198	55	320	30
Populus Deltiodes	197	60	240	25

The total lignin content in biomass sample:

$$\%\text{Lignin} = \frac{m_{AIL} + m_{ASL}}{0.3000} * 100\%$$

Reference:

4. Sluiter, A., Hames, B., Ruiz, R., Scarlata, C., Sluiter, J., Templeton, D., Crocker, D. *Laboratory Analytical Procedure: Determination of Structural Carbohydrates and Lignin in Biomass*. National Renewable Energy Laboratory (NREL). 2012
5. Mahood, S. A., Cable, D. E. *The chemistry of wood*. J. Ind. Eng. Chem. 1922, 14 (10), 933–934.
6. Sluiter, A., Hames, B., Ruiz, R., Scarlata, C., Sluiter, J., Templeton, D. *Laboratory Analytical Procedure: Determination of Ash in Biomass*. National Renewable Energy Laboratory (NREL). 2005
7. Hames, B., Scarlata, C., Sluiter, A. *Laboratory Analytical Procedure: Determination of Protein Content in Biomass*. National Renewable Energy Laboratory (NREL). 2008

Appendix iii: Determination of Moisture Content in Solid Biomass

Reagents:

(2) Dry biomass samples (40mesh particle size)

Materials:

(2) Disposable aluminum moisture pan

Instruments:

(2) Mettler Toledo HE73 moisture analyzer (moisture balance)

Procedures:

1. Set the moisture balance as: ramp to 105^{o}C in 60 seconds, then hold at 105^{o}C for 50 seconds.
2. Weigh three portions of solid biomass sample. Each portion has at least 0.5000g of biomass.
3. Disperse each biomass sample evenly on a disposable aluminum moisture pan and place on moisture balance.
4. Turn on the heating program and run the measurement.
5. The percentage of mass loss can be directly read from moisture balance which represents the moisture content.
6. Allow 5 minutes between each measurement to have the moisture balance cooling down to room temperature.
7. Record the three readings from moisture balance, $\%Moisture_1$, $\%Moisture_2$, and $\%Moisture_3$.
8. Compare the difference between three readings. If the difference is less than 0.3%, then take the average value of the three measurements as the moisture content of the biomass sample. If the difference is greater than 0.3%, then obtain another two portions of biomass sample and repeat steps through 3 to 5 till the difference is less than 0.3%. Then take the average of the measurements as the moisture content of the biomass sample.

Mass Balance:

Dry Biomass[1,2]

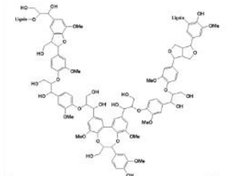

Lignin (15 – 25%)

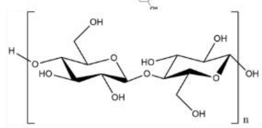

Cellulose (30 – 50%)

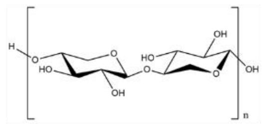

Hemicellulose (22 – 35%)

Others (7 – 15%)

- Moisture (5 – 10%)
- Ash (1 – 2.5%)
- Protein
- Extractives

Example of Poplar wood (WT – 717, 40 mesh):

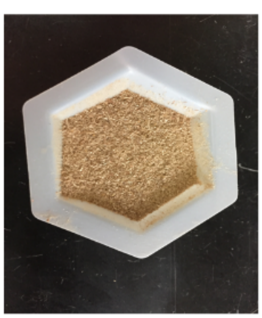

40 mesh dry Poplar

Cellulose	43.4%
Hemicellulose	21.2%
Arabinan	0%
Acetyl	1.8%
Acid insoluble lignin	15.46%
Acid soluble lignin	5.9%
Ash	0.7%
Glucose	0.99%
Xylose	0.79%
Arabinose	0%
Acetic acid	0%
Water extractives	5.41%
Ethanol extractives	2.43%

Reference:

1. de Jong, W. (2014). *Biomass Composition, Properties, and Characterization. In Biomass as a Sustainable Energy Source for the Future* (eds W. De Jong and J. R. Van Ommen). Chapter 2, 38 - 68. doi:10.1002/9781118916643.ch2
2. Templeton, D. W., Wolfrum, E. J., Yen, J. H., & Sharpless, K. E. (2015). *Compositional Analysis of Biomass Reference Materials: Results from an Interlaboratory Study*. Bioenergy research, *9*(1), 303-314.